May 2020

Zinc Proteomics: Interactions of Zn2+, Cd2+, and Metal-binding Ligands with Zn-Binding Sites in the Proteome

Eric Daniel Lund
University of Wisconsin-Milwaukee

Zinc Proteomics: Interactions of Zn^{2+}, Cd^{2+}, and Metal-binding Ligands with Zn-binding Sites in the Proteome

by

Eric D. Lund

A Dissertation Submitted in

Partial Fulfillment of the

Requirements for the Degree of

Doctor of Philosophy

in Chemistry

at

The University of Wisconsin-Milwaukee

May 2020

ABSTRACT

ZINC PROTEOMICS: INTERACTIONS OF Zn^{2+}, Cd^{2+}, AND METAL-BINDING LIGANDS WITH ZN-BINDING SITES IN THE PROTEOME

by

Eric D. Lund

The University of Wisconsin-Milwaukee, 2020
Under the Supervision of Distinguished Professor David H. Petering, Ph.D.

Cadmium ion causes toxicity in humans, most prominently in the kidney. This thesis focuses on mechanisms by which Cd^{2+} harms kidney proximal tubule cells. Previous experiments have shown the time-dependent distribution of Cd^{2+} and Zn^{2+} within supernatant of pig kidney, LLC-PK_1 cells after exposure to Cd^{2+} plus the ionophore pyrithione**[1]**. The first part of this research describes the trafficking of cadmium within LLC-PK_1 proximal tubule cells, including the time dependent distribution, speciation, and quantification of Cd^{2+} and Zn^{2+} in cells exposed to Cd^{2+} and Cd^{2+} plus pyrithione. The latter treatment introduces Cd^{2+} into cells at time zero and permits the clean observation of its subsequent trafficking pathway. Cd^{2+} binds first to the Proteome and exchanges with Zn^{2+} bound as specific Zn-proteins. Later, Cd^{2+} shifts into newly synthesized metallothionein. A 1:1 stoichiometry of the Cd-Zn exchange reaction was determined by titrations in cells and isolated cell Proteome. Zn^{2+} displaced from the Zn-Proteome became bound to other, adventitious sites of binding within the entire Proteome. The results support the hypothesis that non-specifically bound Zn^{2+} mobilized by Cd^{2+} activates the transcription factor, MTF-1, leading to the induction of metallothionein synthesis.

With these results in hand, the research turned to understanding at the protein level, how Cd^{2+} interacts with cell constituents. Important questions were what are the identities of the proteins

that bind Cd^{2+}? Are these proteins normally Zn-proteins? How can such proteins be detected analytically? Recently, native SDS-PAGE, or NSDS-PAGE, was developed that showed refined separation of proteins even as their native properties and bound metal ions remained intact[2]. This section of the defense explores the development of a new approach for the identification of zinc- and cadmium-containing proteins in complex mixtures. NSDS-PAGE was used to separate proteins with retention of their zinc and cadmium contents. Then, laser ablation-inductively coupled plasma-mass spectrometry (LA-ICP-MS) was utilized to detect low amounts of these metals in proteins along the length of the gel electrophoresis lane. A companion technique of fluorescent visualization of Zn-proteins with the zinc sensor, TSQ, was used in tandem with LA-ICP-MS to strengthen the detection of Zn- and Cd-proteins[3]. Using these methods, the replacement of Zn^{2+} by Cd^{2+} in Zn-proteins was observed. In the presence of Zn-metallothionein, the restoration of Zn^{2+} into these proteins was also seen for the first time as metallothionein successfully competed for Cd^{2+}.

The last part of this defense addresses the hypothesis that ligand binding to members of the Zn-proteome can occur with a wide variety of ligands. The ability of ligands to form adduct species with specific and non-specifically bound zinc was surveyed using a competitive titration experiment using the Zn^{2+} sensor TSQ. Of direct interest to the Cd^{2+} research, pyrithione can form ternary adducts with both types of cellular zinc.

1. Namdarghanbari, M. et al. J Biol Inorg Chem (2011) 16: 1087
2. Nowakowski, D. et al. Metallomics, 2014, 6, 1068
3. Meeusen, J. et al. *Inorganic Chemistry* 2011 *50* (16), 7563-7573

To my family,
if it was not for you, I would not be where I am today

To my wife,
for the continual dedication and support in which the words ‘thank you’ cannot even begin to express my deepest gratitude

To my friends,
whose support will never go unrecognized or unappreciated

To my professor,
whose unwavering dedication and support will never be lost on me

TABLE OF CONTENTS

LIST OF FIGURES

LIST OF TABLES

LIST OF ABREVIATIONS

AAS	Flame Atomic Absorption Spectroscopy
CA	Carbonic Anhydrase
DPBS	Dulbecco's Phosphate Buffered Saline
EDTA	Ethylenediaminetetraacetic acid
FCS	Fetal Calf Serum
LMW	Low Molecular Weight
LA-ICP-MS	Laser Ablation-Inductively Coupled Plasma-Mass Spectrometry
HMW	High Molecular Weight
MOPS	3-(*N*-morpholino)propanesulfonic acid
NSDS-PAGE	Native Sodium Dodecyl Sulfate-Polyacrylamide Gel Electrophoresis
SDS	Sodium Dodecyl Sulfate
SDS-PAGE	Sodium Dodecyl Sulfate-Polyacrylamide Gel Electrophoresis
TPEN	*N,N,N',N'*-Tetrakis(2-pyridylmethyl)ethylenediamine
MT	Metallothionein
TSQ	Zinc fluorophore
Proteome	Collection of proteins in a cell
Zn-Proteome	Collection of zinc proteins in a cell
Proteome●Zn	Adventitiously bound Zn^{2+} to Proteomic sites in the cell
PYR	2-mercaptopyridine-N-Oxide or Pyrithione
RSD	Relative standard deviation
BSA	Bovine Serum Albumin
HPLC	High performance liquid chromatography
DEAE	Diethyl-aminoethyl

Part I: Introduction

Introduction

Toxicologists lack a satisfactory understanding of cellular chemistry of xenobiotic metal ions that causes toxicity (Petering 2016). It is a common hypothesis that redox stable metals such as Cd^{2+} and Pb^{2+} compete with Zn^{2+} for proteins binding sites and binding would modify their normal biochemical function which would result in cell injury (Petering 2016). To understand how toxic metals cause cell injury requires the identification of intracellular sites of binding that cause changes in the cell biochemistry. With a host of metal binding groups such as carboxylate, amine, thiolate, imidazole structures in proteins, nucleic acids and small molecules; multiple metal binding interactions can be proposed in which $\sum L_i$ represents potential binding sites:

$$M^{n+} + \sum L_i \leftrightharpoons \sum M\text{-}L_i \, (K_i, k_i, k_{-i}) \qquad (1.1)$$

Where K_i is the equilibrium constant of the reaction and the rate constants for formation and dissociation of the complex are k_i and k_{-i}, respectively (Petering 2016).

The chemistry of metals (M^{n+}) differs depending on the location in the periodic table. Zn^{2+} is a d^{10} first row transition metal that primarily associates with nitrogen and sulfhydryl ligands; whereas, Cd^{2+}, just below it in the same family of the periodic table, coordinates most favorably with thiolate ligands (Maret et al. 2013). Metal ion binding reactions commonly are reversible; which means that the forward (k_i) and reverse (k_{-i}) reactions are significant. Cd^{2+} toxicity results directly or indirectly from the particular speciation of M^{n+} among $\sum L_i$ during generic **reaction 1.1** (Petering 2016). Therefore:

$$Cd^{2+} + \sum L_i \leftrightharpoons \sum Cd\text{-}L_i \qquad (1.2)$$

From the formation of a Cd-L complex, changes in structure and reactivity of L_i offer insights into the mechanism by which Cd^{2+} alters cellular biochemistry. The equilibrium constant provides an understanding of the stability of the complex alone or in the presence of other cellular ligands that can compete to bind Cd^{2+}. In turn, this offers information about whether Cd-L can exist in the cell.

A variety of metal ions are required for cellular systems to function. Disruption of normal operations within a cell occurs when the inorganic chemistry of a toxic metal, M_{toxic}^{n+}, overlaps with a native metal ion neighbor of one of the biologically essential metal ions, such as Zn^{2+}. Zn^{2+} and Cd^{2+} reside in the same family on the periodic table and, therefore, share similar chemical properties. Oxygen (O), nitrogen (N) and sulfur (S) ligands form complexes with Zn^{2+} and Cd^{2+} and neither of these elements participates in oxidation-reduction reactions. There are large concentrations and countless sites for Cd^{2+} to bind within cells. Carboxylate(O), imidazole (N), thiolate (S), and amino (N) groups are plentiful on the exterior surface of aqueous proteins (Sovago et al. 2013). Glutathione is another molecule in high concentration that could bind Cd^{2+} (Krezel et al. 1999). Nonspecific affinity for Cd^{2+} is substantial among cellular constituents. Cd^{2+} prefers soft ligands, such as sulfhydryl (S), to harder ligands, such as carboxyl (O) and imidazole (N), and its atomic radius is larger than Zn^{2+} (Maret et al. 2013). Thus, it has been hypothesized that normal Zn^{2+} metabolism and function is interfered with by interaction with Cd^{2+} at the molecular level (Petering 1978).

In addition to many adventitious binding sites for Cd^{2+}, numerous metalloproteins populate cells. Mammalian cells contain an estimated 3,000 Zn-proteins (Zn-P) (Andreini et al. 2006). Zn^{2+} typically contributes to protein conformation (e.g. Zn-finger transcription factors) or the catalytic mechanism of action at enzyme active sites (e.g. carbonic anhydrase and alcohol dehydrogenase) (Petering et al. 2017). When Zn^{2+} is involved with protein conformation, it provides thermodynamic stabilization for the structure and may be involved with the correct

folding of the protein. Considering Zn^{2+} and Cd^{2+} are within the same family on the periodic table, protein (P) may also have significant affinity for Cd^{2+}:

$$Cd^{2+} + P \leftrightharpoons Cd\text{-}P \ (K_{eq}, k_1, k_{-1}) \qquad (1.3)$$

As with **reaction 1.2**, knowledge of the rate constants and equilibrium are crucial for assessing any critical significance for any particular example of this reaction.

A general pathway for the trafficking of Cd^{2+} includes its transport across membranes, intracellular distribution within any given compartment, and final sites of localization (Petering et al. 2017). **Figure 1.1** serves as the foundation for what is known about Cd^{2+} speciation in relation to toxicity. Once in the cell, Cd^{2+} associates with adventitious proteomic binding sites and possibly with glutathione (Cadmium Interaction with Animal Cells 2018). Some of these adventitious Proteomic binding sites, Proteome•Cd, may be toxicologically important. The underlying hypothesis in **figure 1.1** suggests that Proteome•Cd ultimately reacts with metalloproteins, through metal ion exchange, to create Cd-proteins in which the native binding site with M^{n+} becomes a cadmium substituted protein with modified biochemical properties. Because Zn^{2+} and Cd^{2+} share chemical properties, many hypothetical reactions with Cd^{2+} involve Zn-proteins (Petering et al. 2017). The hypothesis is supported by NMR experiments in which Zn^{2+} is replaced in Zn-proteins by $^{113}Cd^{2+}$ to gain information about the nature of the metal binding site (Armitage et al. 2013).

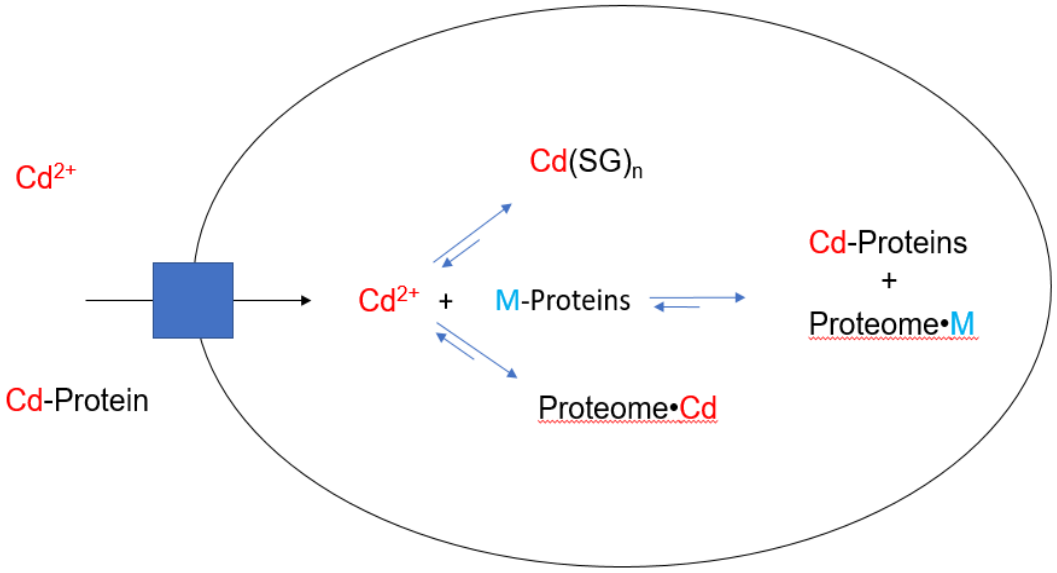

Figure 1.1

General pathway of trafficking of Cd^{2+} within cell compartments. M, native metal in metalloprotein, M-protein; SG, glutathione; box represents transporter connecting compartments. (Recreated from Cadmium Interaction with Animal Cells 2018).

There are also many sites within the cell that can bind Zn^{2+} nonspecifically and, thus, potentially bind Cd^{2+}. Once Cd^{2+} is associated with such a protein (P_1), the product P_1•Cd may transfer its metal ion to other protein ligands through a series of association and dissociation steps, as in **reaction 1.2**. A direct ligand substitution may occur in which the metal exchange between two proteins (P_1 and P_2) occurs without the dissociation of Cd^{2+} from P_1:

$$P_1\text{•Cd} + P_2 \leftrightharpoons P_2\text{•Cd} + P_1 \ (K_{eq}, k_1, k_{-1}) \qquad (1.4)$$

Eventually, the distribution of Cd^{2+} among proteins becomes consistent with all the equilibrium and rate constants of the participating reactions.

Through **reactions 1.3-1.4**, one can generalize that intracellular Cd^{2+} would be readily distributed among many proteins. Based on the chemical properties of Cd^{2+} listed above, it can

be inferred that most of the proteins would contain sulfhydryl ligands. Since glutathione has a cysteine thiol as one of its ligands, Cd^{2+} might also coordinate with it.

Cd^{2+} is hypothesized to eventually find its way into specific metalloprotein binding sites (M-Proteins), based on **figure 1.1**. Focusing on Zn-proteins ($\sum Zn\text{-}P_n$), the interaction with Cd^{2+} might result in Cd-proteins but, also through metal exchange reactions (**reaction 1.5**):

$$\sum Zn\text{-}P_n + \sum Pro_n \bullet Cd \leftrightharpoons \sum Cd\text{-}P_n + \sum Pro_n \bullet Zn \qquad (1.5)$$

One such protein is a sulfhydryl-rich protein called Metallothionein (MT). Much of the research on Cd^{2+} toxicity was shaped by the discovery of Metallothionein (Margoshes et al. 1957). MT has been identified as the protein chiefly responsible for protecting cells against Cd^{2+}. Its best documented function is its participation in cadmium toxicological action (Klaassen et al. 2009).

Mammalian MT has four major isoforms, I-IV (Otvos et al.1980). MT I and II are ubiquitously found throughout the body in organs and tissues, including kidney, and contain 20 cysteine residues placed identically within the 60 amino acid sequence (Vasak et al. 2011). The sulfhydryl side chains allow one molecule of MT to bind up to 7 Cd^{2+} and/or Zn^{2+}.

Fully saturated Cd_{7}- or Zn_7-MT exists in an elongated structure comprised of two domains, each containing a metal thiolate cluster – α domain (M_4S_{11}) and β domain (M_3S_9) (**figure 1.2**) (Petering et al. 2009). When not enough cadmium is present to saturate MT, mixed metal, Cd_n,Zn_{7-n}-MT species are formed (Ejnik et al. 2010). In addition, unsaturated forms can exist such as Cd_n-MT where $n \leq 7$ (Stillman et al. 1987).

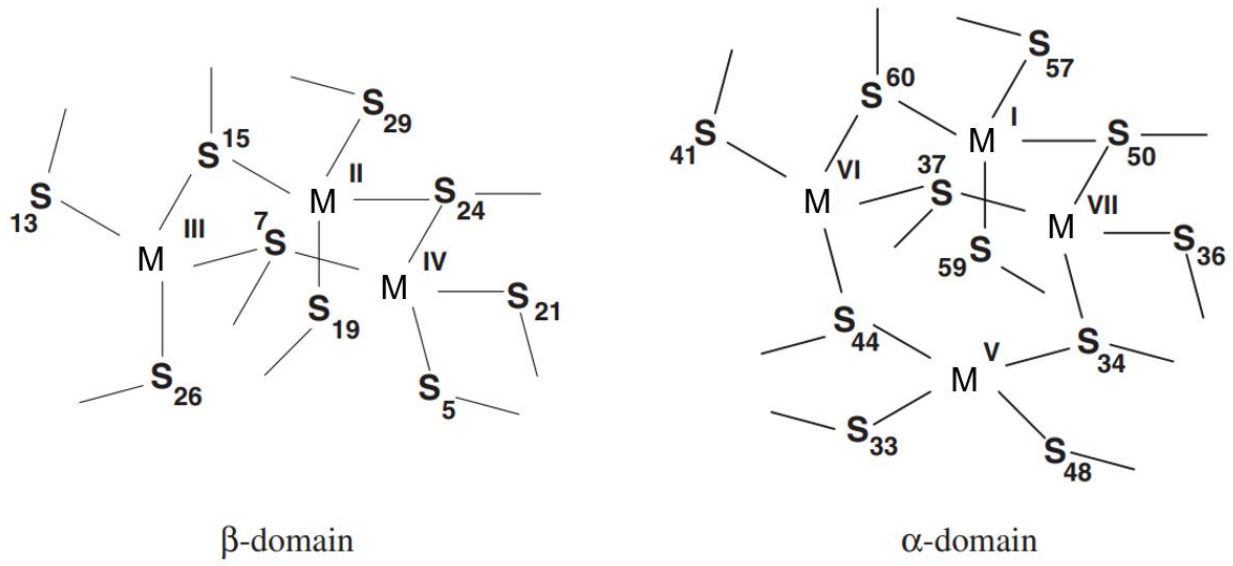

Figure 1.2

M^{2+} -thiolate connectivities in the metallothionein M_3S_9 and M_4S_{11} clusters, located in the N-terminal β-domain and C-terminal α-domain, respectively. (Altered from Petering et al. 2009)

The stability constants for the association of Cd^{2+}, at pH 7, with the α and β domains of mammalian MT are inferred to be in the range from $10^{14\text{-}16}$, three orders of magnitude larger than for Zn^{2+} ($K_{Zn\text{-}MT} = 10^{11\text{-}12}$) (Otvos et al. 1989; Namdarghanbari et al. 2010; Pinter et al. 2014). The explanation for the difference between stability constants of the two metal ions with apo-MT is that on a thermodynamic/equilibrium basis, MT simply binds Cd^{2+} more strongly to sulfhydryl groups (Petering 2016).

Recent experiments have discovered two classes of Zn^{2+} nonspecific Proteomic binding sites (Krezel et al. 2006; Karim et al. 2016). Thiolate ligands, in the concentration of hundreds of micromolar, are involved in the manifold of stronger binding sites and the average stability constant for Zn^{2+}, at pH 7, is 10^{10} (Petering et al. 2017). Since the stability constant for Cd^{2+} interaction with the proteome ($K_{Pro\bullet Cd}$) would be expected to be even larger, on average, because of its avid binding to sulfhydryl groups; it seems probable that Cd_n-MT would be formed when considering the reaction of newly synthesized, metal free, apo-MT with $\sum Pro_n \bullet Cd$.

$$\text{Apo-MT} + \sum \text{Pro}_n\text{.Cd} \leftrightharpoons \text{Cd}_n\text{-MT} + \sum \text{Pro}_n \qquad K = K_{\text{Cd-MT}} / K_{\text{Pro•Cd}} \qquad (1.6)$$

Similarly, apo-MT might favorably react with Cd-Pi that has formed in **reaction 1.5**:

$$\text{apo-MT} + n \sum \text{Zn-P}_i \leftrightharpoons \text{Cd}_n\text{-MT} + n \sum \text{Pro}_i \qquad (1.7)$$

Considering the measured stability constants for Zn-proteins range between $10^{9\text{-}12}$, it could be hypothesized that newly synthesized MT would compete with Zn^{2+} bound as Zn-proteins like in **reaction 1.8**.

$$\text{apo-MT} + 7\ \text{Zn-protein} \leftrightharpoons \text{Zn}_7\text{-MT} + 7\ \text{apo-protein} \qquad (1.8)$$

Based on two observations, apo-MT does not compete for Zn^{2+} bound as Zn-Protein. First, apo-MT or MT lacking its full complement of metals (Less than 7 Zn^{2+} and/or Cd^{2+}) is detected in a variety of cell types under various physiological and pathological conditions, sometimes in high concentration (Petering et al. 2006). MT that is undersaturated with metal ions coexists with Zn-proteins. Second, when the components of **reaction 1.7** are mixed together, *in vitro*, little to no products are formed (Rana et al. 2008). There must be a kinetic barrier to this reaction considering there are at least some Zn-proteins that have relative stability constants for Zn^{2+} that should react with apo-MT. In fact, in the same study, small molecule ligands for Zn^{2+} such as EDTA were shown to undergo reaction with Zn-Proteome (Rana et al. 2008).

An explanation for the high concentration of unsaturated MT may be that the reverse of **reaction 1.9** takes place regularly within cells: hypothetically, the source of Zn^{2+} for newly synthesized apo-Zn proteins is Zn_n-MT.

$$\text{Zn}_n\text{-MT} + n\ \text{apo-protein} \leftrightharpoons \text{apo-MT} + n\ \text{Zn-protein} \qquad (1.9)$$

Reports show that Zn_n-MT can donate Zn^{2+} to apo-carbonic anhydrase (Li et al. 1980; Pinter et al. 2014). Zn^{2+} that binds to high affinity sites within the Proteome ($\sum \text{Pro}_m$•Zn) that are in large concentrations are also kinetically available for donation to apo-carbonic anhydrase (Petering et

al. 2017; Petering et al. 2019). MT is the only protein that has been hypothesized to participate in Zn^{2+} trafficking and supplying Zn^{2+} to apo-Zn-proteins. But recently, Mahim and Petering have demonstrated that **reaction 1.10** gives rise to the equilibrium formation of some $\sum Pro_n \bullet Zn$ and that Zn^{2+} associated non-specifically with the Proteome can serve as a source of Zn^{2+} for the reconstitution of Zn-CA from apo-CA (**reaction 11**) (Petering et al. 2019).

$$Zn_n\text{-MT} + \sum Pro_n \leftrightharpoons \text{apo-MT} + \sum Pro_n \bullet Zn \qquad (1.10)$$

$$\sum Pro_n Zn + n \text{ apo-protein} \leftrightharpoons \sum Pro_n + n \text{ Zn-protein} \qquad (1.11)$$

In cells or organs that have undergone Cd^{2+} uptake, all isolated cadmium metallothioneins contain both Cd^{2+} and Zn^{2+} (Otvos et al. 1980). During the exposure of mouse kidney cortical cells to Cd^{2+}, Cd,Zn-MT begins to appear within three hours of exposure and continues to grow in concentration (Blumenthal et al. 1994). When the mechanism for cluster-specific information of Cd_n, $Zn_{(7-n)}$-MT was probed, Cd^{2+} tends to concentrate in the 4-metal cluster and Zn^{2+} in the 3-metal cluster (Nettesheim et al. 1985). This is due to a complicated metal ion exchange process between two fully saturated MT proteins, Cd_7-MT and Zn_7-MT (Nettesheim et al. 1985):

$$n\ Cd_7\text{-MT} + (7-n)\ Zn_7\text{-MT} \leftrightharpoons 7\ Cd_n, Zn_{(7-n)}\text{-MT} \qquad (1.12)$$

Extracellular Zn^{2+} seems to be the source of Zn_7-MT since cells exposed to Cd^{2+} cause the induction of MT, raises the total intracellular concentration of Zn^{2+} and MT does not seem to compete for protein-bound Zn^{2+} (Petering et al. 1984).

Cells exposed to Cd^{2+} make more MT than is necessary to gather all the invasive metal ion into its structure because, it is hypothesized, MT needs to retain its capacity to donate Zn^{2+} to other sites (**reaction 1.10-1.11**) even as it sequesters Cd^{2+} out of proteins (Otvos et al. 1989).

Zn_7-MT must be formed at some point for **reaction 1.12** to take place and may serve as a precursor of Cd_7-MT according to **reaction 1.13**:

$$Zn_7\text{-MT} + 7\ \text{Pro}\bullet\text{Cd} \leftrightharpoons Cd_7\text{-MT} + 7\ \text{Pro}\bullet\text{Zn} \qquad (1.13)$$

In this case, the overall equilibrium constant is the ratio of $(K_{Cd\text{-}MT}K_{Pro\bullet Zn})/(K_{Zn\text{-}MT}K_{Pro\bullet Cd})$. Whether **reaction 1.12** is energetically feasible lies in both the strongly favorable affinity of Cd^{2+} versus Zn^{2+} for MT $(K_{Cd\text{-}MT})/(K_{Zn\text{-}MT})$ and the relative binding strength of Cd^{2+} and Zn^{2+} to other proteins as well.

The principal hypothesis of **figure 1.1** is that when Cd^{2+} enters cells, it eventually displaces Zn^{2+} in Zn-proteins (**reaction 1.5**), producing an array of Cd-proteins with altered function (Cadmium Interaction with Animal Cells 2018). The properties of **reaction 1.5** have been directly assessed by directly reacting whole proteome, including the complete manifold of Zn-proteins, with Cd^{2+} and measuring the amount of products $\sum Cd\text{-}P_n$ and $\sum Pro_n\bullet Zn$ (Namdarghanbari et al. 2014). The results were consistent with the replacement of Zn^{2+} by Cd^{2+} in Zn-proteins together with the association of Zn^{2+} with nonspecific Proteomic binding sites.

When the product mixture of **reaction 1.5** was reacted with enough apo-MT to coordinate all the cadmium ion, Cd^{2+} was preferentially transferred to apo-MT along with some Zn^{2+} (Namdarghanbari et al. 2014):

$$\sum Cd\text{-}P_n + \sum Pro_m\bullet Zn + \text{apo-MT} \leftrightharpoons \sum P_n + \sum Pro_m + Cd_n,\ Zn_m\text{-MT} \qquad (1.14)$$

The much larger affinity of apo-MT for Cd^{2+} than Zn^{2+} drives **reaction 1.13** energetically and is indicative of the broad reactivity of apo-MT with Cd^{2+} bound in native Zn^{2+} protein sites. When apo-MT was replaced by Zn-MT in **reaction 1.13**, Cd^{2+} moves into the pool of MT, changing the product distribution, as a similar amount of MT-bound Zn^{2+} shifts back into the protein fraction (Namdarghanbari et al. 2014). This reaction possibly restores functional activity to these proteins by placing Zn^{2+} back into its native binding sites:

$$\sum Cd\text{-}P_n + Zn_7\text{-MT} \leftrightharpoons \sum Zn\text{-}P_n + Cd_n,\ Zn_{(7-n)}\text{-MT} \qquad (1.15)$$

The long-standing hypothesis that Zn_7-MT restores functionality to cadmium-altered proteins is supported by two model reactions: metal ion exchange of Zn_7-MT with a Cd-substituted zinc-finger protein, Tramtrak, and Cd-carbonic anhydrase (Otvos et al. 1989, Roesijadi et al. 1998, Ejnik et al. 1999).

An important characteristic of Cd^{2+} intoxication is that as Cd^{2+} reaches the kidney, it remains bound to MT in the form Cd_n, $Zn_{(7-n)}$-MT in a steady state of degradation and resynthesis (Cousins 1979). According to **figure 1.1**, as MT is hydrolyzed into its constituent amino acids, MT must reacquire Cd^{2+} from Cd-proteins and $\sum$Pro•Cd.

According to one hypothesis, once the concentration of Cd^{2+} within cells exceeds the storage capacity of MT, it becomes toxic and spills out of the MT pool into other sensitive sites (Friberg 1984). In this model, cadmium becomes toxic only after long exposure and extensive accumulation in tissues such as the kidney. However, in both animals and cells exposed with a modest concentration of Cd^{2+}, a small residual pool of non-MT-bound Cd^{2+} has been detected even though the sites occupied by Zn^{2+}, in Cd_n, $Zn_{(7-n)}$-MT, should have exchanged with Cd^{2+} (Petering et al. 1984, Blumenthal et al. 1994). This pool of Cd^{2+} hypothesized to initiate cell injury.

It may be useful to compare the concentration of intracellular Zn-proteins to the estimated concentration of non-MT-bound Cd^{2+}. Hundreds of micromolar Zn^{2+} within the cell are contributed by approximately 3000 Zn-proteins ($\sum$Zn-P_n) (Nowakowski et al. 2015). One study places the pool of potentially toxic Cd^{2+} at approximately 4% of the concentration of intracellular zinc and that of MT-bound Cd^{2+} many times larger (Nettesheim et al. 1985).

Cells upregulate the rate of synthesis of MT, in response to Cd^{2+} and Zn^{2+} as well as other metal ions, by activating the molecular switch MTF-1, metal regulatory transcription factor 1 (Gunter et al. 2012). MTF-1 is the transcription factor that binds selectively to metal response elements

(MREs) located in the promoter region of MT and other genes (Laity et al. 2007). The mechanism by which Zn^{2+} influences gene expression has been widely studied. The metal-responsive part of the protein is comprised of six tandem cysteine$_2$, histidine$_2$ (C_2H_2) zinc fingers residing in the DNA binding region. Only in the presence of Zn^{2+} do these structures fold and function properly (**reaction 1.11**) (Berg et al. 1997, Cox et al. 2000)**.**

$$n\ Zn^{2+} + \text{MTF-1}_{\text{inactive}} \leftrightharpoons Zn_n\text{-MTF-1}_{\text{active}}\ (n \leq 6,\ K_{eq} \sim 10^{10\text{-}11}) \qquad (1.16)$$

According to **reaction 1.16**, based on the availability of extracellular Zn^{2+} to the cell, the concentration of Zn^{2+} inactivates MTF-1.

The addition of micromolar amounts of Zn^{2+} were required to stimulate binding of MTF-1•MRE, when using cell lysate as the source of MTF-1 (Dalton et al. 1997). According to the results, the formation of Zn_n-MTF-1 seem to indicate a critical stability constant (K_{eq}) of ca. 10^6. However, the measurement of the equilibrium constant for the association of Zn^{2+} with each of the Zinc-finger domains of MTF-1 is on the order of $10^{10\text{-}11}$ for the association of Zn^{2+} with each of the zinc-finger domains of MTF-1 (Guerrerio et al. 2004). The above results begin to make sense when one recognizes that activation of MTF-1 begins with Zn^{2+} bound to Proteome as Pro•Zn. Pro•Zn has a large affinity for Zn^{2+} and there are large concentrations of such non-specific sites that range into the hundreds of micromolar. As such, the need for micromolar concentrations of Zn^{2+} above reflects the necessity of titrating $\sum Pro_n$ to provide the driving force for transferring Zn^{2+} to MTF-1 (**reaction 1.17**).

$$\sum Pro_n\text{•}Zn + \text{MTF-1} \leftrightharpoons \sum Pro_n + Zn_n\text{-MTF-1} \qquad (1.17)$$

The upregulation of MTF-1 is directly correlated to Cd^{2+} uptake. The initial hypothesis was Cd^{2+} directly binds to MTF-1, as in **reaction 1.16,** but Cd^{2+} actually inactivates MTF-1 (Bittel et al.1998). To rationalize this behavior, a study examined the DNA binding activity of transcription factor IIIA (TF-IIIA), using native Zn- and Cd-substituted Zinc-finger domains. When Cd^{2+} binds

to MTF-1, it prevents zinc fingers from interacting with the 5S ribosomal RNA gene (Huang et al. 2004). C_2H_2 Zinc-finger domains as are found in TF-IIIA and MTF-1 display a ββα secondary structure for each finger (Berg et al. 1988, Lee et al. 1989). The β-sheet provides two thiolate ligands and the α helix provides two imidazole nitrogens for binding of Zn^{2+}. The elements of DNA recognition are the amino acid side chains of the helix in which both Cd- and Zn-peptides have similar conformational folds according to a related NMR structural analysis (Krepkiy et al. 2004). Because Cd^{2+} has a larger ionic radius compared to Zn^{2+} (92 vs. 74 picometers), there is a structural perturbation in the recognition helix so that the amino acid side chains are not properly presented to the base-pair edges in the major groove of cognate DNA. Specific DNA-protein association is lost due to the sub-optimal complementary non-covalent bonding interactions between peptide and base pairs (Krepkiy et al. 2004).

The mechanism of Cd^{2+} inactivation of proteins with multiple, tandem zinc fingers may be more drastic. Cd^{2+} displaces Zn^{2+} in its reaction with Zn_9-TF-IIIA to form $Cd_{4\text{-}5}$-TF-IIIA (Huang et al. 2004). It appears to displace Zn^{2+} causing a rearrangement to favor Cd-C_4 binding of two adjacent fingers and destroying the original finger domain structure:

$$2\ \text{Cd-}(C_2H_2) \leftrightharpoons \text{Cd-}C_4 + 4\ \text{His} + Cd^{2+} \qquad (1.18)$$

According to this research, cadmium does not activate MTF-1 through direct binding to the transcription factor. Alternatively, Zn^{2+} released by the reaction of Zn-MT with Cd^{2+} could explain the activation of the apo-transcription factor, MTF-1 (Zhang et al. 2003). During a recent experiment, functional Zn_n-MTF-1 was generated when inactive MTF-1 and Zn_7-MT were added to a mixture of Cd^{2+} and lysate. Cd^{2+} displaced Zn^{2+} from MT to make it more available for reaction with apo-MTF-1 (Huang et al. 2004). During this reaction, MTF-1 competes with $\sum Pro_n$ for Zn^{2+} as in **reaction 1.17**. Although the above hypothesis explains the activation of MTF-1, the concentration of Zn-MT, in some cells, may not be able to act as a source of Zn^{2+} upon reaction with Cd^{2+}. **Reaction 1.5** is a better starting point for a more general hypothesis of how

MTF-1 is activated by Zn^{2+}. First, $\sum Zn\text{-}P_n$ exchanges metals with $\sum Pro_n \bullet Cd$ and then, as in **reaction 1.17**, $\sum Pro_n \bullet Zn$ undergoes ligand substitution with MTF-1 to yield active Zn_6-MTF-1.

The introduction to this point review what is known about the interactions of Cd^{2+} and Zn^{2+} at a molecular level. Other research has focused on defining the toxicology of Cd^{2+} in mammalian organisms and cells. Still other studies have sought to explain the toxicology in terms of the chemistry of Cd^{2+}.

Epidemiological studies clearly link Cd^{2+} with chronic kidney failure and bone disease (Nordberg 2009; Thevenod et al. 2013; Klaassen et al. 1999; Friberg 1984; Jarup et al. 2009). To rapidly elicit overt kidney injury that mimics human nephrotoxicity, large amounts of Cd^{2+} were injected intraperitoneally into rodents (Klaassen et al. 1999, 2000, 2009). From these experiments, it was determined that the induction of metallothionein synthesis protected animals from Cd^{2+} toxicity. MT-null rodents, that do not contain the MT 1 and 2 genes in their genome, were more susceptible to Cd^{2+} toxicity than wild-type rodents; animals carrying MT transgenes or animals pre-induced to synthesize MT were more resistant to Cd^{2+} toxicity. These studies also discovered that Cd-MT, itself, was the primary agent that caused kidney damage (Klaassen et al. 1988, 1992; Sabolic et al. 2010). When Cd^{2+} was injected into animals, it accumulated principally in the liver causing induction of MT and, consequently, damaging the hepatic cells enough to rupture; releasing a wave of Cd-MT into the plasma. The wave of Cd-MT reaches the kidney where it was filtered by the glomerulus into the tubule, degraded and resorbed. The rapid appearance of Cd^{2+} within the tubule cells resulted in nephrotoxicity.

Due to unusual administration of Cd^{2+} by injection and the focus on acute toxicity, this method of exposure seems to be irrelevant to how humans are usually exposed through the ingestion of small amounts of Cd^{2+}. Cd-MT circulating in the plasma does not seem to be the primary initiator of nephrotoxicity considering MT-null mice develop the same kidney disorder through injections and do not have the capability of making hepatic Cd-MT (Liu et al. 1998). Cd^{2+} and

Cd-MT caused indistinguishable toxic effects in kidney cortical cell cultures (Blumenthal et al. 1996). Thus, during oral intake of Cd^{2+}, it seems that release of Cd^{2+} from the intestine to the plasma, followed by direct glomerular filtration and absorption by proximal tubule epithelial cells is the likely cause of kidney toxicity.

Human and animals slowly develop chronic kidney disease following long-term exposure to Cd^{2+} (Satarug et al. 2004). This disease is usually characterized as a Falconi Syndrome; which is the inability of tubular cells to resorb nutrients such as glucose, amino acids, and phosphate from the plasma glomerular filtrate (Thevenod 2003). Primary mouse kidney cortical cells, rich in proximal tubule cells, were incubated for 24 hours with low micromolar concentrations of Cd^{2+} to understand the disruption of glucose resorption (Blumenthal et al. 1990). It was found that two transporters that mediate sodium-dependent glucose uptake, SGLT 1 and 2, were inhibited in a concentration-dependent manner that did not alter viability or protein or DNA synthesis.

$$\text{Glucose}_{out} + m\ Na^{+}_{out} \leftrightharpoons \text{Glucose}_{in} + m\ Na^{+}_{in} \qquad (1.19)$$

The inhibited kinetics of glucose transport are consistent with loss of functional transporters. Cd^{2+} did not appear to compromise the sodium gradient supporting active transport, the sodium-potassium ATPase which establishes the gradient, or oxidative phosphorylation that supplies ATP to drive the formation of the ion gradient. This was indicated by normal intracellular concentrations of Na^{+}, K^{+}, and ATP.

These results suggest that the synthesis or degradation of SGLT 1 and/or 2 protein is directly impacted by Cd^{2+}. The inquiry into these two processes revealed the selective inhibition of the synthesis of mRNAs for SGLT 1 and 2 in cells exposed to Cd^{2+} (Tabatabai et al. 2001). Further investigations showed multiple GC-rich binding sites on the promoter regions of each gene, sglt 1 and 2, for selective binding of the transcription factor Sp1, a common zinc-finger structure that contains a C_2H_2 metal chelation motif (Tabatabai et al. 2005).

$$Zn_3\text{-Sp1} + GC_{site} \leftrightharpoons Zn_3\text{-Sp1}\bullet GC_{site} \quad (1.20)$$

In the presence of Cd^{2+}, the Sp1-specific cytomegalovirus promoter and the expression of the luciferase gene, driven by these promoters, was downregulated.

Additional experiments showed the inhibitory effect of Cd^{2+} on Sp1 through reduction of *in vivo* binding of Sp1 to cognate DNA (GC_{sites}) in the promoters of sglt 1 and 2, with a chromosomal immunoprecipitation assay (Tabatabai et al. 2003). Direct *in vitro* assays revealed that the concentration of Sp1, in Cd^{2+} treated cells, remains the same while its specific DNA binding activity is drastically depressed.

Another study discovered 8-oxoguanine glycosylase, a DNA repair enzyme, is downregulated by Cd^{2+}, which inhibits the positive transcriptional activity of Sp1 required for its gene expression (Youn et al. 2005). Both studies hypothesized that the generation of Cd_n-Sp1 is the result of Zn^{2+} being displaced by Cd^{2+} and the resultant inactivation of the protein towards selective DNA complexation:

$$Zn_3\text{-Sp1} + 3\ Cd^{2+} \leftrightharpoons Cd_3\text{-Sp1} + 3\ Zn^{2+} \quad (K_{eq}) \quad (1.21)$$

Recombinant human Zn_3-Sp1 was used to probe the properties of this reaction (Kothinti et al. 2010). First, Zn_3-Sp1 was simultaneously mixed with varying Cd^{2+} and Zn^{2+} concentrations to determine the equilibrium (K_{eq}) properties of **reaction 1.21**. It was determined that $K_{eq} \sim 10$ with a slight preference for Cd_3-Sp1. The reaction of Sp1 with GC_{site} diminishes as more Cd^{2+} shifts the reaction to the right (**reaction 1.20-1.21**) but the reaction is reversed with increasing concentrations of Zn^{2+} (**reaction 1.20**) which increases the concentration of Zn_3-Sp1•GC_{site} (**reaction 1.19)**.

The experiment had different results when Zn_3-Sp1 was incubated first with Cd^{2+} for a short time before adding Zn^{2+}. In this case, the inhibition of DNA imposed by Cd^{2+} was not reversed by large concentrations of Zn^{2+}. The results were interpreted in terms of a two-step reaction

sequence: first, Cd^{2+} displaces Zn^{2+} as in **reaction 1.21**. Then, an irreversible rearrangement occurs to create a highly stable Cd_n-Sp1' analogous to what is proposed as the product of the reaction of Cd^{2+} with Zn_9-TFIIIA described above (**reaction 1.22**) (Huang et al. 2004):

$$Cd_3\text{-Sp1} \leftrightharpoons Cd_n\text{-Sp1'} + (3\text{-}n)\ Cd^{2+} \qquad (1.22)$$

In **reaction 1.21**, the substitution of Zn^{2+} by Cd^{2+} probably occurs with minimal conformational change of the three zinc fingers in Sp1 (Krepkiy et al. 2004); whereas, in **reaction 1.21**, Cd^{2+} in Cd_3-Sp1 may rearrange from its C_2H_2 coordination and bind to three or four sulfhydryl groups located on adjacent fingers unfolding and altering the standard C_2H_2 conformation like in **reaction 18** (Huang et al. 2004). This interconversion of Sp1 results in a Cd_n-Sp1 that is highly stable in the presence of Zn^{2+}.

For an appropriate model of the situation, Proteome would need to be in the reaction mixture. Due to their relative affinities of Cd^{2+} and Zn^{2+}, the presence of Proteomic binding sites ($\sum Pro_n$) may influence the formation of Cd_n-Sp1. An experiment was attempted using Cd-EDTA in place of Cd^{2+} (Kothinti et al. 2010). Specific DNA binding of Zn_3-Sp1 was effectively inhibited by Cd-EDTA, even though EDTA has a large affinity for Cd^{2+} ($K_{eq} = 1.4 \times 10^{13}$, pH 7) (**reaction 1.23**) (Anderegg 1964):

$$n\ Cd\text{-EDTA} + Zn_3\text{-Sp1} \leftrightharpoons Cd_n\text{-Sp1'} + n\ Zn\text{-EDTA} + (3\text{-}n)\ Zn^{2+} \qquad (1.23)$$

From an energetics standpoint, the high affinity of EDTA for Zn^{2+} ($K_{eq} = 8.6 \times 10^{12}$, pH 7) balances the large stability of EDTA with Cd^{2+} in the overall reaction (Anderegg et al. 1964). As a result, the reaction is driven towards products due to the strongly favorable formation of Cd_n-Sp1' in a possible Cd-S_4 coordination. The metal exchange mechanism is complicated because the metal ions of both reactants are fully coordinated with ligands. Nevertheless, **reaction 1.23** is kinetically feasible.

In the absence of a GC_{site}, Cd^{2+} and a variety of ligands, including EDTA, readily inactivates Zn_3-Sp1 due to a loss protection from specific DNA binding (Kothinti et al. 2011). If Zn_3-Sp1 is present as Zn_3-Sp1•GC_{site} in a reaction mixture, **reaction 1.21, 1.22** or **1.23** take place slowly or not at all (Kothinti et al. 2010). It appears that the specific transcription factor-DNA complex is protected from reaction with a number of exogenous chemicals, both metal ions and ligands. The nature of the protection could be a kinetic barrier to bimolecular reaction. Or it might be thermodynamic because the formation of the adduct if an energetically favorable reaction that needs to be overcome for these other reactions to occur.

Mechanistic features of these reactions were probed. When the protein was associated with nonspecific DNA, the protective effect was not observed. In the cell, it is likely that a pool of non-GC_{site}-bound Zn_3-Sp1 is reactive with Cd^{2+} and the details of inhibition are determined by the dynamics of selective DNA-protein interactions (**reaction 1.24**-**1.25**):

$$Zn_3\text{-Sp1} + DNA_{non\text{-}specific} \leftrightharpoons Zn_3\text{-Sp1}\bullet DNA_{non\text{-}specific} \quad (1.24)$$

$$Zn_3\text{-Sp1}\bullet DNA_{non\text{-}specific} + GC_{site} \leftrightharpoons Zn_3\text{-Sp1}\bullet GC_{site} + DNA_{non\text{-}specific} \quad (1.25)$$

In this context, Cd^{2+} would react with Zn_3Sp1•$DNA_{non\text{-}specific}$. Thus, the concentration of active Zn_3-Sp1•GC_{site} is reduced by shifting **reaction 1.25** to the left.

There are nearly 1000 Zn-finger proteins with C_2H_2 ligands, with Zn_3-Sp1 being only one of them (Andreini et al. 2006). Considering the structural similarity of zinc binding sites in these Zn-finger proteins, it seems unlikely that Cd^{2+} only targets Zn_3-Sp1. **Reactions 1.24-1.25** may give insight into Cd^{2+} selectivity along with the possible exchange reaction of Zn_n-MT with Cd^{2+} bound to cadmium-substituted proteins (**reaction 1.15**). The steady-state localization of Cd^{2+} among cellular binding sites may be limited by the capacity of Zn_n-MT or apo-MT to compete for Cd^{2+} with these proteins. Nevertheless, it is clear that non-MT bound Cd^{2+} exists in cells. Some of it may represent Cd-substituted zinc finger proteins.

An experiment with primary mouse kidney cortical cells showed the kinetics of reaction and trafficking of Cd^{2+} as it enters cells over the course of 24 hours (Blumenthal et al. 1994). At time 0, Cd^{2+} begins entering the proteome and stimulates MT mRNA synthesis, starting at 1 hour. After 3 hours, Cd^{2+} begins to appear in newly synthesized MT. Throughout 24 hours of observation, the downregulation of glucose transport, beginning at 3 hours, is thought to be the result of a small pool of Cd^{2+} remaining bound to Proteome, despite the synthesis of Cd_n, $Zn_{(7-n)}$-MT. The toxicity of Cd^{2+} may be prevented by the pre-induction of Zn_7-MT, prior to exposure. Without a significant pool of endogenous MT, Cd^{2+} is partitioned into protein binding sites important for toxicity. These reactions are thought to be the direct cause of toxicity, recognizing that the cadmium-containing proteins can coexist with a growing pool of MT and may set into motion pathways that cannot be reversed by MT sequestering Cd^{2+} out of these proteins.

As knowledge of the chemistry underlying the cellular toxicity of Cd^{2+} continues to develop, there are important questions that remain: what are the identities of the proteins that bind Cd^{2+} even in the presence of metallothionein? Are these proteins normally Zn-proteins? How can such proteins be detected analytically? These questions stimulated the work in this thesis.

Fluorescence zinc sensors are compounds that undergo a change in fluorescence emission in the presence of Zn^{2+}. Such multi-dentate ligands have proven to be an attractive technique for *in vivo* monitoring of Zn^{2+} (Jiang et al. 2004). For example, sensors react with free zinc within the cell according to **reaction 1.26**:

$$Zn^{2+} + \text{sensor (S)} \leftrightharpoons \text{Zn-sensor (Zn-S)} \qquad (1.26)$$

Fluorescence changes can be monitored if the equilibrium constant (K_{eq}) of the reaction lies within the range of transient or free Zn^{2+} concentration so that some Zn-S forms and that the concentration of Zn-S complex emits enough fluorescence to be observable. Free Zn^{2+} is the

metal ion concentration that exists in the equilibria that intracellular Zn^{2+} establishes with small molecule ligands and adventitious Proteomic sites.

$$Zn^{2+} + L \leftrightharpoons Zn\text{-}L \text{ (L is Proteomic or small molecule ligands)} \quad (1.27)$$

The zinc sensor may bind and detect Zn^{2+} within this pool depending on the equilibrium constants of the sensor and these other molecules.

$$\sum Zn\text{-}L + S \leftrightharpoons Zn\text{-}S + \sum L \quad (1.28)$$

If the equilibrium constant of the zinc sensor is large enough, it may be able to chelate Zn^{2+} out of Zn-proteins.

$$\sum Zn\text{-Protein} + S \leftrightharpoons Zn\text{-}S + \sum Protein \quad (1.29)$$

One of the most commonly used zinc fluorophores is called TSQ or 6-methoxy-(8-p-toluenesulfonamido)quinoline. TSQ has a very selective character of sensing Zn^{2+} making it an excellent choice to use as a reporter for the Zn^{2+} trafficking pool. It binds in a 2:1 stoichiometric ratio with free Zn^{2+} producing a strongly fluorescent Zn^{2+} complex (Meeusen et al. 2011).

Previous experiments have shown that TSQ forms adducts with Zn-proteins and image a fraction of the Zn-Proteome and do not image free intracellular Zn^{2+} (Meeusen et al. 2011; Nowakowski et al. 2012; Nowakowski et al. 2015). Adducts form either because the Zn-coordination sphere can be expanded or because the Zn^{2+} binding sites of Zn-proteins are unsaturated with ligands (Fatema et al. 2015).

$$TSQ + Zn\text{-Proteome} \leftrightharpoons TSQ\text{-}Zn\text{-Proteome} \quad (1.30)$$

Considering the large swath of Zn-proteins that TSQ is able to bind to, it must be true that other metal binding ligands may also bind to the Zn-Proteome.

Thus far, reagents that modify the Zn-Proteome have been considered. Biologically active metal binding ligands (L_x) that compete with the Zn-Proteome for Zn^{2+} should also be added to that list.

$$\sum Zn\text{-}P + mL_x \leftrightharpoons mZn\text{-}L_x + \sum P \qquad (1.31)$$

N,N,N',N'-tetrakis(2-pyridylmethyl)-ethylenediamine (TPEN) has a stability constant with Zn^{2+} of $10^{15.6}$ at pH 7 and is a membrane-permeant Zn^{2+} chelating agent (Meeusen et al. 2012). TPEN presumably reduces the amount of reactive or trafficking Zn^{2+}, $\sum P \bullet Zn$, to mimic cellular zinc deficiency (Shin et al. 2011; Bernhardt et al. 2011). Approximately 30% of Proteomic Zn^{2+} is removed by TPEN in stoichiometric concentrations (**reaction 1.31**) but also binds a significant portion of adventitiously bound Zn^{2+} (Meeusen et al. 2012). With this finding and the discovery that fluorescence Zn^{2+} sensors like TSQ form ternary adducts with intracellular Zn proteins not free Zn^{2+}, led to the hypothesis that other xenobiotic metal binding ligands might also bind to the Zn-Proteome and exert some of their biological effects by this mechanism (Nowakoski et al. 2011).

$$\sum Zn\text{-}P + mL \leftrightharpoons \sum L\text{-}Zn\text{-}P \qquad (1.32)$$

TSQ binds about 20-25% of Proteomic-bound Zn^{2+}(Meeusen et al. 2011). It was hypothesized that TSQ could be used as an indicator that endogenous or exogenous Zn^{2+} binding ligands (L) form adducts with the Zn-Proteome.

$$TSQ\text{-}Zn\text{-}Proteome + L \leftrightharpoons L\text{-}Zn\text{-}Proteome + TSQ \qquad (1.33)$$

An indication that ligands bind to the Zn-Proteome is seen by the loss of the fluorescent species TSQ-Zn-Proteome and the productions of L-Zn-Proteome.

Some of the research described in this thesis addresses the hypothesis that ligand binding to members of the Zn-Proteome is wide-spread. This was also expanded to include reactions of adventitiously bound Zn^{2+}, Proteome•Zn with such ligands.

Part II: Reaction of LLC-PK_1 Cells with Cd^{2+}

1. Introduction

Experiments have shown that as cadmium enters mammals it becomes concentrated in the liver as Cd-MT (Cousins 1979). Once hepatic cells become overloaded with Cd-MT, they rupture and release Cd-MT to be absorbed by the kidney. Kidney cells degrade Cd-MT, eventually distributing cadmium throughout the Proteome. Dr. Namdarghanbari has shown the time-dependent distribution of Cd^{2+} and Zn^{2+} within cell supernatant once LLC-PK_1 cells uptake cadmium and the exchange of Cd^{2+} for Zn^{2+} occurs within the Zn-Proteome producing Cd-proteins and displacing Zn^{2+}, in a nearly 1:1 ratio (Namdarghanbari et al. 2011). The experiments below were an attempt to expand upon the trafficking of cadmium within LLC-PK1 proximal tubule cells including: the time dependent distribution and quanitation of Cd^{2+} and Zn^{2+} in cells exposed to Cd^{2+} and $Cd(pyrithione)_2$ and the Cd-Zn exchange reaction of the Zn-Proteome and LLC-PK1 cells.

2. Methods

2.1 Chemicals

All chemicals were purchased from either Fisher Scientific or Sigma-Aldrich unless noted and were highest purity available.

2.2 Cell Culture

All cell lines were purchased from the American Tissue Culture Company (ATCC) and cultured in similar fashion unless otherwise described. In general, cells were thawed from -80 °C and transferred into a 75 cm^3 culture flask with 15 mL of complete media and incubated at 37 °C in the presence of 5-6% CO_2 (see below). After 48-72 hours, old media was exchanged with 15

mL of fresh, complete media and 1 mL of fetal calf serum. When confluent, cells were detached from the flask via treatment with 1 mL of trypsin/EDTA solution and divided into either flasks or 100 cm^2 cell culture plates.

Proximal tubule cells from *Sus scofa* (pig) (LLC-PK_1, ATCC #CL-101) were grown in M199/HEPES modified media (Thermo Fisher Scientific) supplemented with 4% fetal calf serum (FCS). 50 mg/L streptomycin and 45-60 mg/L penicillin G were also added to media. LLC-PK_1 cells were grown in the presence of 5% CO_2. In detail, M199/HEPES modified media contains the following components: 25 mM HEPES, L-glutamine and Earle's salts.

2.3 Viability Assay

The toxicity of various reagents was determined in a dose and time dependent fashion. A 1 mL suspension of approximately 1 x 10^6 cells/mL in complete media was decanted and trypsinized. Cells were detached from plates using 400 µL of trypsin (1 mM) followed by 600 µL of horse serum. Trypan Blue assay was used to test for viability. Healthy cells expel Trypan Blue from their interior; the plasma membrane of dead cells becomes leaky and permits the diffusion of Trypan Blue into the cells. In the assay, 20 µL of cells (5 x 10^6/mL) were combined with 20 µL of Trypan Blue dye (0.08% solution). Then, 10 µL of cell suspension was pipetted onto the hemocytometer for cell counting. Four 1 mm^2 areas were counted and then averaged for the final cell count. Cells that have died are stained blue while viable cells were not stained. 100-300 cells per mm^2 are ideal counts. Cell viability is determined by the following equation:

% cell viability = $\frac{total\ viable\ cells\ (unstained)}{total\ cells\ (stained\ plus\ unstained)}\ X\ 100$.

Total amount of cells per culture plate is determined by:

n (Total number of cells counted) x 10^4 per mL x volume of trypsinized cells (mL)

n = the total number of dead and viable cells

The total volume of the four 1mm^2 areas is 1 x 10^{-4} mL.

2.4 Preparation of Cell Supernatant from Whole Cells

Cells were grown on 100 cm^2 culture plates until confluency was reached, typically around 5 days. Media was decanted and the plates were washed 3 times in cold choline phosphate buffered saline (4.7 g NaH_2PO_4, 1.0 g Na_2HPO_4, 32.2 g NaCl, and 25.0 g choline chloride in 3.8 L $_{dd}H_2O$). 1 mL of Dulbecco's phosphate buffered saline (DPBS, Sigma: potassium chloride 200 mg/L, potassium phosphate monobasic anhydrous 200 mg/L, sodium chloride 8 g/L, sodium phosphate dibasic anhydrous 1.15 g/L) was added to each plate and the cells were then gently lifted into suspension using a rubber cell scraper. Cells were transferred using a transfer pipette into a 50 mL centrifuge tube and spun at 680 x g for 4 min at room temperature. The DPBS solution was decanted, and the cell pellet was resuspended in another milliliter of DPBS per 10 plates of cells to which 20 µL of 25 units/ µL Benzonase (nuclease) and 10 µL of 80 mM Phenylmethanesulfonyl fluoride (protease inhibitor) were added. Cells were transferred to a cut off tube and spun again at 13,000 x g for 4 mins**.** The DPBS solution was decanted and the cell pellet was resuspended in 1 mL $_{dd}H_2O$ (18 MΩcm^{-1}). $_{dd}H_2O$ is hypotonic having decreased solute concentration facilitating a net movement of H_2O into the cell causing them to swell and making the sonication process more effective. A sonicator equipped with a flat tip was placed in an ice water bath for five minutes to chill the tip. The suspension was sonicated for 24 seconds at power five for 60 pulses. The sonicates were transferred to 15 mL Corex® tubes and the process was repeated until the all cell suspensions were lysed. The sonicates were then spun at 20,000 x RPM (41,657 x g) for 25 minutes at 4 °C using a Sorvall LYNX 4000 ultracentrifuge (Thermo Fisher Scientific). The resulting supernatant was further separated using chromatographic techniques described in **Part II section 2.5**.

2.5 Chromatography

2.5.1 Sephadex G-75 Gel Filtration Chromatography

For cell supernatant fractionation, Sephadex G-75 gel filtration chromatography (GE Healthcare) were used. Sephadex G-75 beads were hydrated using 20 mM Tris-Cl buffer pH 7.4 for 24 hours for construction of size exclusion columns. Beads were degassed in a sidearm flask via aspiration for at least one hour. Sephadex G-75 beads were poured into a 0.75 cm x 80 cm borosilicate glass column supported by a small amount of glass wool to aid with gravity packing of beads. Columns were eluted by gravity using one-liter round bottom buffer reservoirs connected to the top of the columns using Tygon tubing. Unless otherwise noted, columns were eluted using degassed 20 mM Tris-Cl pH 7.4 to limit the amount of sulfhydryl oxidation in the supernatant TCEP (500 µM) was added. Columns were poured again when the columns lost their seal and dried out or when the flow rate exceeded 1 drop every 20 seconds.

Typical chromatographic runs involved collecting 1.0 mL fractions, corresponding to 20 drops. For Sephadex G-75 separation, 50 one-mL fractions were collected with a total fractionation time of 1.5-3.5 hours. The void volume of the column consisted of the first 8 mL fractions. The high molecular weight (HMW) protein region of the chromatogram, corresponding to fractions 10-20, is the Proteomic pool with molecular sizes >10 kDa. Fractions 20-30 contained molecules with molecular weights around 6-10 kDa. Species with molecular weights lower than 6 kDa (low molecular weight), were found in fractions greater than 30.

2.5.2 HPLC DEAE Ion Exchange Chromatography

HPLC anion exchange chromatography was employed to separate cell supernatant from LLC-PK_1 cells into fractions containing sets of proteins for experiments described below. 5 mL Macro-Prep DEAE ion exchange cartridges were purchased from Bio-Rad. Elution of 5 column

volumes of 5 mM Tris-Cl pH 8.0 containing 1 M NaCl followed by an additional 5 column volumes with 5 mM Tris-Cl pH 8.0 containing no salt was used to generate the ion exchange matrix. A peristaltic pump loaded protein samples (50 mg/mL) onto the column at a rate of 1 mL/min. A stepwise gradient was used for elution of the column. In brief, two 50 mL Erlenmeyer flask were connected to the peristaltic pump using Tygon tubing which then fed the column. One flask containing 5 mM Tris-Cl pH 8.0, 0 mM NaCl and the other containing 500 mM NaCl. Using a constant flow rate of 1 mL/min, 5 mM Tris-Cl pH 8.0 a typical stepwise gradient was conducted using 50 mM NaCl increments from 0-500 mM NaCl. Diethylaminoethyl cellulose is positively charged packing in the column that binds negatively charged molecules, such as proteins. As more anion solution, NaCl, is added to the column, the column competes with the anion solution for the protein and is eluted from the column with increasing anion concentration. 1 mL fractions were collected from the column.

2.5.3 Separation of Proteins by Centrifugal Filtration

Cell supernatant was added to a 100 kDa centrifugal filter unit (Millipore) and spun at 10,000 RPM (6538 g) for 20 minutes in a microcentrifuge (Revolutionary Science) at room temperature. The resultant supernatant was taken for further analysis.

2.6 Fluorescence Spectrophotometry

All fluorescence measurements were performed using a Hitachi F-4500 Fluorescence Spectrophotometer. Most experiments utilized TSQ (refer to structure in **Part IV: figure 4.1**), a probe that fluoresces when it binds to Zn^{2+}. An excitation wavelength of 365 nm was employed to generate an emission spectrum primarily located between 400-600 nm. The photomultiplier voltage was generally set at 950 volts and emission wavelength scans were performed at 240 nm per minute.

Suspended cells, cell supernatant, or solutions were placed in the fluorometer and a background emission spectrum was taken to measure background light scattering (cells) and auto fluorescence. When cells were involved, they were then exposed to TSQ in the dark for at least 60 minutes. During this time, spectra were periodically taken. Cells were mixed frequently using a pipette to ensure a homogenous mixture of the suspension.

2.7 Use of the Fluorescent Probe, TSQ, to detect Zn-Proteins and Proteome•Zn

All spectrofluorimetry experiments were conducted with a Hitachi F4500 fluorescence spectrophotometer. To observe fluorescence emission from Zn^{2+} species interacting with TSQ, experiments were performed using a 365 nm excitation wavelength and scans of the fluorescence emission between 400 and 600 nm. Ternary complexes of TSQ with Zn-proteins display spectra with wavelength maxima near 475 nm; while $Zn(TSQ)_2$ has a wavelength maxima near 490 nm.

2.8 Zn^{2+} and Cd^{2+} determination by Flame Atomic Absorption Spectroscopy (AAS)

Zinc and cadmium concentrations were determined using a GBC 904 flame atomic absorption spectrophotometer. The absorbance was recorded using a zinc or cadmium cathode lamp and a deuterium lamp for background correction. Solutions were nebulized into mixture of 80:20 air-acetylene flame. Data were acquired in running mean mode with a sampling time of 1-3 seconds. Prior to the analysis of the samples, a calibration curve was constructed using standards containing 0.5, 1.0, and 2.0 ppm Zn^{2+} corresponding to 7.6, 15.2, and 30.4 µM Zn^{2+}. Cd^{2+} solutions were also 0.5, 1.0, and 2.0 ppm which corresponds to 4.4, 8.8, 17.8 µM Cd^{2+}. Samples that exhibited concentrations above 17.8 and 30 µM, Cd^{2+} and Zn^{2+}, respectively, were diluted and measured again.

3 Results and Discussion

3.1 Uptake and Distribution Reaction of Cd^{2+} and $Cd(Pyrithione)_2$ In Cells

Why use $Cd(PYR)_2$?

2-Mercaptopyridine-N-Oxide (Pyrithione) is a molecule that forms a 2:1 complex with most divalent transition metals (**figure 2.1**). When complexed with a divalent metal ion, the complex becomes neutral and exhibits hydrophobic character. Complexes of Pyrithione (PYR) with zinc and cadmium were employed in this study. Zinc binds to PYR with equilibrium constants of log $K_1 = 5.9$, log $K_2 = 5.4$, at pH 7.4. In contrast to the slow uptake of Cd into cells over the course of many hours, Pyrithione allows Cd^{2+} to pass through the hydrophobic interior of the plasma membrane and enter the cell and its organelles during 30 minutes of exposure. A defined amount of Cd^{2+} present in the cell at t = 30 mins, or t = 0 for the remainder of the experiment, then reacts with the components of the cell, such as the Proteome. As a result, the reaction of a defined amount of intracellular Cd^{2+} accumulated during 30 mins of exposure can be observed over time.

When comparing $Cd(PYR)_2$ and Cd^{2+} ion, Cd^{2+} is taken up much more slowly by cells over time. Moreover, in the case of Cd^{2+}, the exposure is continuous and increasing amounts of Cd^{2+} appear in the cell over time while previously internalized Cd^{2+} is distributing itself among cellular components such as the Proteome. Thus, for example, metallothionein is synthesized to react with incoming Cd^{2+} at the same time as it being absorbed through the cell membrane and also interaction with the Proteome. Thus, the reactions that Cd^{2+} undergoes are complicated.

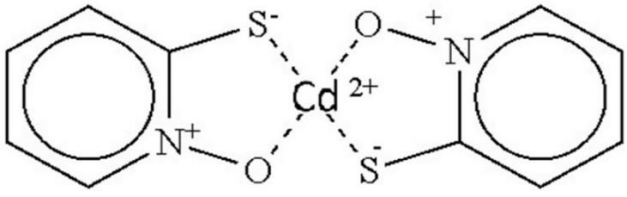

Figure 2.1

Pyrithione forms a 2:1 complex with Cd^{2+} at pH 7.4

3.1.1 Toxicity of Cd^{2+} vs. $Cd(Pyrithione)_2$

Toxicity studies were done in LLC-PK_1 cells to compare Cd^{2+} with that of Cd^{2+} in the presence of Pyrithione. Exposing cells to Cd^{2+} gradually moves the metal ion into cells over a 24-hour period. In contrast, $Cd(Pyrithione)_2$ rapidly delivers a comparatively large bolus of Cd^{2+} into the interior of the cells within 30 minutes, as shown below. Three plates of cells were incubated with Cd^{2+}, Pyrithione and $Cd(PYR)_2$ (3 µM PYR) of varying concentrations to see the limit of concentration. 0, 10, 25, 50, 100, 200 µM Cd^{2+}; 25, 50, 100, 200 µM Pyrithione; and 1.5, 7.5, 15, 30, 60 and 120 µM Cd^{2+} + 3 µM PYR were used. Cd^{2+}, Pyrithione and Cd^{2+} + Pyrithione were incubated in M199 media that does not contain any Zn^{2+}.

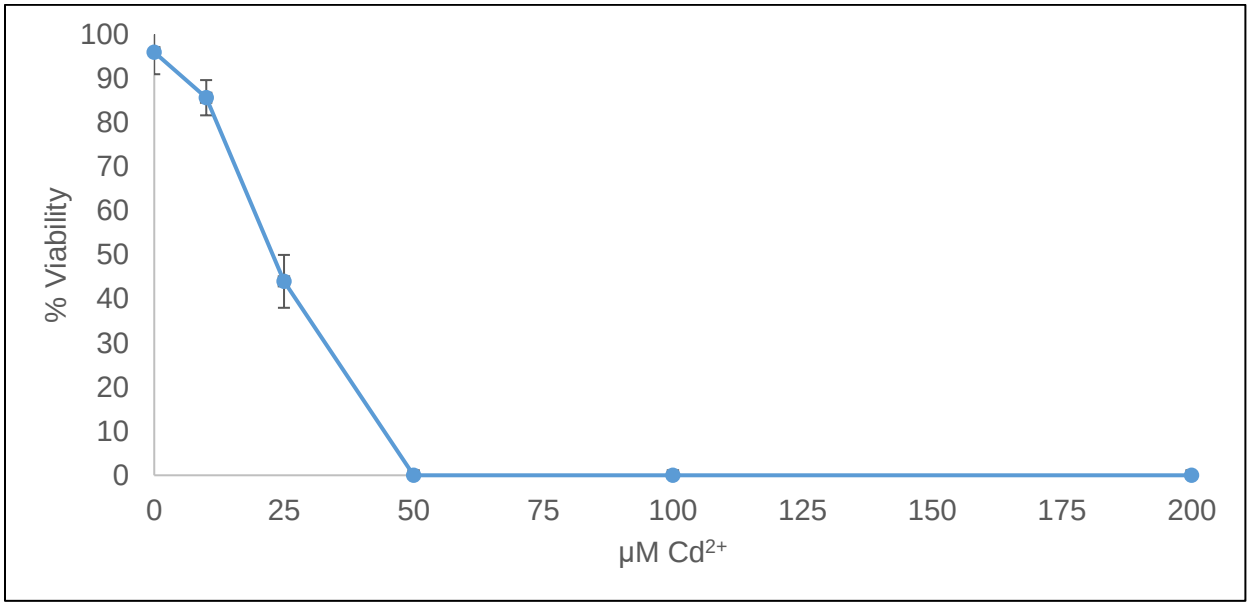

Figure 2.2
Toxicity experiment of Cd^{2+} using Trypan Blue assay. 50, 100, 200 µM Cd^{2+} plates were cell debris for majority of the cells counted. (n = 3, 1.7 x 10^7 cells)

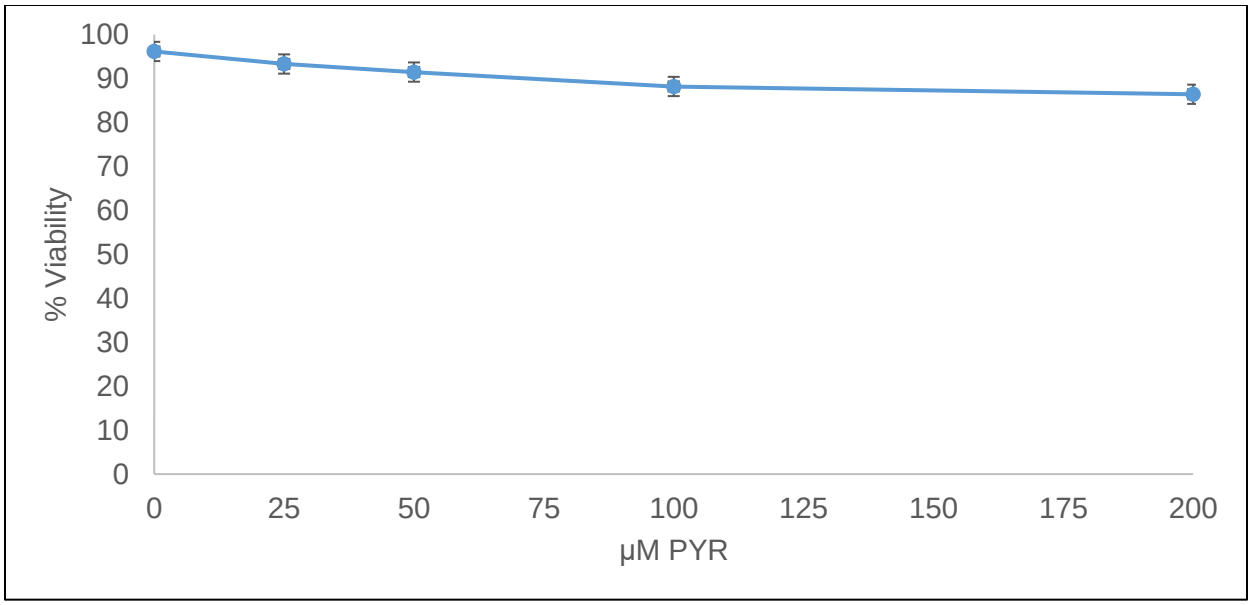

Figure 2.3

Toxicity experiment of Pyrithione using Trypan blue assay. 25, 50, 100, 200 µM Pyrithione were incubated with three plates for 24 hours. (n = 3, 1.7 x 10^7 cells)

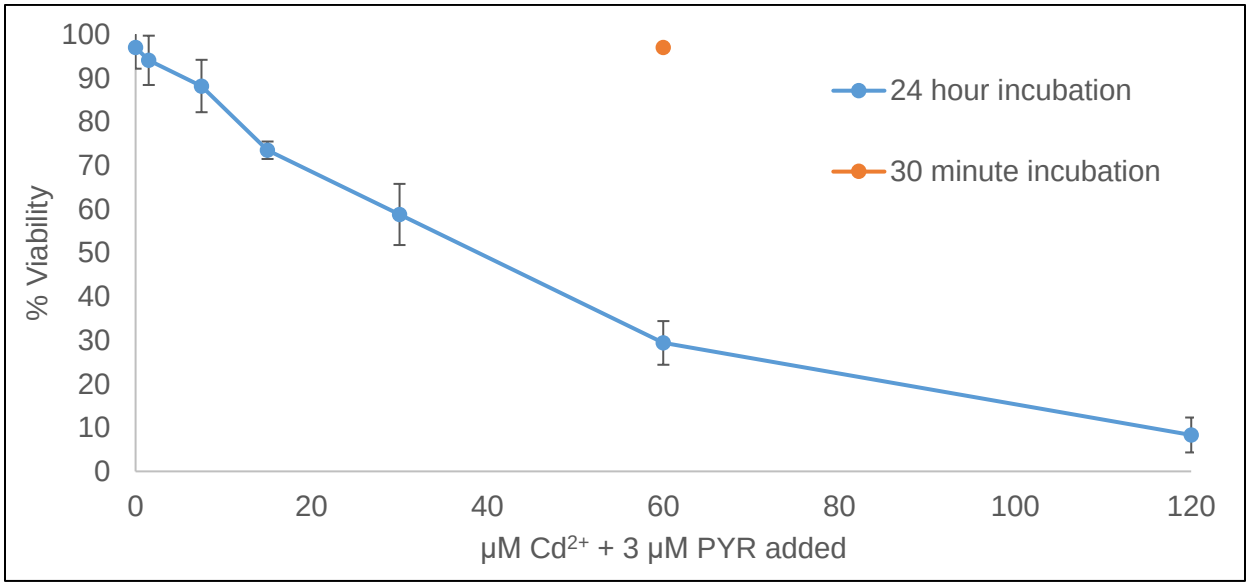

Figure 2.4

Toxicity experiment of $Cd(PYR)_2$ using Trypan blue assay. 0, 1.5, 7.5, 15, 30, 60 and 120 µM Cd^{2+} + 3 µM PYR were incubated with three plates for 24 hours. (n = 3, 1.9 x 10^7 cells)

To study the toxicity of Cd^{2+}, LLC-PK_1 cells were incubated with varying concentrations of Cd^{2+} for 24 hours of incubation. The toxicity experiments show that increasing amounts of Cd^{2+}

drastically decrease viability over 24 hours (**figure 2.2**). Thus, 50-200 μM Cd^{2+} either ruptured the cells or detached them from the plates, as they were not able to be counted for analysis.

Pyrithione did not significantly decrease viability of LLC-PK_1 cells despite incubation for 24 hours with increasing concentrations. Even at 200 μM Pyrithione, the cell viability was 87% after for 1.7 x 10^7 cells (**figure 2.3**).

The toxicity pattern of Cd^{2+} plus PYR differed markedly from that of Cd^{2+} (**figure 2.3**). High concentrations of Cd^{2+} did not cause complete loss of viability when complexed with PYR (**figure 2.4**). 50 μM Cd^{2+} caused completed loss of viability (**figure 2.2**); whereas, 60 μM Cd^{2+} plus 3 μM PYR caused a significant loss of viability (71%) but the remaining cells were still viable (**figure 2.4**). It is clear that when Cd^{2+} complexes with PYR, cell viability is greater than with Cd^{2+} in solution.

For Cd^{2+} experiments, 1.2% of total Cd^{2+} applied is absorbed into cells within 30 minutes of exposure. When 60 μM Cd^{2+} is incubated with 3 μM Pyrithione, 82.5% of total Cd^{2+} applied is absorbed into cells for the same exposure time. A minute amount of Zn^{2+} is detected in the media, around 0.09% (0.06 nmol) after 30 minutes of exposure to 60 μM $Cd(PYR)_2$ (3 μM PYR) and 1.8% (1.19 nmol) after 24 hours of exposure to 4 μM Cd^{2+} measured by Flame Atomic Absorption. The fact that more than 80% of the Cd^{2+} in the medium reached the cell interior in the presence of a concentration of PYR that can maximally form only 1.5 μM $Cd(PYR)_2$ at any one time, demonstrates that PYR acts as a shuttle, repeatedly conducting Cd^{2+} into the cell and returning to the exterior as the free ligand, PYR.

It was surprising that Cd^{2+} plus PYR was less toxic than Cd^{2+} alone, considering that so much more Cd^{2+} entered cells in total and very quickly upon treatment of cells with Cd^{2+} in the presence of PYR. It was beyond the scope of this thesis research to investigate the origin of this unexpected different. But it would be important to study in the future.

3.1.2 Time dependent distribution of Cd^{2+} and Zn^{2+} in cells exposed to $Cd(Pyrithione)_2$

Based on the work of Dr. Jeffrey Meeusen (data not published), the initial experiment consisted of mixing 3 µM Pyrithione with 60 µM Cd^{2+} for 30 minutes. The complex was incubated with cells in DPBS for 30 minutes. This concentration of PYR was chosen because it did not cause loss of cell viability by itself. The larger concentration of Cd^{2+} did not cause toxicity when complexed with PYR. The $Cd(PYR)_2$ uptake reaction was stopped by washing the cells with DPBS then adding media and FCS and allowing the cells to grow for a set amount of time before harvesting the cells. Seven timepoints were chosen for analysis: Control (t = 0), 30 minutes, 1, 2, 3, 6, and 24 hours.

The following reaction scheme was developed as the hypothesis underlying this experiment:

Uptake and Reaction of Cd^{2+} In cells

$$Cd(PYR)_{2\ out} \leftrightharpoons Cd(PYR)_{2\ in} \quad \text{(Cell membrane)} \qquad (2.1)$$

$$Cd(PYR)_2 + Proteome \leftrightharpoons Proteome{\bullet}Cd + 2\ PYR \qquad (2.2)$$

$$Proteome{\bullet}Cd + Zn\text{-proteins} \leftrightharpoons Cd\text{-proteins} + Proteome{\bullet}Zn \qquad (2.3)$$

In **reaction 2.1**, Cd^{2+} binds to Pyrithione (1:2) and is shuttled across the cell membrane as a neutral molecule where it reacts with Proteomic sites and binds to the Proteome (**reaction 2.2**). Zn^{2+} proteins then react with cadmium-bound Proteome, replacing Zn^{2+} in the protein with Cd^{2+} as the two metal ions exchange with one another (**reaction 2.3**). Displaced Zn^{2+} can then bind to Proteomic sites.

The following series of Sephadex G-75 chromatographic profiles displays the time dependent distribution of Zn^{2+} and Cd^{2+} following the initial incubation of cells with $Cd(PYR)_2$ (**figures 2.6-2.12**). Atomic absorption spectrophotometric analysis of fractions separated by Sephadex G-75

gel filtration revealed that at t = 0, all the measurable Zn^{2+} (66.2 nmol) was bound to macromolecular species (I) (**figure 2.5**). No Zn^{2+} was detected in the low molecular weight region (III). Nor was any metal ion found in the metallothionein region, ~10 kDa in apparent molecular weight, centered at fraction 30 (II). No Cd^{2+} was observed. Total Zn^{2+} per 10^8 cells was (66.2 nmol), typical of many measurements on control cells.

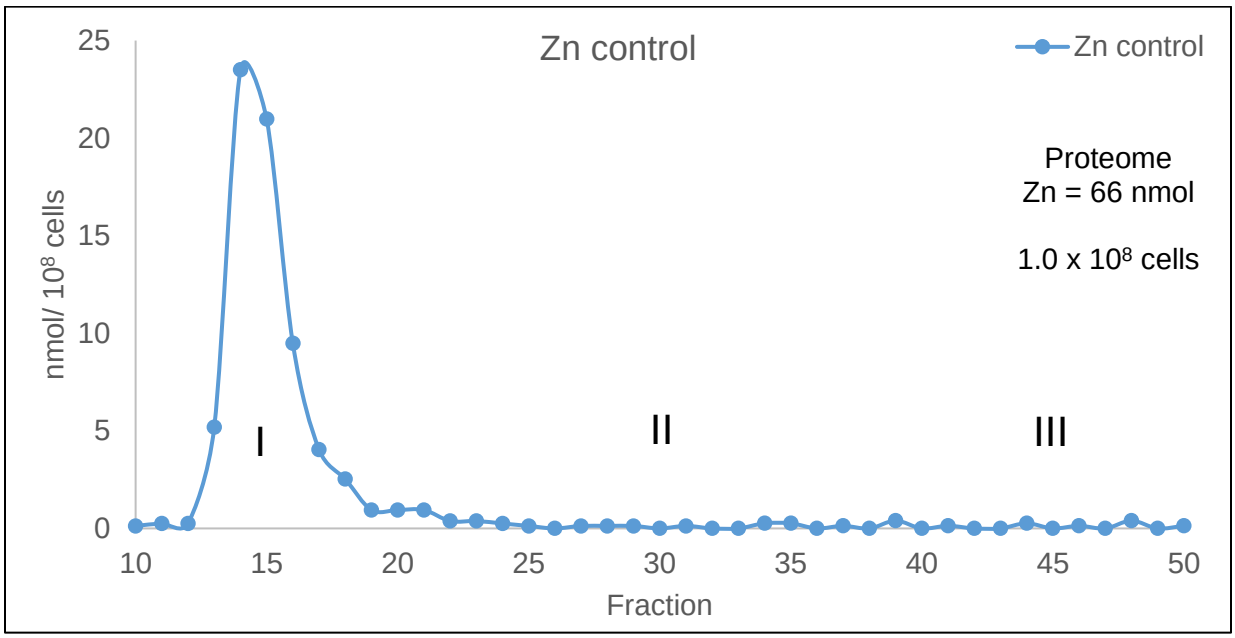

Figure 2.5

Sephadex G-75 chromatography of control LLC-PK_1 cells. No cadmium added. 20 plates of confluent LLC-PK_1 cells were harvested (1.0 x 10^8 cells).

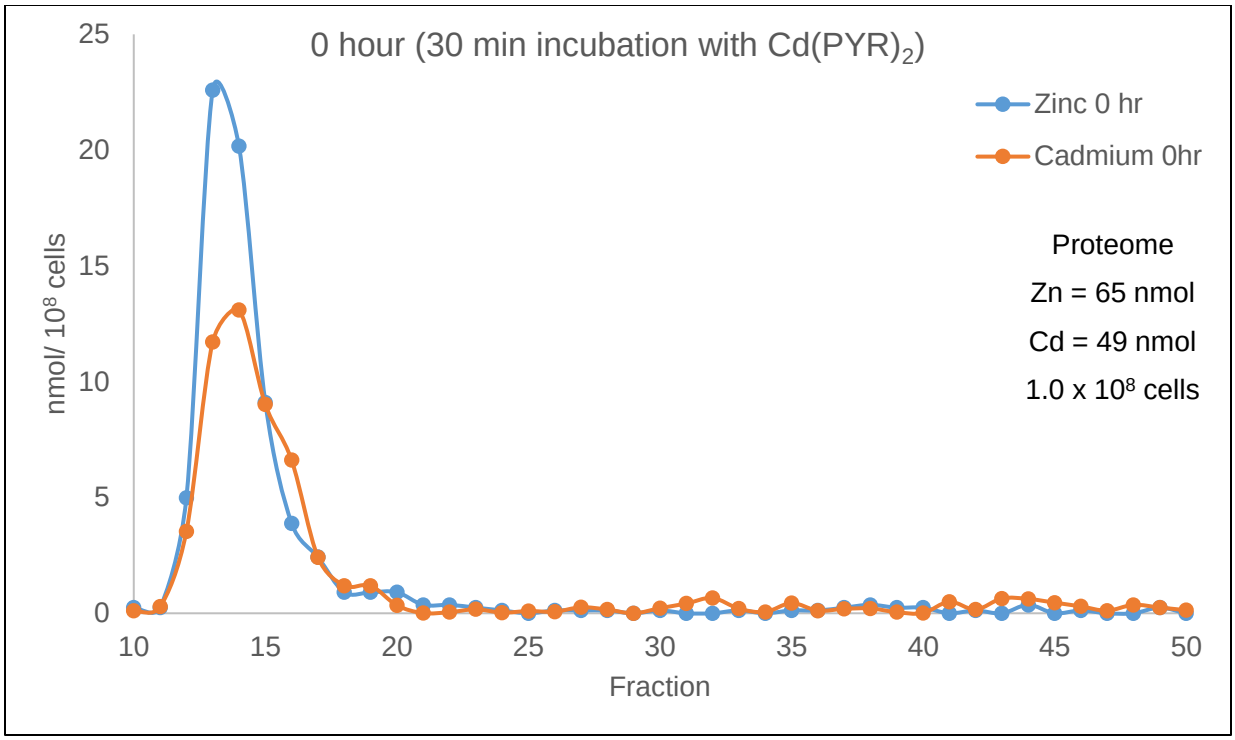

Figure 2.6

Sephadex G-75 filtration of 20 plates of cells treated with Cd^{2+} plus PYR and incubated for 30 minutes. 60 µM Cd^{2+} plus 3 µM PYR exposure for 30 minutes.

At t = 30 minutes, 82.5% of the total Cd^{2+} in the extracellular medium had reacted and become bound to high molecular weight species, basically proteins within the cell Proteome (**figure 2.6**). It did so without changing the total concentration of Proteomic Zn^{2+}. No evidence for Cd-MT was obtained, consistent with the previously established conclusion that neither detectable Zn- nor apo-MT exists in control LLC-PK_1 cells. The latter was inferred because had apo-MT been present, Cd^{2+} entering cells would have been preferentially bound to it (Namdarghanbari et al. 2015). Similar results were obtained with the 1-hour sample of Cd-treated cells with the possible exception that Proteomic Zn^{2+} had marginally declined (**figure 2.7**)

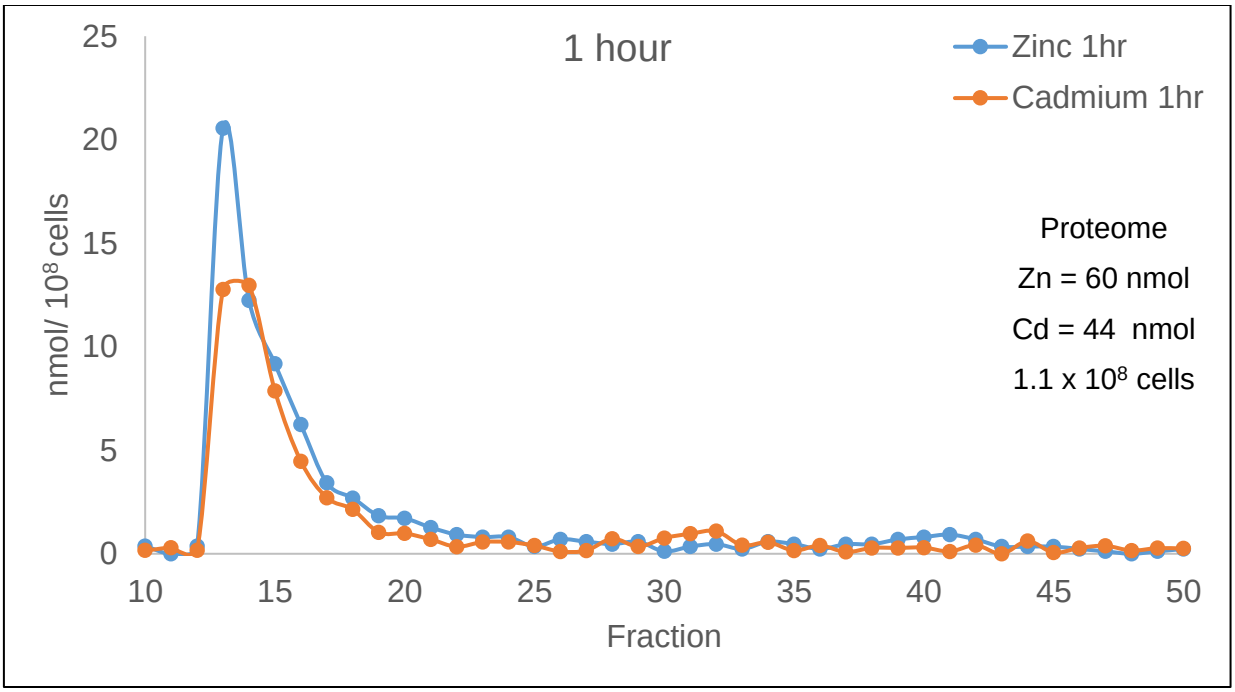

Figure 2.7

Sephadex G-75 filtration of 20 plates of cells treated with Cd^{2+} plus PYR and incubated for 1 hour. 60 µM Cd^{2+} plus 3 µM PYR exposure for 30 min followed by 1-hour incubation in fresh media

After 2 hours of incubation, $Cd(PYR)_2$ exposed cells retained their original content of Zn^{2+} and Cd^{2+}. However, this time point revealed that some (14.2%) of the Cd^{2+} had shifted from the proteome to the MT region, centered at fraction 30, of the chromatogram (**figure 2.8**). Evidently, *de novo* MT protein synthesis had been induced by the presence of Cd^{2+} and the newly synthesized protein was able to compete with the Proteome for binding some of the cellular Cd^{2+}. In addition, MT acquired about an equivalent amount of Zn^{2+} to make a pool of mixed metal, Cd,Zn-MT.

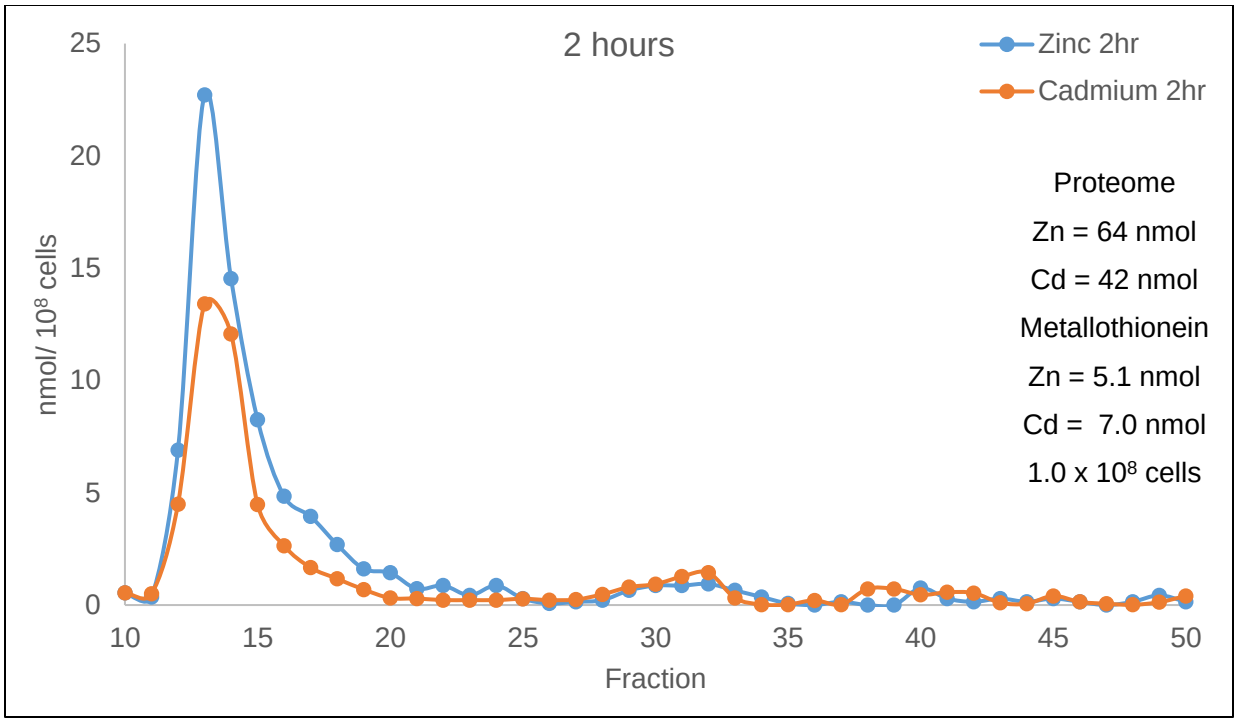

Figure 2.8

Sephadex G-75 filtration of 20 plates of cells treated with Cd^{2+} plus PYR and incubated for 2 hours. 60 µM Cd^{2+} plus 3 µM PYR exposure for 30 min followed by 2 hours incubation in fresh media

After 3 hours of incubation, 16.3% of the Cd^{2+} had shifted into the MT region from the Proteome region of the chromatogram (**figure 2.9**) while maintaining the original content of Zn^{2+}.

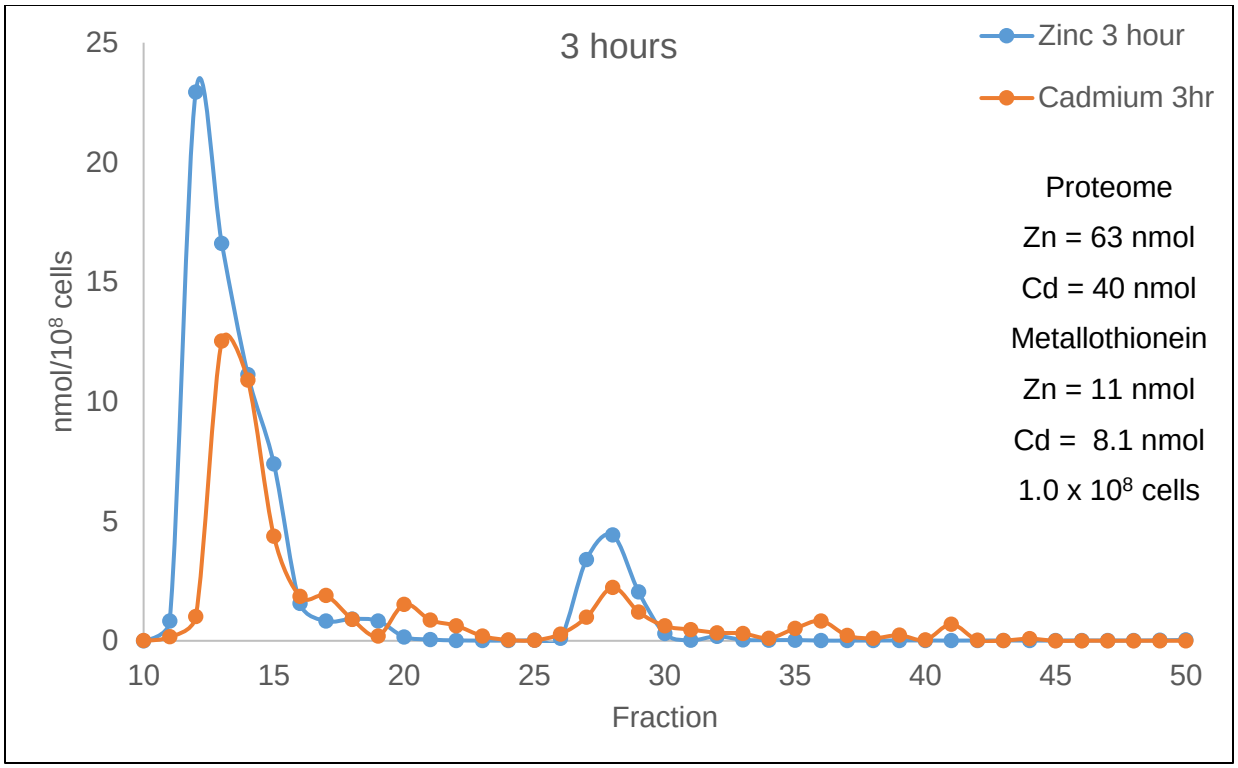

Figure 2.9

Sephadex G-75 filtration of 20 plates of cells treated with Cd^{2+} plus PYR and incubated for 3 hours. 60 µM Cd^{2+} plus 3 µM PYR exposure for 30 min followed by 3 hours incubation in fresh media

After six hours, 66% of Proteome-bound Cd^{2+} was now bound to Metallothionein. Keeping pace with the Cd^{2+} content of MT, a nearly equal amount of Zn^{2+} was also sequestered into the protein (**figure 2.10**). Interestingly, the content of Proteomic Zn^{2+} remained essentially unchanged in comparison with the t = 0 control during the 6 hours of intracellular rearrangement of Cd^{2+}. Evidently, the zinc content of the MT pool must have originated from the extracellular medium.

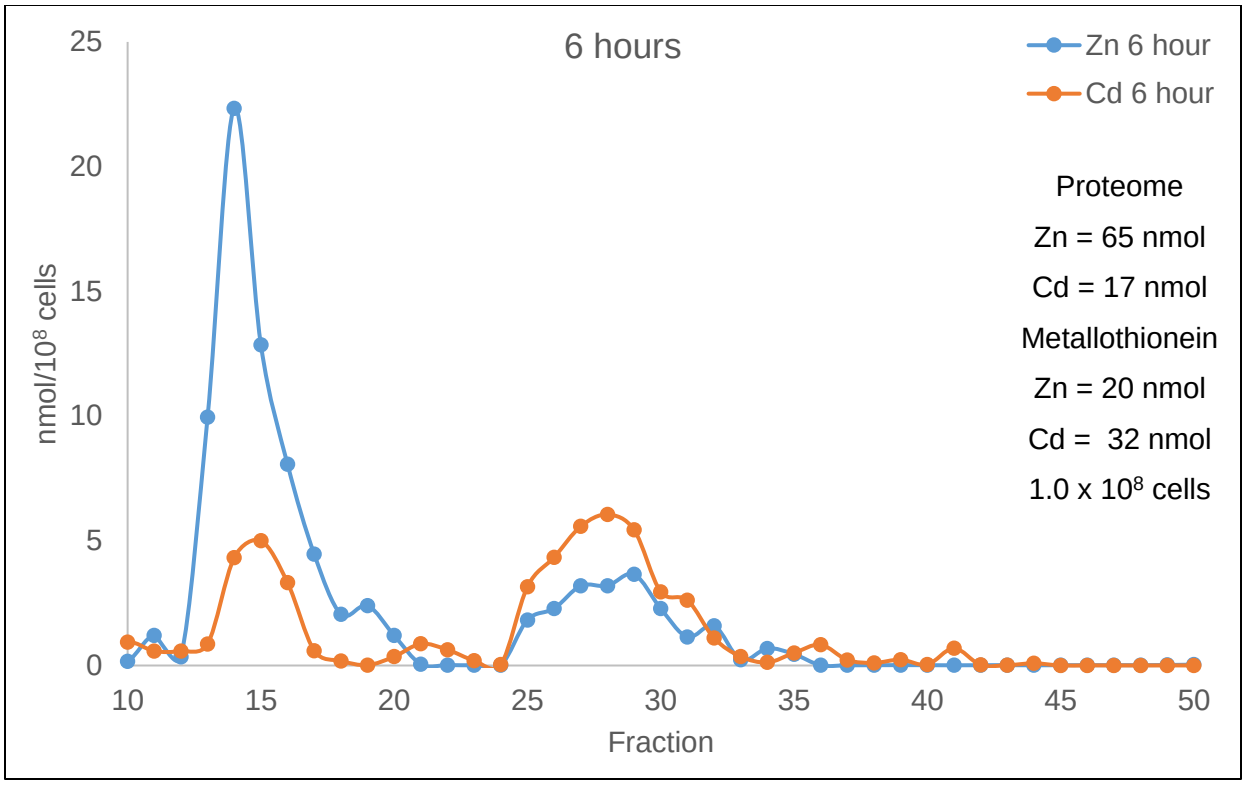

Figure 2.10

Sephadex G-75 filtration of 20 plates of cells treated with Cd^{2+} plus PYR and incubated for 6 hours. 60 µM Cd^{2+} plus 3 µM PYR exposure for 30 min followed by 6 hours incubation in fresh media

Most of the Cd^{2+}, 84%, has been sequestered out of the Proteome by Metallothionein after 24 hours. *De novo* synthesis of metallothionein protein coordinates some extracellular Zn^{2+} and sequesters Cd^{2+} out of the Proteome during the incubation 24-hour period (**figure 2.11**).

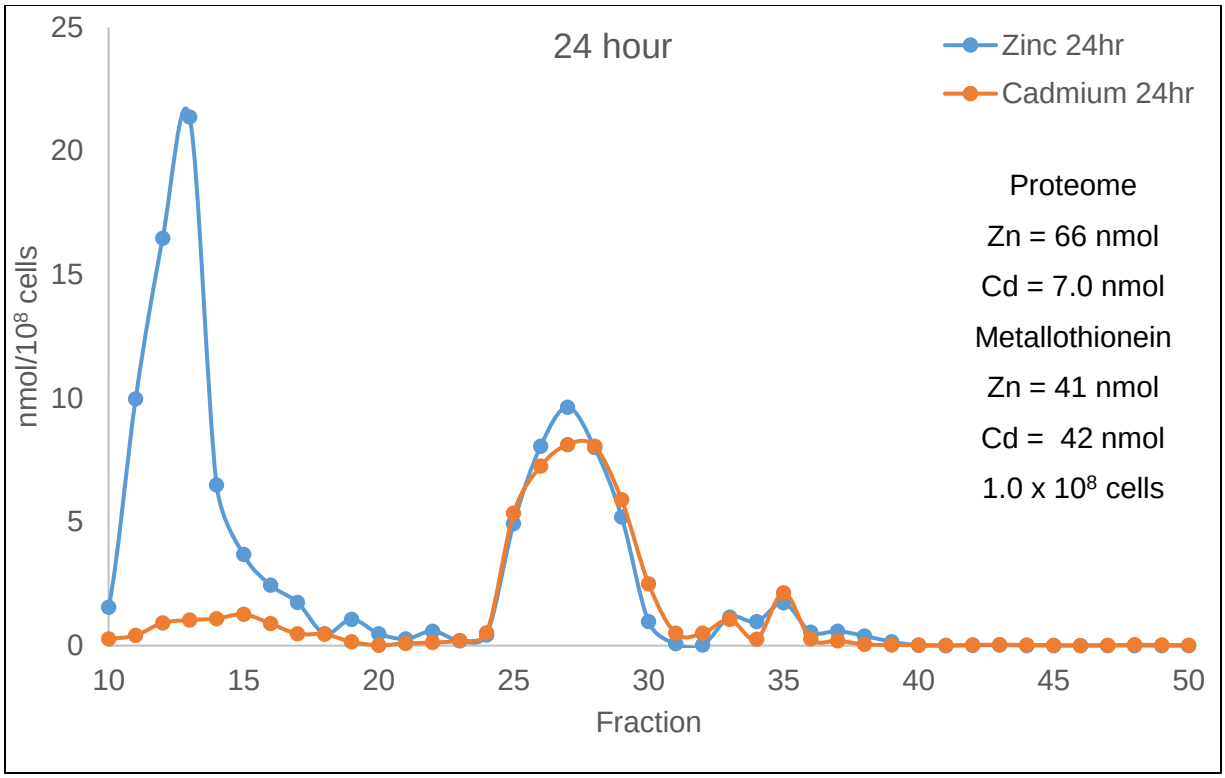

Figure 2.11

Sephadex G-75 filtration of 20 plates of cells treated with Cd^{2+} plus PYR and incubated for 24 hours. 60 µM Cd^{2+} plus 3 µM PYR exposure for 30 min followed by 24 hours incubation in fresh media

The following reactions are hypothesized to explain the evolving speciation of Cd over time:

Uptake and Reaction of Cd^{2+} In cells	$Cd(PYR)_{2\ out} \leftrightharpoons Cd(PYR)_{2\ in}$ (Cellular Membrane)	(2.4)
	$Cd(PYR)_2$ + Proteome ⇋ Proteome•Cd + 2 PYR	(2.5)
Induction of Metallothionein following Cd^{2+} uptake and activation of MTF-1	Proteome•Cd + Zn-proteins ⇋ Cd-proteins + Proteome•Zn	(2.6)
	6 Proteome•Zn + apo-MTF-1 ⇋ Proteome + Zn_6-MTF-$1_{CYTOSOL}$	(2.7)
	Zn_6-MTF-$1_{CYTOSOL}$ ⇋ Zn_6-MTF-$1_{NUCLEUS}$	(2.8)
	Zn_6-MTF-$1_{NUCLEUS}$ + MRE ⇋ Zn_6-MTF-$1_{NUCLEUS}$ • MRE	(2.9)
	Zn_6-MTF-$1_{NUCLEUS}$ • MRE ⇋ MT mRNA transcription and protein synthesis of apo-MT	(2.10)
	apo-MT + Cd-proteins ⇋ Cd_7-MT + apo-proteins	(2.11)
Exchange of Cd^{2+} and Zn^{2+} Between proteins and MT	apo-MT + Proteome•Zn ⇋ Zn_7-MT + Proteome	(2.12)
	(7-m) Zn_7-MT + m Cd_7-MT ⇋ Cd_m, $Zn_{(7-m)}$-MT	(2.13)
	Proteome•Zn + apo-proteins ⇋ Zn-proteins + Proteome	(2.14)
	Cd_m , $Zn_{(7-m)}$ -MT + (7-m) apo-proteins ⇋ Zn-proteins + Cd_m-MT	(2.15)

The membrane-permeant Cd-Pyrithione complex was used to introduce Cd^{2+} into LLC-PK_1 cells at time zero. $Cd(PYR)_2$ crosses the cell membrane and reacts with Proteomic sites (**reaction 2.4-2.5**). As illustrated in **figure 2.6,** Cd^{2+}, hypothetically, distributes itself into Zn-proteins and nonselective Proteomic sites within the Proteome (**reaction 2.5**). Cd_n-MT was not observed at time zero, consistent with LLC-PK_1 cells having a very low concentration of MT. Proteome•Cd undergoes reaction with Zinc proteins (Namdarghanbari et al. 2014). Zinc is displaced by cadmium in these proteins and the released zinc becomes bound to Proteomic sites, completing the exchange process (**reaction 2.6**) (Petering et al. 2017). Proteome-bound zinc reacts with apo-Metal Transcription Factor-1 (MTF-1) and becomes bound to MTF-1 in the cytosol (**reaction 2.7**) (Petering et al. 2017). Zn_6-MTF-1 migrates from the cytosol into the nucleus to react with the Metal Response Elements (MRE) of the metallothionein gene promoters (**reactions 2.8-2.9**) (Radtke et al. 1993). The binding to MRE stimulates transcription of apo-

Metallothionein (MT) mRNA (**reaction 2.10**). Apo-MT can react with cadmium proteins to form Cd_7-MT or with Proteome•Zn to become Zn_7-MT (**reactions 2.11-2.12**) (Namdarghanbari et al. 2014). Alternatively, Zn_7-MT reacts with cadmium proteins to create apo-proteins and mixed metal Cd/Zn-MT (**reaction 2.13**) (Namdarghanbari et al. 2014). In addition, it is hypothesized that Proteome•Zn and Cd/Zn-MT can react with apo-proteins to regenerate zinc proteins (**reaction 2.14** -**2.15**) (Petering et al. 2017). This experiment demonstrates that displacement of Zn^{2+} from Zn-MT does not need to occur for MT synthesis to be induced by Cd^{2+} (Zhang et al. 2003).

With a high affinity for Cd^{2+}, due to its cysteinyl sulfhydryl group ligands, apo-MTF-1 would seem to be a preferred site of reaction with Cd^{2+} entering cells. Yet, MTF-1 seems to initially escape this reaction, adding to the complexity of this model.

3.1.3 Time dependent distribution of Cd^{2+} and Zn^{2+} in cells exposed to Cd^{2+}

Cells that have been incubated with Cd^{2+} react differently than those incubated with $Cd(PYR)_2$. Cadmium, being a charged ion, has a difficulty passing through the cell membrane. Thus, it is hypothesized that less Cd^{2+} will enter cells exposed for 24 hours, than cells treated with $Cd(PYR)_2$ for 30 minutes. As an example, 4 µM Cd^{2+} was incubated for 30 minutes, 6 hours, 12 hours and 24 hours with LLC-PK_1 cells (5 x 10^7 cells). Each population of cells was harvested as above, and its supernatant separated using Sephadex G-75 gel filtration chromatography. The results are shown below.

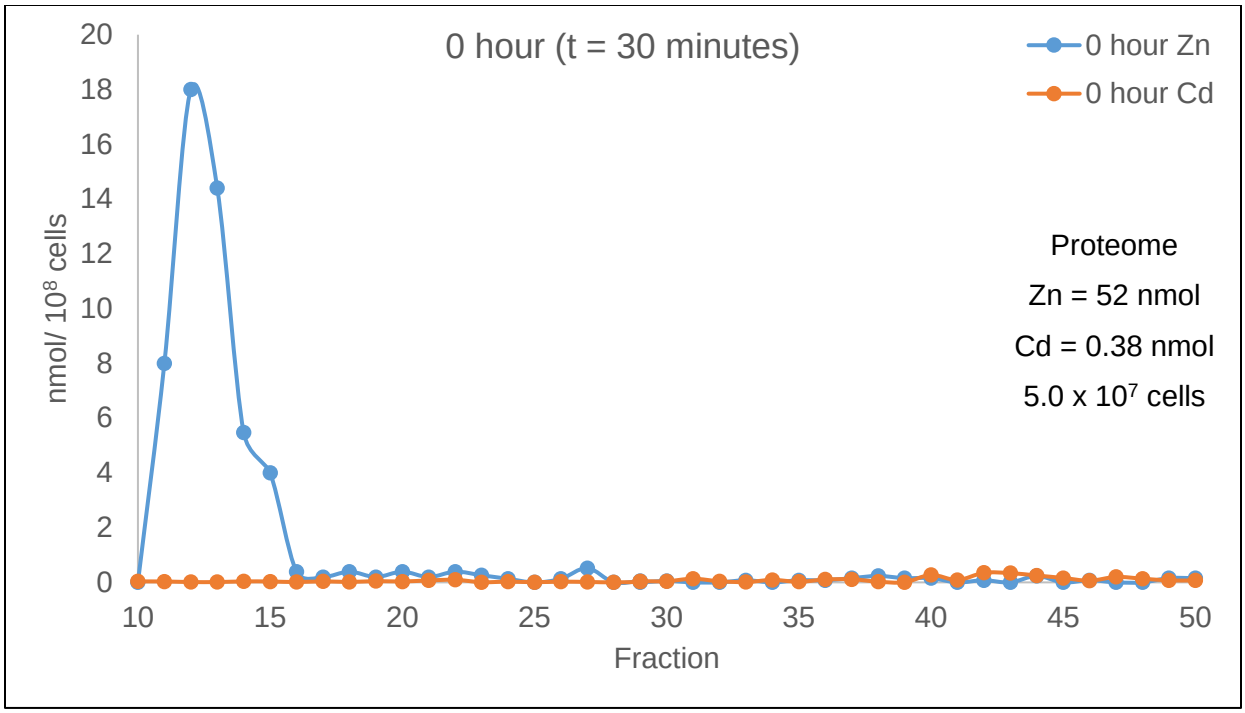

Figure 2.12

Sephadex G-75 chromatography of cells treated with 4 μM Cd for 30 minutes. LLC-PK$_1$ cells were incubated with 4 μM Cd^{2+} for 30 minutes before being harvested.

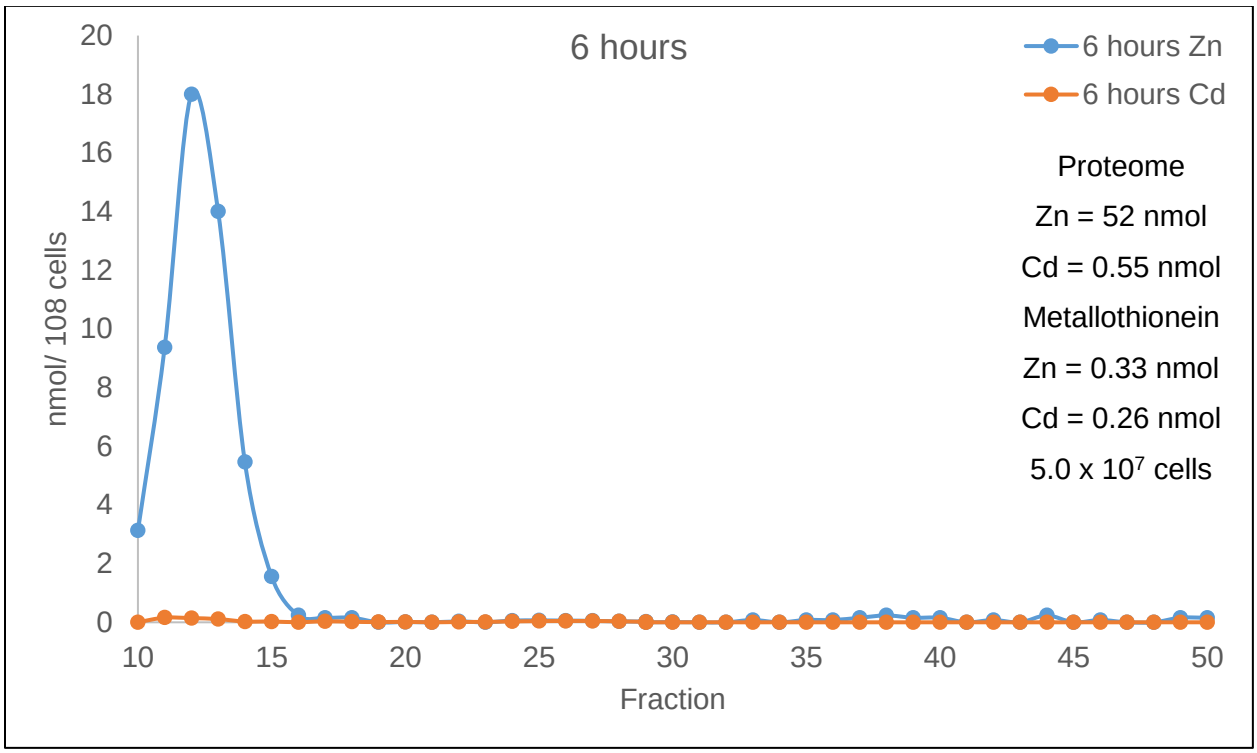

Figure 2.13

Sephadex G-75 chromatography of supernatant from cells incubated for 6 hours with 4 μM Cd^{2+}.

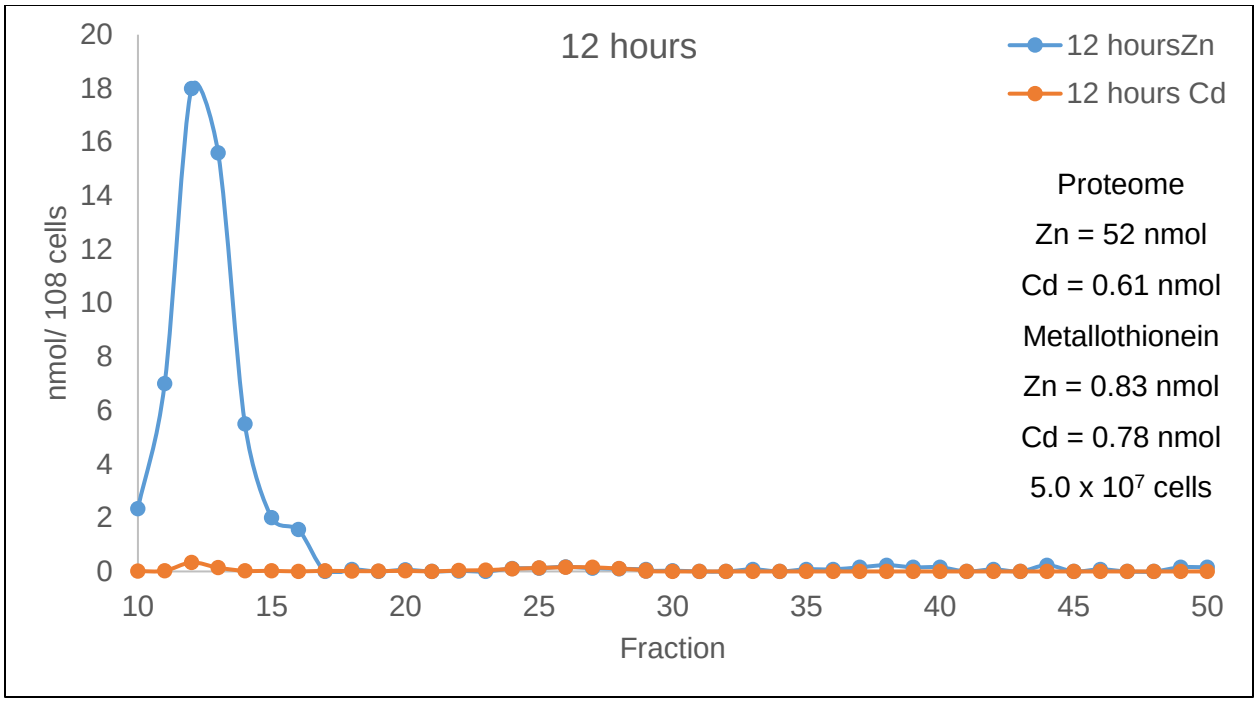

Figure 2.14

Sephadex G-75 chromatography of supernatant from cells incubated for 12 hours with 4 μM Cd^{2+}.

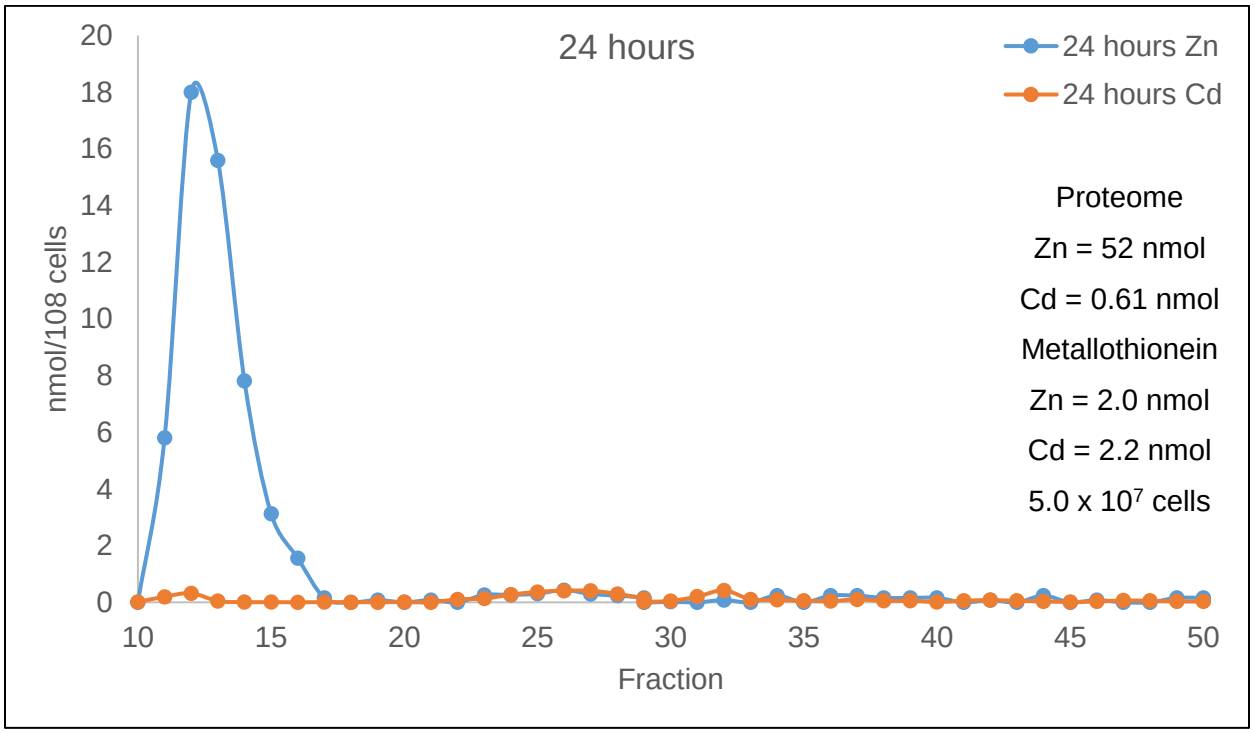

Figure 2.15

Sephadex G-75 chromatography of supernatant from cells incubated for 24 hours with 4 μM Cd^{2+}.

After 24 hours of incubation with 4 μM Cd^{2+}, Metallothionein has sequestered the majority (78.6%) of cadmium that was transported through the outer membrane into the cell interior (**figure 2.15**). The final distribution reflects the progressive uptake of Cd^{2+} followed by its partition into Proteomic binding sites and MT. One could hypothesize that the observed speciation results from reactions analogous to **reaction 2.4**-**2.15** above. Alternatively, once the induction of MT synthesis has occurred, MT may directly compete with Proteomic sites (**reaction 2.5**) for incoming Cd^{2+}:

$$Cd_{intracellular} + \text{apo-MT} \leftrightharpoons \text{Cd-MT} \qquad (2.16)$$

	HMW		MT	
$Cd(PYR)_2$	Zn	Cd	Zn	Cd
CTRL	66	0	0	0
30 mins	65	50	0	0
1	60	44	0	0
2	64	42	5.1	7.0
3	63	40	11	8.1
6	65	17	21	32
24	66	7.0	41	42

Cd^{2+}	HMW		MT	
	Zn	Cd	Zn	Cd
30 mins	52	0.38	0	0
6	52	0.55	0.33	0.26
12	52	0.61	0.83	0.78
24	52	0.61	2.0	2.2

Table 2.1

Metal totals (nmol) for incubation of LLC-PK_1 cells for varying times with $Cd(PYR)_2$ and Cd^{2+}

Cadmium enters through the cell membrane and as it reacts with Proteome, metallothionein sequesters it out. Metallothionein synthesis begins around 2 hours after Cd^{2+} enters the cell. In both experiments, MT was able to sequester 78-82% of the total Cd^{2+} that entered the cell over 24 hours. Cd^{2+} uptake is a much slower process without the use of PYR as a shuttle across the cell membrane. 24 hours of incubation with 4 μM Cd^{2+} resulted in 35% uptake by LLC-PK_1 cells; which is in stark contrast to 83% uptake when incubating with 60 μM $Cd(PYR)_2$ for 30 minutes. Although an average of 80% of Cd^{2+} was sequestered out of the Proteome by MT, there remains ~20% of Cd^{2+} bound. Clearly, not all Cd^{2+} sites participate in the reactions with MT (Namdarghanbari et al. 2011). The presence of non-MT bound Cd^{2+} could explain how the

mRNAs for SGLT 1 and 2 were substantially reduced and the downregulation of Zn_3-Sp1 transcription factor activity continues, despite the synthesis of MT as described by **reaction 1.20-1.24** (Tabatabai et al. 2001; Kothinti et al. 2010).

The puzzle that emerges from these experiments is that exposure to a comparatively small concentrations of over 24 h Cd^{2+} is highly toxic; whereas, treatment with a much larger concentration of Cd^{2+} plus PYR for 30 min is not. In the first experiment, little Cd^{2+} reaches the interior of the cell over time. Arguably, most of it is intercepted by and binds to metallothionein before it can react with other sites. Yet, the residual non-MT bound cadmium is deleterious to the cells. In the second case, a large concentration of Cd^{2+} is deposited in the cell at time zero, where it binds to the Proteomic fraction. Only later is it sequestered from this pool by MT after its induction. But these cells are not impacted by the rapid introduction of the large bolus of Cd^{2+}. Studying the origin of these divergent responses was beyond the scope of this these. At present, we do not understand the basis for the different behavior of these two populations of Cd-exposed cells.

3.2 Reaction of Proteome with $Cd(PYR)_2$: Cd-Zn • Proteome Exchange

To test the validity of the previous experiments, isolated 8 μM Zn-Proteome (1.75×10^8 cells) was titrated with varying concentrations of $Cd(PYR)_2$ (1 Cd^{2+}: 2 PYR) for 30 minutes and the product mixed with EDTA (2 EDTA: 1 Zn^{2+} in the Proteome) to capture *loosely* bound Zn^{2+} and Cd^{2+}. The mixture was then centrifuged in 3kDa Centricon tubes to investigate whether Cd^{2+} had mobilized Zn^{2+} from the Proteome. This is represented by the following equations and figures:

$$Cd(PYR)_2 + Proteome \leftrightharpoons Proteome{\bullet}Cd + 2\ PYR \quad (2.5)$$

$$Cd(PYR)_2 + Zn\text{-}Proteome \leftrightharpoons Cd\text{-}Proteome{\bullet}Zn + 2\ PYR \quad (2.17)$$

$$Proteome{\bullet}Cd + EDTA \leftrightharpoons Cd\text{-}EDTA + Proteome \quad (2.18)$$

$$Cd\text{-}Proteome{\bullet}Zn + EDTA\ (2{:}1\ Zn) \leftrightharpoons Cd\text{-}Proteome + Zn\text{-}EDTA \quad (2.19)$$

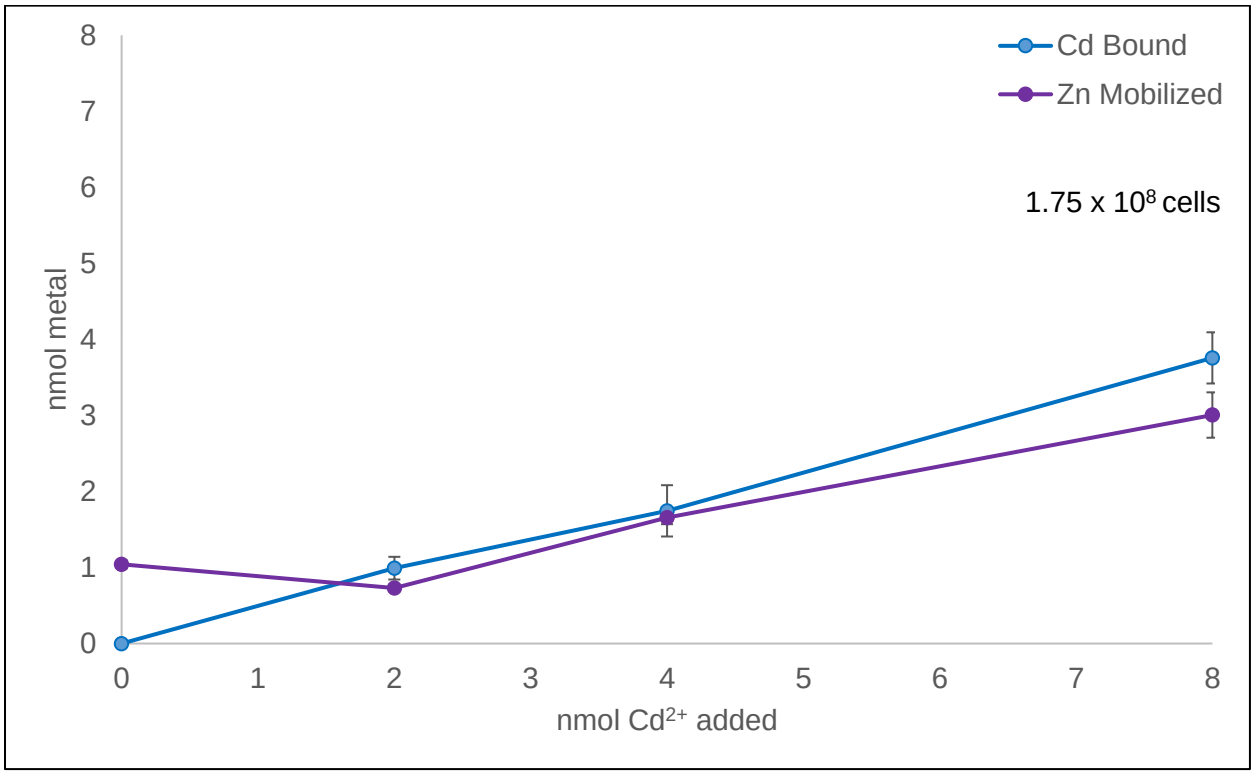

Figure 2.16

Isolated 8 µM Zn-proteome titrated with increasing amounts of $Cd(PYR)_2$. Loosely bound Cd^{2+} and Zn^{2+} was reacted with 16 µM EDTA and the mixture subjected to 3 kDa Centricon filtration. Blue line: cadmium measured in the retentate (Proteome). Purple line: zinc present in the filtrate. (n = 3)

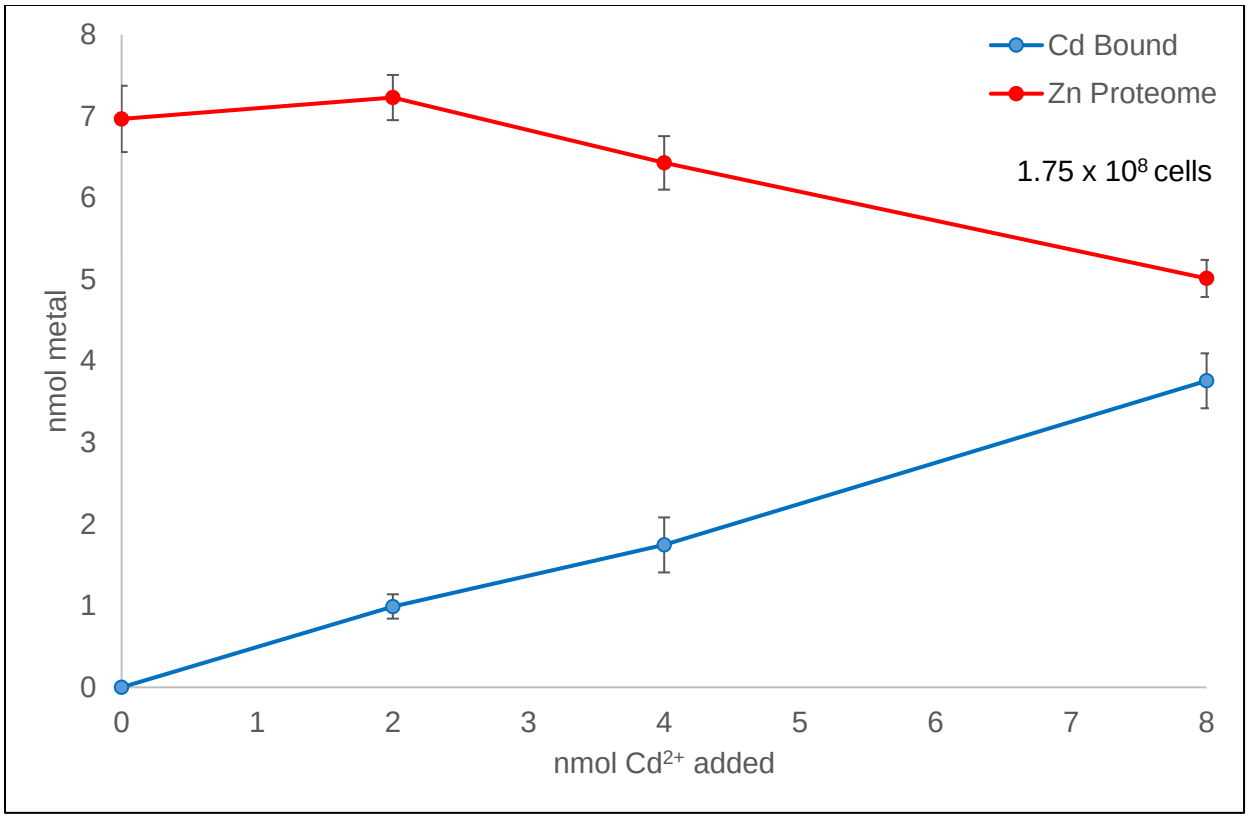

Figure 2.17

Isolated 8 µM Zn-proteome incubation with increasing amounts of $Cd(PYR)_2$. Loosely bound Cd^{2+} and Zn^{2+} was reacted with 16 µM EDTA and the mixture subjected to 3 kDa Centricon filtration. Blue line: cadmium measured in the retentate (Proteome). Red line: zinc present in the Proteome.

Increasing amounts $Cd(PYR)_2$ were titrated with isolated 8 µM Zn-proteome (**reaction 2.17**). As the concentration of Cd^{2+} increased, the amount of Zn^{2+} mobilized and accessible to EDTA increased (Namdarghanbari et al. 2014) (**reaction 2.18**). Despite EDTA having an equilibrium constant 1.62 times larger for Cd^{2+} (K_{eq} = 1.4 x 10^{13}, pH 7) than for Zn^{2+} (K_{eq} = 8.6 x 10^{12}, pH 7), 47.0% (3.76 nmol) of the total cadmium became tightly bound to Proteome, or inaccessible to EDTA, within 30 minutes of incubation. The amount of cadmium that was tightly bound displaced Zinc (3.0 nmol) from the Proteome in a nearly 1:1 ratio (**figure 2.16**). Clearly, not all Proteomic sites (~37%) are reactive to Cd^{2+} or at least some of those sites have a larger stability constant for Cd^{2+} than EDTA (**figure 2.17**). We hypothesize that the observed speciation results from reactions analogous to **reaction 2.5**-**2.6** above.

This reaction was monitored another way, using Cd^{2+} in place of $Cd(PYR)_2$. The zinc fluorescent sensor, TSQ, forms ternary adducts with about 25% of the total concentration of Zn-Proteome that fluorescence with a 470-475 nm wavelength maximum (Meeusen et al. 2011):

$$\text{TSQ} + \text{Zn-Proteome} \leftrightharpoons \text{TSQ-Zn-Proteome} \qquad (2.20)$$

It also reacts with Proteome•Zn in the same way:

$$\text{Proteome•Zn} + \text{TSQ} \leftrightharpoons \text{Proteome•Zn-TSQ} \qquad (2.21)$$

Although TSQ can react with similar Cd^{2+} structures, its fluorescence intensity is only about 10% of the corresponding zinc adducts (**Part III: section 3.1**). In **figure 2.18,** two stages of TSQ fluorescence were observed. First, TSQ was reacted with the Zn-Proteome before Cd^{2+} addition. The adduct forms slowly (**reaction 2.20**, orange spectrum).

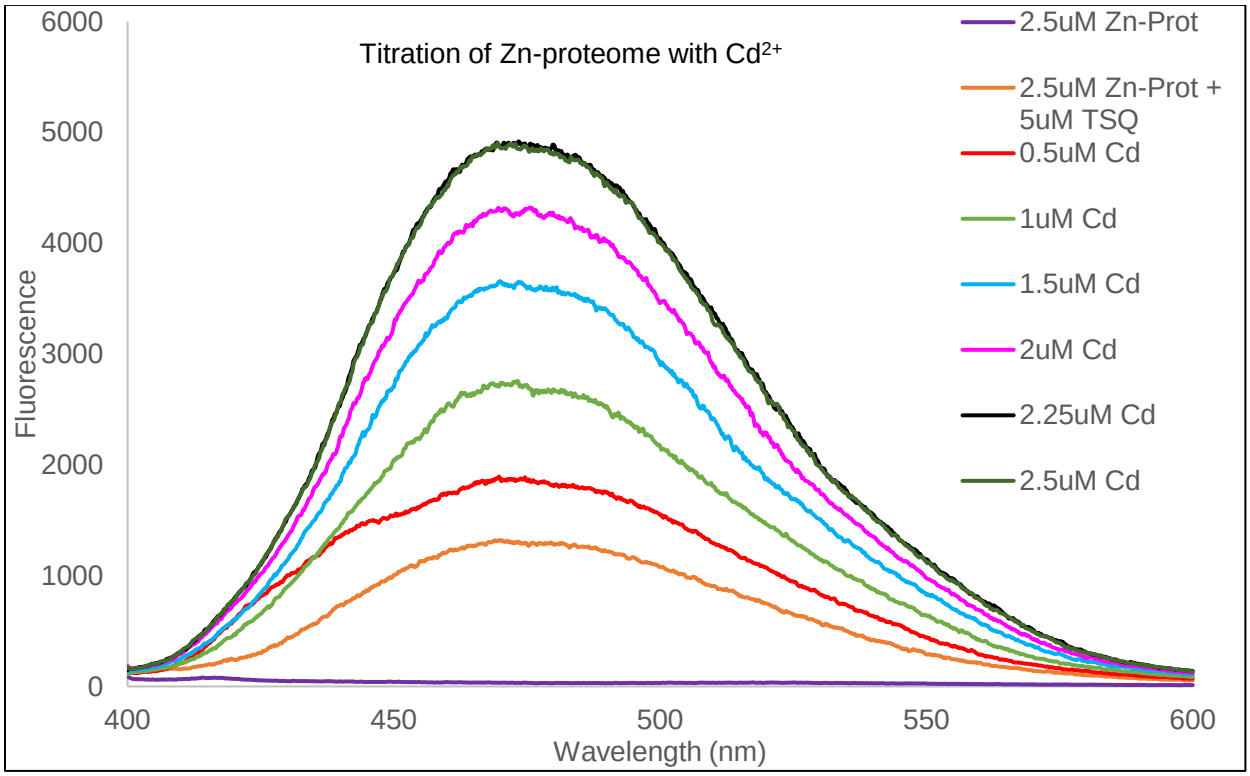

Figure 2.18

Titration of Zn-proteome with Cd^{2+}. 2.5 µM Zn-Proteome in 20 mM Tris pH 7.4 incubated with 5 µM TSQ for 60 minutes prior to additions of Cd^{2+}. 2 minutes in between additions of Cd^{2+}. Excitation wavelength was 365 nm. Emission wavelength window was 400-600 nm.

Then Cd^{2+} was titrated into the solution, reaching a maximum concentration equal to the concentration of Zn^{2+} in the Proteome. Each addition rapidly increased the fluorescence emission as seen in both **figure 2.18** and **figure 2.19** that summarizes the titration results. Because TSQ-Cd complexes fluoresce poorly, the large increase in fluorescence must imply the increasing availability of Zn^{2+} mobilized by Cd^{2+} for reaction with the Proteome to generate Proteome•Zn. Similar results were seen when Proteome was titrated with Zn^{2+} in the presence of TSQ (**figure 3.20**). In turn, TSQ reacts with this pool of Zn^{2+} as in **reaction 2.21** to produce fluorescent Proteome•Zn-TSQ. Notably, the titration is complete at 2.25 µM Cd^{2+}, nearly stoichiometric with the concentration of Zn^{2+} in the Proteome sample.

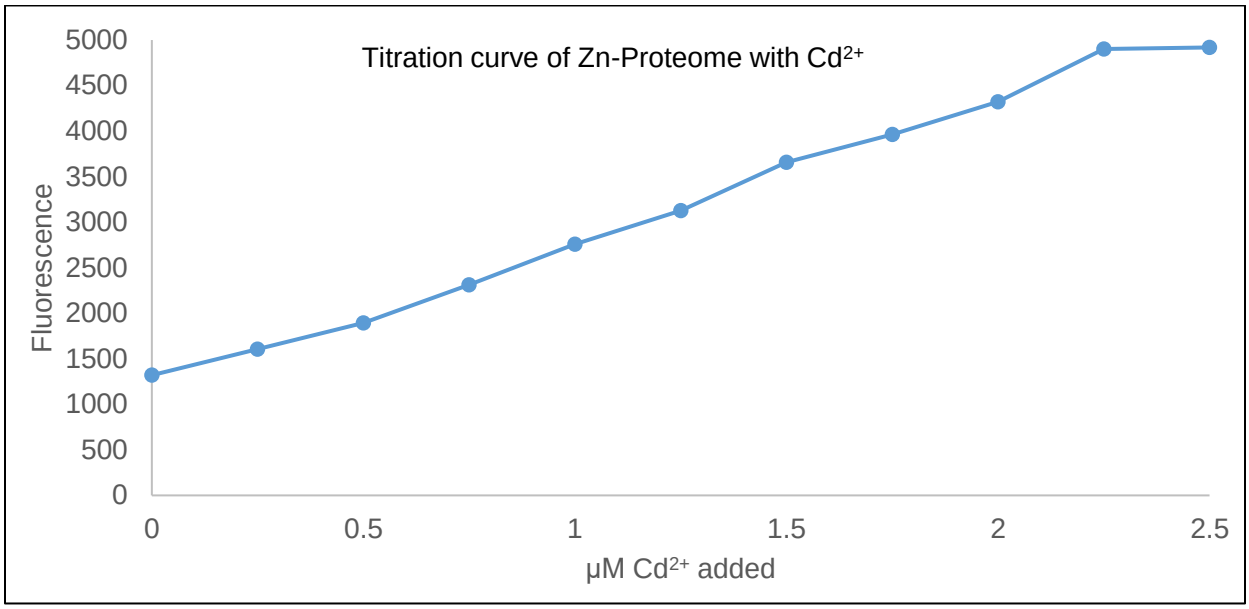

Figure 2.19

Titration curve of Zn-Proteome with Cd^{2+}. 2.5 µM Zn-Proteome in 20 mM Tris pH 7.4 incubated with 5 µM TSQ for 60 minutes prior to additions of Cd^{2+}. 1 minute in between additions of Cd^{2+}.

3.3 Reaction of Cells with $Cd(PYR)_2$: Cd-Zn●Proteome Exchange

10 plates of confluent LLC-PK_1 cells (5.7×10^7 cells) were incubated with $Cd(PYR)_2$ (3 µM PYR, 60 µM Cd^{2+}) for 30 minutes then washed with DPBS and harvested at 0 minutes, 30 minutes, 2 hours and 4 hours. The 2- and 4-hour time points were incubated with FCS and media prior to

harvesting. The supernatant of these reactions was incubated with EDTA (2:1 Zn^{2+} in the cell Zn-Proteome) to capture *loosely* bound Zn^{2+} and Cd^{2+}. The mixture was then centrifuged in 3kDa Centricon tubes to investigate whether Cd^{2+} had mobilized Zn^{2+} from the supernatant using Atomic Absorption Spectroscopy. This is represented by **figures 2.20-2.21** below.

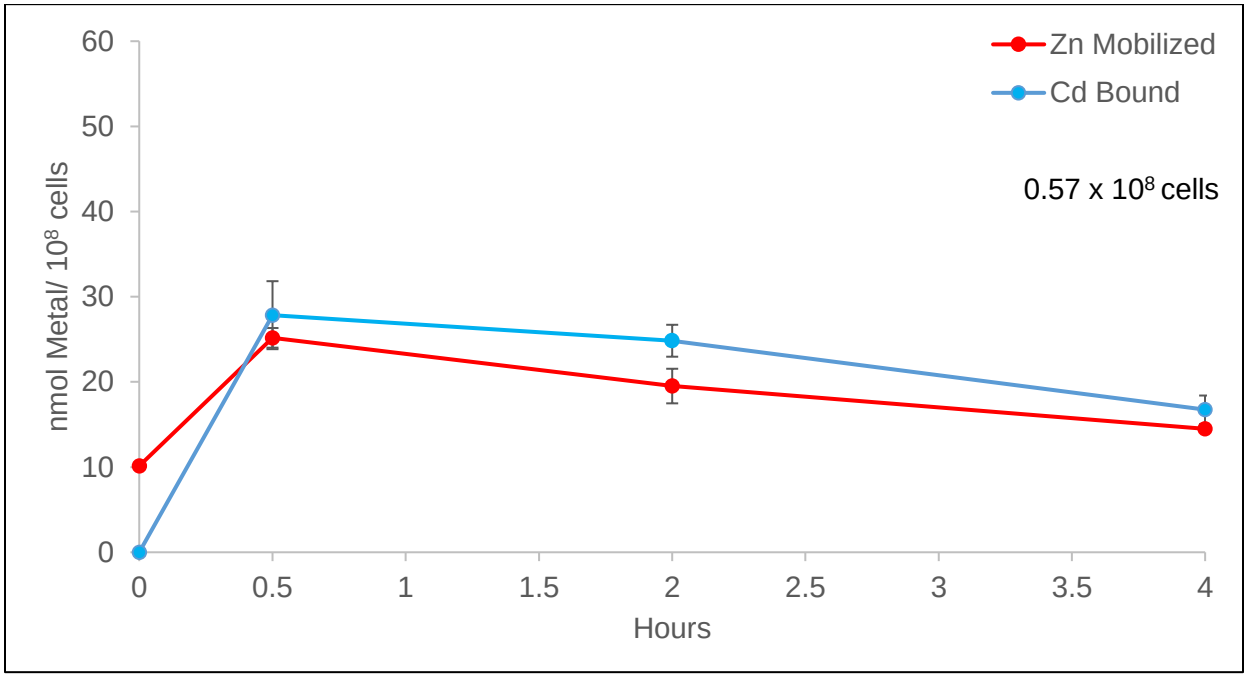

Figure 2.20

Reaction of Cd^{2+} with Zn-Proteome *in vivo*. Ten plates of confluent LLC-PK1 cells were incubated with $Cd(PYR)_2$ (3 µM PYR, 60 µM Cd^{2+}) for 30 min in DPBS and then transferred to FCS and media for 2 and 4 h time point. At 0, 0.5, 2, and 4 h supernatant, Proteome was isolated and treated with EDTA (2:1 Zn). The mixture was subjected to 3 kDa Centricon filtration. Blue line: cadmium measured in the retentate (Proteome). Red line: zinc present in the filtrate. (n = 3)

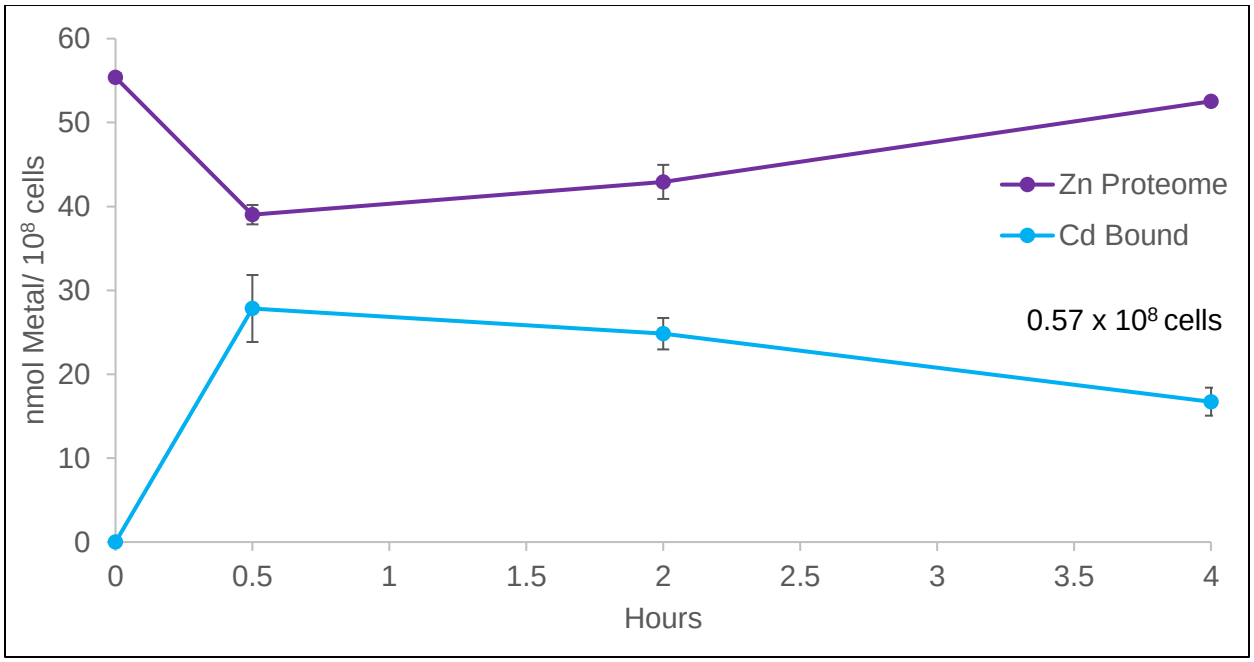

Figure 2.21

Reaction of Cd^{2+} with Zn-proteome *in vivo*. Ten plates of confluent LLC-PK1 cells were incubated with $Cd(PYR)_2$ (3 µM PYR, 60 µM Cd^{2+}) for 30 min in DPBS and then transferred to FCS and media for 2 and 4 h time point. At 0, 0.5, 2, and 4 h supernatant, Proteome was isolated and treated with EDTA (2:1 Zn). The mixture was subjected to 3 kDa Centricon filtration. Blue line: cadmium measured in the retentate (Proteome). Purple line: zinc present in the Proteome. (n = 3)

Analogous to **figure 2.16**-**2.17**, these figures show that $Cd(PYR)_2$ rendered Zn^{2+} from Zn-Proteome available for reaction with EDTA. $Cd(PYR)_2$ was incubated with LLC-PK_1 cells for 30 minutes, 82.0% (49 nmol) of the cadmium entered the cell (**reaction 2.4**). 56.5% (28 nmol) of the Cd^{2+} remained tightly bound, compared to 47.0% (3.8 nmol) in **figure 2.20**, or inaccessible to EDTA. The amount of cadmium that was tightly bound was similar to the amount of displaced zinc (25 nmol) from the Proteome in a nearly 1:1 ratio (**figure 2.16**) (**reaction 2.17-2.18**). Not all Proteomic sites (~42%), compared to ~37% in **figure 2.17**, are reactive with EDTA or some of those sites have a larger stability constant for cadmium ion than EDTA. Possibly, there are kinetic barriers to reaction of EDTA with Cd-Proteome. As MT was being synthesized at 2- and 4-hour time points, cadmium is seen being sequestered out of the Proteome (and EDTA resistant) and Proteome-bound zinc being restored (**figure 2.21**)

(**reactions 2.11-2.15**). After 2 hours, 11% (3.0 nmol) of the Proteome-bound cadmium was sequestered by the synthesis of MT and 5.8% (3.9 nmol) zinc was restored into the Proteome (**reaction 2.14-2.15**). 4 hours post incubation with $Cd(PYR)_2$ revealed a 40% (11 nmol) loss of Proteome-bound Cd^{2+} with a restoration of 20% (14 nmol) Zn^{2+} (**figure 2.21**). Both the displacement of Zn^{2+} from the Proteome induced by Cd^{2+} and its restoration to the Proteome as Cd^{2+} shifts into MT show a one to one stoichiometry.

4. Conclusion

An investigation into the uptake and distribution of Cd^{2+} and $Cd(PYR)_2$ in cells was undertaken. The initial hypothesis (**reaction 1.1**-**1.3**) was examined using Cd^{2+} and $Cd(PYR)_2$. $Cd(PYR)_2$ (3 µM PYR, 60 µM Cd^{2+}) was incubated with LLC-PK_1 (1×10^8) cells for 30 minutes and the distribution of Zn^{2+} and Cd^{2+} was monitored at six time points: 0 hour (30 minutes), 1 hour, 2 hours, 3 hours, 12 hours, 24 hours. At t = 30 minutes, 82% (50 nmol) of the total cadmium in the extracellular medium had reacted and become bound to high molecular weight species (**figure 2.6**). The observed uptake and distribution are explained by **reactions 2.4**-**2.6**. This is consistent with the reaction seen when Cd^{2+} was reacted with isolated Zn-Proteome (Namdarghanbari et al. 2014). Presumably, over the next two hours, **reactions 2.7-2.10** are occurring, inducing the synthesis of apo-MT. After 2 hours post-incubation with $Cd(PYR)_2$, metallothionein is first seen being synthesized; centered at fraction 30 (**figure 2.8**). The synthesis of apo-MT sequestered 14% (7.0 nmol) of cadmium out of high molecular weight species and a nearly an equal amount of zinc was sequestered into the protein (**reactions 2.10-2.12**). Later, 24 hours post-incubation with $Cd(PYR)_2$, 84% (42 nmol) of Proteome-bound cadmium was sequestered into MT along with an equal amount (41 nmol) of zinc (**figure 2.11**); results were consistent with and expanded upon other experiments involving incubation of $Cd(PYR)_2$ with Proteome from LLC-PK_1 cells (Namdarghanbari et al. 2014).

A different set of reactions occurred when LLC-PK_1 cells (5.0×10^7 cells) were incubated with cadmium ion. Four time points were taken for analysis of the distribution of Zn^{2+} and Cd^{2+}: 30 minutes, 6 hours, 12 hours and 24 hours incubation with Cd^{2+} (**figures 2.12-2.15**). Within 30 minutes of exposure, 1.2% of the total extracellular Cd^{2+} was transported through the outer membrane into the cell interior (**figure 2.12**); compared to 83% using PYR as a shuttle (**figure 2.6**). 5.64 nmol of Cd^{2+} was found within 10 plates of LLC-PK_1 cells following 30 minutes incubation with 60 μM Cd^{2+}. The uptake through the cell membrane is much slower because cadmium ion is charged and must enter through a limited number of transporters. Consistent with incubation of cells with $Cd(PYR)_2$, Cd^{2+} can be seen being sequestered out of the high molecular weight species at the 6-hour time point by MT (**figure 2.13**). After 24 hours of incubation with 4 μM Cd^{2+}, 35% (2.1 nmol) of the total extracellular Cd^{2+} was taken up by cells and 79% (1.6 nmol) was sequestered into MT (**figure 2.15**). In both experiments, a small amount of Cd^{2+} is seen bound to high molecular weight species indicating that not all cadmium sites are reactive with MT (Namdarghanbari et al. 2011). The observed speciation may be explained by reactions analogous to **2.4-2.15** above, with the exception that upon synthesis, apo-MT may directly compete for incoming Cd^{2+} from Proteomic sites (**reaction 2.16**).

Experiments were undertaken to further examine **reactions 2.5** and **2.6**. Isolated Zn-Proteome (1.75×10^8 cells) was reacted with increasing amounts of $Cd(PYR)_2$, then that mixture reacted with EDTA (2:1 Zn^{2+}), and finally separated by 3kDa filtration (**figure 2.16-2.17**). Within 30 minutes of incubation with $Cd(PYR)_2$, an average of 47% of the total incubated cadmium became bound to Proteome displacing zinc in a nearly 1:1 ratio (**figure 2.16**). **Figures 2.16-2.17** can be summed up by the following: as the concentration of Cd^{2+} increased, the amount of Zn^{2+} mobilized and accessible to EDTA increased in parallel, stoichiometric fashion. A more limited but similar set of results were also seen in previous experiments that utilized Cd^{2+} instead of $Cd(PYR)_2$ as the source of cadmium ion (Namdarghanbari et al. 2014).

The reaction of Cd^{2+} with the Zn-Proteome was also followed using the fluorescent sensor for Zn^{2+}, TSQ (**figures 2.18**-**2.19**). Like the previous studies, the changes in fluorescence indicated that Zn^{2+} was mobilized from the Proteome by Cd^{2+} and that the reaction appeared to be nearly stoichiometric.

In vivo analysis of **reactions 2.5-2.6** revealed similar results (**figures 2.20-2.21**). LLC-PK_1 cells (5.7×10^7 cells) were incubated with 60 μM $Cd(PYR)_2$ for 30 minutes; following the procedure listed in **section 2.2**. Like the previous experiment, 57% (28 nmol) of cadmium was found tightly bound to the Proteome, displacing zinc (25 nmol) in a nearly 1:1 ratio (**figure 2.20**) (**reaction 2.18**). At 2- and 4-hour time points, MT is seen being synthesized, consistent with **reactions 2.8**-**2.12**, and sequestering cadmium out of the Proteome; while zinc is being restored into the Proteome (**reactions 2.14**-**2.15**) (**figure 2.21**).

As cadmium crosses the cell membrane, it reacts with Proteomic sites (**reaction 2.4-2.5**) (**figure 2.6, 2.16, 2.20**). Cadmium becomes bound to these Proteomic sites (**reaction 2.5**) displacing zinc in these proteins, in a nearly 1:1 ratio (**figure 2.16** and **2.20**). Displaced zinc becomes bound to non-specific Proteomic sites (**reaction 2.6**), making it more accessible to EDTA (**figure 2.17** and **2.21**) (**reaction 2.18**). Proteome-bound zinc initiates transcription of apo-MT (**reaction 2.7**-**2.10**) (**figures 2.6**-**2.11**). Apo-MT reacts with cadmium proteins (**reaction 2.11**) and Proteome•Zn (**reaction 2.12**) to restore functionality back to zinc proteins and the Proteome (**reaction 2.14-2.15**) (**figure 2.20-2.21**).

Part III: Methodology to measure Zn-proteins and their Interaction with Cd^{2+} using LA-ICP-MS

1. Introduction

Inductively coupled plasma mass spectrometry (ICP-MS) is one of the most successful methods in atomic spectrometry due to its multi-element capabilities and high detection power. The first use of ICP-MS for elemental analysis of aqueous sample solutions was in 1980 (Houk et al. 1980). Since the development of commercial instruments in the 1980's, ICP-MS has evolved into a standard method of multi-elemental and isotopic ratio analysis of diverse biological and geological samples (Hieftje et al. 1992). Calibration against aqueous standards, picogram / mL detection limits, a wide coverage of elements and direct analysis of solutions are just some of the recognized advantages of ICP-MS (Durrant 1999).

Elemental analysis in this thesis was performed using a Thermo Fisher Scientific Element 2 sector field ICP-MS (Thermo Fisher Scientific Waltham, MA). After the sample is ionized by the plasma, the generated ions are passed through a sampler cone to concentrate the elemental isotope of interest. The ions are further concentrated by the skimmer cone and then passed onto the optics system of the ICP-MS. A typical sector field instrument consists of an entrance slit, a magnetic and electrostatic sector field and the exit slit. This instrument uses a so-called 'reverse geometry' with the electrostatic analyzer placed behind the magnetic sector because it is considered advantageous (Cromwell et al. 1996). With this reverse geometry, ions are separated first magnetically according to their mass and energy; those magnetically separated ions, of the selected analyte mass, are fed into an electrostatic analyzer for energy focusing (Schechter et al. 1997).

ICP-MS is not without analytical difficulties. Some matrices resist dissolution requiring laborious procedures that could take hours or days to perform. Even when successful, the procedure could involve potentially dangerous reagents and any handling of the sample involves some risk of contamination and the loss of volatile elements. These dissolution reagents often contribute elements that are interferents with isotopes of analytical interest or that are incorporated into polyatomic interferences (Durrant 1999). Nevertheless, analytical merit is limited by interferences both spectroscopic and non-spectroscopic (Jarvis et al. 1992).

The elemental isotope of interest may be spectroscopically interfered with by atomic and molecular ions having the same mass or secondary discharges taking place in the interface region, explained below. Spectroscopic interferences are subdivided into several groups: isobaric atomic ions, multiply charged ions and molecular ions. Isobaric ions refer to isotopes of different elements that have the same nominal mass as the analyte of interest. Choosing an isotope that is free from isobaric overlap is usually the best option for reducing these interferences (Jakuboski et al. 1998). Constituents of the sample matrix and gases are frequent contributors of multiply charged and molecular ions.

Multiply charged and molecular ions cause the most severe problems among all these spectroscopic interferences (Jakubowski et al. 1998). The ionization processes in the plasma and interface generate ions with double or multiple charges due to secondary charges in the interface region. Molecular interferences are created from cluster ions from Argon gas in the plasma and the analytical sample itself.

Numerous strategies have been employed in order to try to minimize or circumvent the formation of spectral interferences, listed above, which include: special sample introduction systems, special plasma parameters, collision/dynamic reaction cells and mathematical corrections. Sector-field mass spectrometry simply distinguishes the analyte from interference by difference in mass (Thermo Fisher Scientific 2008). Double focusing sector-field mass

spectrometry was first developed and introduced to the market in 1988 for organic analysis (Bradshaw et al. 1989). The earliest known use of this technique coupled to an ICP for isotopic analysis was in 1998 (Wildner 1998).

Non-spectroscopic interferences, or matrix effects, can be split into two groups: matrix induced spectral overlap problems and matrix induced signal intensity changes (Tan et al. 1987). These interferences can be reduced by ion acceleration at high voltages (Jakubowski et al. 1998). The Element 2 is equipped with a high acceleration voltage of -8 kV resulting in a mass independent detector response for ion transmission stability (Thermo Fisher Scientific 2008).

The first use of laser ablation for locating metals within a biological sample date back to 1993 (Countant et al. 1993). An ArF* (Argon Fluoride excited state complex), 193 nm, nanosecond Analyte Excite Excimer Laser Ablation system from CETAC industries was employed throughout this thesis (CETAC Industries, Ohama, NB). A 193 nm excimer laser is ideal for ablation of polyacrylamide gels, which are nearly transparent, because deep ultraviolet light is absorbed more efficiently, laser energy is concentrated in a smaller sample volume which is more completely vaporized in the argon plasma of the ICP, and particles produced are smaller and more uniform than with 213 or 266 nm lasers (Guillong et al 2003).

Fractional ablation, any non-representative sub-sampling of non-analyte, is a serious problem associated with LA-ICP-MS which occurs during ablation and transport of material to the ICP-MS (Durant et al. 1999). For reduced fractionation, 193 nm nanosecond excimer lasers were found to be superior compared to infrared laser ablation. As well, they result in better reproducibility, spatial resolution (space between laser pulses), quantification and sensitivity (Geertsen et al. 1994). Transport efficiency of ablated material is greatly increased to around 90% using Helium as an ablation cell/carrier gas because ions in the Helium atmosphere allow the plasma plume to expand further, giving more time for material to condense out of the cooling plasma (Eggins et al. 1998).

Studies described above have revealed that some intracellular Zn-Proteins interact with Cd^{2+} and presumably become functionally perturbed. Identification of proteins that are the loci of reactions with Cd^{2+} was the initial aim of this research. The downregulation of sodium-dependent glucose transport into kidney cortical cells led to the discovery of Cd^{2+} interaction with Zn_3-Sp1 (Tabatabai et al. 2005; Kothinti et al 2010). Out of potentially thousands of Zn-proteins with similar binding motifs, Sp1 is only one of the generic C_2H_2 proteins that have been identified as reacting with Cd^{2+}. **Section II** of this thesis provide much *in vitro* and *in vivo* support for the hypothesis that Cd^{2+} replaces Zn^{2+} in Zn-proteins (**reaction 1.5**) (Namdarghanbari et al 2014). But the identity of specific proteins that have undergone reaction with Cd^{2+} remains unknown. Robust methods are needed to evaluate the distribution of Cd^{2+} and other metal ions like Zn^{2+} within the Proteome.

Using a solid support, such as polyacrylamide gel, to separate the Proteome, then searching for metals through ablation with a laser and inductively coupled plasma mass spectrometery (LA-ICP-MS) for the identification of those metals is one strategy that may accomplish this aim (Sussulini et al. 2011). Protein denaturation and loss of bound metal ions occur in high-resolution separation methods, particularly in sodium dodecylsulfate polyacrylamide gel electrophoresis (SDS-PAGE). This constitutes one of the major problems at the front end of this method (Sussulini et al. 2011).

Recently, native SDS-PAGE or NSDS-PAGE, a modification of SDS-PAGE, was developed that showed refined separation of proteins with their native properties and bound metal ions intact (Nowakowski et al. 2014). Early experiments have shown that many zinc proteins can be resolved and separated using this technique in combination with LA-ICP-MS (Nowakowski et al. 2014). This combination of NSDS-PAGE and LA-ICP-MS may provide a new, powerful approach for identification of cadmium-containing proteins and propel the understanding of the chemical biology of cadmium.

2. Methods

2.1 Chemicals

All chemicals were purchased from either Thermo Fisher Scientific or Sigma-Aldrich unless noted and were the highest purity available. Cd^{2+} and Zn^{2+} standard solutions were from SPEX Certiprep for routine analytical measurements and creation of standard curves. All gel electrophoretic methods were performed using Novex® NuPAGE® 12% Bis-Tris polyacrylamide precast gels, from Thermo Fisher Scientific, in conjunction with the XCell SureLock™ Mini-Cell electrophoresis chamber available from Invitrogen.

2.2 Native Sodium Dodecyl Sulfate (NSDS)-PAGE

NSDS-PAGE is a recently developed method for the high-resolution separation of proteins with the retention of native properties such as the metal content and maintaining native confirmation (Nowakowski et al. 2014). The SDS concentration was lowered from 0.1% to 0.0375% which results in SDS binding to proteins in low concentration without grossly altering their native structures; whereas, higher concentrations of SDS binds in larger stoichiometry, causing protein denaturation. It has been shown that this technique both resolves protein mixtures and maintains bound Zn^{2+} that forms fluorescent ternary adducts with the Zn^{2+} sensor, TSQ, for the location of Zn-proteins within a polyacrylamide gel (Meeusen et al. 2011).

Before protein preparation, NSDS run buffers (50 mM Tris, 50 mM MOPS, 0.0375% SDS, pH 7.6) were chilled to 4 °C. In addition, NuPAGE® 12% Bis-Tris precast gels were assembled in the electrophoresis chamber and run at 200 V, for at least 30 minutes, using $_{dd}H_2O$ as the run buffer. Then $_{dd}H_2O$ was replaced by chilled NSDS run buffer. The electrophoresis chamber was surrounded by ice prior to starting run, in case the system overheats during the electrophoretic process possibly melting the gel. Protein samples were mixed with 25% glycerol. Electrophoresis was run at 30 mA until the dye front migrated 60 mm. Gels were stained for

protein using Coomassie R-250 stain (**section 2.3.1**), dried for laser ablation (**section 2.3.2**) or TSQ stain (**section 2.3.3**).

2.3 Gel Staining

2.3.1 Coomassie R-250 protein band staining

After gels were removed from their casings, a 100 mL fixing solution was added to gels containing 40% methanol and 10% acetic acid. It was microwaved for 45 seconds and put on a shaker for 30-45 minutes. The fixing solution was decanted and 50 mL of staining solution (30% methanol, 10% acetic acid, 0.002% Coomassie R-250) was added. Gels were microwaved for 45 seconds and placed once again on a shaker for 30 minutes. Staining solution was decanted, and the gels were destained using 100 mL of 8% acetic acid placed in a microwave for 45 seconds and agitated for 45 minutes. The destaining solution was replaced with more destaining solution overnight on a shaker.

2.3.2 Passive Drying of PAGE gels

All PAGE gels were dried in partial accordance with the method advised for the Invitrogen DryEase® Mini-Gel Drying System. First, gels were soaked in ddH_2O for 5 mins to wash gel of any buffer solution. Then a drying solution containing 24% ethanol, 1.2% isopropyl alcohol, 4% glycerol, 1.8% methanol and 69% $_{dd}H_2O$ (vol/vol) was added to the gel and agitated for 10 minutes. One side of the gel drying frame was placed on the drying base followed by a piece of cellophane wetted with the drying solution (**figure 3.1**; panel A).

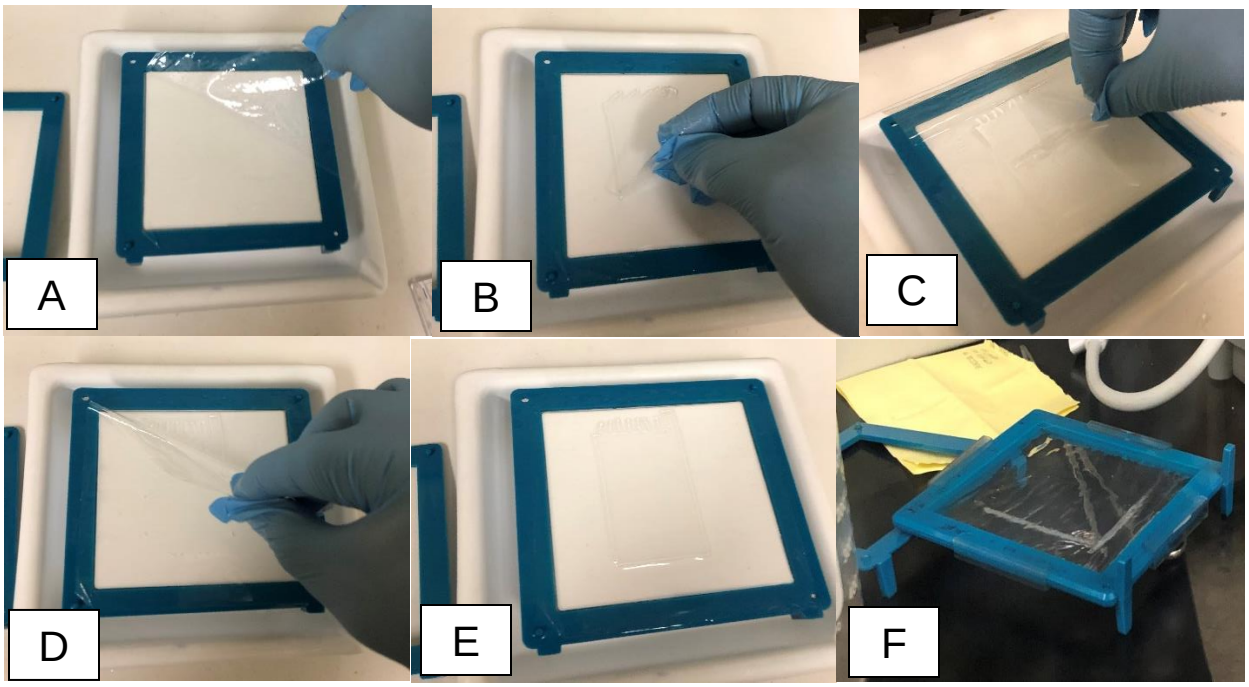

Figure 3.1

Passive drying of a polyacrylamide gel using Invitrogen DryEase® Mini-Gel Drying System. See text for explanation of A-F

The gel was cut in half, to fit the laser ablation apparatus, and the gel was placed on top of the piece of cellophane (panel B), followed by two pieces of cut saran wrap (panel C) and a second piece of wetted cellophane layered on the other side of the gel (panel D). Air bubbles were removed between the layers of gel, saran wrap, and cellophane to prevent gel cracking (panel E). The other half of the drying frame was placed on the base and the frame was secured with binder clamps. The frame, containing the gel, was transferred, saran wrap face down, to a closed fume hood with an atmospheric humidity of 55% (panel F). Any humidity above 30% prevents the gel from drying too quickly and cracking. After 24 hours, the dried sandwich was kept in the frame and placed in a book—to prevent warping—until the gel was ready for analysis via LA-ICP-MS.

2.3.3 TSQ Staining of NSDS-PAGE Gels

Previous experiments have shown that TSQ can be used to find Zn-proteins within polyacrylamide gels (Nowakowski et al. 2015). All TSQ gel staining experiments were carried out at the UWM CLS Department of Biological Sciences. Protein samples were incubated with TSQ for one hour prior to electrophoresis using the NSDS-PAGE technique (**section 2.2**). Later, after the plastic casting was removed, gels were washed twice in 100 mL of ddH_2O. An initial background of the gel was taken to rule out auto-fluorescent protein bands. The gel was transferred into a UVP EpiChemi II Darkroom UV transilluminator gel box set at the long UV wavelength (approximately 365 nm, the fluorescence excitation wavelength maximum of $Zn(TSQ)_2$ and TSQ-Zn-ligand adducts). Images of the gel were taken using a digital camera with a SYBYR GOLD (580-640 nm) emission filter and processed using LabWorks software version 4.5. This wavelength window was not optimal for TSQ-Zn species but was the best available filter. Typical exposure times for fluorescent images were between 1-5 minutes. In some cases, the gels were additionally incubated in 50 mL of $_{dd}H_2O$ containing a ligand for 5 minutes and additional images were captured.

2.4 Laser Ablation

2.4.1 Optimization of Analyte Excite Excimer Laser Ablation System

Laser Ablation was performed using 193 nm nanosecond Analyte Excite Excimer Laser Ablation system (Cetac Industries, Ohama, NB). Dried gels, already cut in half, were prepared for ablation by removing the saran wrap-cellophane cover, exposing the gel on one side while leaving the cellophane beneath the gel on the other side. Half of the gel was attached to a frosted glass slide using double-sided tape (

3.2; Panel A).

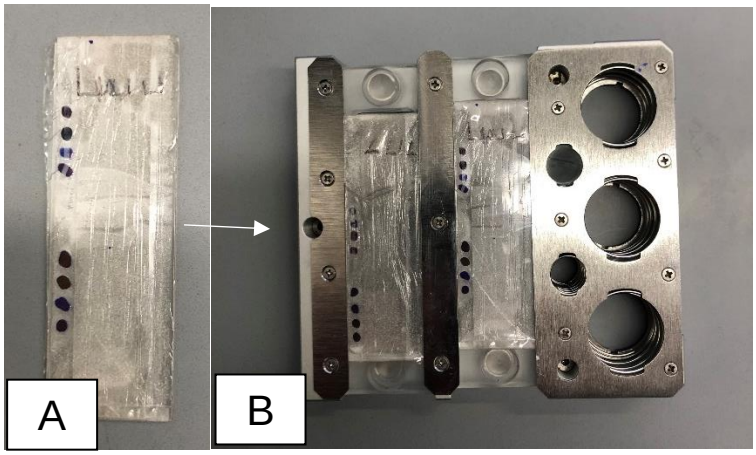

Figure 3.2

Sample preparation of a dried NSDS-PAGE gel (panel A) placed in Helex II sample cell (panel B) with 1 µL dried standard solutions (lane of stained circles).

It is essential to optimize both laser power (fluence) and laser pulse frequency to maximize small sized particles and soft agglomerates. Smaller sized particles or soft agglomerates reduce fractionation due to incomplete ionization of the particles in ICP; incomplete ionization leads to 'spiky' signal behavior (Diwakar et al. 2015). Optimization of the laser ablation instrument was as follows. A procedure defined by CETAC was used to find the power and frequency necessary to ablate the polyacrylamide gel to reduce fractionation effects. ^{66}Zn and ^{114}Cd were monitored on the Thermo Fisher Scientific Element 2 ICP-MS. Both isotopes were chosen because isobaric (different element, same mass) and polyatomic interferences (sample and matrix molecules that have same mass) are either nonexistent or negligible. Isotope studies were done to see if isotopic ratios of zinc were correct after LA-ICP-MS. ^{66}Zn and ^{114}Cd are used throughout experiments unless otherwise noted.

2.4.2 Laser Ablation Parameters

As described above, the optimization of laser power (fluence) and frequency (laser pulses) is essential to reduce fractionation effects in the ICP. Laser ablation parameters were determined

from ablating a small section of gel, at a constant speed of 50 µm/s, that had dried ICP-MS grade standard solution with a volume of 5 µL applied to the gel by the apparatus in **figure 3.3**.

Figure 3.3

Spotting apparatus used for optimization made of stainless steel. 5 µL of standard was pipetted into the space between the arrows then applied by pushing the apparatus onto the gel. This created a uniform line to perform optimization on.

The section of gel, with 5 µL of dried ICP-MS grade standards, was ablated three times to determine the average and relative standard deviation (% RSD), used to correlate the precision and repeatability of an experiment. The %RSD, of registered counts per second (CPS), was calculated by the equation: $\sigma = \sqrt{\left(((\sum(Xavg - X1))^2)/(N-1)\right)}$ x 100 (X_{avg} is the average of the sum of total CPS; X_1 is the value of interest; and N is number of line scans). The resulting % RSD was compared for each variable (1.5, 2.0, 2.5, 3.0, 3.5 mJ and 15, 25, 35 Hz) to determine what value of each parameter was best optimized for the laser ablation system.

Figure 3.4 describes, in detail, how intensity (CPS) and laser power are related (blue curve). As expected, they are directly related to one another. Power (fluence) determines how much

energy is involved with laser-sample interaction. Ablated Particles can be lost on the transport tube walls due to inertial impact, gravitational settling, or laminar and turbulent diffusions (Jeong et al. 1999). There is an optimal fluence in which the particle sizes generated from the ablated material is within an ideal size distribution: particles less than 5 nm in diameter are lost by diffusion (**figure 3.4; section 1**) and particles more than 3 μm settle in the transfer tube due to gravity (**figure 3.4; section 2**) (Durrant 1999). In **figure 3.4 (section 1**), inefficient ablation refers to suboptimal laser power producing ablated particles less than 5 nm in diameter. These particles are lost in the transport tubing due to diffusion from the ablation instrument to the plasma in the ICP (Jeong et al. 1999). Larger particles (> 3 μm) are formed from too much power within the laser-sample interaction causing melting of the sample and creating transport limited particles. There is a loss of ablated sample reaching the plasma from these particles having greater gravitational force acting on them from particles settling within the transport tubing (**figure 3.4; section 2**) (Garcia et al. 2008). The results indicate that the lowest % RSD occurs at 3 mJ (**figure 3.5**).

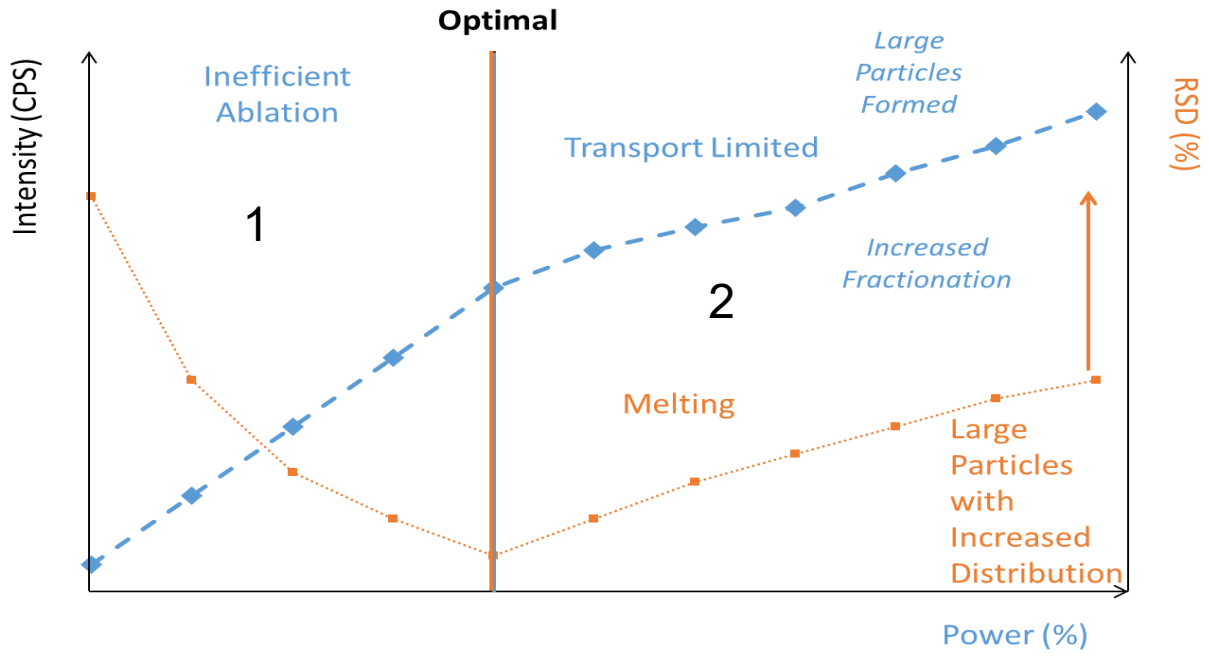

Figure 3.4

Power tuning of the Laser Ablation instrument. Picture modified from CETAC protocol manual. Blue curve plots Intensity vs. Power. Orange line plots % RSD vs. Power. The terms shown in the figure are described in the text.

The results of the optimization of the instrument indicated that the lowest % RSD occurs at 3 mJ (**figure 3.5**).

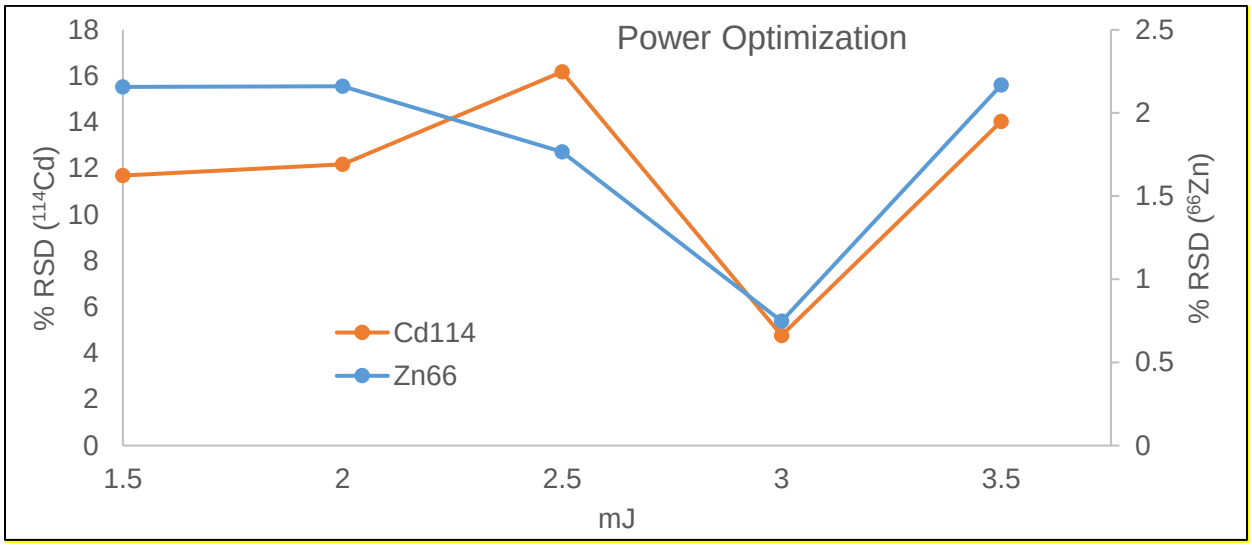

Figure 3.5

Power optimization results from CETAC protocol procedure. Lowest % RSD was determined from line scans (n = 3). 3 mJ was chosen. ^{114}Cd (orange); ^{66}Zn (blue).

Intensity (CPS) is a function of frequency of laser pulses (Hz). The higher the frequency, the higher the intensity. Frequency is also related to scan speed. The faster the scan speed, the higher the frequency needed for reduction of other fractionation effects and mass loading, the incomplete ablation and clumping of ablated material that give rise to a "spiky signal" (Diwakar et al. 2015). Essentially, higher frequency of laser pulses leads to more total material ablation requiring higher scan speeds for less ablated area overlap (Bonta et al. 2015). **Figure 3.6** shows that the optimal frequency is one that has the lowest % RSD.

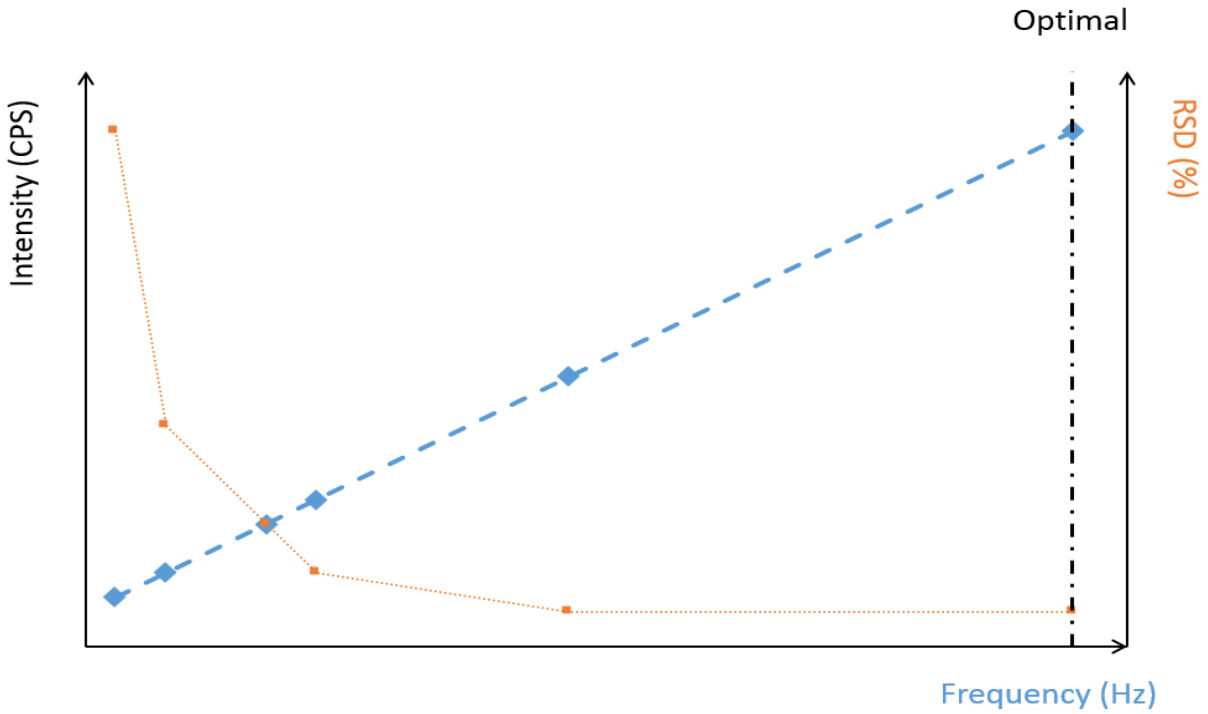

Figure 3.6

Frequency Optimization picture modified from CETAC protocol. Intensity (counts per second) is a function of Frequency. As the Frequency (of laser pulses) increases, the Intensity (CPS) increases. Plot of intensity vs. Frequency (blue curve); plot of % RSD vs Frequency (orange curve).

Using a scan speed of 50 µm/s, the optimal frequency is 25 Hz (**figure 3.7**).

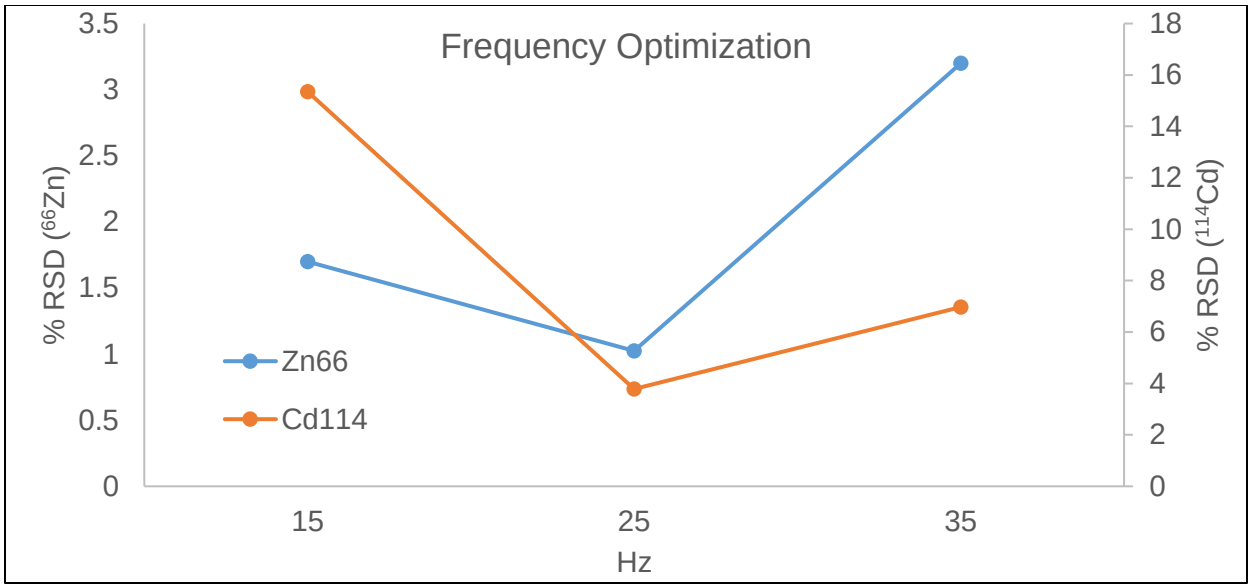

Figure 3.7

Frequency optimization (CETAC protocol procedure). Lowest % RSD was determined from line scans (n = 3). 25 Hz was chosen. ^{114}Cd (orange); ^{66}Zn (blue)

In summary, during the analysis of the distribution of metal along lanes of an electrophoretic gel, it is typical to ablate each lane six times for reasons described below. In addition, there can be up to eight lanes that need ablation per gel. A typical polyacrylamide gel lane is approximately six centimeters long. A scan rate of 50 µm/s or 20 mins/scan was chosen because of time constraints when running multiple line scans on a single lane. The values of lowest % RSD (CPS for ^{66}Zn and ^{114}Cd) corresponding to 3.0 mJ and 25 Hz were selected as seen in **figure 3.5** and **3.7**, respectively.

The HelEX II laser ablation cell has ability to independently control the gas flow. The gas flow keeps the plume of ablated material constrained within the lower part of the cup which minimizes transport induced fractionation and greatly enhances washout speed (Teledyne 2018). The flow rate of the gasses inside the cup of the laser ablation system had to be optimized. A final value of 1.00 L/min Helium gas was chosen as no significant changes to CPS were seen when manually adjusting the flow of cup gasses (data not shown).

Ablation parameters and laser energy were controlled by the Chromium 2.3 program that was part of the software of the instrument. Using the program controls, the stage holding the gel was homed, to give a reference point, in all three axes (X, Y, Z). Then, line scans were generated during ablation of each lane consisting of three to six 85 µm width lines per lane with a spacing of 190 µm between lines, which isolated ablation runs from one another and prevented debris from previous line scans from contaminating current line scans. The laser was set at 25 Hz with 3.0 mJ of power and a scan rate of 50 µm/s. The laser must exchange ArF* excimer gas every two weeks, or the laser power becomes unstable and incomplete ablation occurs on the surface of the gel.

The ablation chamber was evacuated by pulling a vacuum down to 9 psi slowly over 20 pumping cycles. Subsequently, helium was flooded into the chamber for a duration of 10 mins at a rate of 1 L/min. The helium was turned off and the plasma was ignited. Once the plasma stabilized, after 45 minutes, helium was turned back on with the final helium carrier gas flow rate set at 1 L/min. The laser was warmed up by firing at 15 Hz into a shutter for the duration of plasma ignition.

2.5 Elemental Analysis using LA-ICP-MS

Elemental analysis was performed using a Thermo Fisher Scientific Element 2 ICP-MS powered by Thermoelement 3.1 software (Thermo Fisher Scientific Waltham, MA). The detailed operational settings are listed below.

The settings for argon (Ar) gas, used to ignite and maintain the inductively coupled plasma, included a gas flow rate of 17.0 L/min, which cools the torch to prevent melting, an auxiliary Ar gas flow rate, which generates and shapes the plasma, of 1.0 L/min and a sample Ar gas flow (the analyte gas) of 0.936 L/min.

Torch position was optimized as follows: X-position at 1.79 mm, Y-position at 1.45 mm and Z-position at -5.00 mm. The forward power, power generated by the RF (radio frequency) generator to create a steady-state plasma, was set at 1233 W. This steady-state plasma was produced when the rate at which electrons are released by ionizing collisions equals the rate at which they are lost by recombination.

The Guard Electrode was turned on to decouple the plasma from the RF generator in order to reduce the energy spread of ions increasing the ion transmission and delivering superior sensitivity (Thermo Fisher Scientific 2008).

Optic lenses, used to focus and shape the ion beam, were also optimized to be as follows: Extraction lens -1900 V, Focus lens -1461.8 V, X-deflection 6.10 V, Y-deflection -0.10 V and Shape lens 137.0 V.

Once the plasma torch was ignited, helium from the LA unit was introduced at the minimal flow rate of 100 mL/min which was increased until 1000 mL/min was reached. The plasma was warmed up for at least 45 minutes to avoid plasma fluctuations.

The laser was coupled to the settling time of the detector in the mass spectrometer to be 2.5 laser pulses (LA instrument) per elemental mass scan (mass spectrometer), in order to attain the highest resolution possible. The total time per elemental mass scan in the mass spectrometer was 0.101 s while the pulse rate of the laser was 25 Hz (0.04 s/pulse). Data were collected in the Thermoelement software 3.1 and transferred to Microsoft Excel for further analysis.

2.5.1 Spotted Standards for Quantification

In order to quantify metals located in the gel by LA-ICP-MS, 1 µL of standards, from SPEX Certiprep, of Zn^{2+} and Cd^{2+} were spotted near the edge of the gel using a micropipetter and allowed to dry before ablation (see **section 3.4**). For the standard curves, 1 µL drops of 33.1,

66.3, 132.5, 265.1 pmol Zn^{2+} and 20.0, 39.9, 79.9, 159.7 pmol Cd^{2+} were mixed with Coomassie R-250 dye and applied to gels using a micropipette. The standards dried for approximately 20 mins before the start-up of the laser ablation instrument and plasma of the ICP-MS. The plasma was warmed up for 45 minutes, to avoid plasma fluctuations, before ablation began. Three 85 µm line scans per element were run at 50 µm/s and then each set of data points was subjected to Grubbs' test for outliers (see **section 2.6**). The area under the scanned curve was obtained by subtracting the average background from the set of data points, then summing them up to obtain total counts per second (CPS). The integrated area under the curve was equated to the corresponding number of moles applied to the gel.

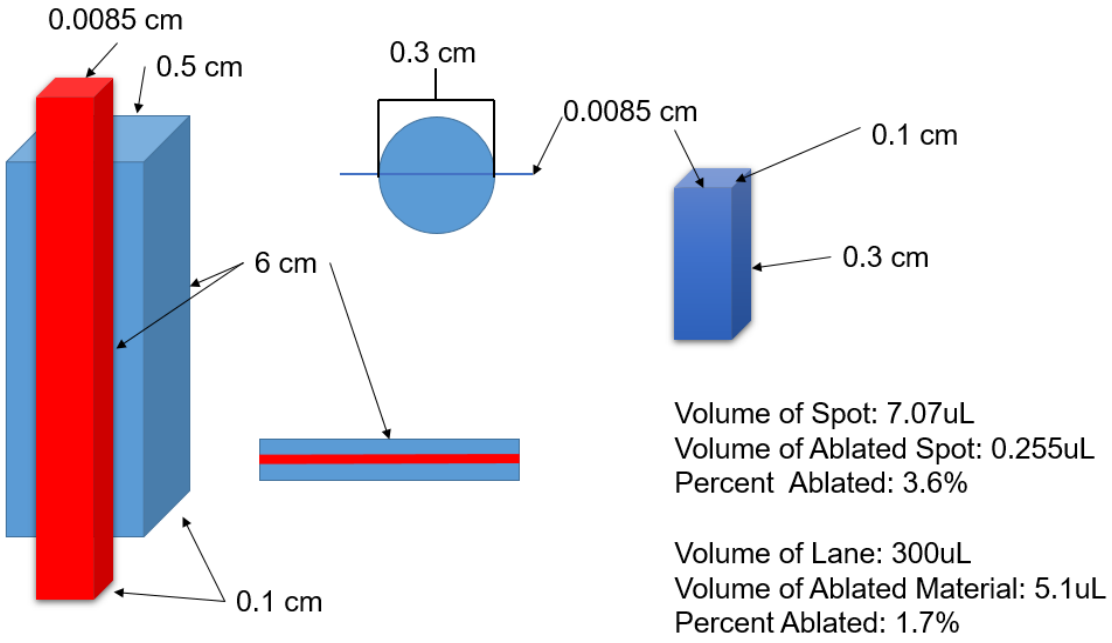

Figure 3.8

Calculation of amount of gel that is ablated.

The calculation of material ablated for a 1 µL standard and a single line scan of a polyacrylamide gel is shown in **figure 3.8**. The ratio of the area/volume of the lane and the total area/volume of the spot was calculated to adjust CPS to equate to the total moles applied to the gel. A standard curve can be established from those values and the slope is used to determine

the amount of metal detected during a line scan (**figure 3.8**). In the example shown, the counts per second were averaged from a blank line scan of a portion of gel to determine the background contribution of ^{66}Zn (**figure 3.9**) and ^{114}Cd (**figure 3.10**). Those values were subtracted from the area under the curve to achieve a more accurate standard curve (**figure 3.11-3.12**). The following equations are comprised of the averages ± standard deviation of 10 determinations of standard curves over a six-month period.

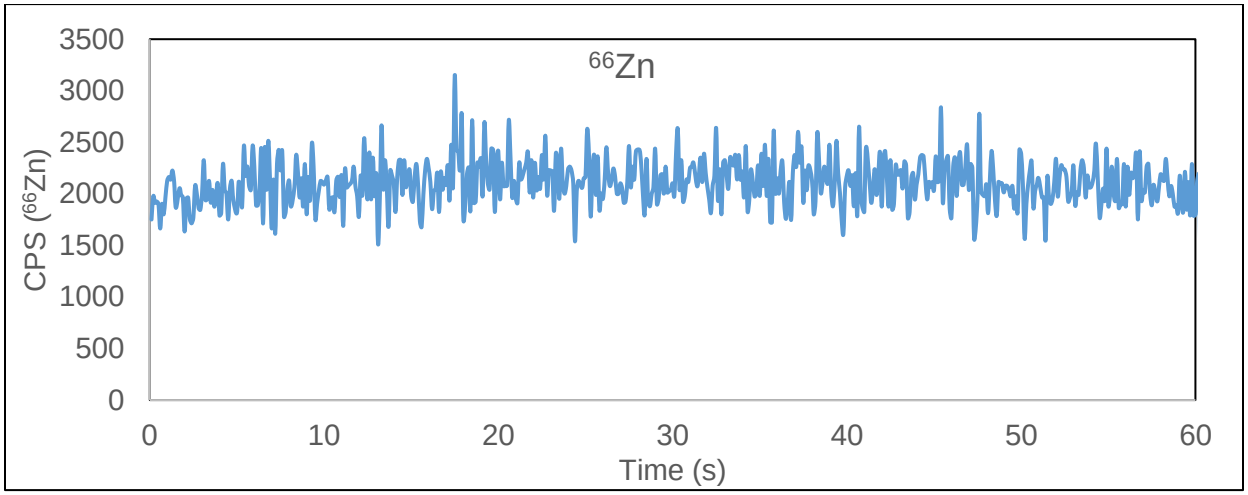

Figure 3.9

^{66}Zn background scan using optimized ablation parameters. Average CPS for the background is around 2000.

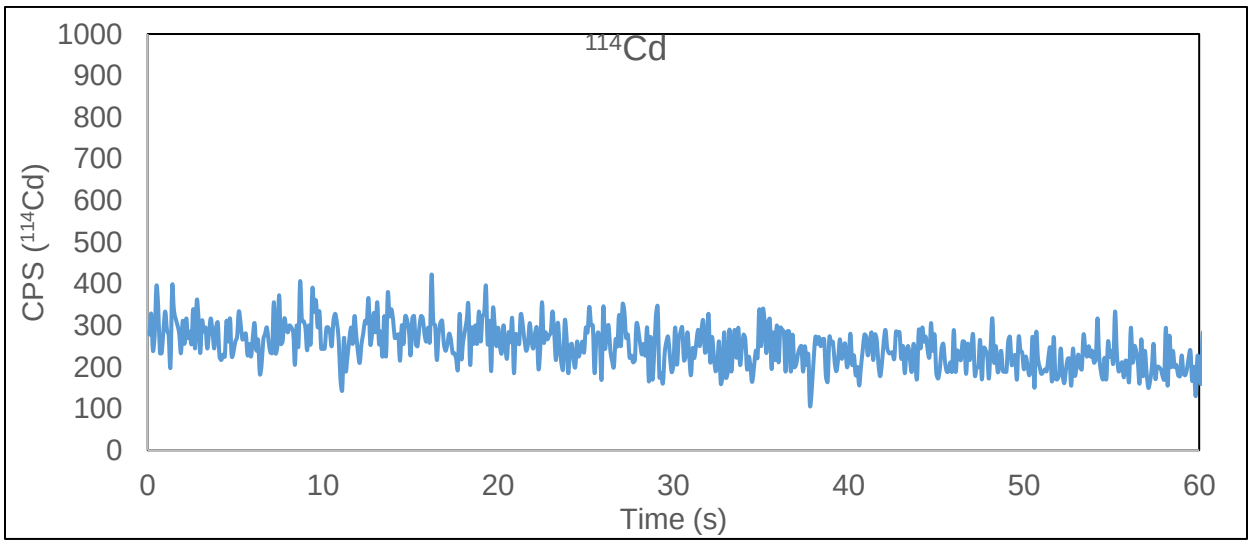

Figure 3.10

^{114}Cd background scan using optimized ablation parameters. Average CPS for the background is around 250.

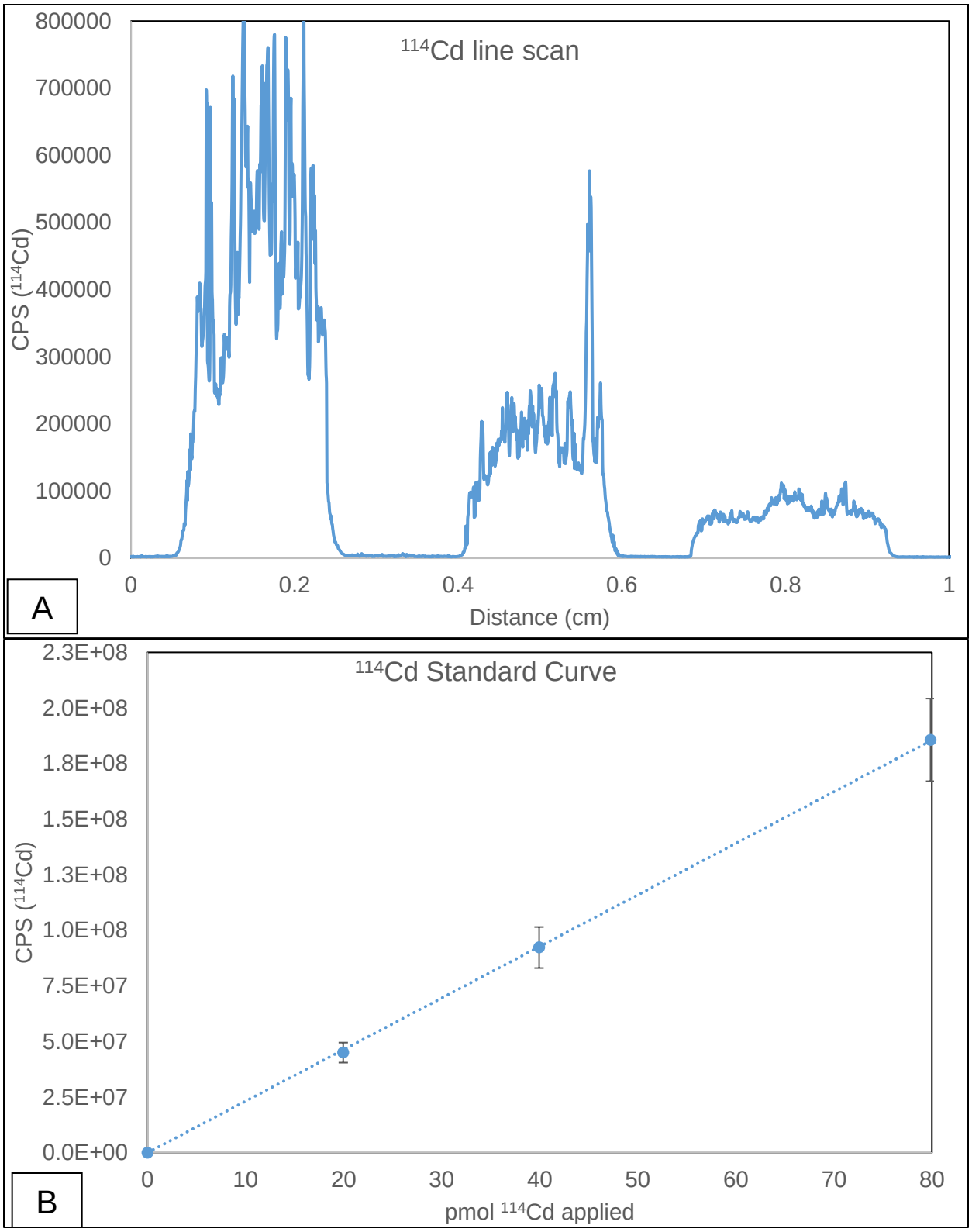

Figure 3.11

Ablation scan (Panel A) and standard curve of ^{114}Cd spotted standards (n = 10) (Panel B)

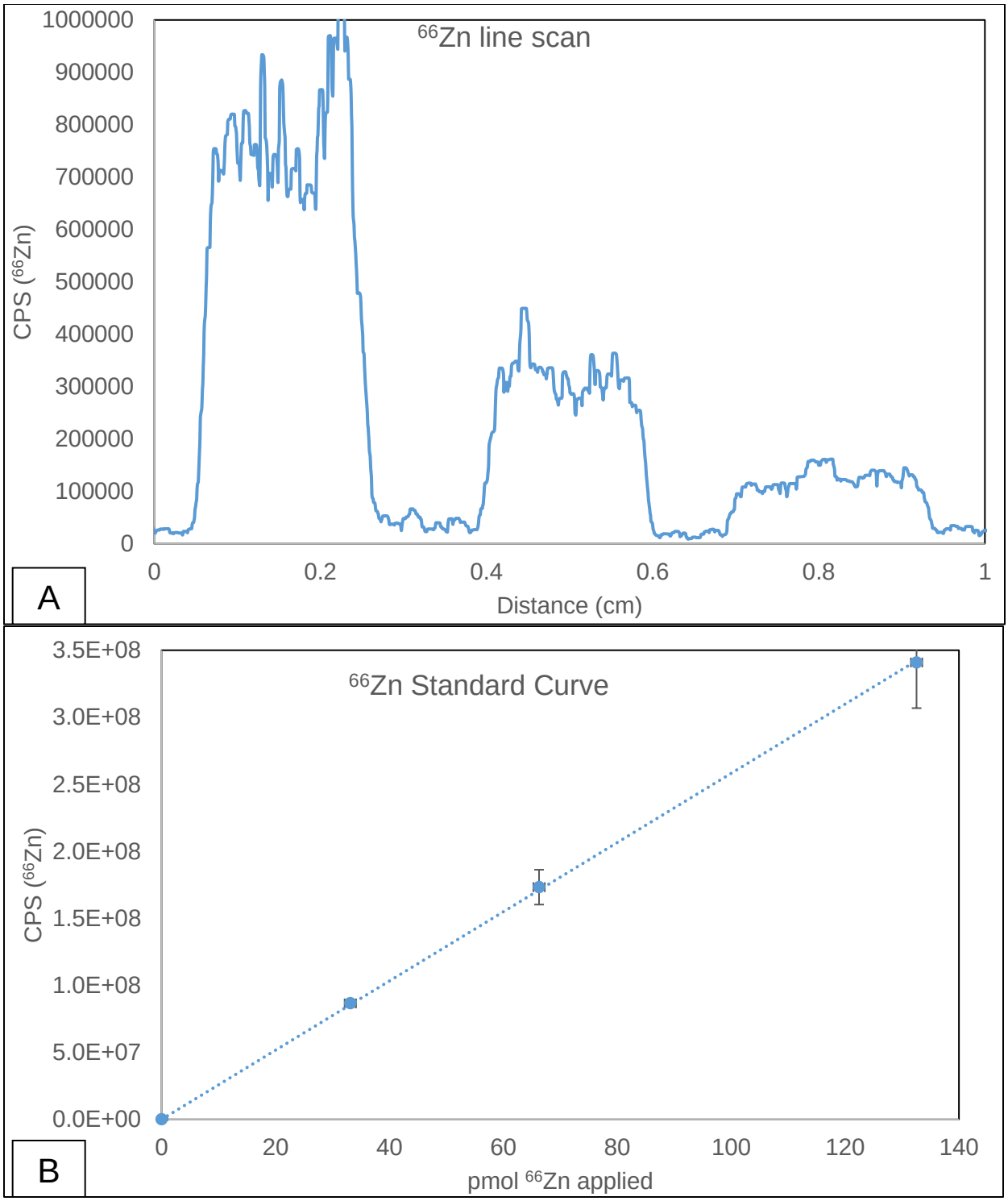

Figure 3.12

Ablation scan (Panel A) and standard curve of ^{66}Zn spotted standards (n = 10) (Panel B)

2.5.2 Isotopes

There are several isotopes to choose from that could be used for analysis of Zn^{2+} or Cd^{2+}. Zinc has five stable isotopes; cadmium has eight stable isotopes. ^{66}Zn and ^{114}Cd were chosen because isobaric (**figure 3.13**) and polyatomic interferences (**figure 3.14**) are negligible or non-existent. Isobaric interferences refer to atoms that might have the same mass as the isotope under examination but stem from different elements. Examples of possible polyatomic interferences for the isotope ^{66}Zn, which has an atomic mass of 65.92 amu, would be the following molecules correspond to that mass: $^{50}Ti^{16}O^{+}$, $^{34}S^{16}O_2^{+}$, $^{33}S^{16}O_2{}^{1}H^{+}$, $^{32}S^{16}O^{18}O^{+}$, $^{32}S^{17}O_2^{+}$, $^{33}S^{16}O^{17}O^{+}$, $^{32}S^{34}S^{+}$, $^{33}S_2^{+}$. Titanium is not present in the gel, the LLC-PK_1 cells, or standard proteins and is negligible. The isotope ^{33}S, although present, is 0.75% abundant and can be ignored. ^{32}S, being the most abundant isotope at 94.99%, would be a potential source of polyatomic interferences but ^{17}O is 0.04% abundant. The combination would be insignificant. ^{34}S is 4.25% abundant and a source of potential interference. Considering ^{114}Cd, $^{98}Mo^{16}O^{+}$ and $^{98}Ru^{16}O^{+}$ are not present in LLC-PK_1 cells, the gel, or the standards and are, thus, negligible when monitoring ^{114}Cd at 113.9 amu.

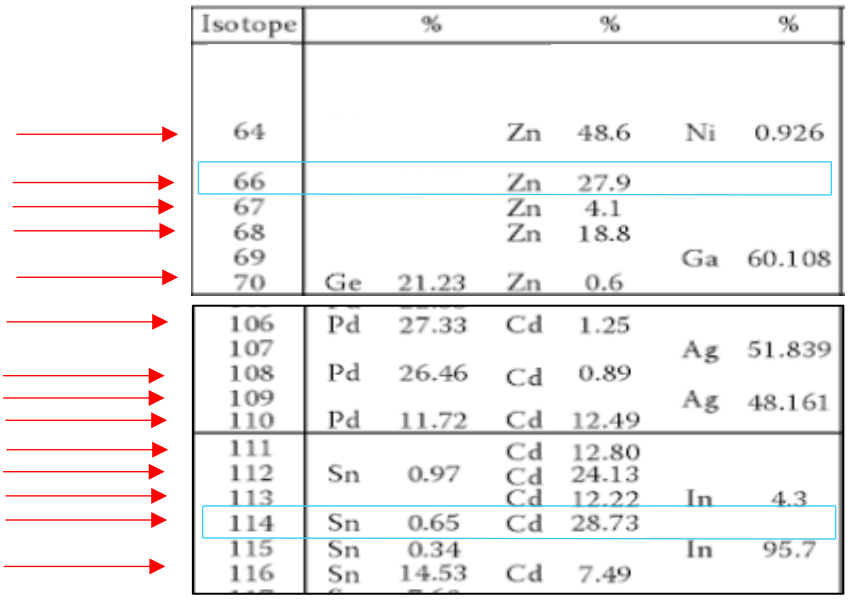

Isotope	%		%		%
64			Zn	48.6	Ni 0.926
66			Zn	27.9	
67			Zn	4.1	
68			Zn	18.8	
69					Ga 60.108
70	Ge	21.23	Zn	0.6	
106	Pd	27.33	Cd	1.25	
107					Ag 51.839
108	Pd	26.46	Cd	0.89	
109					Ag 48.161
110	Pd	11.72	Cd	12.49	
111			Cd	12.80	
112	Sn	0.97	Cd	24.13	
113			Cd	12.22	In 4.3
114	Sn	0.65	Cd	28.73	
115	Sn	0.34			In 95.7
116	Sn	14.53	Cd	7.49	

Figure 3.13

List of potential isobaric interferences.

Atomic Spectroscopy
Vol. 19(5), Sep./Oct. 1998

A Table of Polyatomic Interferences in ICP-MS (cont'd)

Isotope	Abundance	Interference
^{110}Cd	12.5	$^{39}K_2{}^{16}O^+$
^{111}Cd	12.8	$^{95}Mo^{16}O^+$, $^{94}Zr^{16}O^1H^+$, $^{39}K_2{}^{16}O_2{}^1H^+$
^{112}Cd	24.1	$^{40}Ca_2{}^{16}O_2$, $^{40}Ar_2{}^{16}O_2$, $^{96}Ru^{16}O^+$
^{113}Cd	12.22	$^{96}Zr^{16}O^1H^+$, $^{40}Ca_2{}^{16}O_2{}^1H^+$, $^{40}Ar_2{}^{16}O_2{}^1H^+$, $^{96}Ru^{17}O^+$
^{114}Cd	28.7	$^{98}Mo^{16}O^+$, $^{98}Ru^{16}O^+$
^{116}Cd	7.49	$^{100}Ru^{16}O^+$
^{64}Zn	48.89	$^{32}S^{16}O_2{}^+$, $^{48}Ti^{16}O^+$, $^{31}P^{16}O_2{}^1H^+$, $^{48}Ca^{16}O^+$, $^{32}S_2{}^+$, $^{31}P^{16}O^{17}O^+$ $^{34}S^{16}O_2{}^+$, $^{36}Ar^{14}N_2{}^+$
^{66}Zn	27.81	$^{50}Ti^{16}O^+$, $^{34}S^{16}O_2{}^+$, $^{33}S^{16}O_2{}^1H^+$, $^{32}S^{16}O^{18}O^+$, $^{32}S^{17}O_2{}^+$, $^{33}S^{16}O^{17}O^+$, $^{32}S^{34}S^+$, $^{33}S_2{}^+$
^{67}Zn	4.11	$^{35}Cl^{16}O_2{}^+$, $^{33}S^{34}S^+$, $^{34}S^{16}O_2{}^1H^+$, $^{32}S^{16}O^{18}O^1H^+$, $^{33}S^{34}S^+$, $^{34}S^{16}O^{17}O^+$, $^{33}S^{16}O^{18}O^+$, $^{32}S^{17}O^{18}O^+$, $^{33}S^{17}O_2{}^+$, $^{35}Cl^{16}O_2{}^+$
^{68}Zn	18.57	$^{36}S^{16}O_2{}^+$, $^{34}S^{16}O^{18}O^+$, $^{40}Ar^{14}N_2{}^+$, $^{35}Cl^{16}O^{17}O^+$, $^{34}S_2{}^+$, $^{36}Ar^{32}S^+$, $^{34}S^{17}O_2{}^+$, $^{33}S^{17}O^{18}O^+$, $^{32}S^{18}O_2{}^+$, $^{32}S^{36}S^+$
^{70}Zn	0.62	$^{35}Cl^{35}Cl^+$, $^{40}Ar^{14}N^{16}O^+$, $^{35}Cl^{17}O^{18}O^+$, $^{37}Cl^{16}O^{17}O^+$, $^{34}S^{18}O_2{}^+$, $^{36}S^{16}O^{18}O^+$, $^{36}S^{17}O_2{}^+$, $^{34}S^{36}S^+$, $^{36}Ar^{34}S^+$, $^{38}Ar^{32}S^+$

Figure 3.14

List of potential polyatomic interferences

2.5.3 Isotopic Distribution

An investigation was made into the isotopic ratio of Zn^{2+} on a polyacrylamide gel using LA-ICP-MS. Being a Sector ICP-MS, the instrument has the distinct ability to separate ions based on mass (see **Part III: Introduction**). Zinc is primarily composed of five stable isotopes: ^{64}Zn (49.17%) at 63.93 amu, ^{66}Zn (27.73%) at 65.93 amu, ^{67}Zn (4.04%) at 66.92 amu, ^{68}Zn (18.45%) and ^{70}Zn (0.61%), at 67.92 and 69.92 amu, respectively. If the isotopic ratio obtained from this experiment are correct, then it can be concluded that interferences are negligible not only for ^{66}Zn but other zinc isotopes as well. In turn, it should be safe to assume that the ^{66}Zn concentration is correct and representative of all the Zn^{2+} within a polyacrylamide gel.

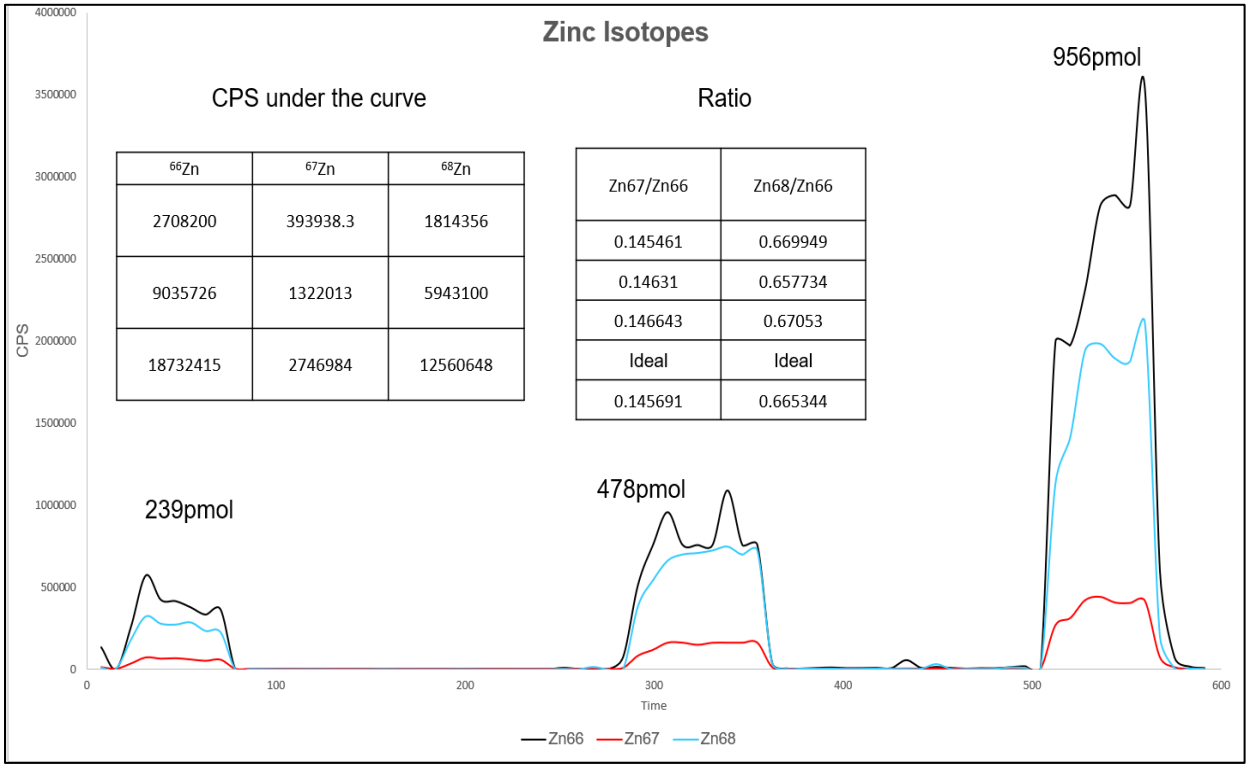

Figure 3.15

Distribution of zinc isotopes during ablation

^{66}Zn was the primary Zn^{2+} isotope of interest; therefore, ^{66}Zn was used in determining the ideal isotopic ratios of ^{66}Zn to ^{68}Zn and ^{67}Zn. The ratios were determined by ablating a section of gel after 1 µL standards were spotted on top and the CPS underneath the curve were determined.

The accepted ideal ratio (% to %) of ^{67}Zn (4.04%) to ^{66}Zn (27.73%) is 0.1457; while the ideal ratio of ^{68}Zn (18.45%) to ^{66}Zn (27.73%) is 0.6653. According to **figure 3.15**, the measured ratio of ^{67}Zn to ^{66}Zn is 0.1461 ± 0.0005 which is a 0.31% deviation from the accepted value. The measured ratio of ^{68}Zn to ^{66}Zn is 0.6661 ± 0.0059, which is a 0.11% deviation. **Figure 3.15** shows the isotopic ratio of Zn^{2+} experimentally obtained from ablation of a standard within a polyacrylamide gel are almost indistinguishable from the ideal ratios. Therefore, isotopic analysis of standards shows that the isotopic ratio is maintained and, therefore, ^{66}Zn and ^{114}Cd (data not shown) can be used for analysis.

2.6 Grubbs' Test for Outliers

Grubbs' test for outliers was developed to detect a single outlier in a data set that resides outside the approximate normal distribution (Grubbs et al. 1972). During successive runs using LA-ICP-MS, there are outliers in the data that would seem to be indicative of interferences during the ablation. Some interferences include those that have been listed in **figure 3.13-3.14**. Other potential interferences may come from mass loading, or other fractionation effects, in the ICP-MS. The Grubbs' Test for Outliers equation is listed below.

Grubbs' Test for Outliers

$$g = \frac{\max_{i=1..n} \left| x_i - \bar{x} \right|}{s}$$

Average

Standard Deviation

Equation 3.1

Grubb's Test for Outliers equation where X_i is the value of interest, X(bar) is the average of the values and S is the standard deviation of those values.

The Grubbs' Test uses a critical value table when n = 3. The critical value, ***g***, is defined as the absolute value of the datum in question minus the average of all the data points, the difference

divided by standard deviation among all data points. ***g*** must be less than 1.15, according to the critical table value; otherwise the value is considered an outlier and can be ignored. For this dissertation, the ***g*** value was set more stringently to 0.8 in the data analysis.

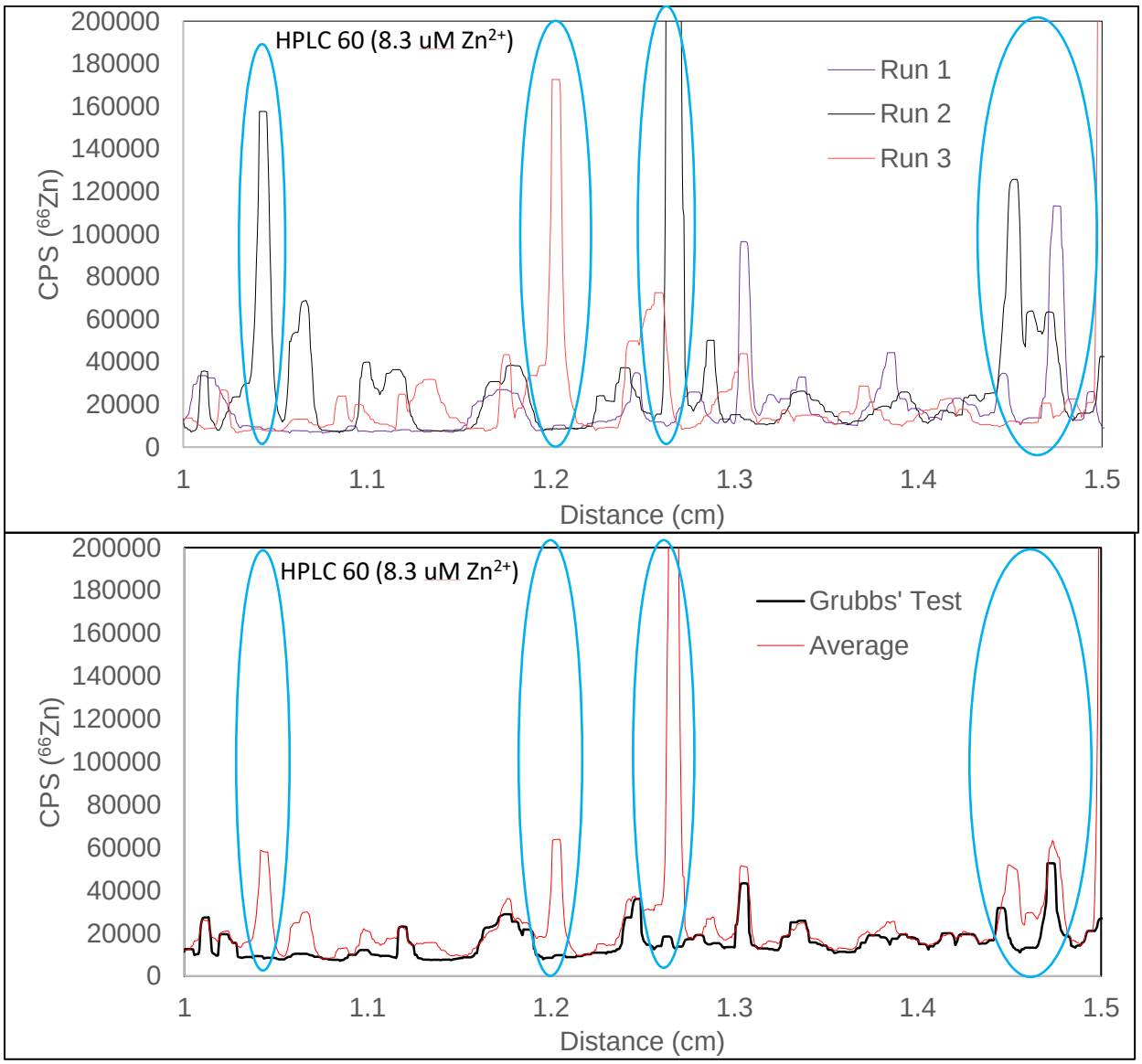

Figure 3.16

Grubbs' test applied to LA-ICP-MS spectra. Circles denotate areas where Grubbs' Test was applied.

Potential spikes that appear as mass loading or fractionation are shown in **figure 3.16** and are denoted by the circles. When **equation 3.1** was applied to the data from the lane ablation, the

second spectra was the result. Looking at the second spectra, the average of the three laser ablation runs (Red line) was much less correlated than when Grubbs' test was applied (Black line).

3. Results and Discussion

3.1 Background experiments with the Zinc Fluorophore, TSQ

Zinc fluorescent sensors have been developed to detect Zn^{2+}. Our laboratory discovered that a major sensor, TSQ, binds to Zn-proteins in the Proteome, Zn-Proteome, and non-specific zinc binding sites that are also part of the Proteome, Proteome•Zn, and in the process emits fluorescence centered at about 475 nm (Meeusen et al. 2011).

$$\text{Zn-Proteome} + \text{TSQ} \leftrightharpoons \text{TSQ-Zn-Proteome} \quad (3.2)$$

$$\text{Proteome•Zn} + \text{TSQ} \leftrightharpoons \text{Proteome•Zn-TSQ} \quad (3.3)$$

Previous studies have shown that TSQ-Zn-protein complexes can be separated by NSDS-PAGE and then be detected fluorometrically (Nowakowski et al. 2015). It was important to compare the results of the new method of detection, LA-ICP-MS, with this method. Several experiments were conducted to prepare for this comparison.

We compared the fluorescence intensities derived from the interaction of Zn^{2+} and Cd^{2+} with TSQ. As seen in **figure 3.17-3.18**, TSQ reacts with both Zn^{2+} and Cd^{2+} to generate a 2:1 complex.

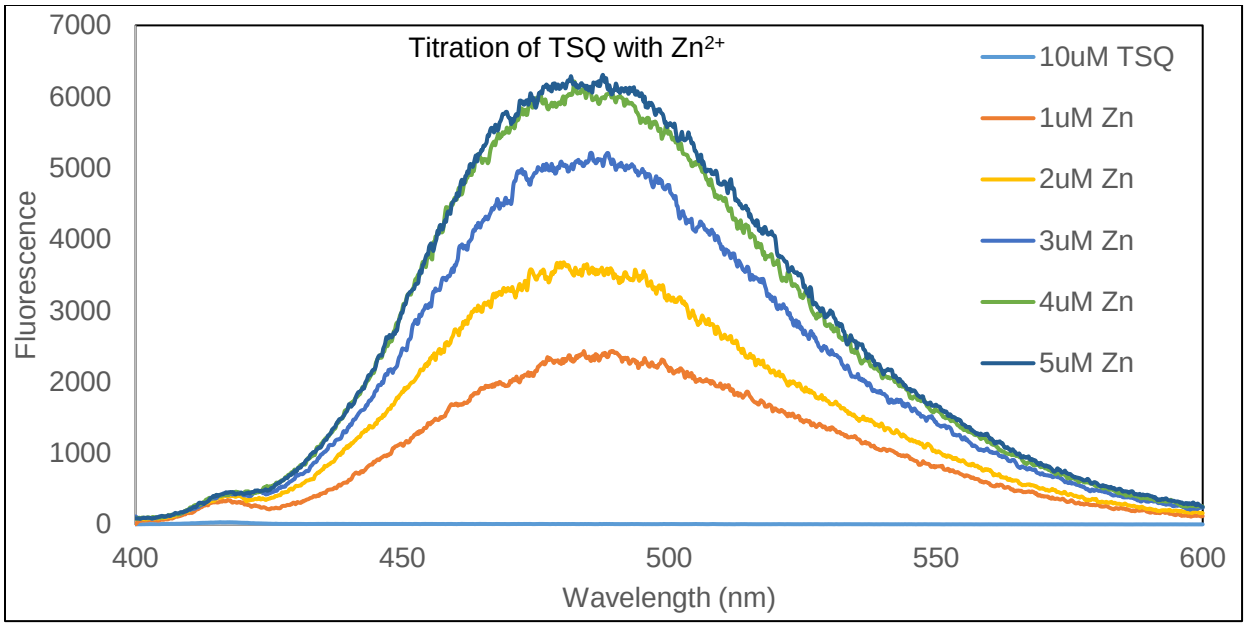

Figure 3.17

Titration of TSQ with Zn^{2+}. Titration of 10 μM TSQ in 20 mM Tris pH 7.4 with Zn^{2+}. 10 minutes in between additions. Excitation wavelength was 365 nm. Emission wavelength span was 400-600 nm.

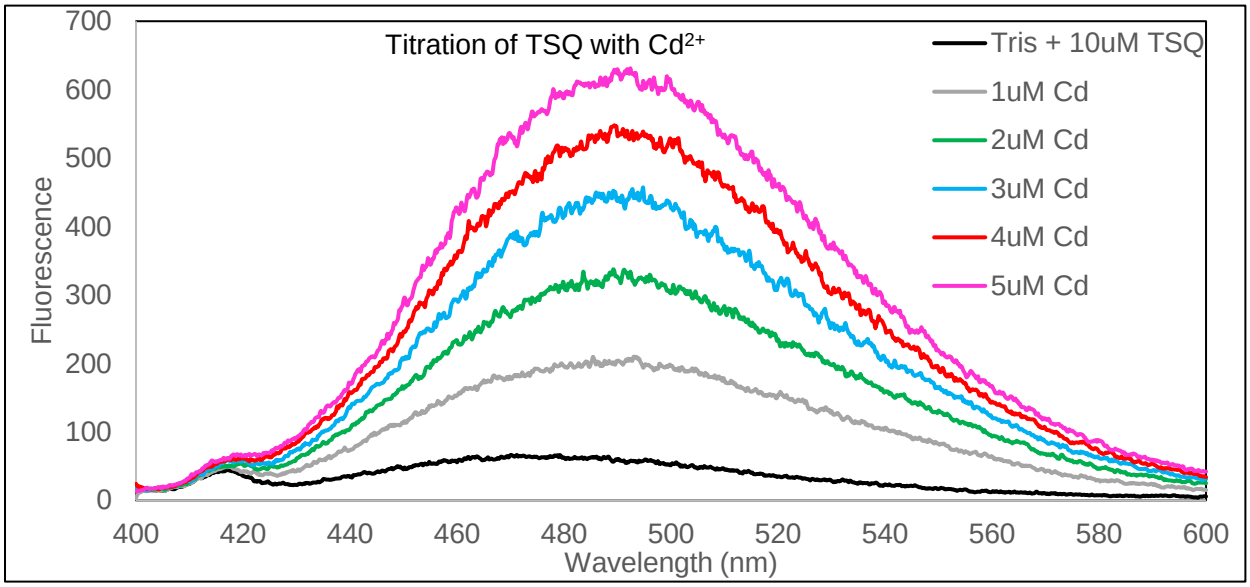

Figure 3.18

Titration of TSQ with Cd^{2+}. Titration of 10 μM TSQ in 20 mM Tris pH 7.4 with Cd^{2+}. 10 minutes in between additions. Excitation wavelength was 365 nm. Emission wavelength was 400-600 nm.

Both $Zn(TSQ)_2$ and $Cd(TSQ)_2$ display a fluorescence emission maximum at 490 nm. Notably, the fluorescence intensity of the zinc complex was 10 times that of the cadmium complex.

Next, the properties of the reaction of TSQ with Zn-Proteome + Proteome•Zn was investigated. In the first experiment, an excess of TSQ was added to Zn-Proteome to generate TSQ-Zn-Proteome. Then, the sample was titrated with Zn^{2+}. **Figure 3.19**-**3.20** describe the results.

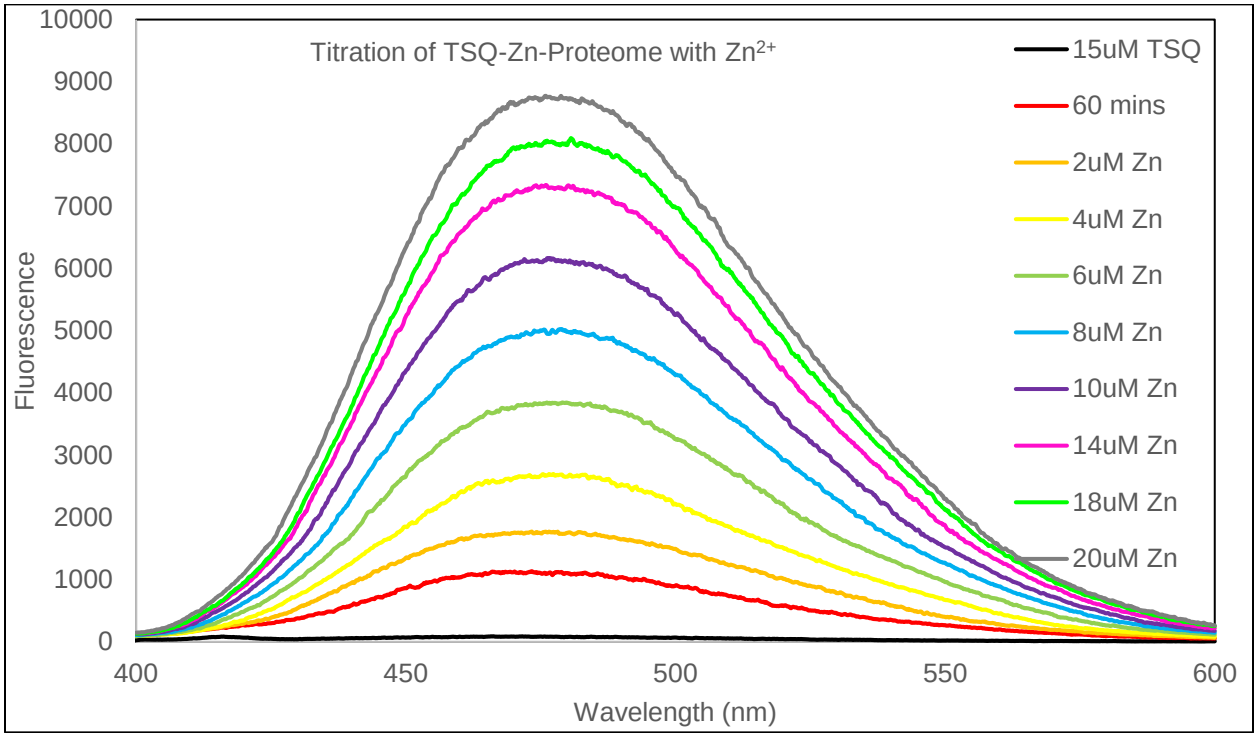

Figure 3.19.
Titration of TSQ-Zn-Proteome with Zn^{2+}. 2.5 µM Zn-Proteome was incubated with 15 µM TSQ in 20 mM Tris pH 7.4 for 60 minutes prior to addition of Zn^{2+}. 1 minute in between additions. Excitation wavelength was 365 nm. Emission wavelength span was 400-600 nm.

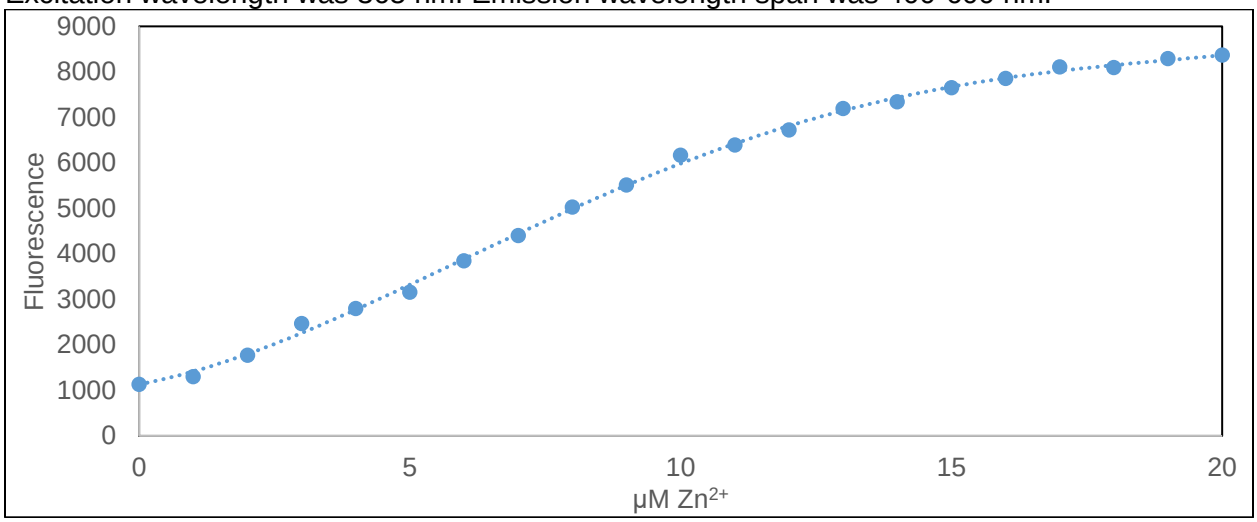

Figure 3.20.
Titration curve of TSQ-Zn-Proteome with Zn^{2+}. 2.5 µM Zn-Proteome was incubated with 15 µM TSQ in 20 mM Tris pH 7.4 for 60 minutes prior to addition of Zn^{2+}. 1 minute in between additions. Excitation wavelength was 365 nm. Emission wavelength span was 400-600 nm.

The initial spectrum reflected the formation of TSQ-Zn-Proteome after 60 min of incubation of the Zn-Proteome with TSQ. Thereafter, additions of Zn^{2+} led mostly to the steady increase in the intensity of the fluorescence emission with the spectral wavelength maximum remaining between 475- 485 nm, consistent with the formation of ternary adducts throughout the titration (**figure 3.19**). Toward the end of the titration, it appears that a measurable equilibrium is established between 'free' and bound Zn^{2+} (**figure 3.20**). Notably, whereas the formation of TSQ-Zn-Proteome occurred slowly over the course of 60 min, the production of Proteome•Zn-TSQ occurred quickly within 1 minute**.**

3.2 Individual Zinc Proteins

3.2.1 Bovine Serum Albumin

Zinc trafficking in plasma is centered on serum albumin (Dyke et al. 1987). In our experiments, Bovine Serum Albumin (BSA) was utilized. Serum Albumin plays an essential role in the transport and metabolism of Zn^{2+} based on its moderate stability constant for Zn^{2+} of $10^{7.3}$ at pH 7.4 (Masuoka et al. 1993). The concentration of Humans Serum Albumin is ~600 μM (Finali et al. 2012). As to the extent of research done investigating LA-ICP-MS and Zn-proteins, no work was found that involved LA-ICP-MS of Bovine Serum Albumin after PAGE separation.

At the outset, 11.7 mg of Zn-BSA powder (Sigma) was mixed with 2 mL $_{dd}$H2O to make 88 μM Zn-BSA. Then, 15.9 μL was mixed with 4.1 μL glycerol and applied to the polyacrylamide gel for electrophoresis using NSDS-PAGE (**section 2.2**). Two gels were run in tandem for experimentation: one gel was stained for protein using Coomassie R-250 (**section 2.3.1**) and TSQ stain (**section 2.3.3**); the other gel was dried for LA-ICP-MS (**section 2.3.2**). Using the optimized conditions (**section 2.4**-**2.5**), the dried polyacrylamide gel was ablated and analyzed. Typical results are found in **figure 3.21**. Each lane was ablated at least three times (separated by 190 μm) then subjected to Grubbs' Test (**section 2.6**).

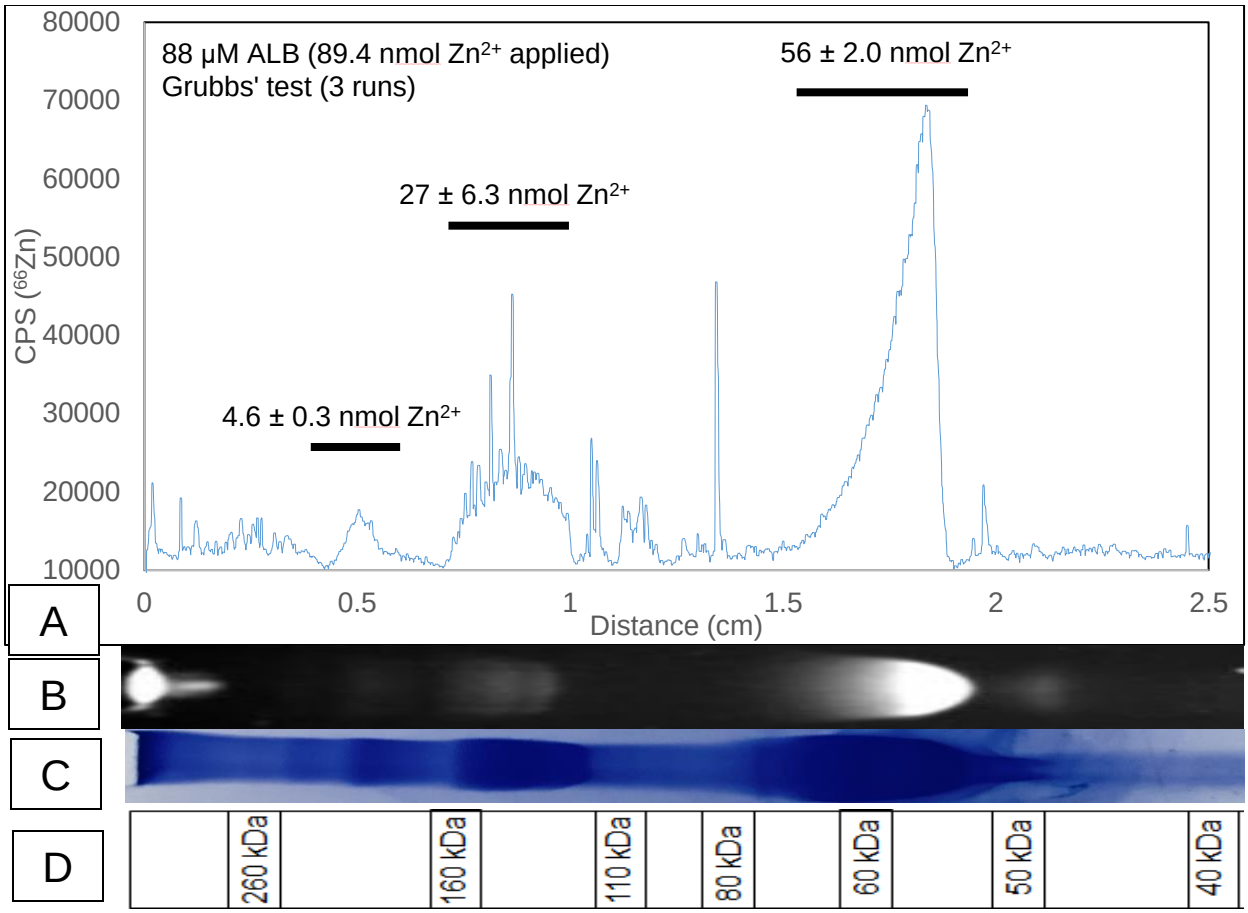

Figure 3.21

A. LA-ICP-MS spectra of 88 µM BSA (89.4 nmol Zn^{2+} applied) separated using NSDS-PAGE. Quantitation from Zn^{2+} standards run that day. Standard deviation based on the quanitation of 3 ablated runs.
B. TSQ stained polyacrylamide gel
C. Coomassie stained polyacrylamide gel
D. 12% Bis-Tris Gel migration chart (reproduced from Thermo Fisher Scientific website).

LA-ICP-MS revealed two strong bands of Zn^{2+} (one peak centered at 1.75 cm and another at 0.75 cm) and one weaker band (peak centered at 0.5 cm) (**figure 3.21;** panel A). According to the migration chart (**figure 3.21**; panel D) that is based on the migration of proteins through 12% Bis-Tris under denaturing conditions in SDS-PAGE, these bands respectively correspond to molecular weights centered around 60, 130, and 200 kDa. BSA has a molecular weight of 66.5 kDa. Thus, these bands correspond to monomer, dimer, and trimer species of Zn-Albumin. Moreover, the integrated content of zinc within these three bands is 88 nmol (Black lines), an

excellent agreement with the amount of zinc that was placed onto the gel at the beginning of electrophoresis. Similarly, in panel C (**figure 3.21**), the same three regions of the gel contain protein as indicated by presence of the Coomassie Blue stain. Together, panels A and C demonstrate the congruent migration of zinc and Albumin through the gel as Zn-$(Albumin)_n$ where n varies from 1 to 3.

In data not shown, it was demonstrated that TSQ reacts with Zn-Albumin to form a fluorescent adduct with emission wavelength maximum at 475 nm.

$$\text{Zn-Albumin} + \text{TSQ} \leftrightharpoons \text{TSQ-Zn-Albumin} \qquad (3.4)$$

The TSQ-stained gel also reveals two clearly fluorescent bands at 60 and 130 kDa and a very faint band at 200 kDa (**figure 3.21**; panel B). Their presence further supports the finding of several species of Zn-Albumin along the electrophoresis lane. A small fluorescent band remains at the origin and surely represents Zn-Albumin that did not enter the gel.

These results are also significant in that they demonstrate (**1**) that under conditions of electrophoresis that are thought to retain native structural characteristics of proteins, 66 kDa Zn-Albumin migrates much like it would during SDS-PAGE. In addition, (**2**) under native conditions, self-association occurs so that dimer and trimer forms are detected as well. Furthermore (**3**), Albumin retains its complement of moderately strongly bound Zn^{2+} (binding affinity of $10^{7.3}$ at pH 7.4), showing that the native conditions of electrophoresis permit the retention of Zn^{2+} by Albumin, even though the binding site is not kinetically inert to ligand substitution and metal ion exchange.

3.2.2 Carbonic Anhydrase

Carbonic anhydrase (CA) was the first zinc-dependent metalloenzyme discovered and has been under intense investigation since 1933 (Meldrum et al. 1933). Three histidine ligands are directly coordinated to the catalytic zinc metal center (Hurst et al. 2010). Compared to BSA, CA

has a Zn^{2+} bound within its structure with an association constant of 10^{12} at pH 7.4 (Hunt et al. 1997). Previous experiments have shown that Zn-CA can be separated using non-denaturing conditions and retain its metal-protein complex in the process (Raab et al. 2009). Zn-CA was used to examine a limit of detection for Zn-proteins, using LA-ICP-MS, for further applications to apply to a collection of Zn-proteins, such as the Proteome.

A stock solution of 4.64 mg of Zn-CA powder was mixed with 10 mL $_{dd}$H2O to make 15.47 µM Zn-CA. 15.0 µL was mixed with 5 µL glycerol and applied to the polyacrylamide gel before being separated using NSDS-PAGE (**section 2.2**). Serial dilutions were made with the stock solution of Zn-CA for analysis. Two gels were run in tandem for the experiment: one gel was stained for protein using Coomassie R-250 (**section 2.3.1**) and the fluorescent detection of Zn-protein with TSQ stain (**section 2.3.3**); the other was dried for laser ablation (**section 2.3.2**). Using the optimized conditions (**section 2.4**-**2.5**), the dried polyacrylamide gel was subjected to LA-ICP-MS and the results are found below (**figure 3.22** – **3.25**).

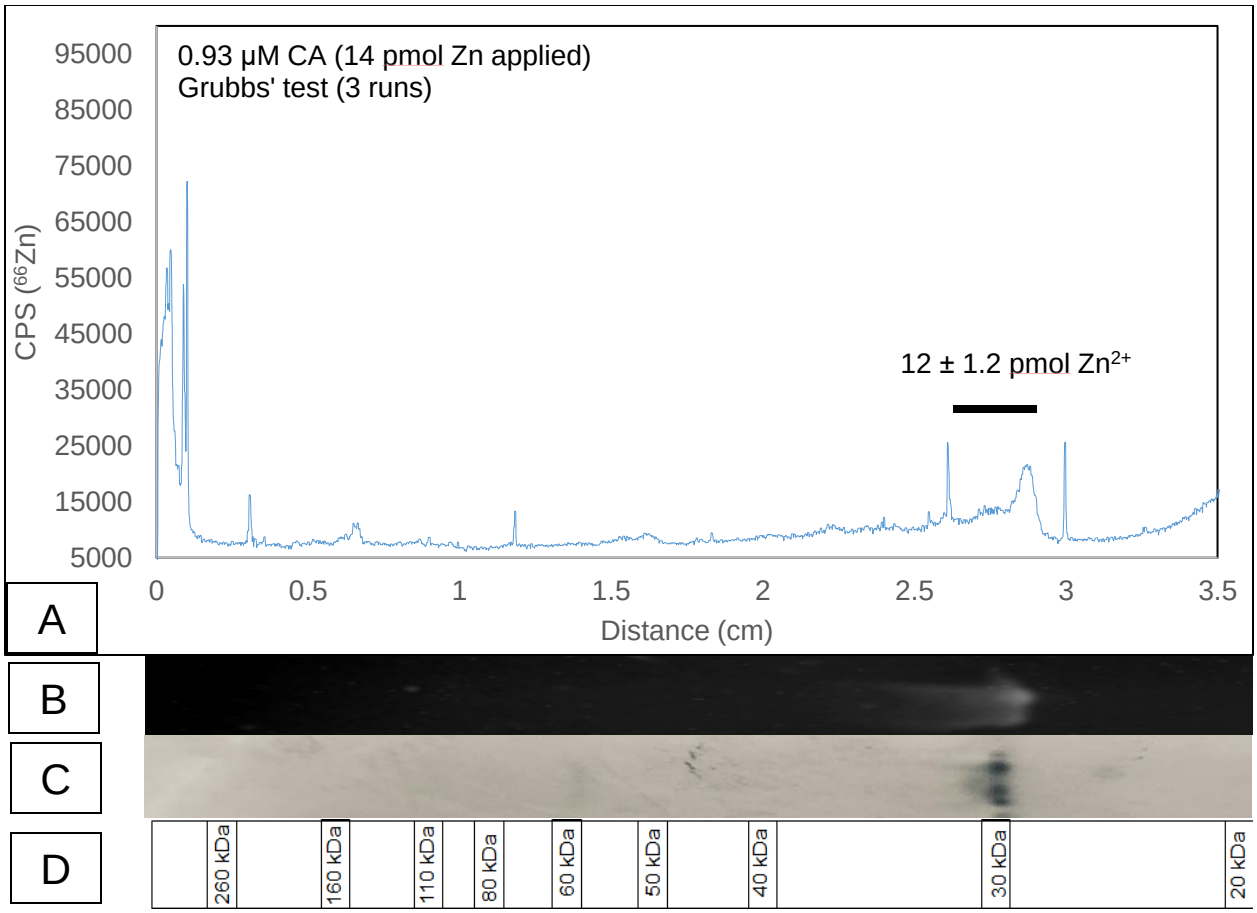

Figure 3.22

A. LA-ICP-MS spectra of 930 nM Zn-CA (14 pmol Zn^{2+} applied) separated using NSDS-PAGE. Quantitation based on Zn^{2+} standards run that day. Standard deviation based on the quanitation of 3 ablated runs.
B. TSQ stained polyacrylamide gel
C. Coomassie stained polyacrylamide gel
D. 12% Bis-Tris Gel migration chart (reproduced from Thermo Fisher Scientific website).

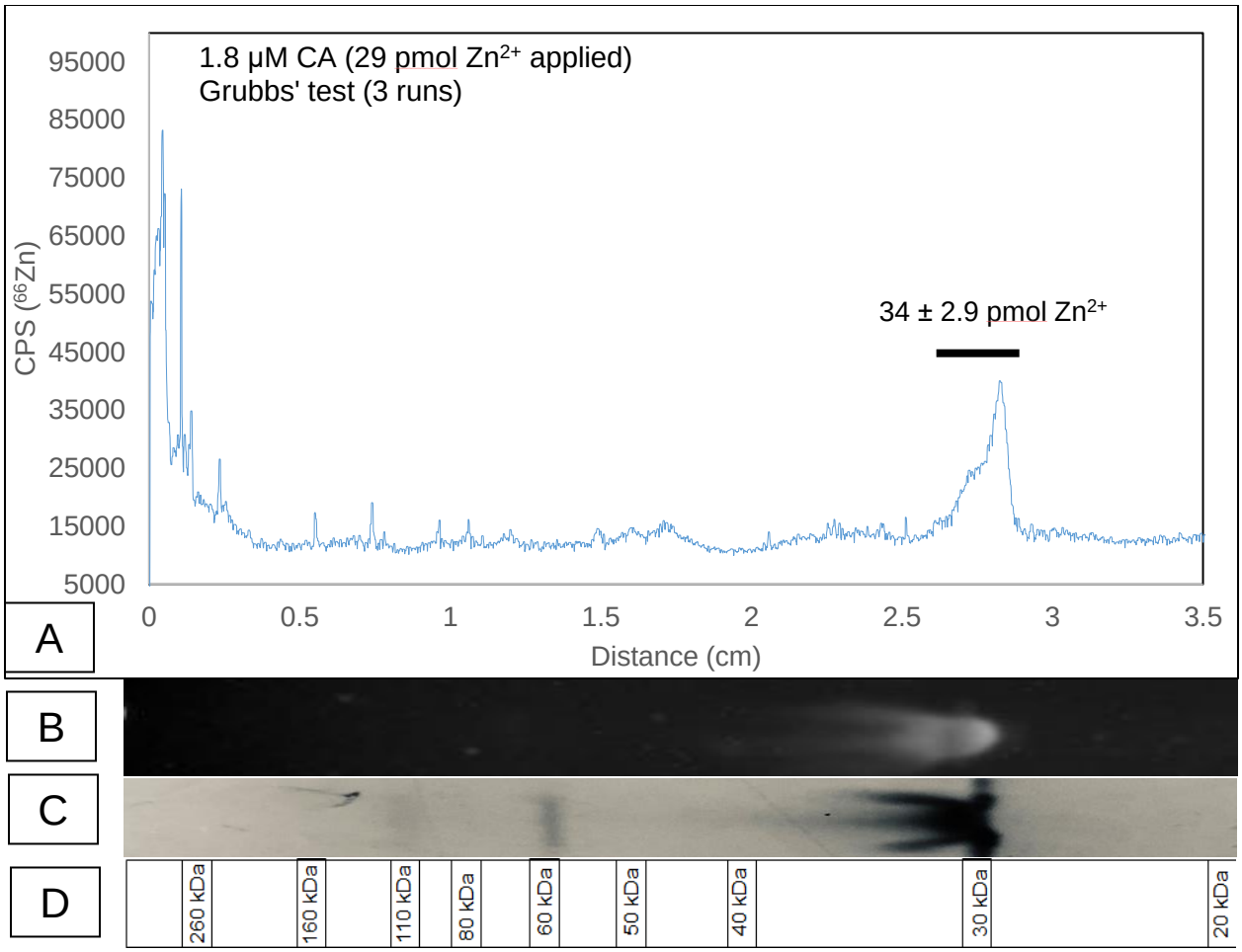

Figure 3.23

A. LA-ICP-MS spectra of 1.86 µM Zn-CA (29 pmol Zn^{2+} applied) separated using NSDS-PAGE. Quantitation based on Zn^{2+} standards run that day. Standard deviation based on the quanitation of 3 ablated runs.
B. TSQ stained polyacrylamide gel
C. Coomassie stained polyacrylamide gel
D. 12% Bis-Tris Gel migration chart (reproduced from Thermo Fisher Scientific website).

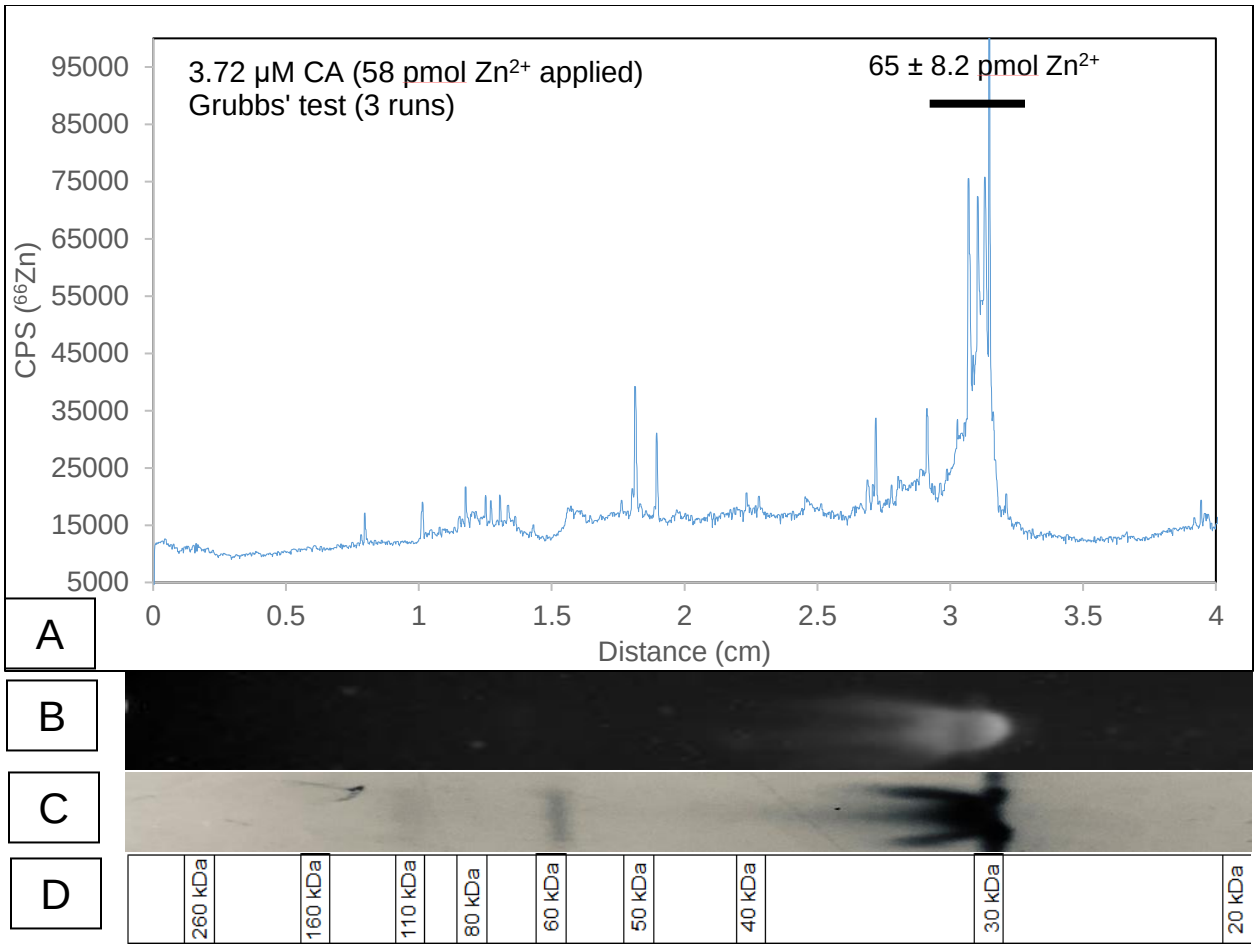

Figure 3.24

A. LA-ICP-MS spectra of 3.72 µM Zn-CA (58 pmol Zn^{2+} applied) separated using NSDS-PAGE. Quantitation based on Zn^{2+} standards run that day. Standard deviation based on the quanitation of 3 ablated runs.
B. TSQ stained polyacrylamide gel
C. Coomassie stained polyacrylamide gel
D. 12% Bis-Tris Gel migration chart (reproduced from Thermo Fisher Scientific website).

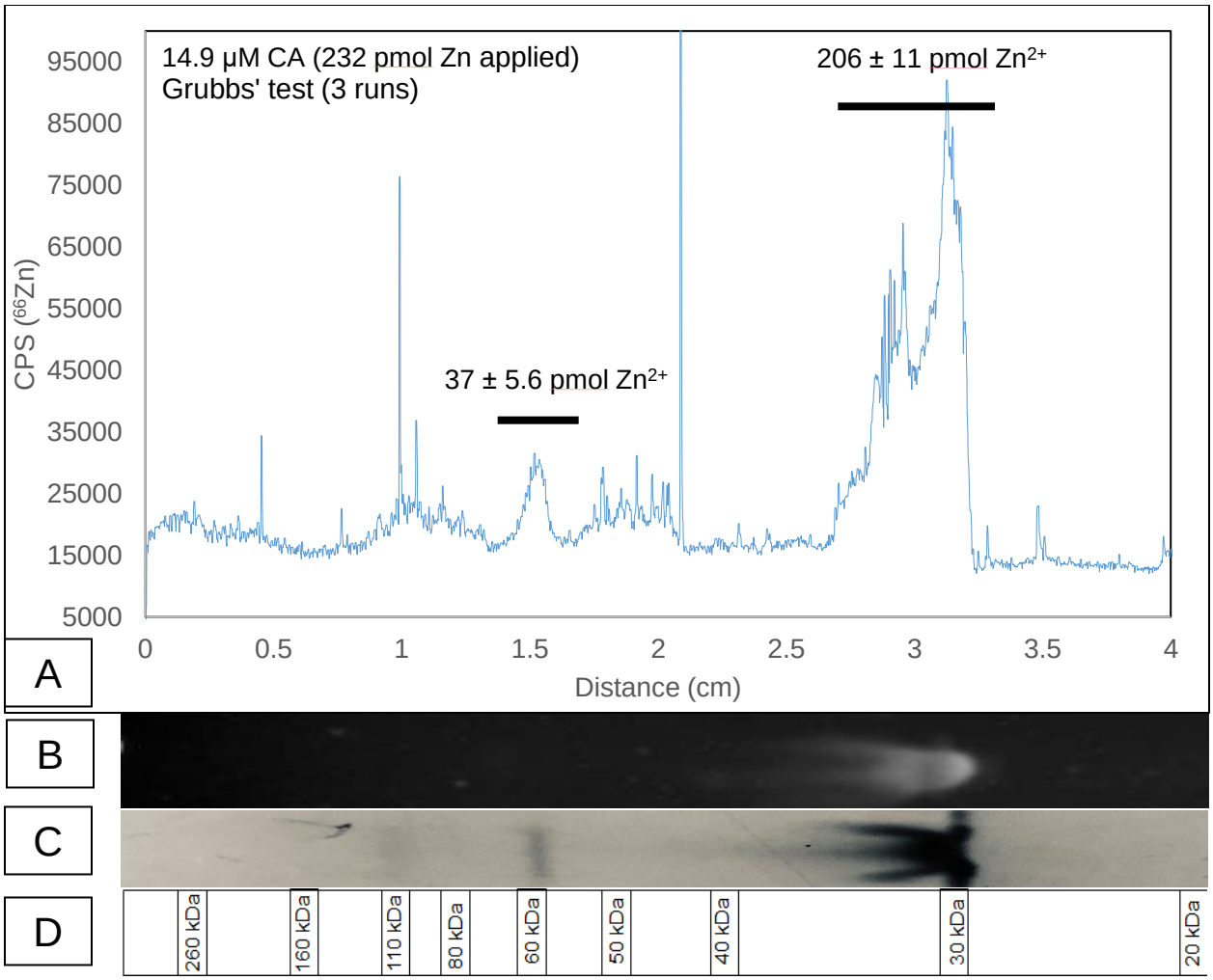

Figure 3.25

A. LA-ICP-MS spectra of 14.9 µM Zn-CA (232 pmol Zn^{2+} applied) separated using NSDS-PAGE. Quantitation based on from Zn^{2+} standards run that day. Standard deviation based on the quanitation of 3 ablated runs.
B. TSQ stained polyacrylamide gel
C. Coomassie stained polyacrylamide gel
D. 12% Bis-Tris Gel migration chart (reproduced from Thermo Fisher Scientific website).

Carbonic anhydrase has a molecular weight of approximately 30.0 kDa (29,000). The migration chart of proteins through a 12% Bis-Tris polyacrylamide gel is shown (**figure 3.22-3.25**; panel C). The major peak, centered around 3 cm, is indicative of 30 kDa monomer, based on the migration chart and the LA-ICP-MS spectra (**figure 3.22-3.25**; panel A). Both the TSQ and Coomassie stain display a band around 3 cm (**figure 3.22-3.25**; panel B and panel C). As the

concentration of CA increased, another band is formed at 1.5 cm and lines up with 60 kDa, indicative of a possible dimer formation. The TSQ stain displays the fluorescence from adduct formation of TSQ to Zn-proteins, in this case Zn-CA. A fluorescent band is not apparent for a putative dimer, probably because its' concentration is too low to observe. Since the bands revealed by LA-ICP-MS, TSQ staining and Coomassie staining are coincident, it is clear the LA-ICP-MS measurements detect ^{66}Zn bound to CA after NSDS-PAGE separation, consistent with the maintenance of the native conformation of the protein and its' retention of Zn^{2+}. The activity of Carbonic Anhydrase was previously tested following a NSDS-PAGE separation (**section 2.2**) and was found to be active, also indicative of an intact native conformation (Nowakowski et al. 2014).

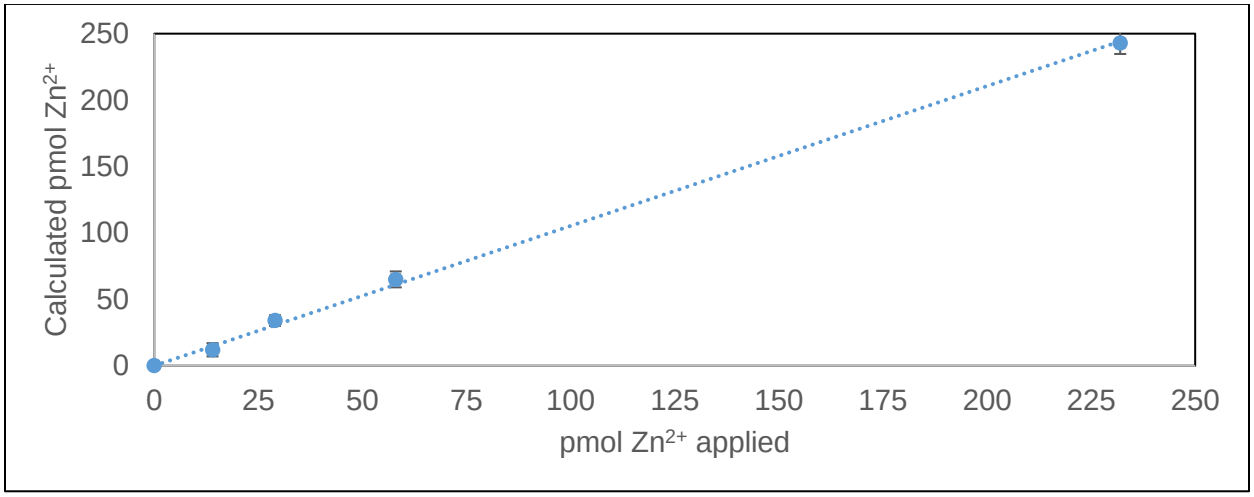

Figure 3.26

Zn-CA: Amount of Zn^{2+} applied vs. Zn^{2+} calculated based on Zn^{2+} standard curve.

Figure 3.26 plots the observed amount of zinc found in the four experiments versus the applied amounts for these electrophoretic runs. Both the linear relationship and the good agreement between applied and detected amounts of zinc show that the method provides quantitative results. Moreover, bands containing low pmol amounts of zinc can be readily detected in this type of experiment. The limit of detection for Zn-CA is around 14 pmol applied (**figure 3.22**). Attempts to go lower in concentration results in a S/N ratio that rendered Zn-protein recognition

improbable. The peak of Zn-CA seen in **figure 3.22** is comprised of three individual measurements. That being the case, it is clear that the LA-ICP-MS system can detect on the order of ~150 fmol of zinc delivered from the gel in a single laser pulse.

3.3 HPLC fraction 60

In the search of Zn-proteins inhibited by Cd^{2+} through the Cd-Zn exchange reaction, HPLC-DEAE was employed for the separation of Zn-proteins from the Proteome into 100 fractions for a more manageable number of Zn-proteins per fraction. Initially, 40 plates of confluent LLC-PK1 cells were harvested (**Part II: section 2.4**). The supernatant was put over a DEAE column for separation into 100 1 mL fractions (**Part II: section 2.5.2**) (**figure 3.27**). The absorbance at 280 nm was taken as a relative measure of protein concentration within the fractions. Fractions 52-60 were chosen for further analysis as they had the highest Zn^{2+} content (inlet **figure 3.27**). Fractions 55-60 were concentrated through a 3 kDa filter to give a collective fraction "60" which had a Zn^{2+} content of 8.3 μM.

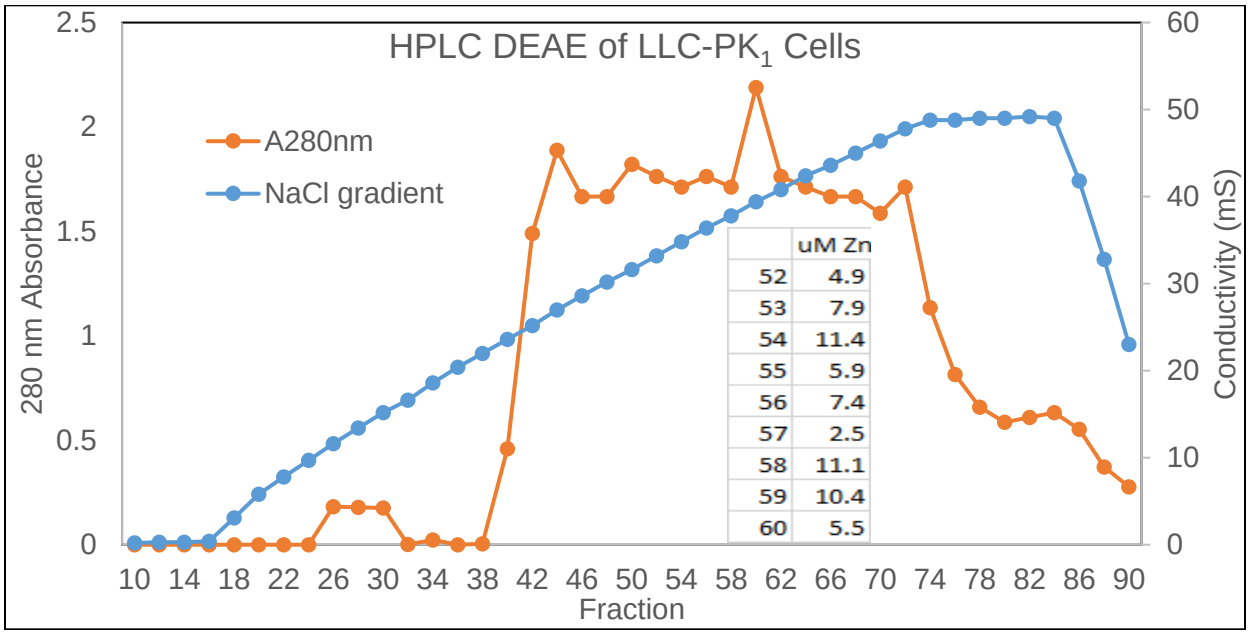

Figure 3.27
DEAE-HPLC separation of Proteome. 40 plates of confluent LLC-PK_1 cells were harvested and then separated by a DEAE column.

3.3.1 Reproducibility of the NSDS-PAGE LA-ICP-MS method

3.3.1.1 Reproducibility of NSDS-PAGE LA-ICP-MS within a lane

Reproducibility was a major concern regarding the analysis of a collection of Zn-proteins in solution separated by NSDS-PAGE. To test the reproducibility of this novel method within a single lane, HPLC fraction 60 was chosen for analysis. A 15 µL sample (5 µL glycerol added) was added to a 12% Bis-Tris polyacrylamide lane, electrophoresed by NSDS-PAGE (**section 2.2**) and subjected to analysis using LA-ICP-MS (**section 2.4-2.5**). One lane was subjected to three LA-ICP-MS line scans and the resulting profiles compared (**figure 3.28-3.30**; panel A). Also shown in panel B are the patterns of Zn-proteins that have formed TSQ-Zn-protein adducts (see **section 2.7**). Panel C provides the Coomassie Blue staining profile for protein, followed by the standard molecular weight markers for proteins migrating during SDS-PAGE (panel D).

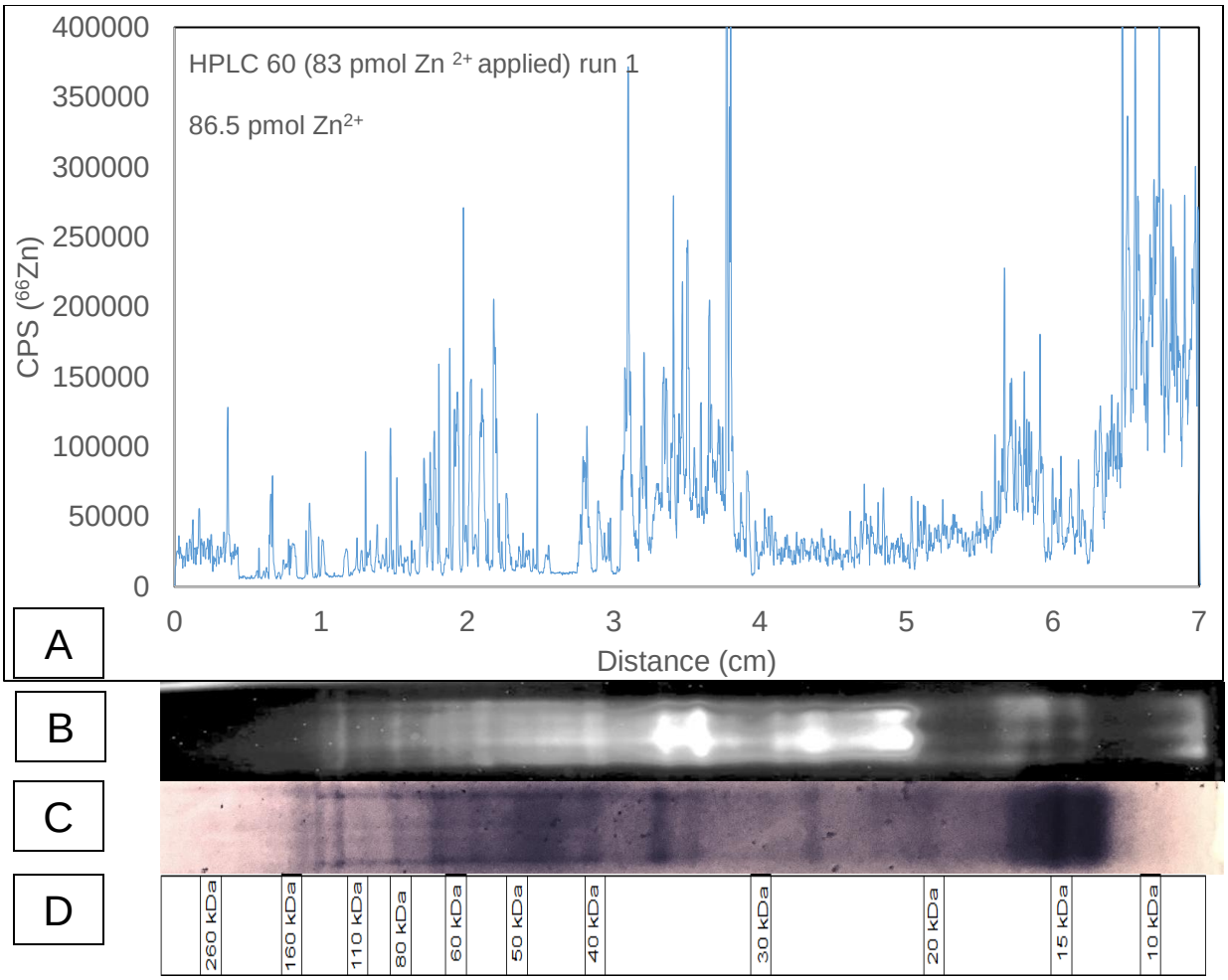

Figure 3.28

A. LA-ICP-MS spectra of HPLC fraction 60 run 1 (83 pmol Zn^{2+} applied) separated using NSDS-PAGE. Quantitation based on Zn^{2+} standards run that day.
B. TSQ stained polyacrylamide gel
C. Coomassie stained polyacrylamide gel
D. 12% Bis-Tris Gel migration chart (reproduced from Thermo Fisher Scientific website).

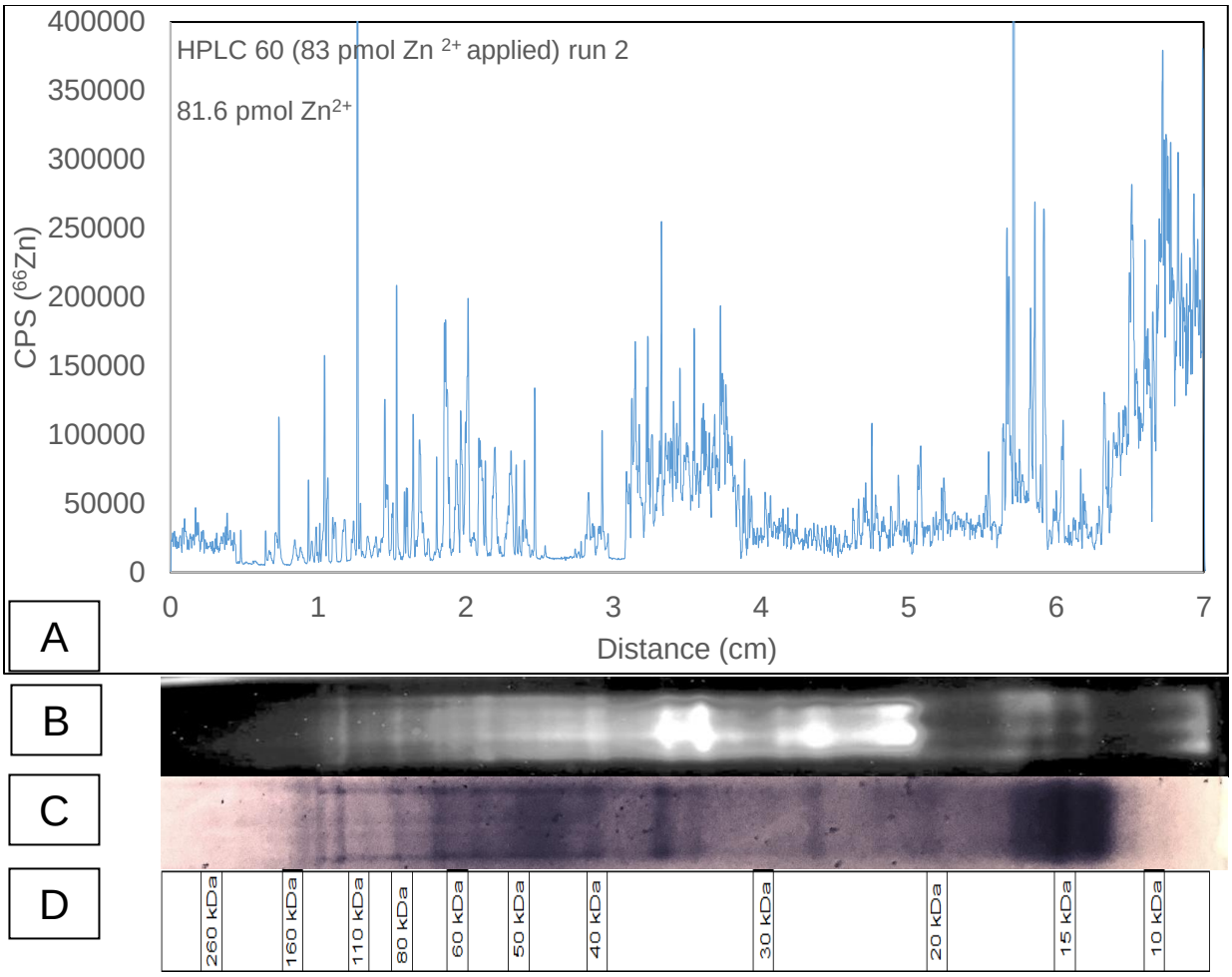

Figure 3.29

A. LA-ICP-MS spectra of HPLC fraction 60 run 2 (83 pmol Zn^{2+} applied) separated using NSDS-PAGE. Quantitation based on Zn^{2+} standards run that day.
B. TSQ stained polyacrylamide gel
C. Coomassie stained polyacrylamide gel
D. 12% Bis-Tris Gel migration chart (reproduced from Thermo Fisher Scientific website).

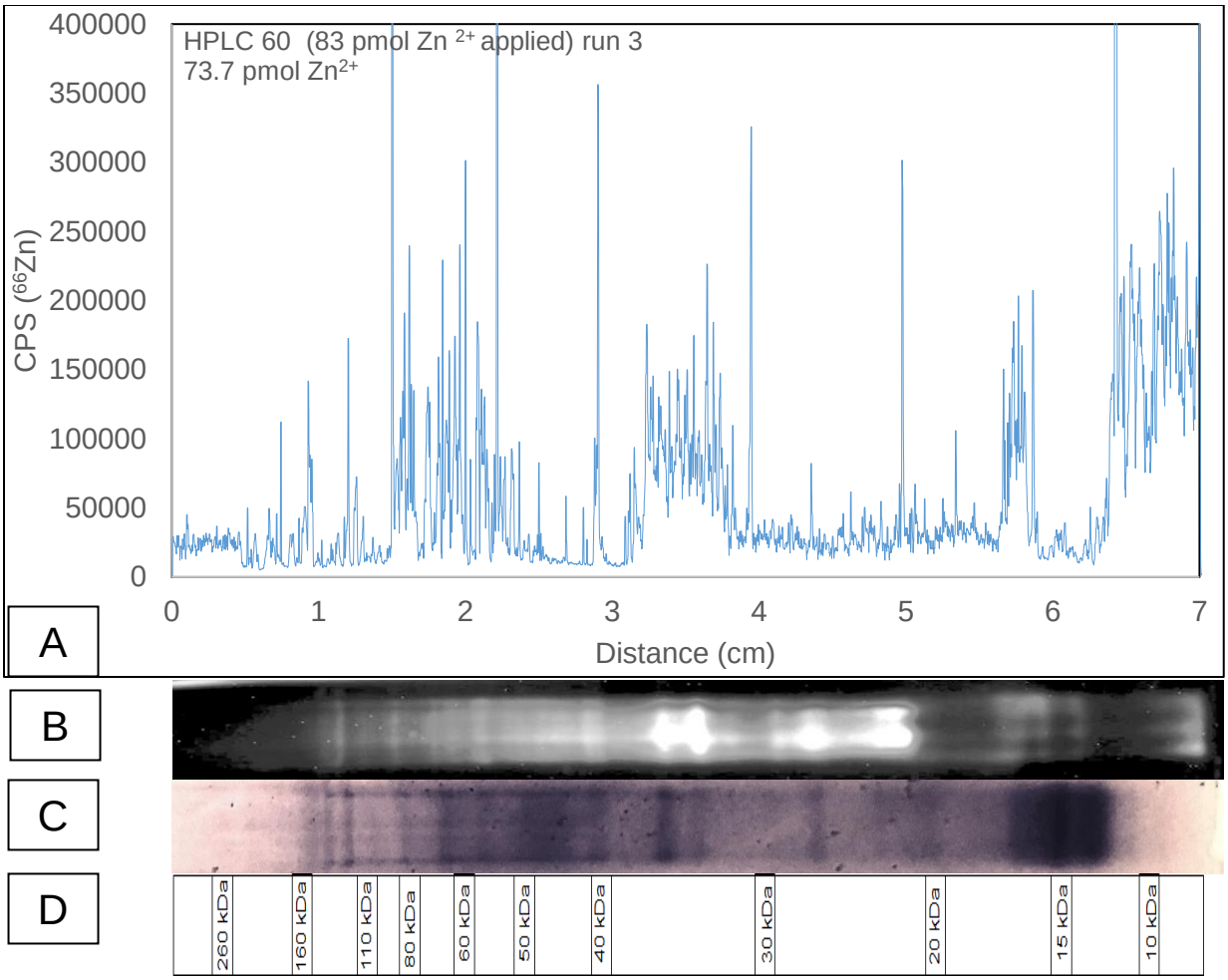

Figure 3.30

A. LA-ICP-MS spectra of HPLC fraction 60 run 3 (83 pmol Zn^{2+} applied) separated using NSDS-PAGE. Quantitation based on Zn^{2+} standards run that day.
B. TSQ stained polyacrylamide gel
C. Coomassie stained polyacrylamide gel
D. 12% Bis-Tris Gel migration chart (reproduced from Thermo Fisher Scientific website).

A comparison of the LA-ICP-MS patterns (panel A) derived from three line scans shows that they closely resemble one another (**figure 3.31**). Integration of the amount of Zn^{2+} present across each profile shows that all line scans contained amounts of zinc (86, 82, 74 pmol, respectively) in good agreement with that of the starting sample (83 pmol). Regions of the profiles that contain apparent concentration of ablated material are marked with horizontal lines. Taken alone these results demonstrate that LA-ICP-MS profiles of the same sample run within a lane on the same gel are reproducible.

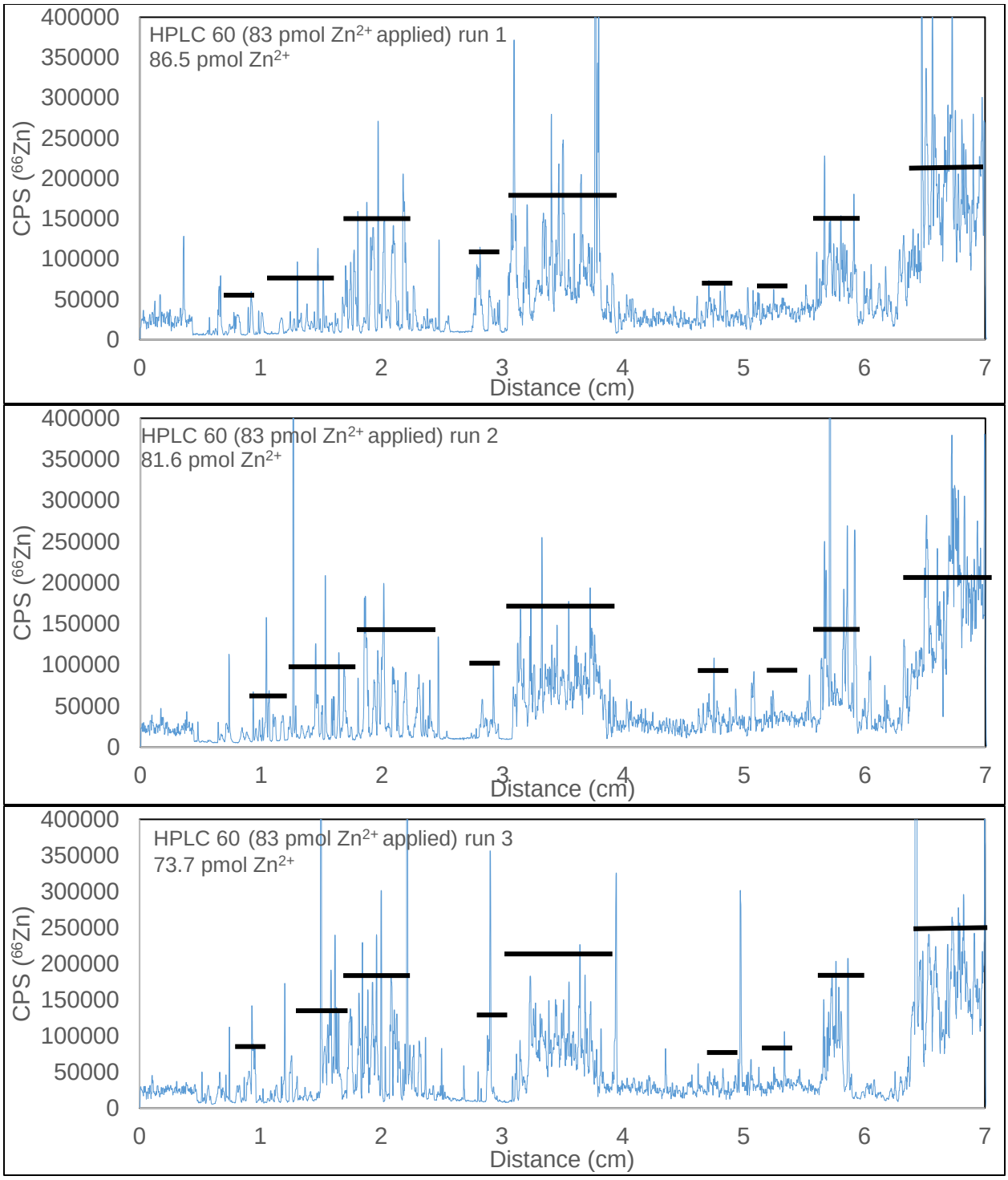

Figure 3.31

Comparative analysis of three LA-ICP-MS line scans (**figure 3.28-3.30**; panel A) within a lane using HPLC fraction 60 as the sample.

These three runs are summed up after Grubbs' Test is applied, in **figure 3.32**. It is also worth noting that the distribution of Zn-Proteins can be investigated in this experiment because the separation method, NSDS-PAGE both leaves proteins in their native conformations with metals bound and separates them with high resolution (Nowakowski et al. 2014).

3.3.1.2 Reproducibility of NSDS-PAGE LA-ICP-MS Between Lanes

The reproducibility of the method was further tested by examining reproducibility of results obtained from the same gel but different lanes. The same procedure was used as in **section 3.2.1**. To test the reproducibility of this method between lanes, HPLC fraction 60 was again chosen for analysis. 15 µL of sample (5 µL glycerol) was added to three separate lanes, electrophoresed by NSDS-PAGE (**section 2.2**) and subjected to analysis using LA-ICP-MS (**section 2.4-2.5**). As before, each lane consisted of three ablated line scans that were subjected to Grubbs' test (**section 2.6**). **Figure 3.32** and **3.33** were run on the same day and **figure 3.34** was run the following day to see any differences (9 ablated line scans, three for each lane, total). Standards were run prior to ablation of the sample, in each experiment. Standard deviation based on the quanitation of three ablated line scans.

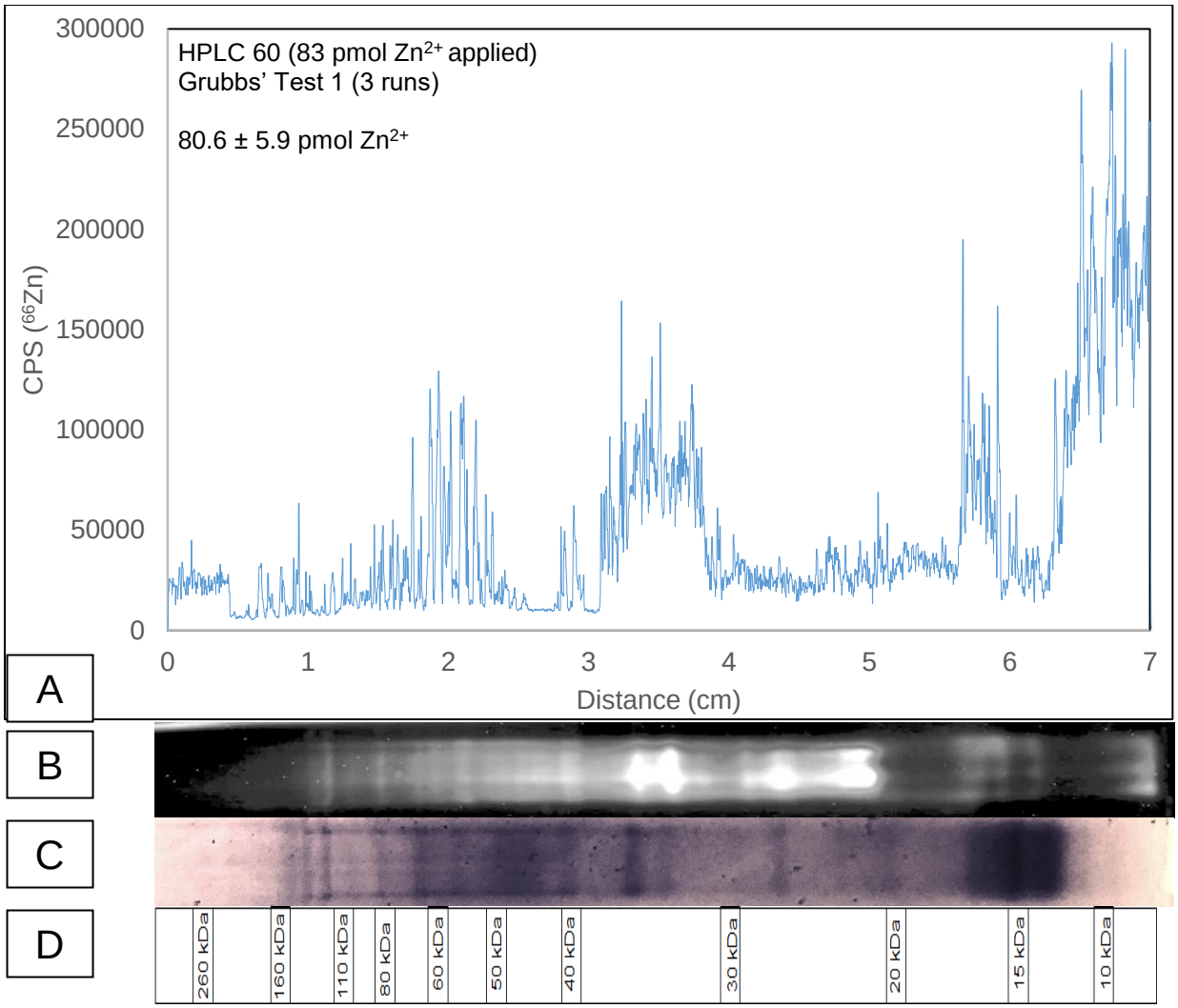

Figure 3.32

A. LA-ICP-MS spectra of HPLC fraction 60 (83 pmol Zn^{2+} applied) separated using NSDS-PAGE. Quantitation based on Zn^{2+} standards run that day. Standard deviation based on the quanitation of 3 ablated runs.
B. TSQ stained polyacrylamide gel
C. Coomassie stained polyacrylamide gel
D. 12% Bis-Tris Gel migration chart (reproduced from Thermo Fisher Scientific website).

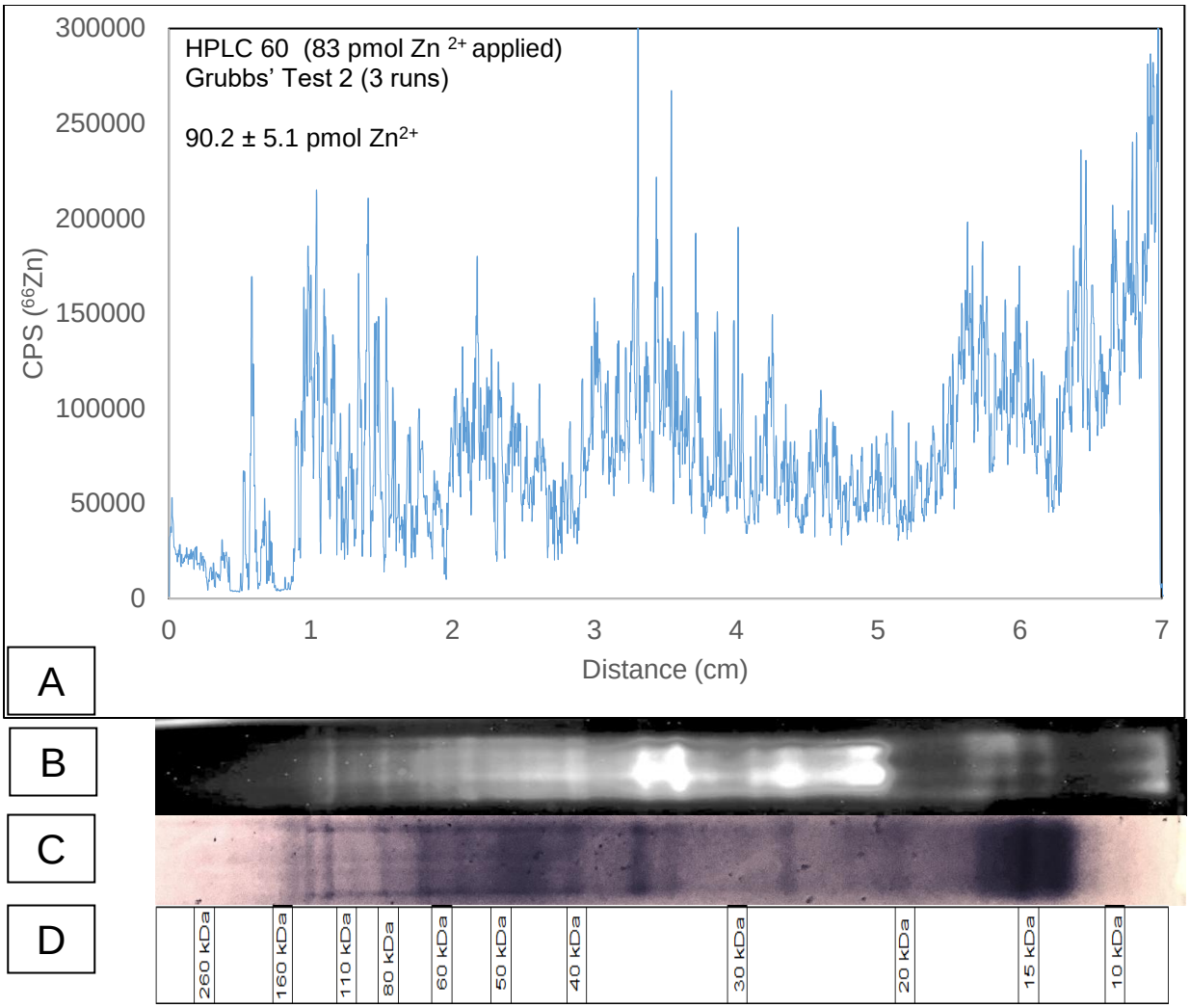

Figure 3.33

A. LA-ICP-MS spectra of HPLC fraction 60 (83 pmol Zn^{2+} applied) separated using NSDS-PAGE. Quantitation based on Zn^{2+} standards run that day. Standard deviation based on the quanitation of 3 ablated runs.
B. TSQ stained polyacrylamide gel
C. Coomassie stained polyacrylamide gel
D. 12% Bis-Tris Gel migration chart (reproduced from Thermo Fisher Scientific website).

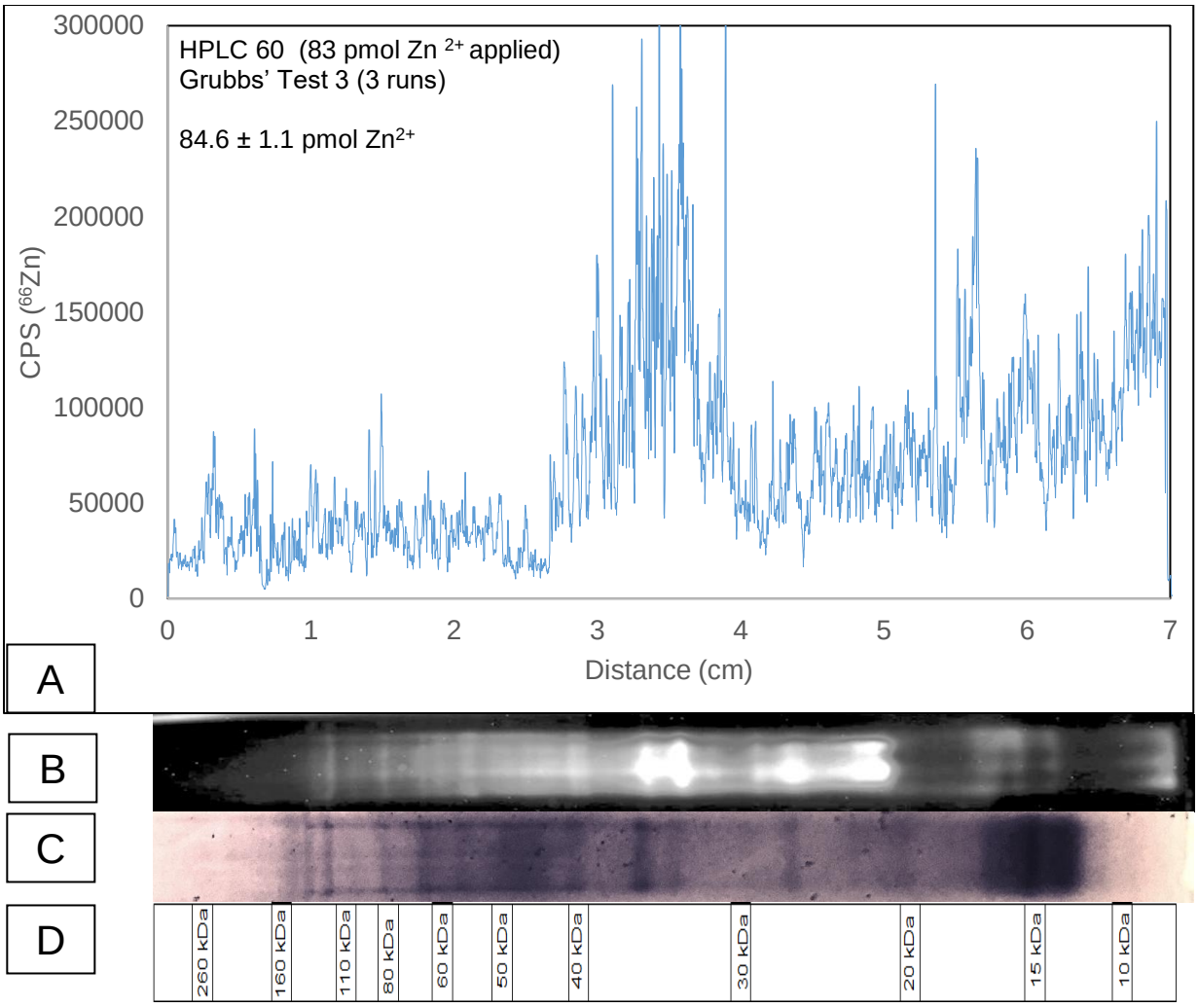

Figure 3.34

A. LA-ICP-MS spectra of HPLC fraction 60 (83 pmol Zn^{2+} applied) separated using NSDS-PAGE. Quantitation based on Zn^{2+} standards run that day. Standard deviation based on the quanitation of 3 ablated runs.
B. TSQ stained polyacrylamide gel
C. Coomassie stained polyacrylamide gel
D. 12% Bis-Tris Gel migration chart (reproduced from Thermo Fisher Scientific website).

Typical LA-ICP-MS experiments have 13-18% RSD (using Standard Reference Materials, SRM), but previous research has not explored the results of ablating 1-D polyacrylamide gels (Durrant et al. 2005). In **figure 3.32-3.34**, the % RSD is 4.3%, when calculating the area under the curve using the standard curve from spotted standards, making this method more precise than referenced work (**section 2.5.1**). The LA-ICP-MS traces (panel A) of **figure 3.32-3.34** are directly compared for patterns of intensity and evidence of resolved bands of zinc in **figure 3.35**.

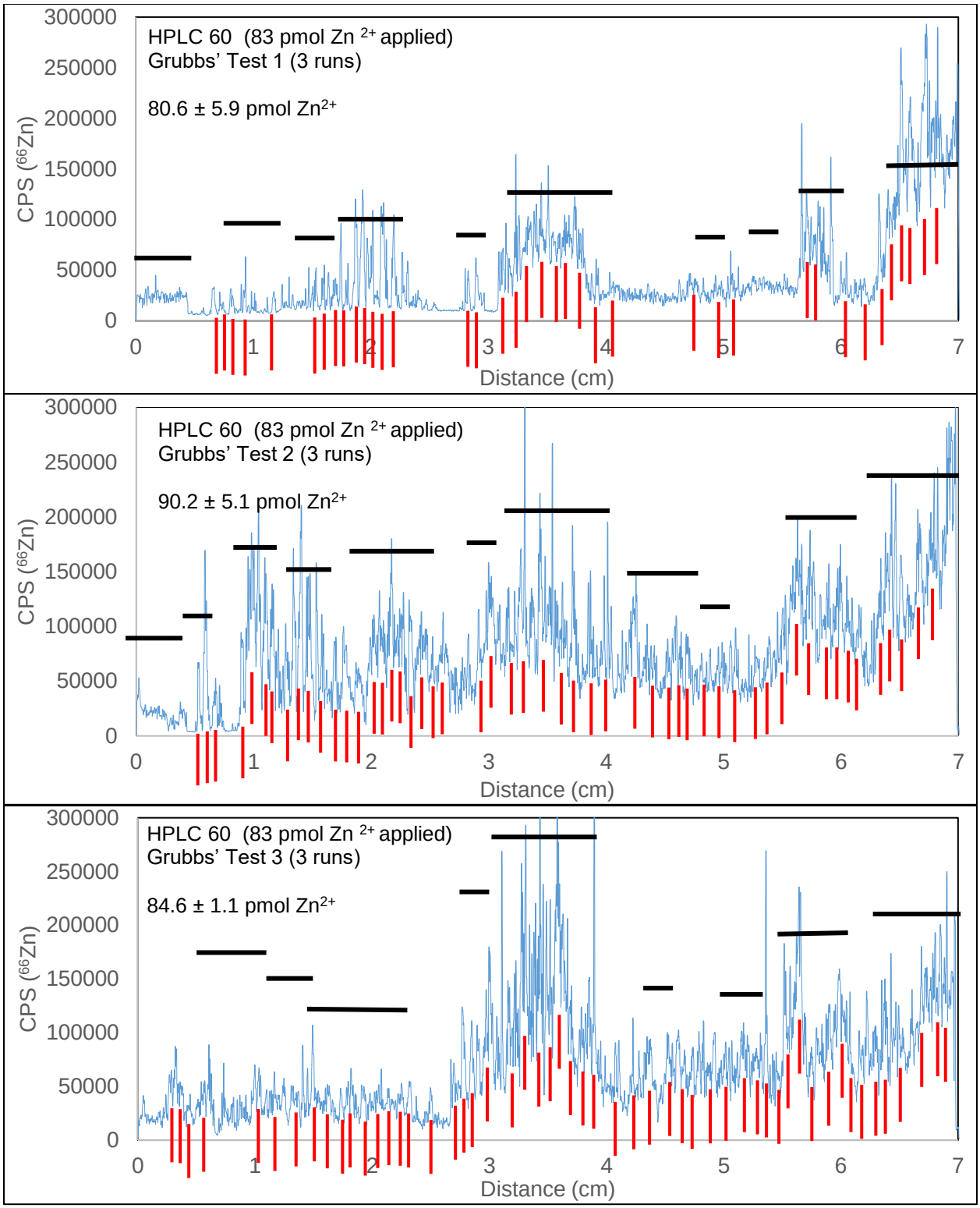

Figure 3.35

Comparative analysis of nine LA-ICP-MS runs (**figure 3.32-3.34**) within three lanes using HPLC fraction 60 as the sample. The horizontal black bars indicate areas of intensity. The vertical red lines indicate possible peaks of zinc.

Although there is some discrepancy between the runs, the overall contours are quite similar as noted with the black bars (**figure 3.35**). The resolution of the bands into individual peaks is visualized by the vertical red lines. As many as 55 peaks were assigned in **figure 3.34**. Whether each of these represents a band of zinc is considered below in the section on TSQ staining of Zn-proteins (**section 3.3.2**). The total zinc detected in each of these profiles (81, 90, and 85 pmol; respectively) was similar to what was seen in the previous runs (**figures 3.28-3.30**). These results indicate that good degree of reproducibility can be achieved by ablating a sample of Zn-proteins electrophoresed through a polyacrylamide gel on different lanes.

3.3.1.3 Reproducibility of NSDS-PAGE LA-ICP-MS on Different Gels

Reproducibility was also investigated using the same protocol as above but on different 12% Bis-Tris polyacrylamide gels. Two gels were run in tandem: one gel was Coomassie and TSQ stained; the other gel was dried for laser ablation. HPLC fraction 60 was separated by NSDS-PAGE then ablated on three separate occasions; each lane was run three times and then subjected to Grubbs' Test for outliers to obtain the final graph of zinc content along the gel (**figure 3.36-3.38**; panel A). **Figure 3.39** shows the comparison of the LA-ICP-MS results for each gel (panel A). Standards were run prior to ablation of the sample, in each experiment. Standard deviation based on the quanitation of 3 ablated runs.

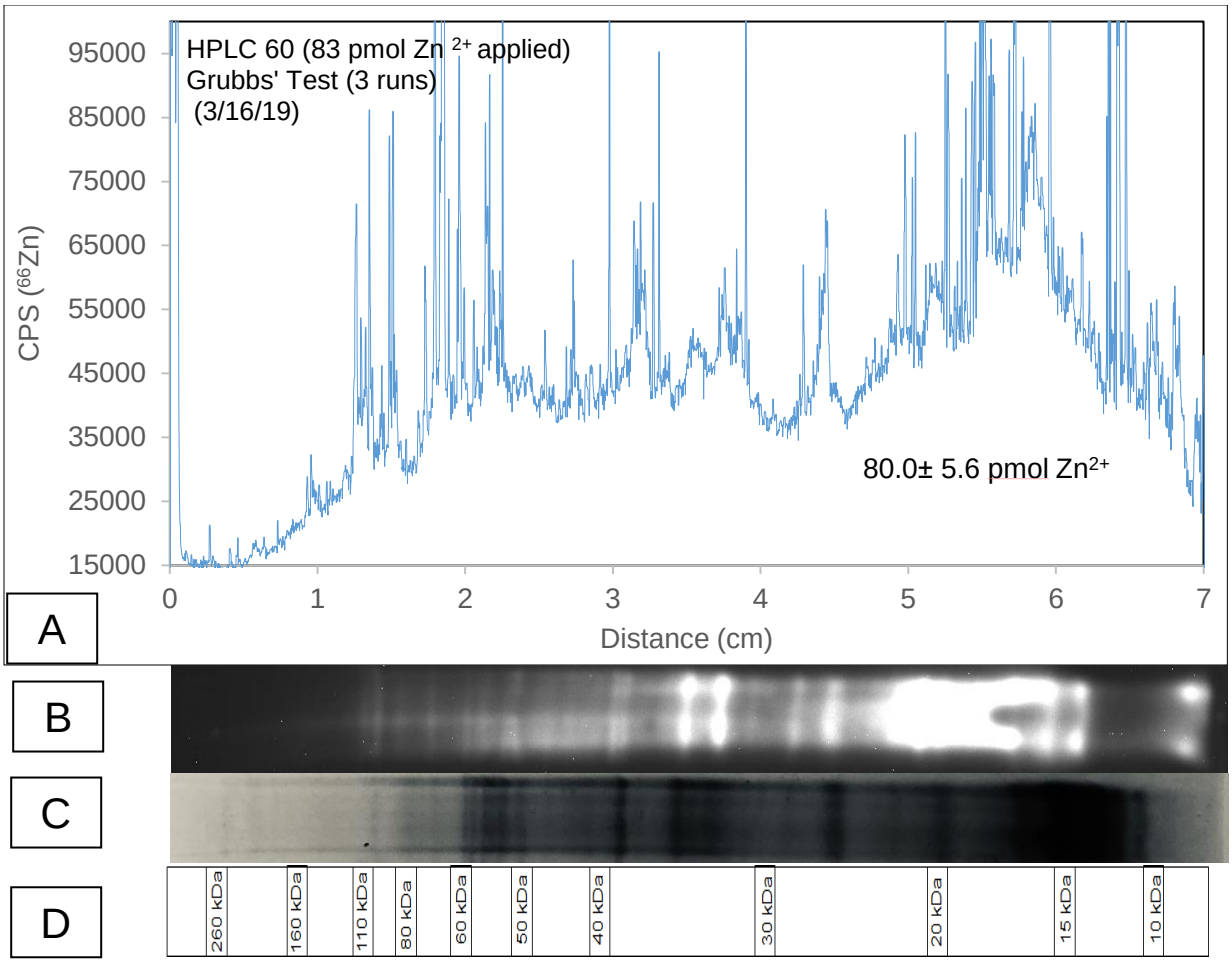

Figure 3.36

A. LA-ICP-MS spectra of HPLC fraction 60 (83 pmol Zn^{2+} applied) separated using NSDS-PAGE. Quantitation based on Zn^{2+} standards run that day. Standard deviation based on the quanitation of 3 ablated runs.
B. TSQ stained polyacrylamide gel
C. Coomassie stained polyacrylamide gel
D. 12% Bis-Tris Gel migration chart (reproduced from Thermo Fisher Scientific website).

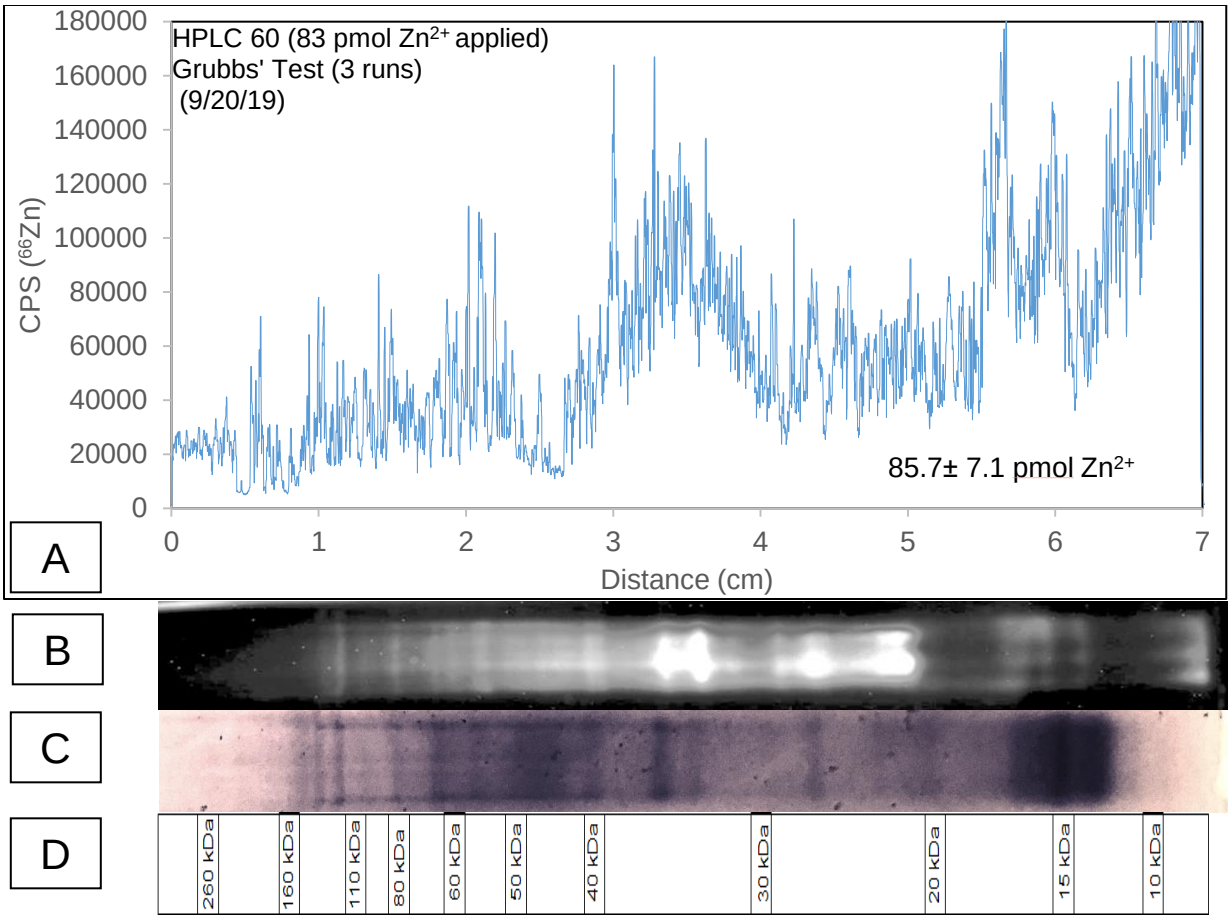

Figure 3.37

A. LA-ICP-MS spectra of HPLC fraction 60 (83 pmol Zn^{2+} applied) separated using NSDS-PAGE. Quantitation based on Zn^{2+} standards run that day. Standard deviation based on the quanitation of 3 ablated runs.
B. TSQ stained polyacrylamide gel
C. Coomassie stained polyacrylamide gel
D. 12% Bis-Tris Gel migration chart (reproduced from Thermo Fisher Scientific website).

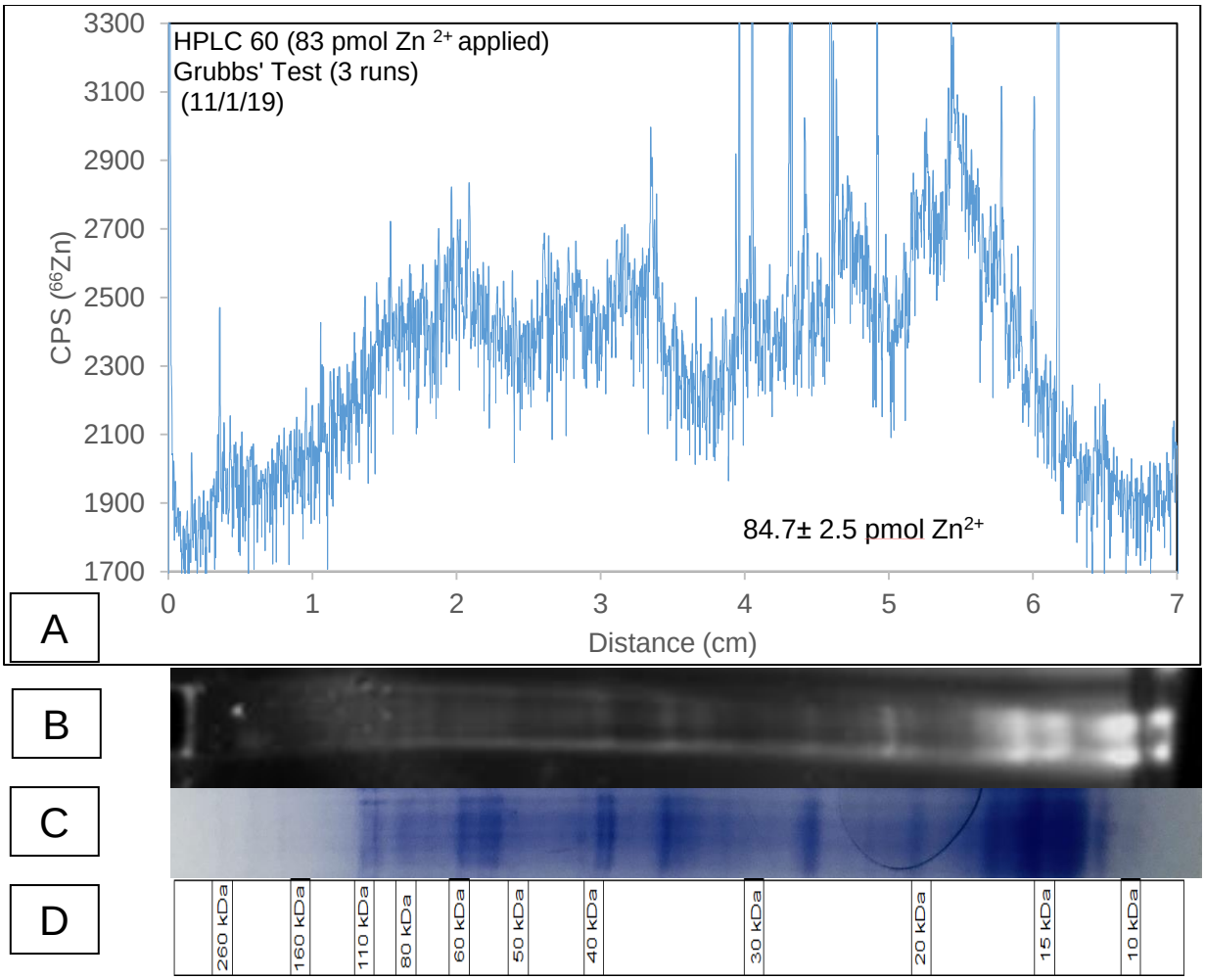

Figure 3.38

A. LA-ICP-MS spectra of HPLC fraction 60 (83 pmol Zn^{2+} applied) separated using NSDS-PAGE. Quantitation based on Zn^{2+} standards run that day. Standard deviation based on the quanitation of 3 ablated runs.
B. TSQ stained polyacrylamide gel
C. Coomassie stained polyacrylamide gel
D. 12% Bis-Tris Gel migration chart (reproduced from Thermo Fisher Scientific website).

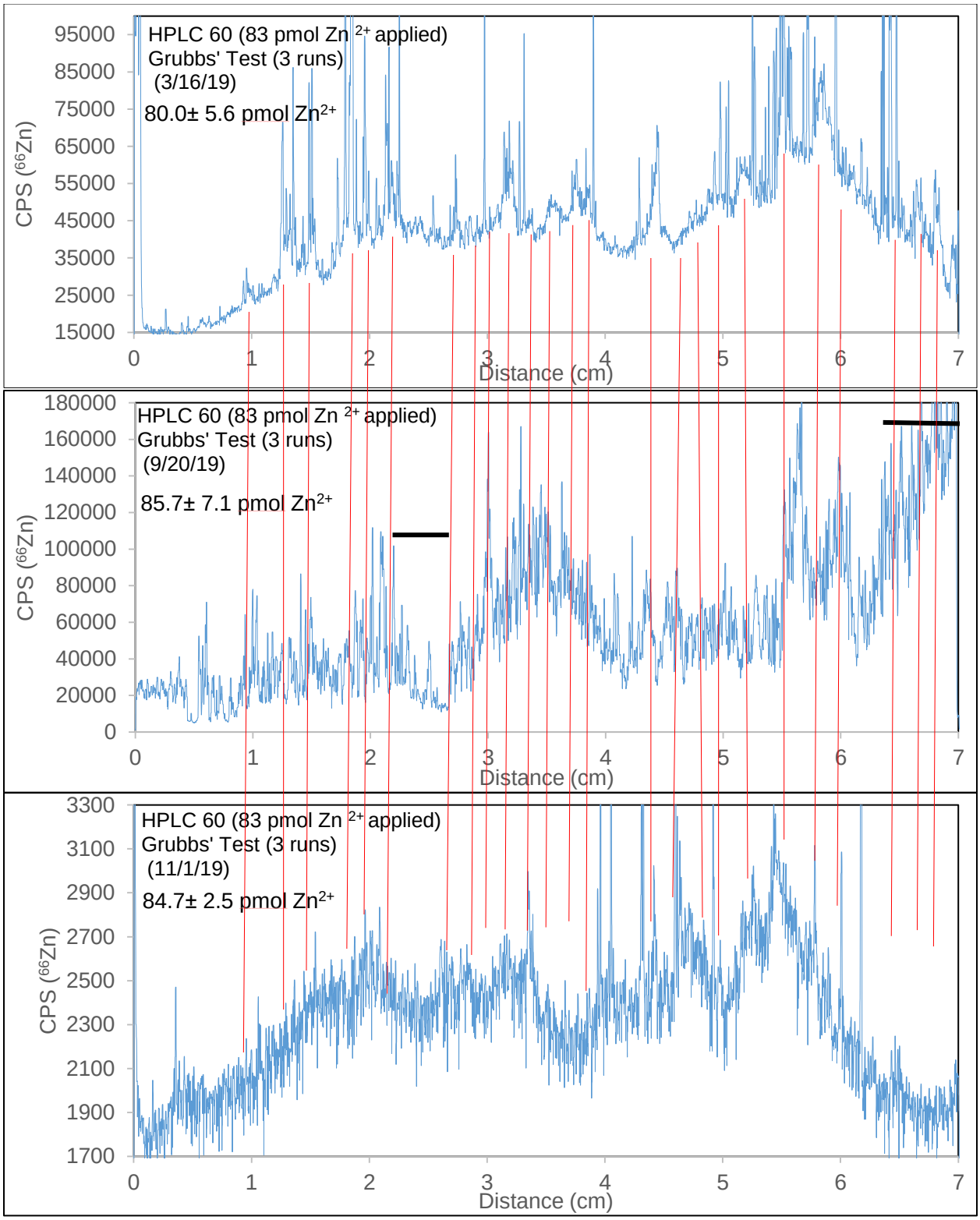

Figure 3.39

Comparison of Panel A (**figure 3.36-3.38**, top to bottom). The black bands in the middle panel (**figure 3.37**) show regions of the profile that differ from the other panels. The red lines show peaks that are common among at least 2 or 3 profiles

Three LA-ICP-MS HPLC fraction 60 profiles of ^{66}Zn that were taken over the course of several months are compared in **figure 3.39**. The runs display a number of similar features noted by the red lines. **Figure 3.37** differs from the other two particularly in the regions noted by the black bars where between 2 and 3 cm little zinc was detected and at the end of the gel between 6 and 7 cm where more zinc was observed. It is important to note the scales for the CPS are indicative of zinc concentration. Each is different, reflecting the fact that standard curves for the elements under investigation must be run each time an analysis is done.

3.3.2 Detection of Zn-proteins by staining with TSQ

In the previous studies of the reproducibility of LA-ICP-MS results, parallel lanes were also stained with TSQ to visualize Zn-proteins as TSQ-Zn-proteins (**figure 3.36-3.38**; panel B). A sampling of those lanes are shown in **figure 3.40.**

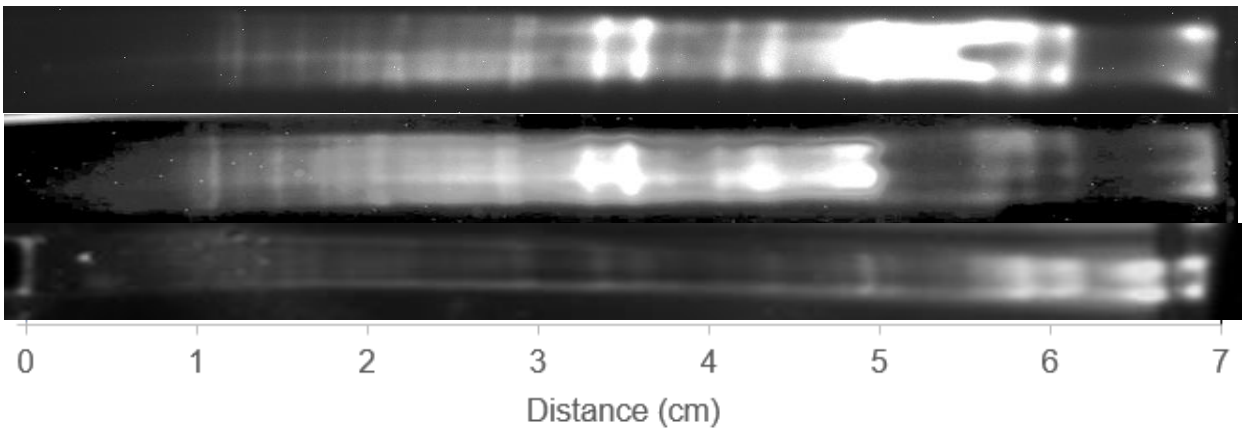

Figure 3.40

Comparison of TSQ staining of Zn-proteins after NSDS-PAGE taken from different days

The lanes shown in **figure 3.40,** which are taken from different experiments conducted on different days and months, reveal in high resolution the same pattern of fluorescence from the formation of TSQ-Zn-proteins. This pattern is clearly reproducible.

We compared the banding of zinc and fluorescence seen **figure 3.36** (panel B), which displays the best resolution in the LA-ICP-MS profile (**figure 3.36**; panel A).

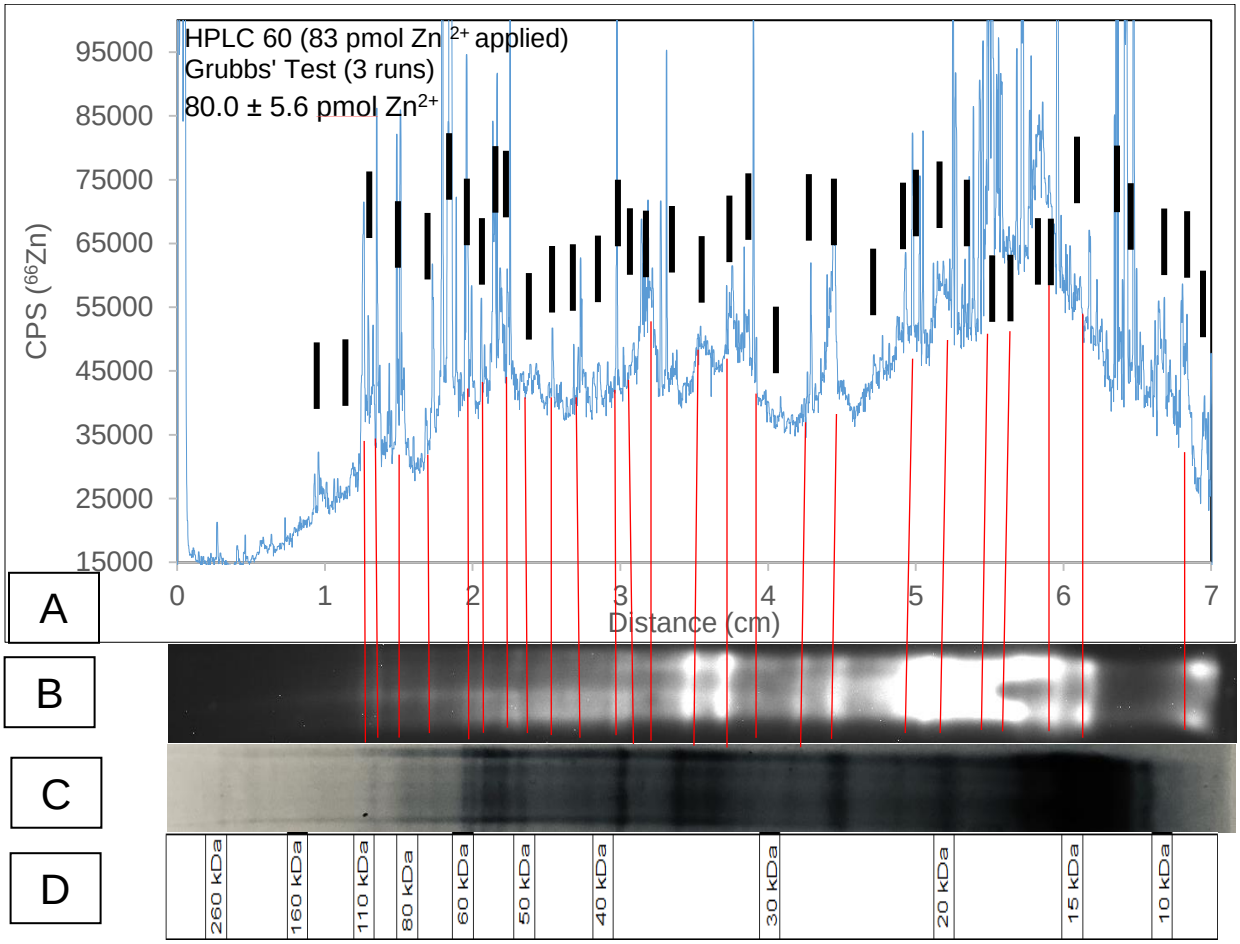

Figure 3.41

Overlap of TSQ-Zn-protein staining with LA-ICP-MS ^{66}Zn profile

A. LA-ICP-MS spectra of HPLC fraction 60 (83 pmol Zn^{2+} applied) separated using NSDS-PAGE. Quantitation based on Zn^{2+} standards run that day. Standard deviation based on the quanitation of 3 ablated runs.
B. TSQ stained polyacrylamide gel
C. Coomassie stained polyacrylamide gel
D. 12% Bis-Tris Gel migration chart (reproduced from Thermo Fisher Scientific website).

Figure 3.41 shows that there are 39 peaks in the LA-ICP-MS profile of zinc (panel A; black marks). In comparison, there are 25 bands of fluorescence in the TSQ stained lane (panel B;

red marks). Of these, 24 overlap and suggest that both methods are detecting the same Zn-proteins. With significant CPS along the length of the LA-ICP-MS lane from 0.5 cm to 7 cm, there may be a number of other Zn-proteins that remain unresolved. In fact, the observable bands could contain more than one Zn-protein. It is recalled that TSQ visualizes about one-quarter of the zinc in the Proteome (Meeusen et al. 2011). If fraction 60 is similar to the Proteome, one would expect that there are many more bands of Zn-protein that are unresolved by electrophoresis and LA-ICP-MS.

Section 3.3.1 demonstrates the reproducibility of using NSDS-PAGE coupled to LA-ICP-MS for the location of Zn-proteins within a polyacrylamide gel. Efforts into protein identification have typically utilized 2-D protein separation and elemental mapping (Becker et al. 2009). Eight possible experiments can be run on a typical polyacrylamide gel which would require a total of 154 hours to completely map every lane; in addition, 2-D gel separation typically utilizes SDS-PAGE in one dimension and isoelectric focusing in the other which destabilize most metal-protein complexes (Raab et al. 2009). **Section 3.2** shows that NSDS-PAGE followed by LA-ICP-MS can be a useful tool for identification of Zn-proteins in gels. Native protein structure is maintained, and zinc remains bound under the conditions of NSDS-PAGE (Nowakowski et al. 2014). Alternatively, Zn-proteins may be visualized with the zinc fluorophore TSQ as TSQ-Zn-proteins as shown above.

3.3.3 Reaction of fraction 60 with Cd^{2+} and Zn-MT

In **Part II** of this thesis, it was shown that Zn-proteins can undergo an exchange reaction with Cd^{2+} to produce Cd-proteins + Proteome•Zn (**Part II: section 3.4**, **reaction 2.6**). Then, as Zn-MT was being synthesized, Cd-proteins were being restored back to their native Zn^{2+} conformation (**Part II: section 3.5, reaction 2.11-2.15**). A hypothesis was tested utilizing NSDS-PAGE followed by LA-ICP-MS or TSQ staining to probe whether Cd^{2+} displaces Zn^{2+} from Zn-proteins through the Cd-Zn exchange reaction and whether subsequent reaction with

zinc metallothionein can sequester Cd^{2+} from these proteins and restore Zn^{2+} to its' original binding sites.

Fraction 60 was subjected to two experiments. The first, investigating if any Zn-proteins within fraction 60 would undergo an exchange reaction with Cd^{2+} to produce Cd-proteins + Proteome•Zn (**reaction 2.6**) and could be visualized on a LA-ICP-MS. Theoretically, these proteins would be indicated by peaks on the ^{114}Cd profile, due to the exchange of Cd^{2+} for Zn^{2+}. Those ^{114}Cd peaks would need to correlate with the loss of intensity of ^{66}Zn peaks within the same lane, compared to a control lane of fraction 60. This exchange reaction could also be visualized by TSQ staining due to the loss of fluorescence when Cd^{2+} replaces Zn^{2+}, considering that $Zn(TSQ)_2$ is 10 times more fluorescent than $Cd(TSQ)_2$ (**figure 3.17-3.18**).

The second experiment is also an extension of **Part II** of this thesis. Cd-proteins have been shown to transfer zinc into a growing pool of MT to generate Cd, Zn-MT (**figures 2.3 – 2.9**). Hypothetically, if the Cd-proteins•Zn were incubated with Zn-MT, the zinc content of the proteins could be restored and appear as an increase of CPS and related peaks in the ^{66}Zn LA-ICP-MS profile. In addition, the correlating ^{114}Cd spectrum peaks should decrease in CPS. This can be further corroborated by the restoration of zinc-dependent fluorescence on a TSQ stain. The results are shown below (**figure 3.42-3.47**) and the comparison of all the ^{66}Zn profiles are shown in **figure 3.48**.

Figure 3.42 (the same electrophoretic run as **figure 3.36**) shows the original distribution of Zn^{2+} bound to Zn-proteins fraction 60 of Proteome. Like earlier experiments, the integrated sum of measured Zn^{2+} was 80 pmol. Prior to the addition of Cd^{2+}, the background distribution of Cd^{2+} was virtually zero (0.64 pmol) (**figure 3.43**). For later comparison, the black lines indicate bands of zinc seen in the native LA-ICP-MS profile. The red lines mark bands of TSQ-Zn-protein.

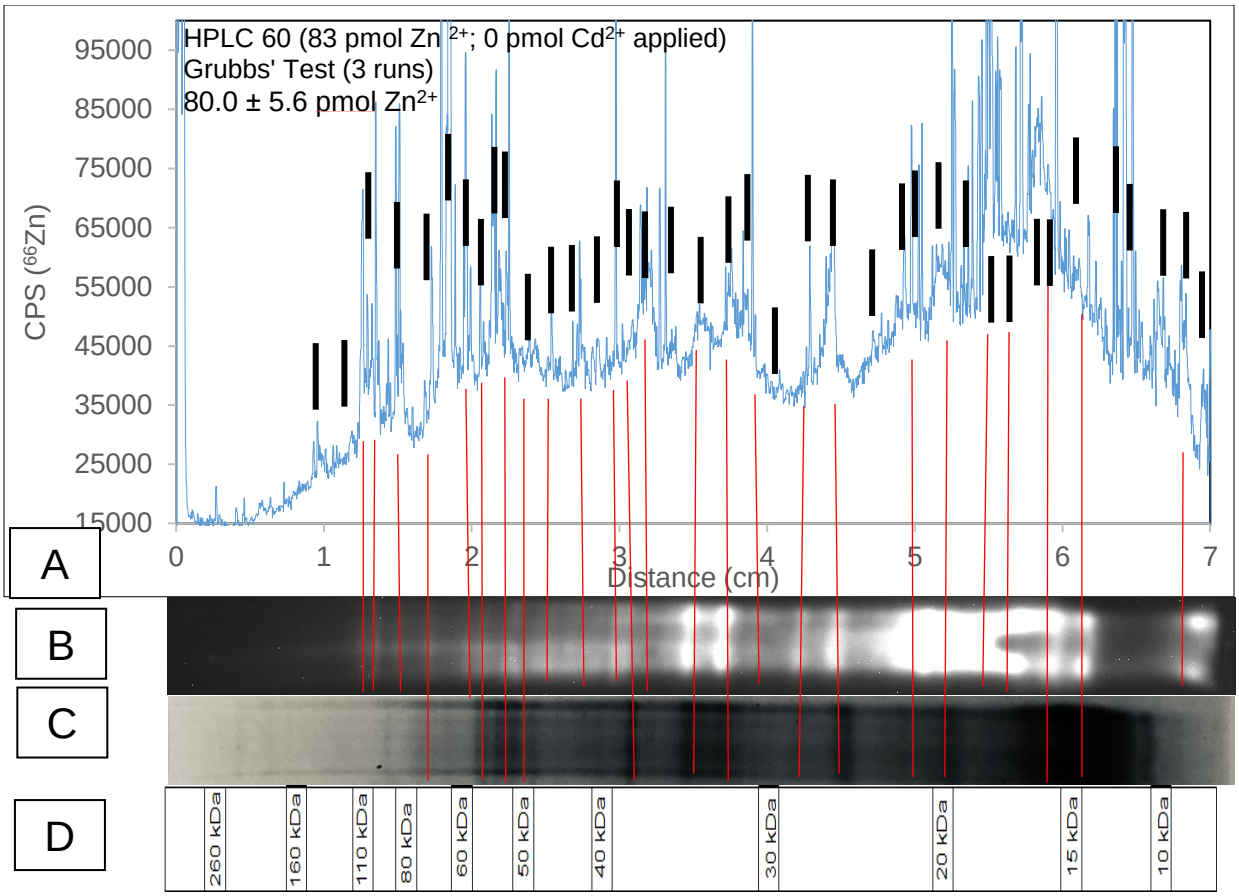

Figure 3.42

LA-ICP-MS spectra of fraction 60- control ^{66}Zn profile

A. LA-ICP-MS spectra of HPLC fraction 60 (83 pmol Zn^{2+} applied) separated using NSDS-PAGE. Quantitation based on Zn^{2+} standards run that day. Standard deviation based on the quanitation of 3 ablated runs.
B. TSQ stained polyacrylamide gel
C. Coomassie stained polyacrylamide gel
D. 12% Bis-Tris Gel migration chart (reproduced from Thermo Fisher Scientific website).

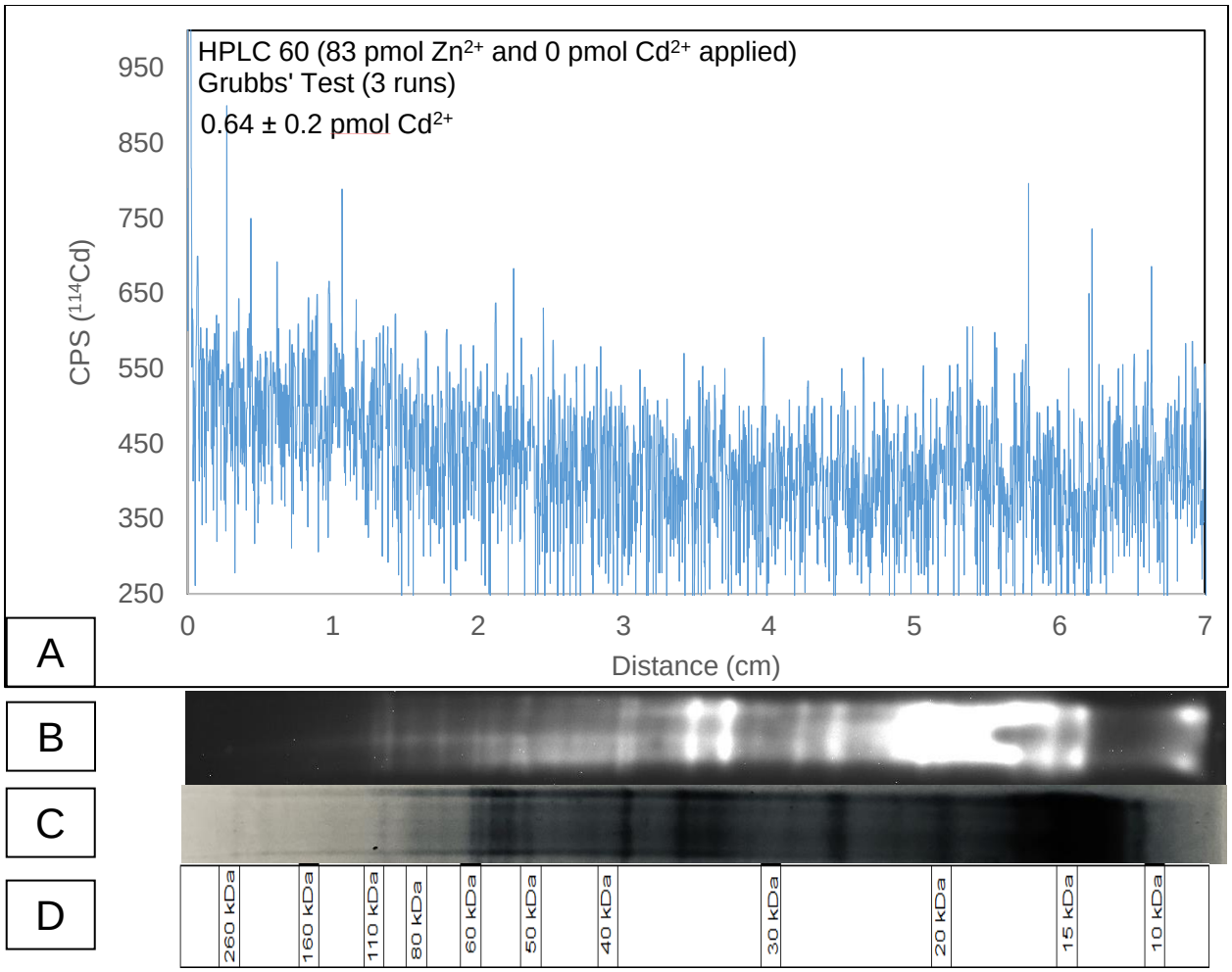

Figure 3.43

LA-ICP-MS spectra of fraction 60- control ^{114}Cd profile

A. LA-ICP-MS spectra of HPLC fraction 60 (83 pmol Zn^{2+} and 0 pmol Cd^{2+} applied) separated using NSDS-PAGE. Quantitation based on Cd^{2+} standards run that day. Standard deviation based on the quanitation of 3 ablated runs.
B. TSQ stained polyacrylamide gel
C. Coomassie stained polyacrylamide gel
D. 12% Bis-Tris Gel migration chart (reproduced from Thermo Fisher Scientific website).

Next, 100 pmol of Cd^{2+} was incubated with 83 pmol of Zn^{2+} from fraction 60 for 30 minutes. At that point, the mixture was either electrophoresed and then subjected to LA-ICP-MS or treated with TSQ (200 pmol) prior to NSDS-PAGE. The results are shown in **figure 3.44-3.45**.

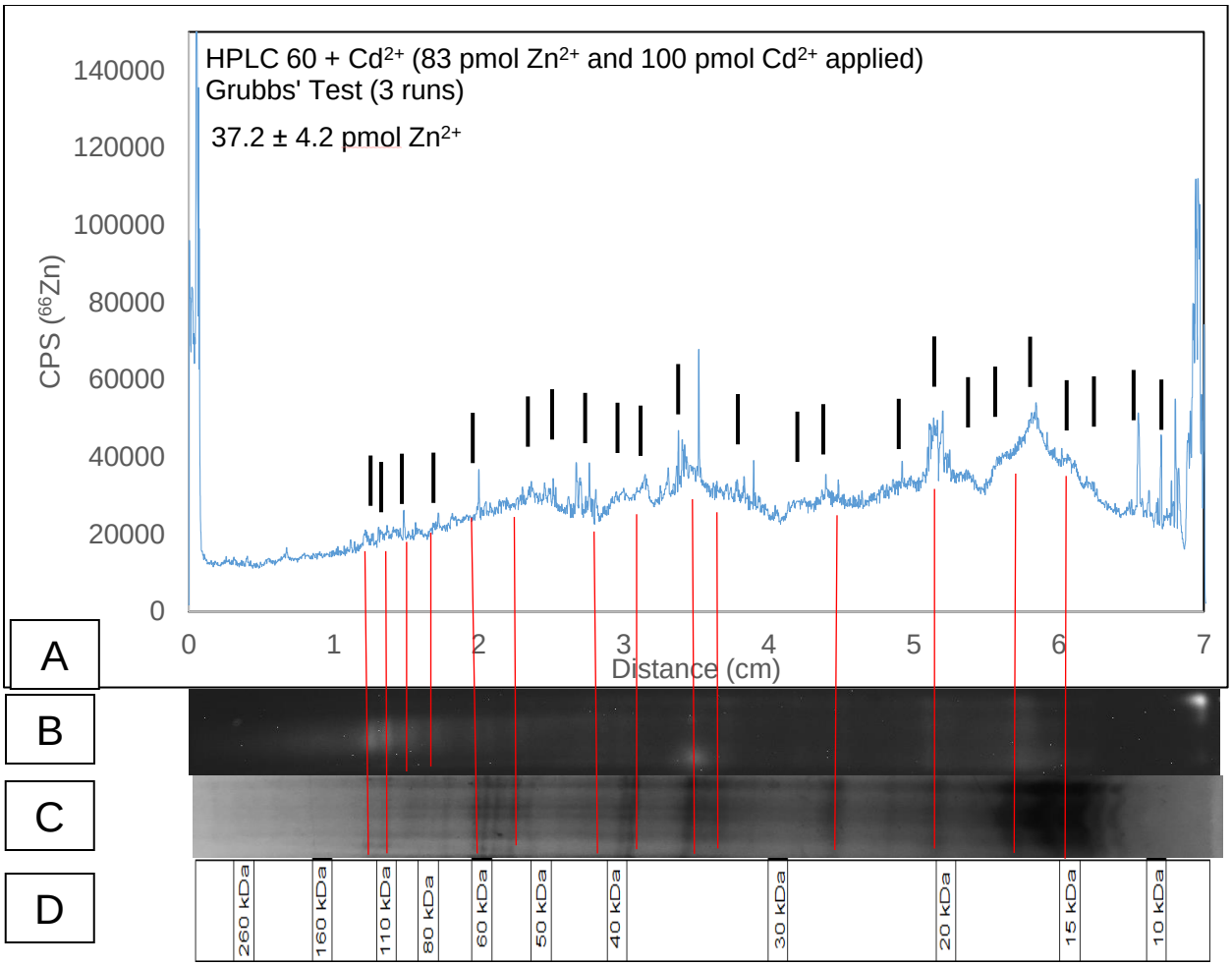

Figure 3.44

LA-ICP-MS spectra of fraction 60 + Cd^{2+} - ^{66}Zn profile

A. LA-ICP-MS spectra of HPLC fraction 60 + Cd^{2+} (83 pmol Zn^{2+} and 100 pmol Cd^{2+} applied) separated using NSDS-PAGE. Quantitation based on Zn^{2+} standards run that day. Standard deviation based on the quanitation of 3 ablated runs.
B. TSQ stained polyacrylamide gel
C. Coomassie stained polyacrylamide gel
D. 12% Bis-Tris Gel migration chart (reproduced from Thermo Fisher Scientific website).

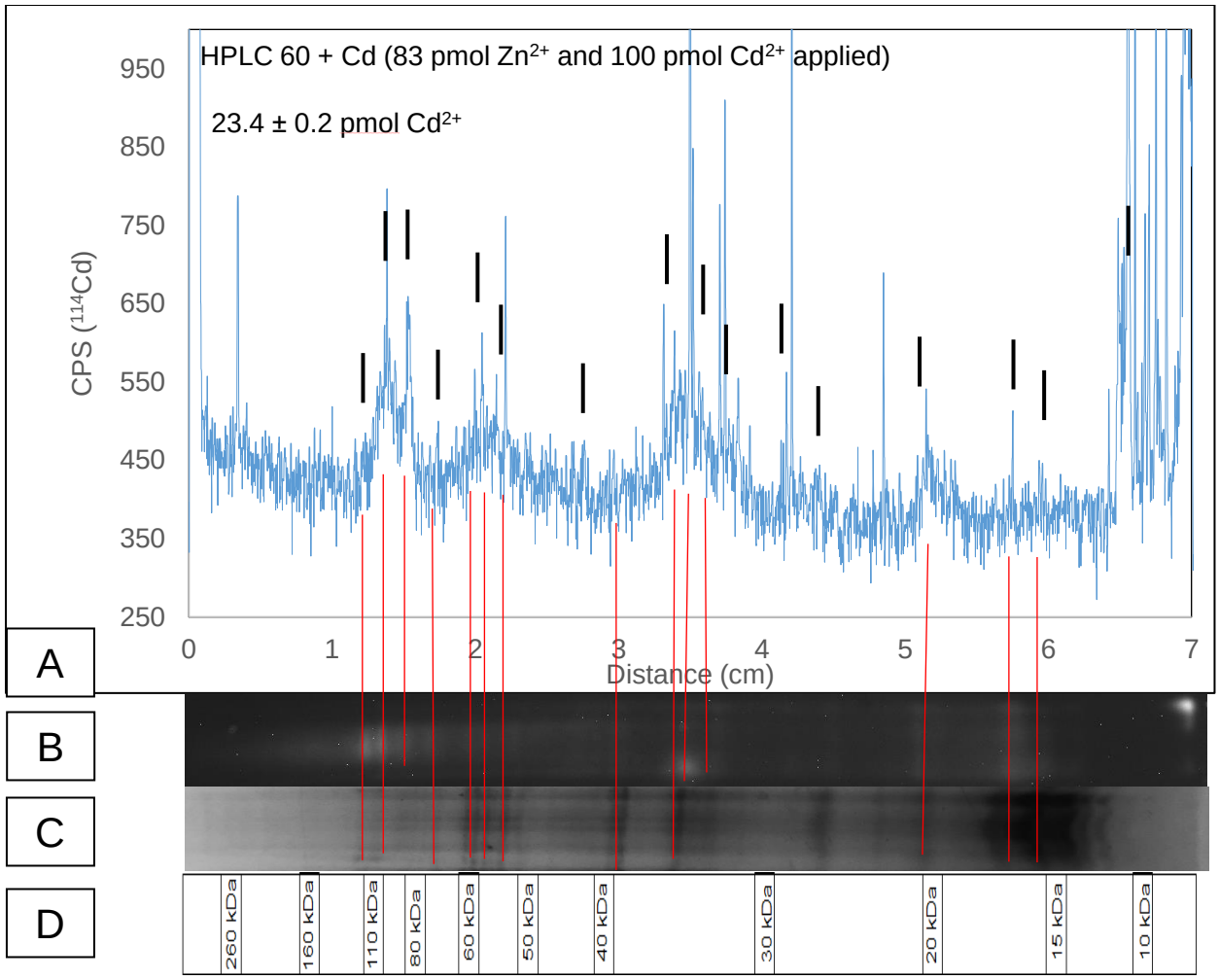

Figure 3.45

LA-ICP-MS spectra of fraction 60 + Cd^{2+} - ^{114}Cd profile

A. LA-ICP-MS spectra of HPLC fraction 60 + Cd^{2+} (83 pmol Zn^{2+} and 100 pmol Cd^{2+} applied) separated using NSDS-PAGE. Quantitation based on Cd^{2+} standards run that day. Standard deviation based on the quanitation of 3 ablated runs.
B. TSQ stained polyacrylamide gel
C. Coomassie stained polyacrylamide gel
D. 12% Bis-Tris Gel migration chart (reproduced from Thermo Fisher Scientific website).

It is immediately evident that much CPS intensity has been lost from the profile. The measured total, recovered zinc was 37 pmol, indicating that Cd^{2+} had induced the loss of 43 pmol of Zn^{2+} from the profile and much of the detail of the profile. Strikingly, most of the TSQ-dependent fluorescence had disappeared. At the same time, examination of the gel for the presence of

^{114}Cd (**figure 3.45**) showed that 23 pmol of cadmium had become bound and was now distributed across the profile. The profiles are directly compared in **figure 3.46**.

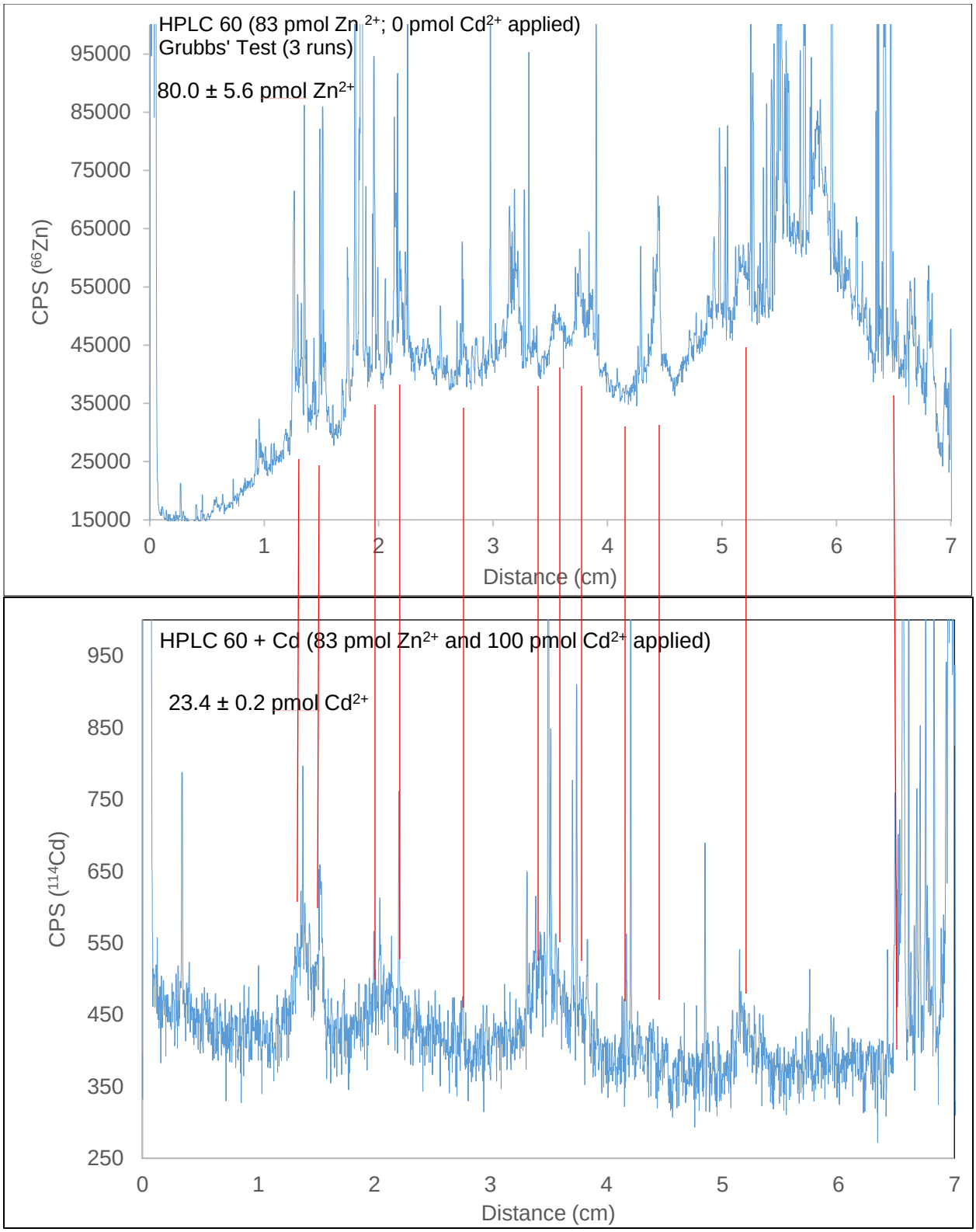

Figure 3.46.

Comparative profiles of control Zn-proteins (**figure 3.43**) and Cd-proteins (**figure 3.45**). Red vertical lines show ^{114}Cd peaks and corresponding ^{66}Zn peaks in the control

Based upon the hypothetical scheme of reaction of Cd^{2+} with the Zn-Proteome in **reaction 2.6**,

$$\text{Proteome•Cd + Zn-proteins} \leftrightharpoons \text{Cd-proteins + Proteome•Zn} \qquad (2.6)$$

the products should be Cd-proteins plus Zn^{2+} bound to non-specific sites in the Proteome, Proteome•Zn. The results reveal the presence of Cd-Proteins but not Proteome•Zn, which has been lost during the electrophoresis. It was apparent that once Zn^{2+} had been mobilized, it was not stably bound to the Proteome during electrophoresis and as a positively charged ion, migrated out of the gel.

Similarly, in an earlier study when Proteome•Zn-TSQ was formed, it did not migrate with components of the fraction (Nowakowski et al. 2015). In addition, TSQ can make adducts with Cd-proteins. But according to **figure 3.44-3.45** (panel B), Cd^{2+} is much less effective than Zn^{2+} in stimulating the fluorescence emission of TSQ. For these reasons, the profile of fluorescence was greatly diminished. With these limitations understood, the results of displacement of Zn^{2+} from Zn-proteins by Cd^{2+} is observed by two methods at the individual protein level of detection.

At this point, the hypothesis was tested that Cd-proteins together with Proteome•Zn would react with Zn-MT and undergo exchange to restore Zn-proteins and produce Cd-MT (Namdarghanbari et al. 2014). In **figures 3.47-3.48**, the outcome of the reaction of the products of **figure 3.44-3.45** with Zn-MT (50 pmol of Zn^{2+} as Zn-MT) is shown. The Zn^{2+} profile provided by LA-ICP-MS has been largely restored as 73 pmol of zinc are present in the profile (up from 37 pmol) (**figure 3.47**). The profiles are directly compared in **figure 3.49**. Similarly, the fluorescence pattern resembles much of the original one in **figure 3.42** as shown in **figure 3.50**. Measurement of ^{114}Cd in **figure 3.48**, indicates that much of the Cd^{2+} that had previously been bound was removed (23 to 5 pmol). Cd-MT has not been located in this profile, probably because it is a small protein that is highly negatively charged and may run at the gel front.

Based on this experiment, **reaction 3.4** describes the overall metal exchange that occurs and is clearly visible in this set of figures:

$$\text{Cd-proteins} + \text{Zn-MT} \leftrightharpoons \text{Zn-proteins} + \text{Cd-MT} \qquad (3.4)$$

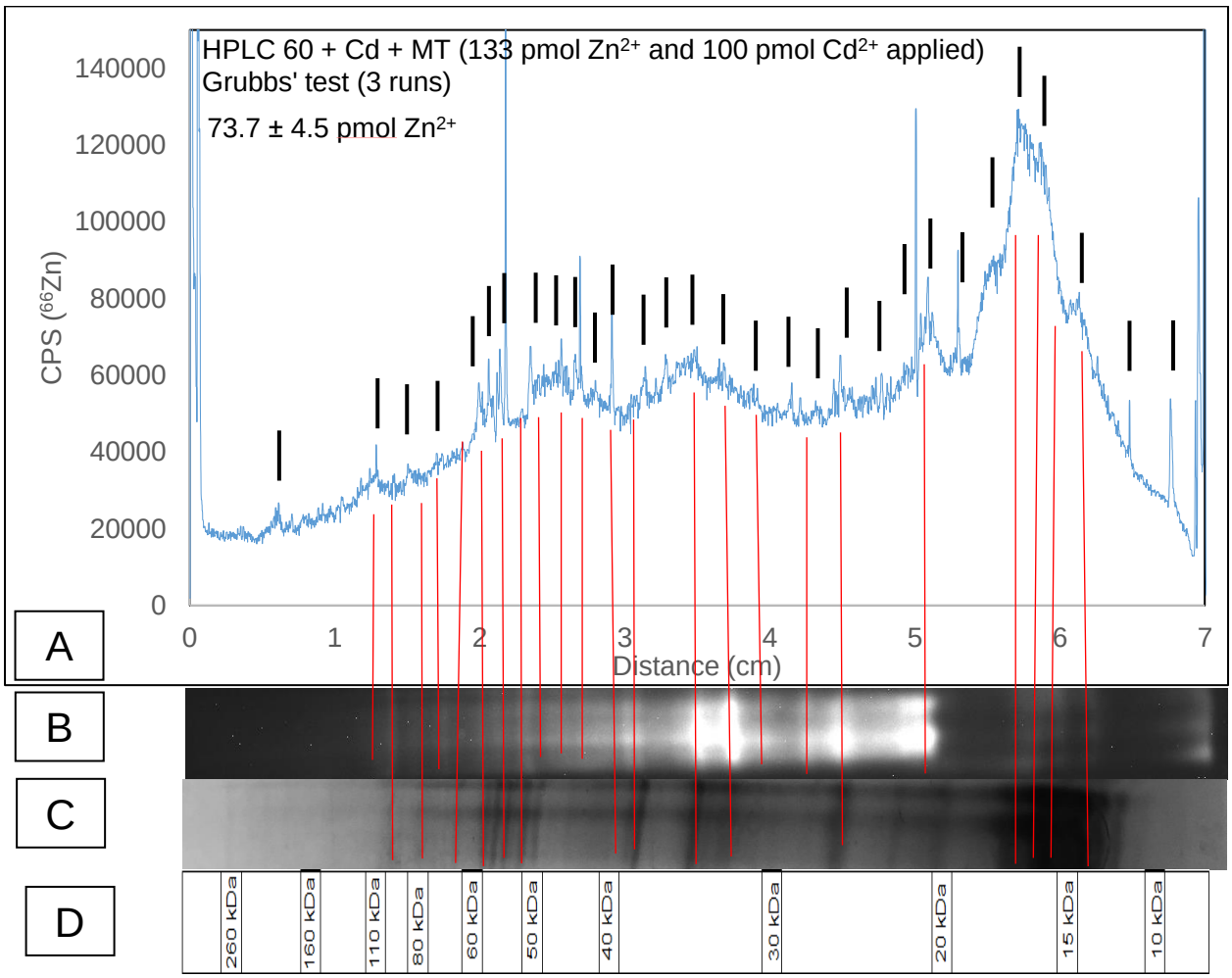

Figure 3.47

LA-ICP-MS HPLC fraction 60 + Cd^{2+} + Zn-MT - ^{66}Zn profile

A. LA-ICP-MS spectra of HPLC fraction 60 + Cd^{2+} + Zn- MT (133 pmol Zn^{2+} and 100 pmol Cd^{2+} applied) separated using NSDS-PAGE. Quantitation based on Zn^{2+} standards run that day. Standard deviation based on the quanitation of 3 ablated runs.
B. TSQ stained polyacrylamide gel
C. Coomassie stained polyacrylamide gel
D. 12% Bis-Tris Gel migration chart (reproduced from Thermo Fisher Scientific website).

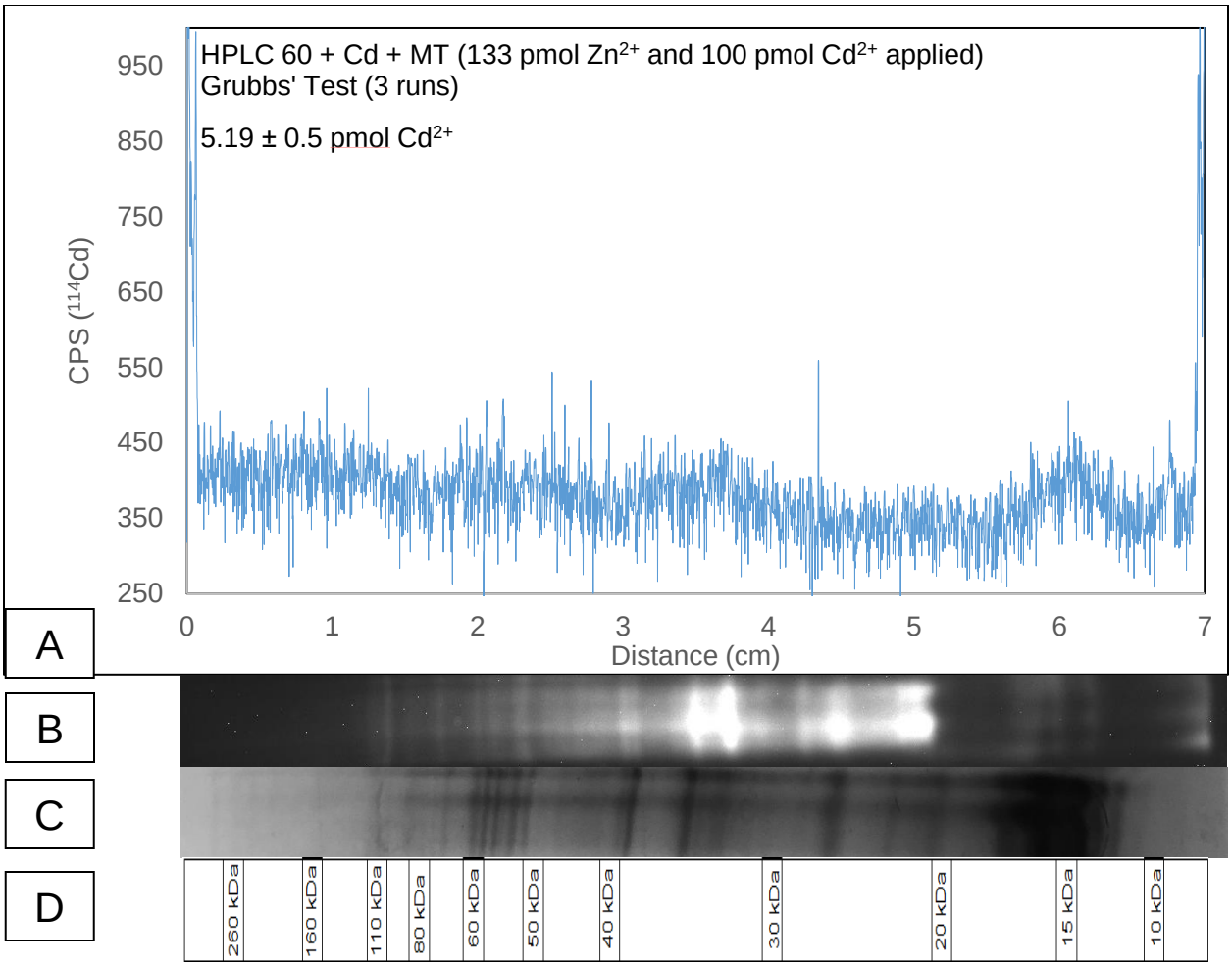

Figure 3.48

LA-ICP-MS HPLC fraction 60 + Cd^{2+} + Zn-MT – ^{114}Cd profile

A. LA-ICP-MS spectra of HPLC fraction 60 + Cd^{2+}+ MT (133 pmol Zn^{2+} and 100 pmol Cd^{2+} applied) separated using NSDS-PAGE. Quantitation based on Cd^{2+} standards run that day. Standard deviation based on the quanitation of 3 ablated runs.
B. TSQ stained polyacrylamide gel
C. Coomassie stained polyacrylamide gel
D. 12% Bis-Tris Gel migration chart (reproduced from Thermo Fisher Scientific website).

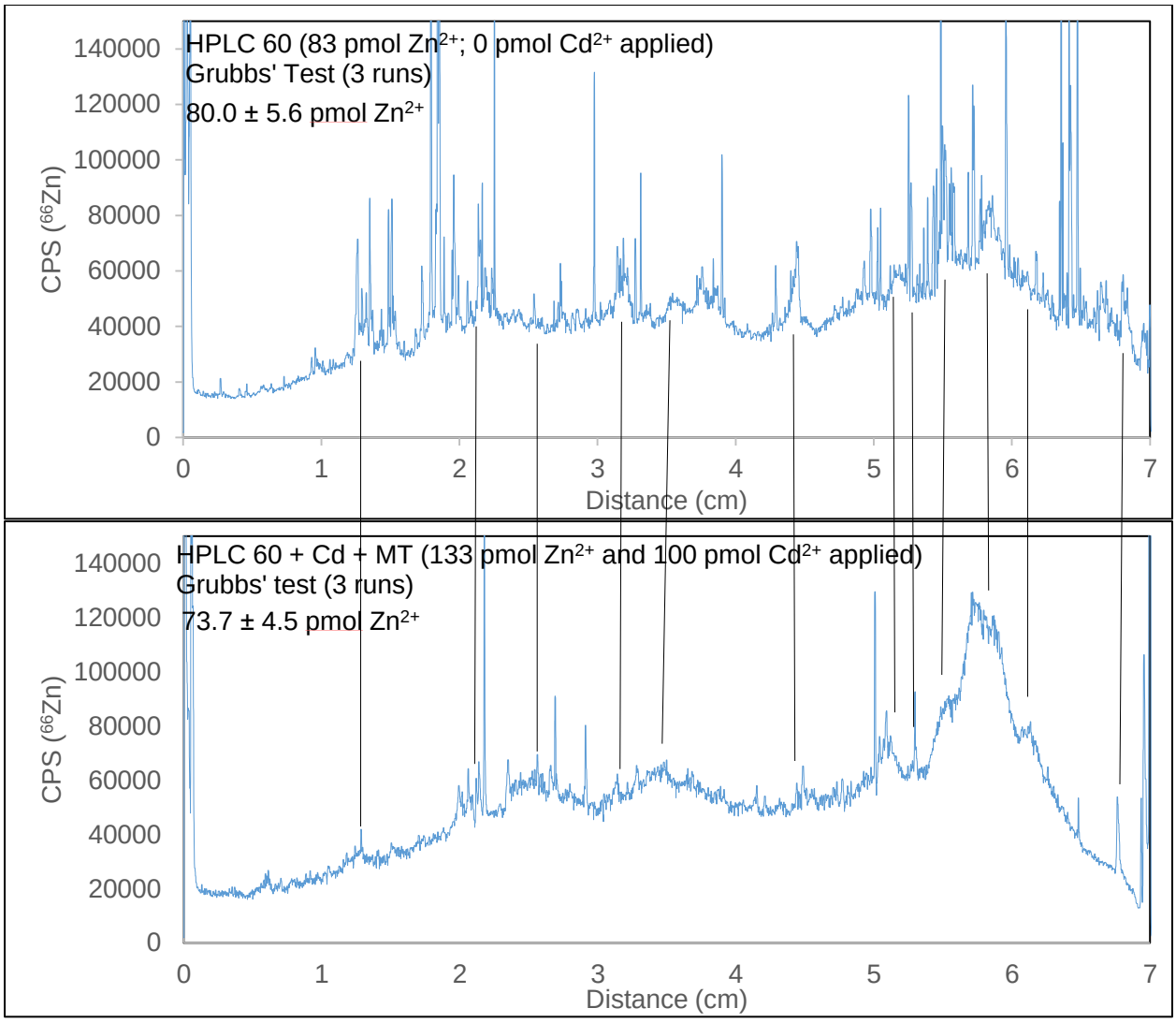

Figure 3.49

Comparison of HPLC fraction 60 ^{66}Zn LA-ICP-MS profiles (**figure 3.42-3.47**) (black marks indicate TSQ overlap)

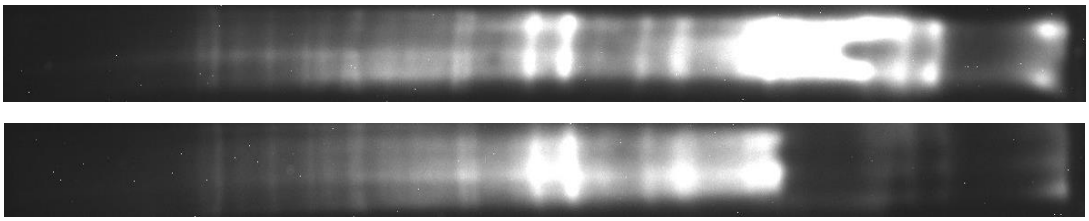

Figure 3.50

Comparison of TSQ staining in control (**figure 3.42**, top) and Cd-treated plus Zn-MT samples (**figure 3.47**, bottom)

4. Conclusion

An initial inquiry was made into the development of a method utilizing NSDS-PAGE (**section 2.2**) coupled to LA-ICP-MS (**section 2.4-2.5**) for the identification of zinc proteins. Bovine serum albumin (BSA) and Carbonic Anhydrase (CA) were the individual zinc proteins used for method development. BSA was separated by NSDS-PAGE then ablated three times and subjected to Grubbs' Test for outliers (**figure 3.11**; panel A). TSQ and Coomassie stains (**figure 3.11**; panel B and C) revealed zinc peaks that line up directly with the ablated material. These results demonstrated (**1**) that under conditions of electrophoresis that are thought to retain native structural characteristics of proteins, 60 kDa Zn-Albumin migrates much like it would during SDS-PAGE. In addition (**2**), under native conditions, self-association occurs so that dimer and trimer forms are detected as well. Furthermore (**3**), Albumin retains its complement of moderately strongly bound Zn^{2+}, showing that the native conditions of electrophoresis permit the retention of Zn^{2+} by Albumin.

Next, Carbonic anhydrase was employed to investigate the limit of ^{66}Zn detection applying this novel method. **Figure 3.12-3.15** show increasing concentrations of CA protein bands revealed by LA-ICP-MS, TSQ and Coomassie staining are coincident with the location of zinc on the gel. The results indicate that the LA-ICP-MS measurements detect ^{66}Zn bound to CA after NSDS-PAGE separation, consistent with the maintenance of the native conformation of the protein and its retention of Zn^{2+}. A plot of the observed amount of zinc versus the applied zinc (**figure 3.16**) shows that this method provides quantitative results because of the linear relationship and the good agreement between applied and detected amounts of zinc. Moreover, CA protein bands containing low pmol amounts of zinc can be readily detected in this type of experiment. The limit of detection for Zn-CA was found to be around 14 pmol applied Zn^{2+} (**figure 3.12**).

HPLC fraction 60 was the first mixture of Zn-proteins utilized for furthering this method development. Reproducibility was first addressed (**section 3.3.1**). Fraction 60 was electrophoresed through a polyacrylamide gel and subjected to LA-ICP-MS to investigate how well three runs of the same sample were correlated (**section 3.3.1.1**). A comparison of the LA-ICP-MS patterns derived from three line scans show that they closely resemble one another (**figure 3.20**; panel A). Integration of the amount of Zn^{2+} present across each profile shows that all lanes contained amounts of zinc in good agreement with that of the starting sample (83 pmol). Taken alone these results demonstrate that LA-ICP-MS ^{66}Zn profiles of the ablated line scans of the same lane are reproducible.

Next, reproducibility of the same sample between lanes on the same gel was explored (**section 3.3.1.2**). Fraction 60 was electrophoresed through three separate lanes on the same polyacrylamide gel (**figure 3.28-3.30**). Although there is some discrepancy between the runs, the overall contours are quite similar. The total zinc detected in each of these profiles (81, 90 and 85 pmol; respectively) was similar to what was seen in the previous runs indicating that a good degree of reproducibility can be achieved across different lanes of the same gel.

Fraction 60 was also used to investigate the reproducibility of the same sample electrophoresed through different gels and ablated on different days (**section 3.3.1.3**). The correlation of zinc profiles, the TSQ staining (**section 3.3.2**) and the total zinc detected in each of these profiles (80, 85, 86 pmol Zn^{2+}; respectively) indicated that a good degree of reproducibility can be achieved using the same sample across different gels.

Lastly, NSDS-PAGE followed by LA-ICP-MS or TSQ staining of fraction 60 was utilized to probe whether Cd^{2+} displaces Zn^{2+} from Zn-proteins through the Cd-Zn exchange mechanism and whether subsequent reaction with zinc metallothionein can remove Cd^{2+} from these proteins and restore Zn^{2+} to its original binding sites (**section 3.3.3**). **Figure 3.42** shows the original distribution of Zn^{2+} bound to Zn-proteins in fraction 60 with an integrated sum of measured Zn

around 80 pmol and Cd virtually zero (0.64 pmol) (**figure 3.43**). After the addition of 100 pmol Cd^{2+}, much ^{66}Zn intensity has been lost from the profile indicating that Cd^{2+} had induced the displacement of 43 pmol of Zn^{2+} from the profile (80 to 37 pmol) (**figure 3.44**). At the same time, examination of the gel for the presence of ^{114}Cd (**figure 3.45**) showed that 23 pmol of cadmium had become bound and was now distributed across the profile. Coincidentally, most of the TSQ dependent fluorescence had disappeared (**figure 3.44-3.45**; panel B). The location of the new bands of ^{114}Cd coincided with positions of peaks of ^{66}Zn in the original, control profile of untreated fraction 60 (**figure 3.46**). The cadmium-treated fraction (**figure 3.44-3.45**) was then incubated with 50 pmol of Zn^{2+} as Zn-MT (**figures 3.47-3.48**). The ^{66}Zn profile measured by LA-ICP-MS (panel A) was largely restored to the profile of the control sample (37 to 73 pmol). Similarly, the fluorescence pattern resembles much of the original one (**figure 3.50**). Measurement of ^{114}Cd (**figure 3.48**), indicates that much of the Cd^{2+} that had previously been bound was removed (23 to 5 pmol).

The results of **section 3.3.3** confirm the capability of utilizing NSDS-PAGE coupled to LA-ICP-MS for the location of Zn-proteins that undergo an exchange reaction with Cd^{2+} and are restored back to their native Zn^{2+} conformation using Zn-MT. There are many peaks in **figure 3.49** that line up the LA-ICP-MS ^{66}Zn profile to visibly show **reaction 3.4**.

More generally, these results complete the studies of the Cd-Zn exchange process that began with the exposure of LLC-PK_1 cells to Cd^{2+} plus Pyrithione (**figures 2.3**-**2.9**). The presence experiments like earlier ones demonstrate that Cd^{2+} displaces Zn^{2+} from Proteomic sites with approximate one to one stoichiometry. Uniquely, these experiments show that the presence of Zn-MT shifts Cd^{2+} out of the Proteome and restores a native distribution of Zn^{2+} among Zn-proteins. The initial stage of this complicated process presumably involves the direct reaction of Zn-MT with Cd-proteins:

$$\text{Zn-MT} + \text{Cd-proteins} \leftrightharpoons \text{Cd-MT} + \text{Zn-proteins} \qquad (3.4)$$

Direct exchange might occur, leading to reconstitution of the Zn-Proteome. Or, perhaps, Proteome•Zn forms as an intermediate, prior to the restitution of Zn^{2+} into its protein binding sites:

$$\text{Zn-MT + Cd-proteins + Proteome} \leftrightharpoons \text{Cd-MT + Proteome•Zn + apo-Zn-proteins} \quad (3.5)$$

$$\text{Proteome•Zn + apo-Zn-proteins} \leftrightharpoons \text{Proteome + Zn-proteins} \quad (3.6)$$

Part IV: Ligand Binding to Zinc Proteome

1. Introduction

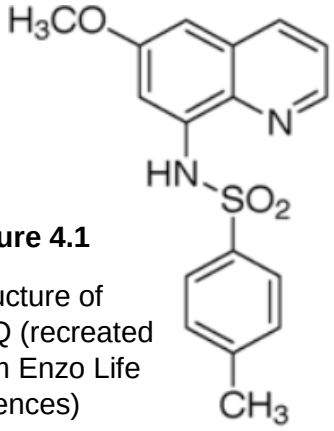

Figure 4.1

Structure of TSQ (recreated from Enzo Life Sciences)

The fluorescent zinc probe TSQ (**figure 4.1**) reacts with members of the cellular Zn-Proteome to form ternary adducts, TSQ-Zn-Proteome (Nowakowski et al. 2015). The availability of extra coordination sites among Zn-proteins that can bind the bidentate ligand TSQ suggests that other ligands may be able to bind to Zn-proteins as well. A previous study showed that 1,10-phenanthroline was able to do so (Fatema 2015). It became of interest to broaden the exploration of ligand binding to the Zn-Proteome as we were considering how $Cd(Pyrithione)_2$ interacts with cellular constituents as it delivers Cd^{2+} into cells. Besides the focus on Cd^{2+}, we wondered whether Pyrithione free of Cd^{2+} might form adducts with Zn-proteins.

In addition, it is recognized that Zn^{2+} mobilized from Zn-proteins by exchange with Cd^{2+} subsequently binds to non-specific Zn^{2+} binding sites in the Proteome. Hypothetically, these sites, Proteome•Zn, can also form complexes with ligands:

$$\text{Proteome•Zn} + \text{L} \leftrightharpoons \text{Proteome•Zn-L} \qquad (4.1)$$

We decided to explore this reaction as well.

In order to be able to detect these reactions, we set up a competitive titration experiment in which Zn-Proteome or Proteome•Zn were originally reacted with TSQ to form fluorescent products and then a ligand was titrated into the solution as a competitor that quenches the fluorescence as it displaces TSQ from its binding sites:

$$\text{TSQ-Zn-Proteome} + \text{L} \leftrightharpoons \text{L-Zn-Proteome} + \text{TSQ} \quad (4.2)$$

$$\text{Proteome•Zn-TSQ} + \text{L} \leftrightharpoons \text{Proteome•Zn-L} + \text{TSQ} \quad (4.3)$$

2. Methods

2.1 Fluorescence Spectrometry

Refer to **Part II: section 2.6**

2.2 Chemicals

All chemicals were purchased from either Thermo Fisher Scientific or Sigma-Aldrich unless noted. For the experiments below, stock solutions of these chemicals were prepared as follows:

2-mercaptopyridine-N-oxide was dissolved in DMSO; 1,10-phenanthroline, L-Cysteine, L-Glutathione, and pyridine-2,6-dicarboxylic acid were dissolved in $_{dd}H_2O$; 8-hydroxyquinoline and 2,2'-bipyridyl were dissolved in ethanol.

2.3 TSQ Staining of Gels

Part III: section 3.10 describes the basic method of doing NSDS-PAGE in the presence of TSQ to stain Zn-proteins. To assess the reaction of ligands with TSQ-Zn-proteins separated by NSDS-PAGE, individual ligands were added in solution to gels and incubated for 10 min before their impact on fluorescence was assessed.

3. Results and Discussion

3.1 Titration of Zinc-Proteome with TSQ

Previous research has demonstrated that TSQ (**figure 4.1**) preferentially forms ternary adducts with Zn-proteins (**reaction 3.2**). TSQ slowly reacts with the Zn-proteins of the Proteome (Zn-Proteome) *in vitro* or *in vivo* to generate these complexes.

A typical titration is shown in **figure 4.2**. **Figure 4.3** provides the summary.

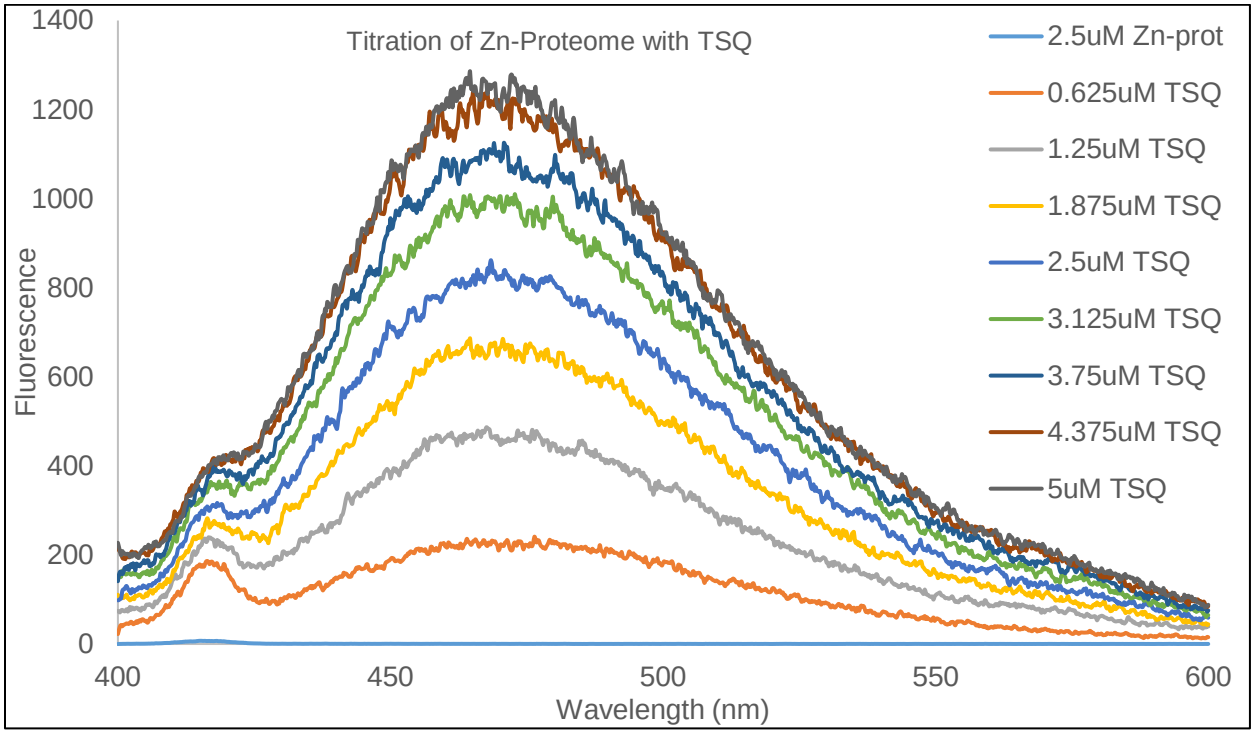

Figure 4.2

Titration of Zn-Proteome with TSQ. 2.5 µM isolated Zn-Proteome (1.43 x 10^8 cells) in 20 mM Tris pH 7.4 was titrated with TSQ. Excitation wavelength was 365 nm. Emission wavelength range was 400-600 nm. 15 minutes between each addition of TSQ to insure final, stable fluorescence.

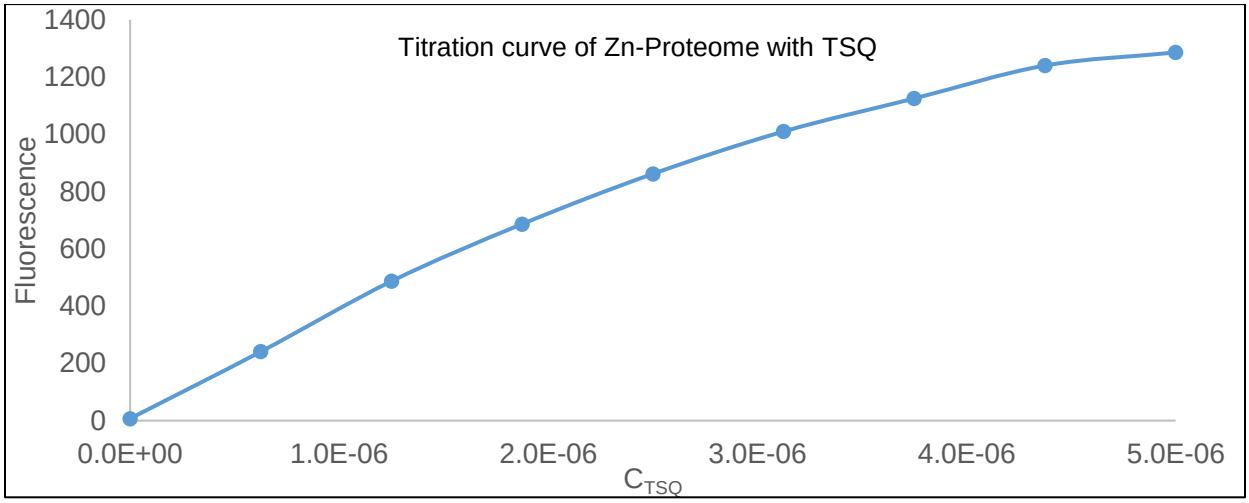

Figure 4.3

Titration curve of Zn-Proteome with TSQ. 2.5 µM isolated Zn-Proteome (1.43 x 10^8 cells) in 20 mM Tris pH 7.4 was titrated with TSQ. Excitation wavelength was 365 nm. Emission wavelength range was 400-600 nm. 15 minutes between each addition of TSQ to insure final, stable fluorescence.

The titration was treated as a simple equilibrium reaction (**reaction 4.4**).

$$\text{Zn-Proteome} + \text{TSQ} \leftrightharpoons \text{TSQ-Zn-Proteome} \qquad (K_1) \qquad (4.4)$$

The apparent equilibrium constant (K_1) for the reaction was derived from the following expressions:

$$Y \text{ (fractional saturation of Zn-Proteome with TSQ)} = [\text{TSQ}]_{free} / (K_d + [\text{TSQ}]_{free}) \qquad (4.5)$$

$$C_{total,[\text{TSQ-Zn-Proteome}]} = 0.24 \times C_{Total,[\text{Zn-Proteome}]} \text{ (Meeusen et al. 2011)} \qquad (4.6)$$

$$[\text{TSQ}]_{free} = C_{total,[\text{TSQ}]} - [\text{TSQ-Zn-Proteome}] =$$

$$C_{total,[\text{TSQ}]} - [\,(F - F_{Minimum}) / (F_{Maximum} - F_{Minimum}) \times C_{total,[\text{TSQ-Zn-Proteome}]}] \qquad (4.7)$$

Previous experiments indicated that TSQ binds to 24% of the total concentration of Proteomic zinc (**reaction 4.6**). $F_{maximum}$ is the maximum fluorescence indicative of the saturation of Zn-Proteome binding sites, F is the fluorescence at any point during the titration, and $F_{minimum}$ is the minimum fluorescence at the start of the titration.

A plot of (1 / Y) vs 1 / $[\text{TSQ}]_{free}$ as shown in **figure 4.4** yielded a straight line with an intercept of 0.38 and a slope of K_d. From this plot, an equilibrium constant (log K_1) of 5.62 was determined.

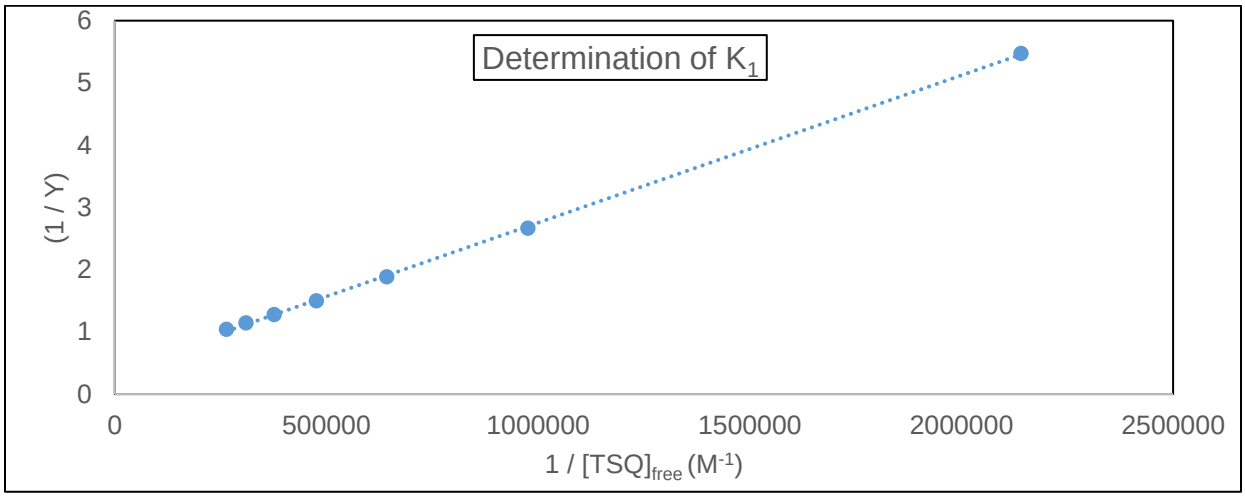

Figure 4.4

Plot of (1 / Y) vs $[\text{TSQ}]_{free}$ for determination of K_1

The fact that the plot does not have an intercept of 1 indicates that the reaction is more complicated than portrayed above. Recently, we realized that TSQ, itself, binds adventitiously to the Proteome:

$$\text{Proteome} + \text{TSQ} \leftrightharpoons \text{TSQ-Proteome} \quad (K_2) \tag{4.8}$$

As a result, the above analysis is not correct. In order to be able to determine the absolute value of K_1, we would need to study and evaluate the above reaction.

3.2 Adduct formation of ligands with Zn-Proteome and Proteome•Zn

We surveyed the ability of ligands to form adduct species with Zn-Proteome and Proteome•Zn using a competitive titration experiment. After completing the titrations, products were filtered through a 3 kDa filter to separate Proteomic zinc (retentate) from low molecular weight zinc-ligand complexes (filtrate). The results are shown in each titration as a table inset along with the log of conditional stability constants for each zinc-ligand complex at pH 7.4 (taken from Stability Constants Supplement No. 1, Special Publication 25).

3.2.1 1,10-Phenanthroline

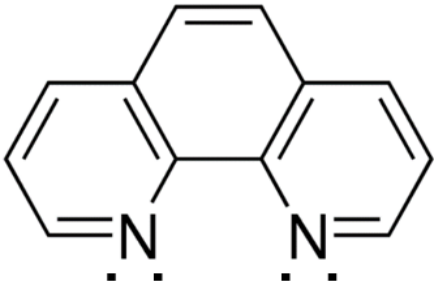

Figure 4.5

Structure of 1,10-phenanthroline pH 7.4 (recreated from Sigma website)

We started out by repeating and extending the work of Kaniz Fatema on the reaction of 1,10-phenanthroline (Phen) with TSQ-Zn-Proteome (**structure figure 4.5**). **Figure 4.6** shows the competitive reaction titration with Phen and **figure 4.7** summarizes the results of the titration.

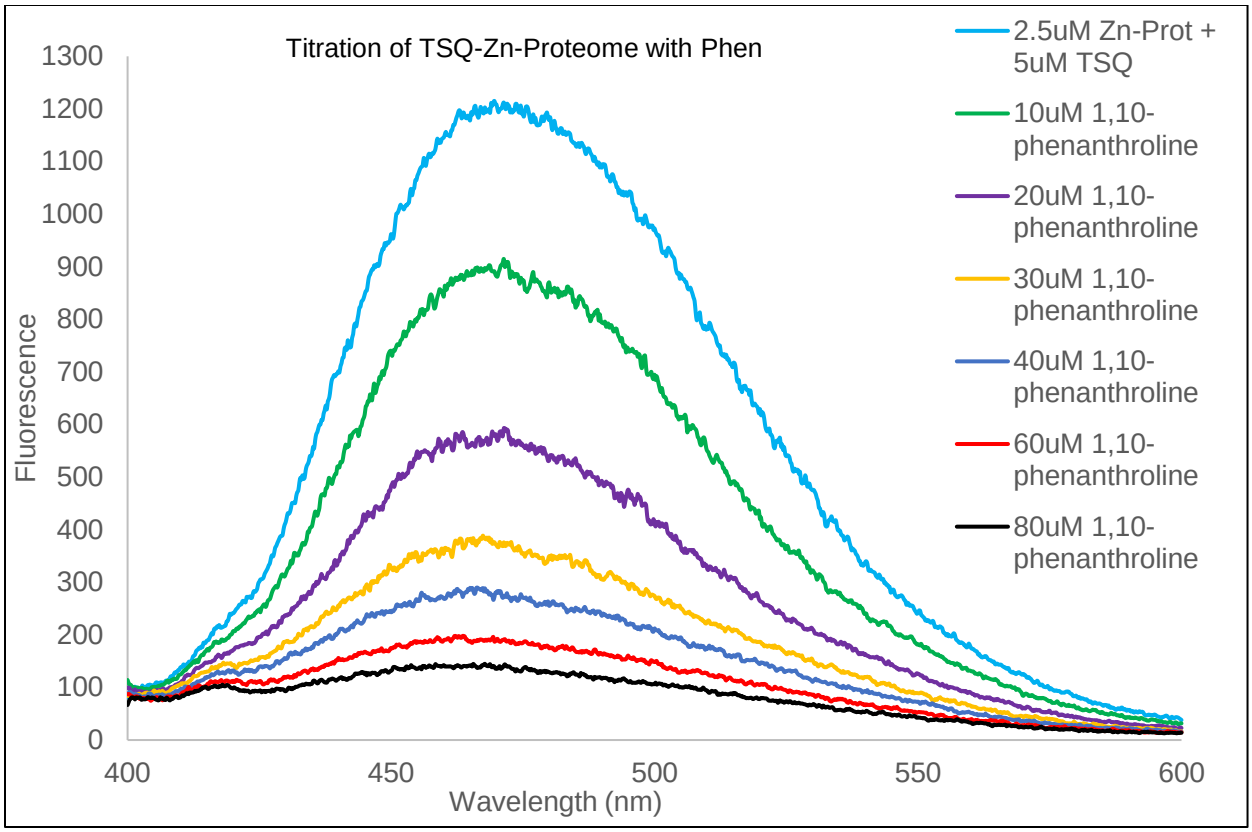

Figure 4.6

Titration of TSQ-Zn-Proteome with Phen. 2.5 µM Zn-Proteome in 20 mM Tris pH 7.4 was incubated with 5 µM TSQ for 60 mins prior to addition of Phen. 5 minutes between additions of Phen. Excitation wavelength was 365 nm. Emission wavelength span 400-600 nm.

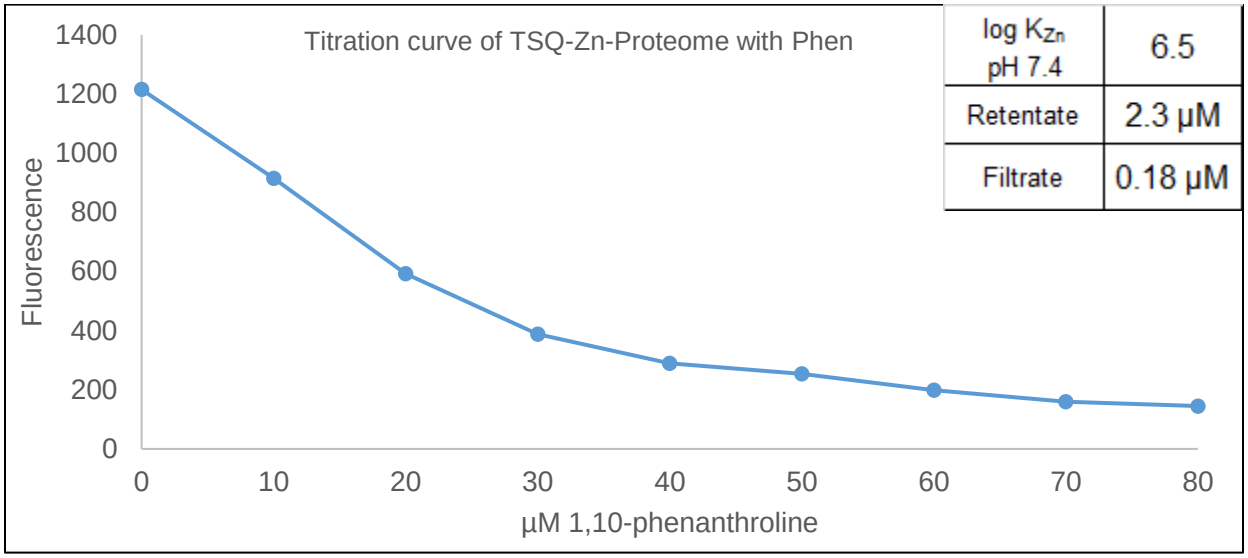

Figure 4.7

Titration curve of TSQ-Zn-Proteome with Phen. 2.5 µM Zn-Proteome in 20 mM Tris pH 7.4 was incubated with 5 µM TSQ for 60 mins prior to addition of Phen. 5 minutes between additions of Phen. Excitation wavelength was 365 nm. Emission wavelength span 400-600 nm.

The initial fluorescence was due to the formation of TSQ-Zn-Proteome adducts with about 25% of the zinc in the sample (Meeusen et al. 2011). Upon addition of Phen, the proposed competitive exchange reaction occurred with the loss of fluorescence (**reaction 4.2**). The reaction was 50% complete at about 15 µM Phen and neared completion at 50 µM ligand. According to the inset of **figure 4.7**, Phen mobilized only 7% of Proteomic zinc as filterable $Zn(Phen)_{2\text{-}3}$; so the observed reaction was largely an exchange process.

The reaction was also examined by NSDS-PAGE. TSQ-Zn-proteins were initially separated by this native PAGE method. Then, they were exposed in the gel to 100 µM Phen. **Figure 4.8** shows that Phen completely dissociated the TSQ-Zn-protein complexes as it fully extinguished the fluorescence.

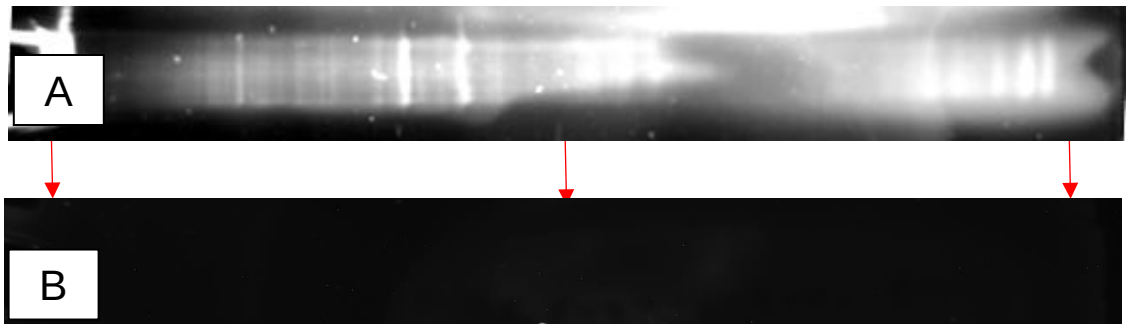

Figure 4.8

A. NSDS-PAGE separated Zn-Proteome stained with TSQ.
B. Gel incubated with 100 µM Phen for 10 minutes before taking another exposure spectra.

Next, the combined reactions of TSQ-Zn-Proteome and Proteome•Zn-TSQ with Phen were studied (**figures 4.9- 4.10**). This experiment with each of the ligands below was conducted under conditions in which all the added Zn^{2+} was bound to higher affinity binding sites in the Proteome that have sulfhydryl groups as part of their ligand sets (Petering et al. 2017).

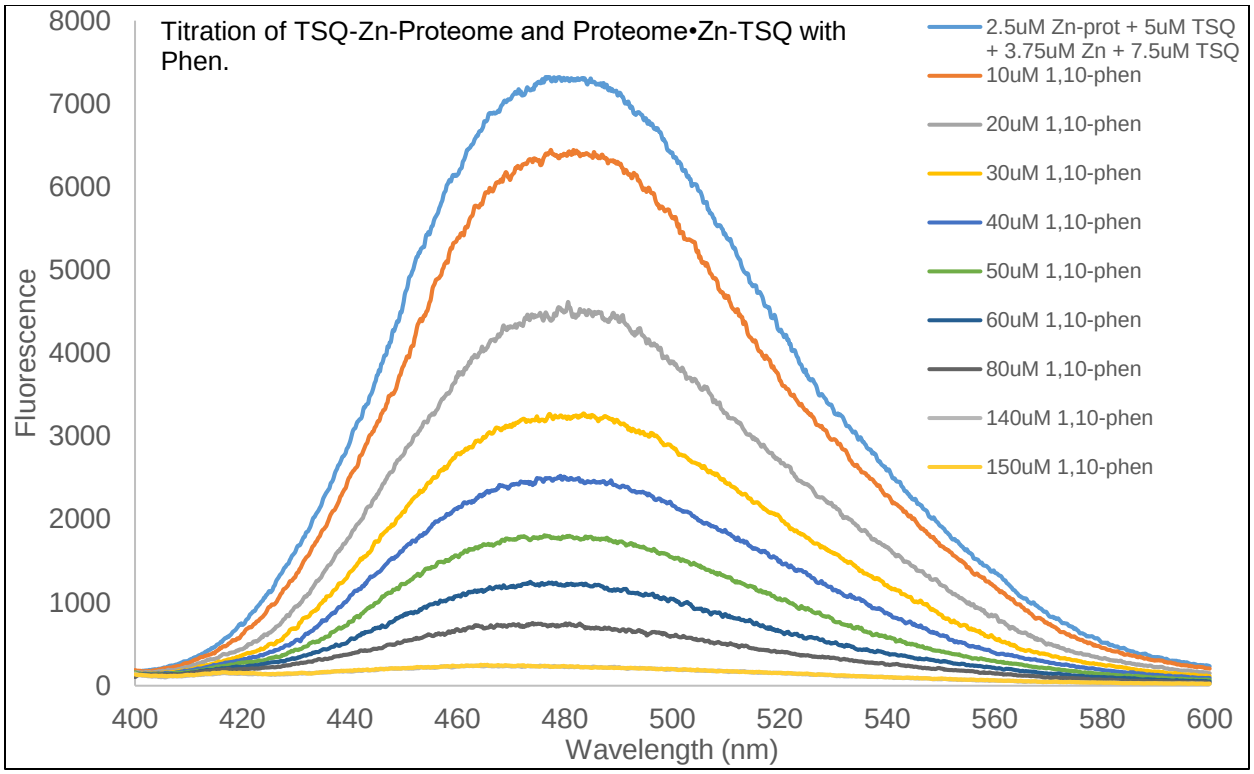

Figure 4.9

Titration of TSQ-Zn-Proteome and Proteome•Zn-TSQ with Phen. 2.5 µM Zn-Proteome in 20 mM Tris pH 7.4 was incubated with 5 µM TSQ for 60 mins prior to addition of 3.75 µM extra Zn^{2+}. Additional 7.5 µM TSQ was added, after 30 minutes of Zn^{2+} addition, prior to addition of Phen. 5 minutes in between additions of Phen. Excitation wavelength was 365 nm. Emission wavelength span 400-600 nm.

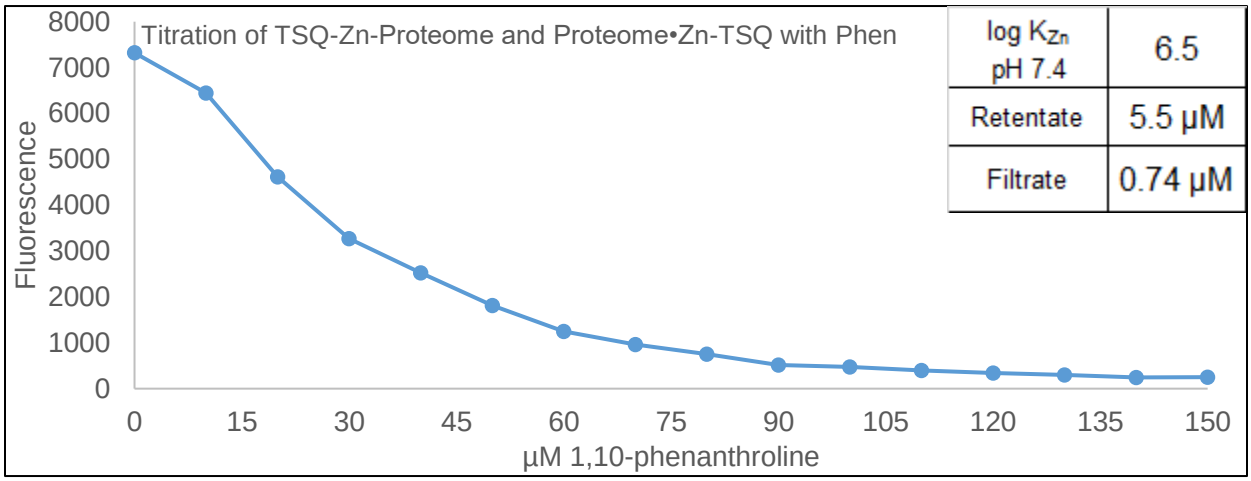

Figure 4.10

Titration curve of TSQ-Zn-Proteome and Proteome•Zn-TSQ with Phen. 2.5 µM Zn-Proteome in 20 mM Tris pH 7.4 was incubated with 5 µM TSQ for 60 mins prior to addition of 3.75 µM extra Zn^{2+}. Additional 7.5 µM TSQ was added, after 30 minutes of Zn^{2+} addition, prior to addition of Phen. 5 minutes in between additions of Phen. Excitation wavelength was 365 nm. Emission wavelength span 400-600 nm.

First, the summary titration curve shows that the starting fluorescence was much higher in this titration (**figure 4.10**). That was because extra Zn^{2+} was present that could react with high affinity Proteomic binding sites to form Proteome•Zn. When Phen was added, the fluorescence dropped 50% after the addition of about 25 µM Phen, representing the exchange of Phen for TSQ in Proteome•Zn (**reaction 4.3**). Some of this zinc was competitively removed by Phen when its concentration had reached 150 µM. At 25 µM, much less would have been in the form of $Zn(Phen)_{2\text{-}3}$.

Phen, like TSQ, also binds to Proteome. Given that it effectively and completely competes with bound TSQ at low µM concentrations, it seems likely that Phen may broadly bind to Proteomic sites containing zinc in the absence of TSQ.

3.2.2 2-mercaptopyridine-N-oxide (PYR)

Next, we moved to a ligand of particular interest in this thesis research, 2-mercaptopyridine-N-oxide (PYR) (**structure figure 2.1**). **Figures 4.11-4.14** describe its reactions with TSQ-Zn-Proteome and Proteome•Zn-TSQ.

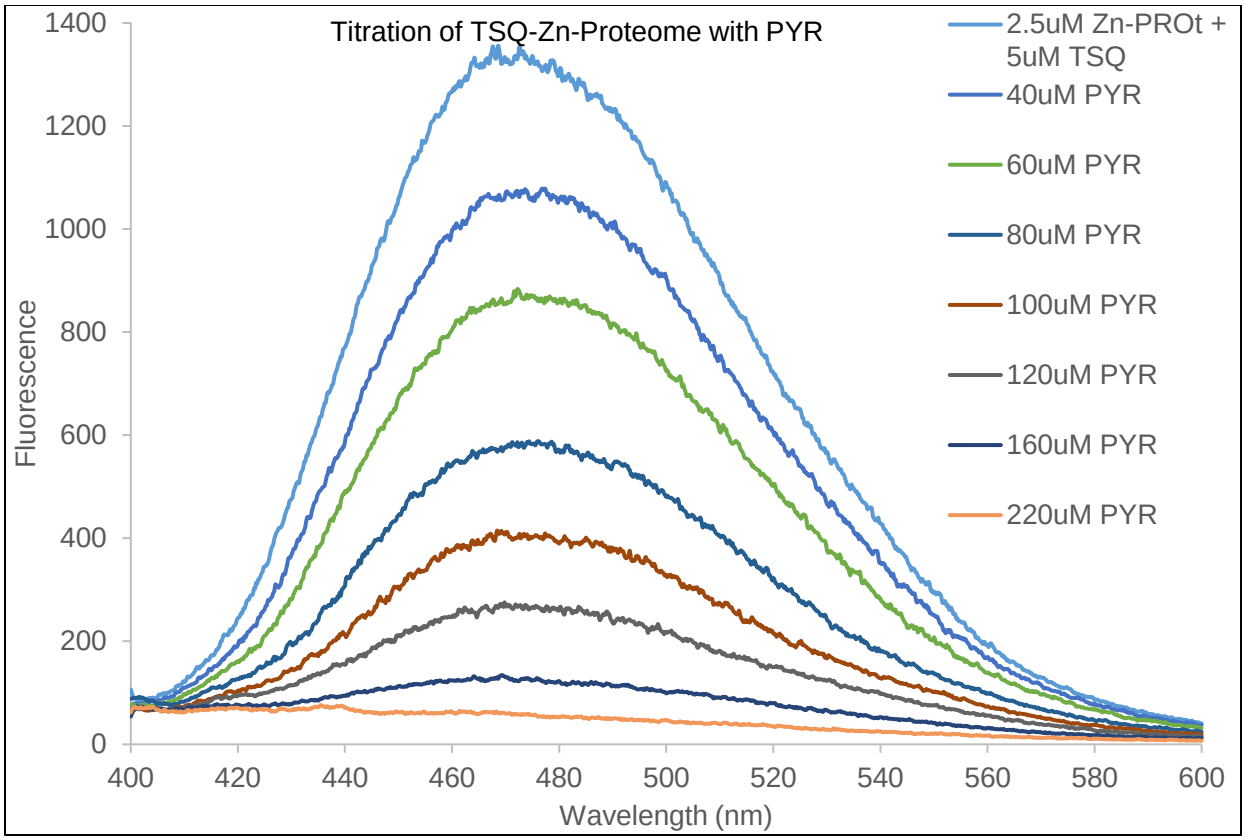

Figure 4.11

Titration of TSQ-Zn-Proteome with PYR. 2.5 µM Zn-Proteome in 20 mM Tris pH 7.4 was incubated with 5 µM TSQ for 60 mins prior to addition of PYR. 5 minutes in between additions of PYR. Excitation wavelength was 365 nm. Emission wavelength span was 400-600 nm

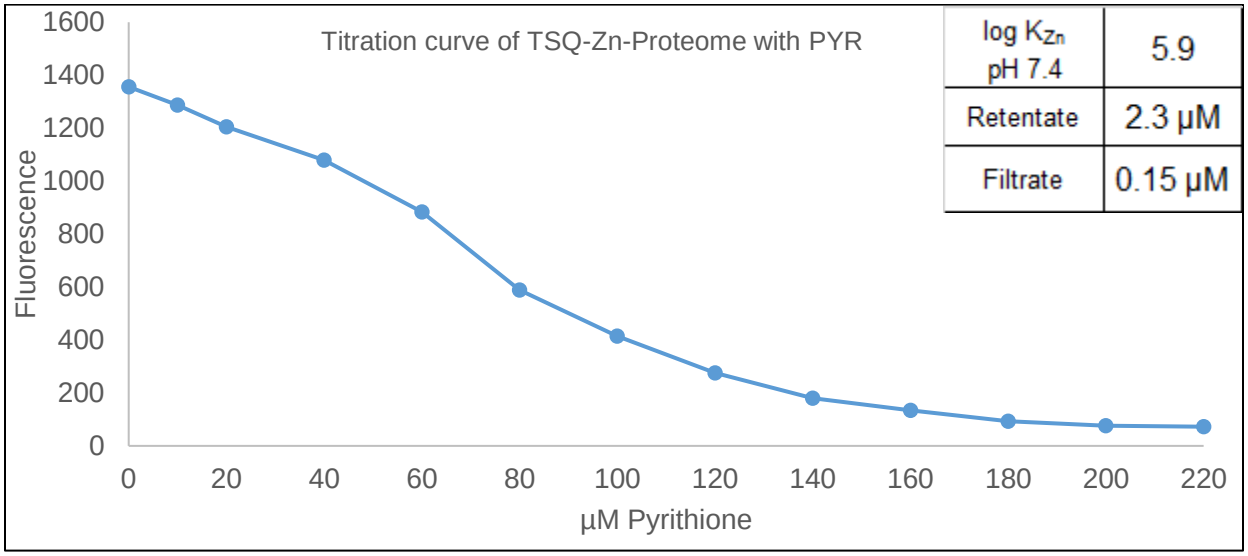

Figure 4.12

Titration curve of TSQ-Zn-Proteome with PYR. 2.5 µM Zn-Proteome in 20 mM Tris pH 7.4 was incubated with 5 µM TSQ for 60 mins prior to addition of PYR. 5 minutes in between additions of PYR. Excitation wavelength was 365 nm. Emission wavelength span was 400-600 nm

Upon addition of PYR, the proposed competitive exchange reaction occurred with a biphasic loss of fluorescence with the first part less sensitive to PYR than the second (**reaction 4.2**). The overall reaction was 50% complete at about 70 µM PYR. According to the inset of **figure 4.12**, PYR mobilized only 6% of Proteomic zinc as filterable $Zn(PYR)_2$; so the observed reaction was largely an exchange process (**reaction 4.9**):

$$\text{TSQ-Zn-Proteome} + \text{PYR} \leftrightharpoons \text{PYR-Zn-Proteome} + \text{TSQ} \qquad (4.9)$$

Reaction 4.9 shows that the interaction of the Zn-Proteome with PYR may have further implications that were not explored in **Section II**. If PYR can bind to the Zn-Proteome, then **reaction 2.5** becomes:

$$Cd(PYR)_2 + \text{Zn-Proteome} + \text{Proteome} \leftrightharpoons \text{PYR-Zn-Proteome} + \text{Proteome•Cd-PYR} \qquad (4.10)$$

Therefore, PYR may participate in the intracellular chemistry of Cd^{2+} in previously unrecognized ways. For example, the exchange reaction of Cd^{2+} and Zn^{2+} may involve the products of **reaction 4.10**:

$$\text{PYR-Zn-Proteome} + \text{Proteome•Cd-PYR} \leftrightharpoons \text{PYR-Cd-Proteome} + \text{Proteome•Zn-PYR} \qquad (4.11)$$

Figure 4.13 shows the competitive reaction titration of TSQ-Zn-Proteome and Proteome•Zn-TSQ with PYR and **figure 4.14** displays the summary of the titration.

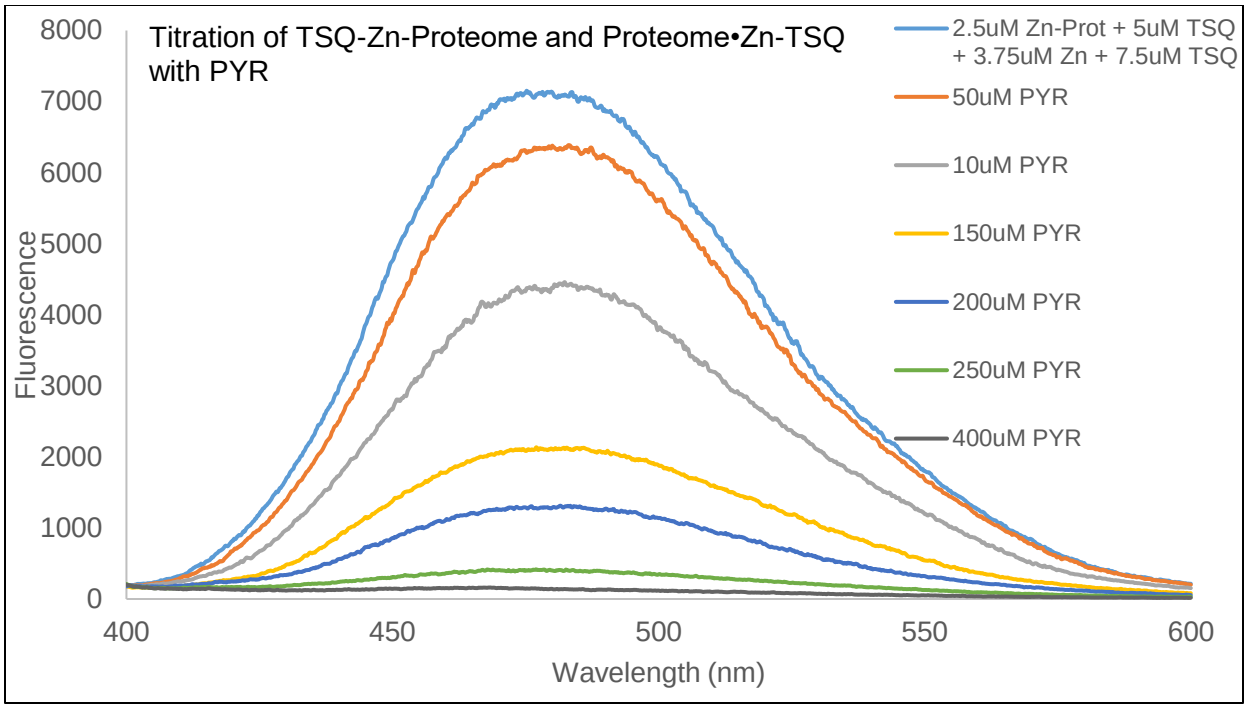

Figure 4.13

Titration of TSQ-Zn-Proteome and Proteome•Zn-TSQ with PYR. 2.5 µM Zn-Proteome in 20 mM Tris pH 7.4 was incubated with 5 µM TSQ for 60 mins prior to addition of 3.75 µM extra Zn^{2+}. Additional 7.5 µM TSQ was added, after 30 minutes of Zn^{2+} addition, prior to addition of PYR. 5 minutes in between additions of PYR. Excitation wavelength was 365 nm. Emission wavelength span 400-600 nm.

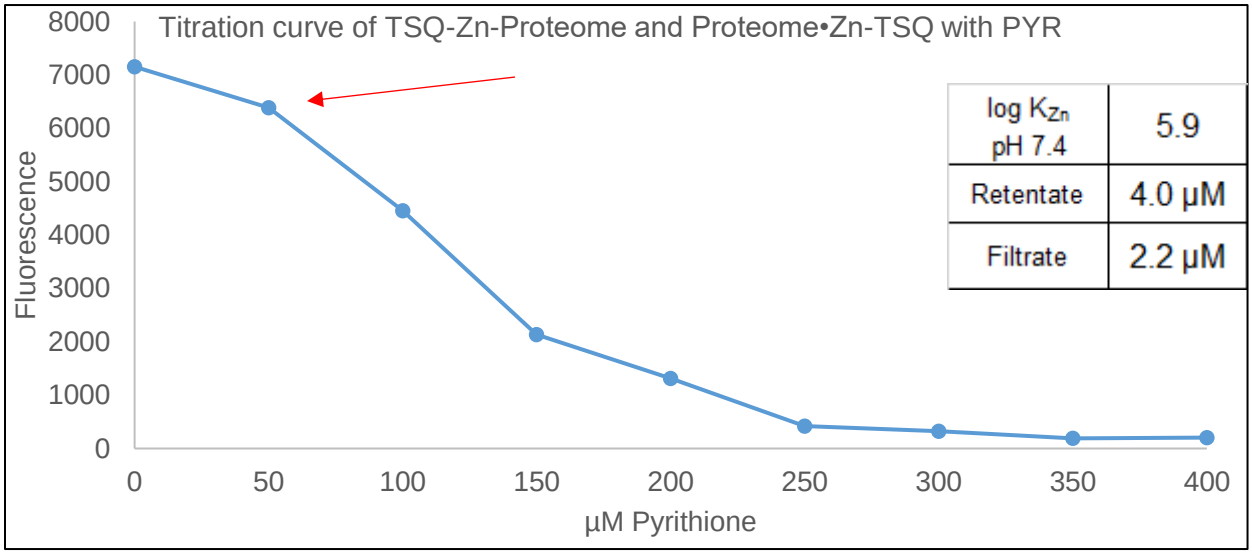

Figure 4.14

Titration curve of TSQ-Zn-Proteome and Proteome•Zn-TSQ with PYR. 2.5 µM Zn-Proteome in 20 mM Tris pH 7.4 was incubated with 5 µM TSQ for 60 mins prior to addition of 3.75 µM extra Zn^{2+}. Additional 7.5 µM TSQ was added, after 30 minutes of Zn^{2+} addition, prior to addition of PYR. 5 minutes in between additions of PYR. Excitation wavelength was 365 nm. Emission wavelength span 400-600 nm.

There appear to be two reactions occurring upon addition of PYR (**figure 4.14**). Initially (up to ~50 µM), there is a lag in the decrease of fluorescence during the first additions of PYR (**figure 4.14;** red arrow). Possibly, PYR is binding non-specifically to the Proteome, making is less available to compete with TSQ for zinc binding sites. This lag also appears, to a lesser extent, in **figure 4.12**.

The second reaction represents the interaction of PYR with Proteome•Zn-TSQ. This reaction was 50% complete at about 125 µM PYR; nearly double the amount needed in **figure 4.12**. According to the inset of **figure 4.14**, PYR mobilized 35% of Proteomic zinc as filterable $Zn(PYR)_2$ at 400 µM PYR. At lower concentrations, the observed decrease in fluorescence would be largely due to PYR-TSQ exchange. The chelatable Zn^{2+} was presumably in the form of Proteome•Zn, considering PYR did not complex a significant amount of zinc (7%) when reacting with Zn-Proteome alone (**figure 4.12;** inset).

Based on the results from **figure 4.13-4.14**, a different set of reactions occurs with Proteome•Zn, depending on the concentration of PYR, compared to the reaction with Zn-Proteome:

$$\text{TSQ-Zn-Proteome} + \text{Proteome•Zn-TSQ} + 2\ \text{PYR} \leftrightharpoons \text{PYR-Zn-Proteome} + \text{Proteome•Zn-PYR} + 2\ \text{TSQ} \qquad (4.12)$$

$$\text{Proteome•Zn-PYR} + \text{PYR} \leftrightharpoons Zn(PYR)_2 + \text{Proteome} \qquad (4.13)$$

3.2.3 L-Cysteine

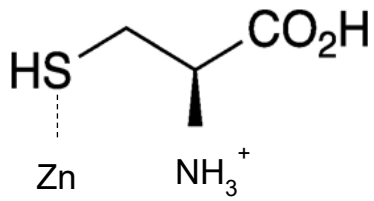

Figure 4.15

Structure of L-Cysteine pH 7.4 (recreated from Sigma website)

L-Cysteine (Cys) is a biologically reactive molecule (**structure figure 4.15**). L-Cysteine is a nutritionally semiessential amino acid. Intracellular L-Cysteine plays an important role in cellular homeostatsis, as a precursor for protein synthesis, and for production of structural motifs in L-glutathione (Yin et. al. 2016). **Figures 4.16-4.17** show the primary data for the titration of TSQ-Zn-Proteome with Cys and the resulting titration plot.

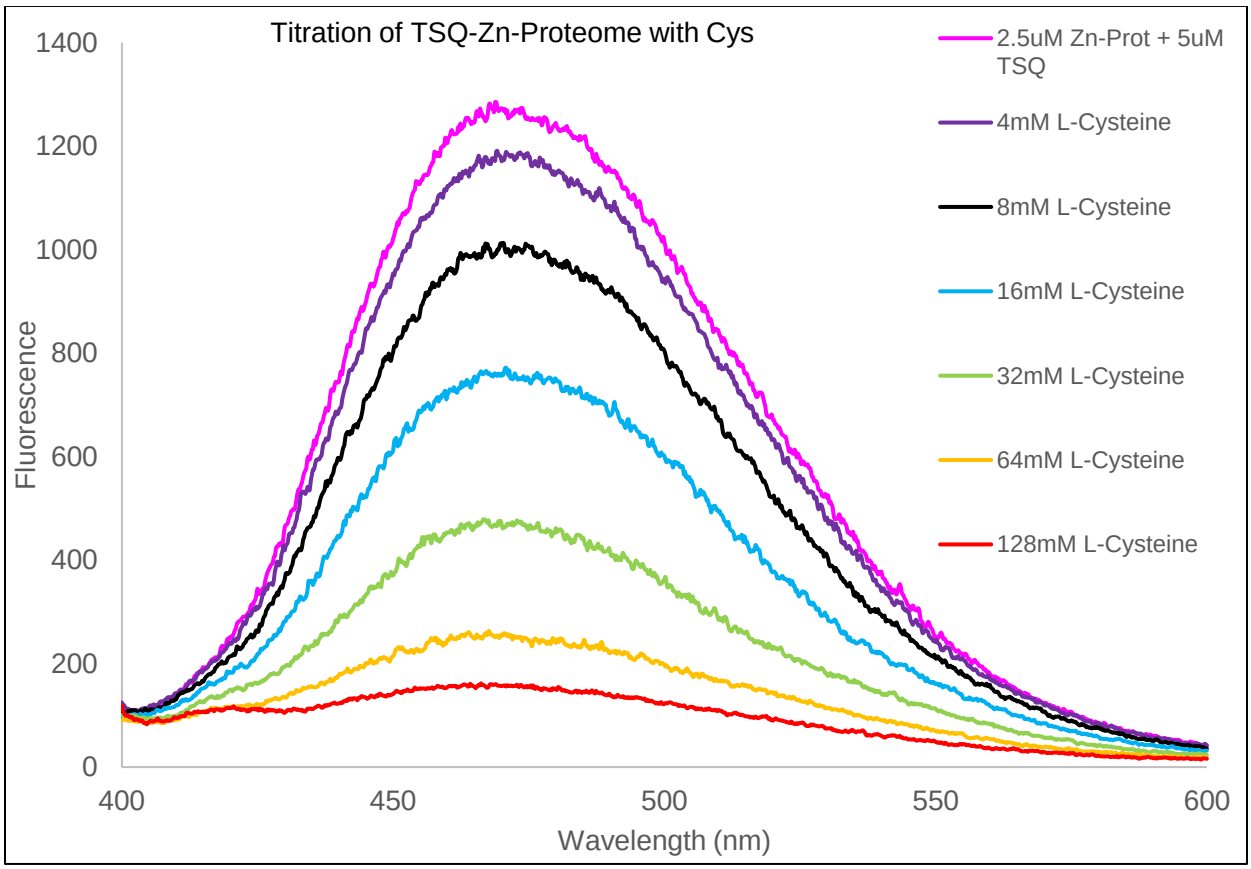

Figure 4.16

Titration of TSQ-Zn-Proteome with Cys. 2.5 µM Zn-Proteome in 20 mM Tris pH 7.4 was incubated with 5 µM TSQ for 60 minutes prior to addition of Cys. 5 minutes in between additions of Cys. Excitation wavelength was 365 nm. Emission wavelength span was 400-600 nm.

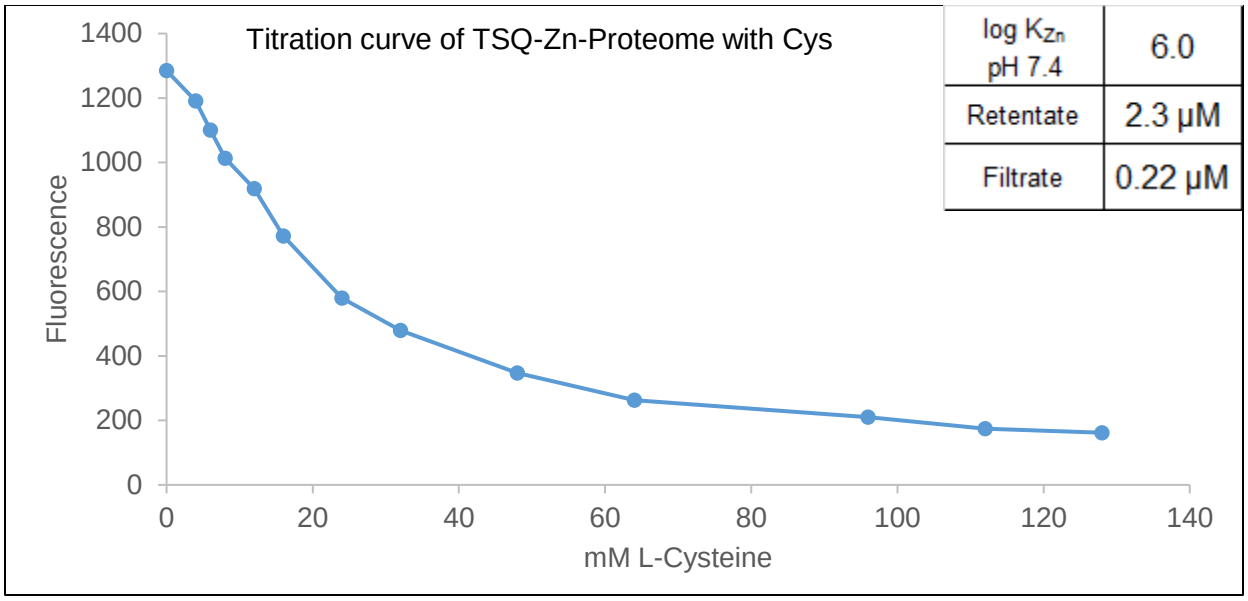

Figure 4.17

Titration curve of TSQ-Zn-Proteome with Cys. 2.5 µM Zn-Proteome in 20 mM Tris pH 7.4 was incubated with 5 µM TSQ for 60 minutes prior to addition of Cys. 5 minutes in between additions of Cys. Excitation wavelength was 365 nm. Emission wavelength span was 400-600 nm.

Cysteine was an effective but poor competitor of TSQ for Zn-Proteome. The exchange reaction was 50% complete at 16 mM Cys, about three orders of magnitude larger than what was needed for Phen and PYR. To reduce the fluorescence further to 15% of the original required approximately an additional 80 mM Cys. The observed loss of fluorescence was almost exclusively the result of a true exchange reaction. This was shown by the small 9% extraction of zinc from the Proteomic pool into the small molecular weight pool (**figure 4.17;** inset) at the end of the titration determined by centrifugal filtration through a 3 kDa filter.

The titration was repeated after additional Zn^{2+} and TSQ were added to the starting sample of Proteome. In this case, both TSQ-Zn-Proteome and Proteome•Zn-TSQ were in the reaction mixture. **Figures 4.18-4.19** show the primary data and resultant titration curve.

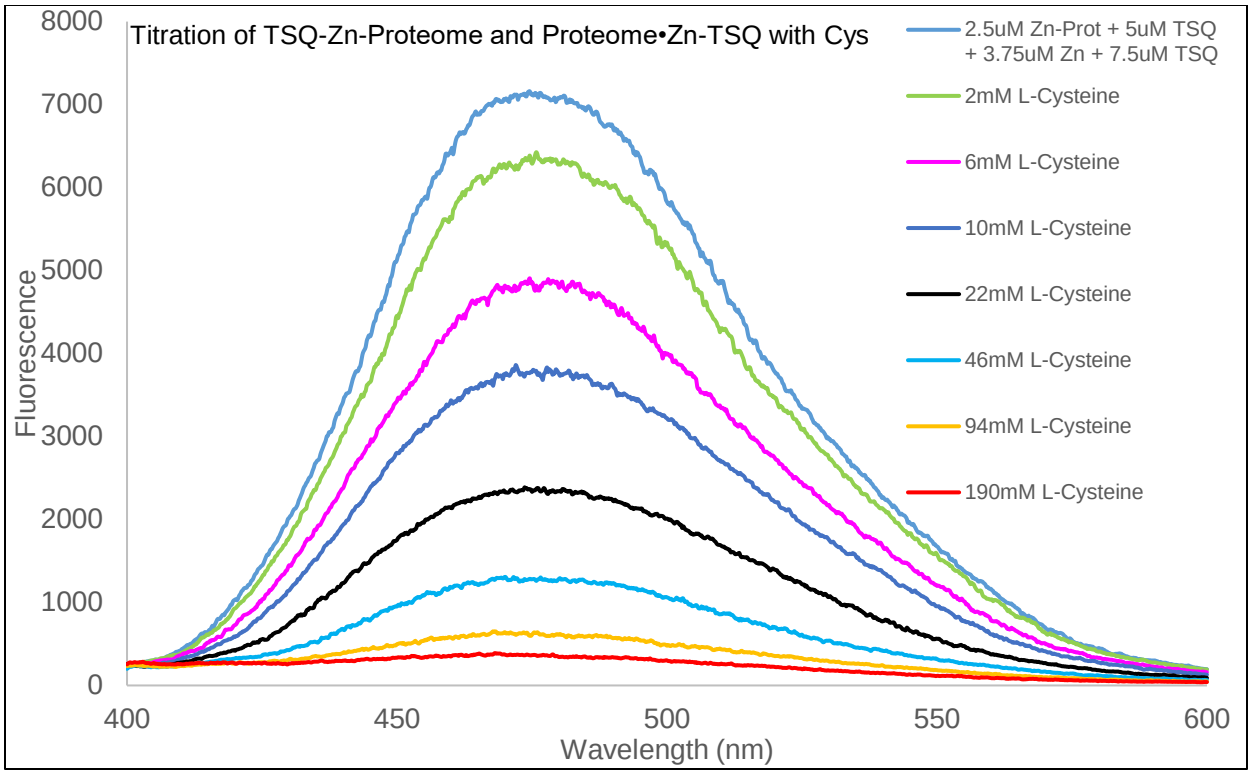

Figure 4.18

Titration of TSQ-Zn-Proteome and Proteome•Zn-TSQ with Cys. 2.5 µM Zn-Proteome in 20 mM Tris pH 7.4 was incubated with 5 µM TSQ for 60 mins prior to addition of 3.75 µM extra Zn^{2+}. Additional 7.5 µM TSQ was added, after 30 minutes of Zn^{2+} addition, prior to addition of Cys. 5 minutes in between additions of Cys. Excitation wavelength was 365 nm. Emission wavelength span 400-600 nm.

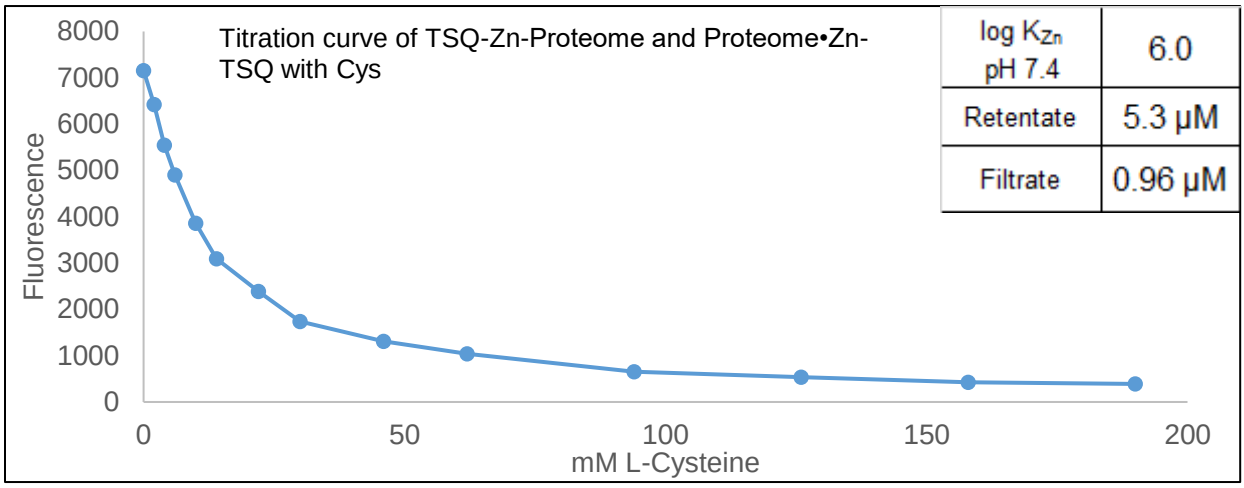

Figure 4.19

Titration curve of TSQ-Zn-Proteome and Proteome•Zn-TSQ with Cys. 2.5 µM Zn-Proteome in 20 mM Tris pH 7.4 was incubated with 5 µM TSQ for 60 mins prior to addition of 3.75 µM extra Zn^{2+}. Additional 7.5 µM TSQ was added, after 30 minutes of Zn^{2+} addition, prior to addition of Cys. 5 minutes in between additions of Cys. Excitation wavelength was 365 nm. Emission wavelength span 400-600 nm.

The starting fluorescence for this reaction was about five times larger than for the titration in the absence of added Zn^{2+} because of the formation of a relatively large concentration of Proteome•Zn-TSQ (**figure 4.18**). The early, steep decline in fluorescence was likely due to the reaction of Cys with Proteome•Zn-TSQ which was nearly complete at 30 mM Cys (**figure 4.19**). The rest of the titration is similar to that described in **figure 4.17**. Although some additional zinc was mobilized from the proteome by Cys when extra Zn^{2+} was present, most of it remained bound as Zn-Proteome and Proteome•Zn. Like the reaction of Cys with native TSQ-Zn-proteins, it was relatively ineffective in competition with TSQ bound as Proteome•Zn-TSQ. This was not because of a lack of affinity for Zn^{2+}. Its log K_{Zn} is similar to those for Phen and PYR. The implication is that protein binding sites for Zn^{2+} prefer Phen and PYR to Cys.

3.2.4 Glutathione

Glutathione (GSH) is an important biomolecule for cellular protection against oxidants and electrophiles (Pizzorno 2014). It is a tripeptide, glutamate-cysteine-glycine, that utilizes the cysteine thiol group to accomplish its protective functions (**structure figure 4.20**). GSH also binds Zn^{2+} with modest affinity ($K_{Zn} = 10^{4.7}$ at pH 7.4) (Walsh et al. 2013). Because it exists in cells in mM concentration (1-10 mM), it is possible that it plays significant roles in zinc biochemistry. **Figures 4.21-4.24** describe how GSH interacts with TSQ-Zn-Proteome and Proteome•Zn-TSQ.

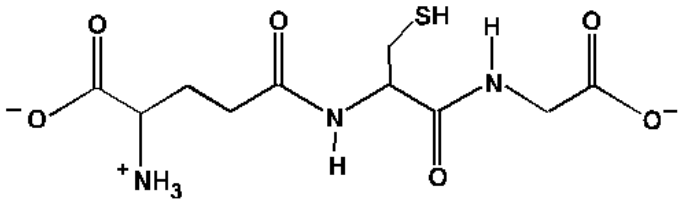

Figure 4.20

Structure of L-Glutathione pH 7.4 (reproduced from Sigma website)

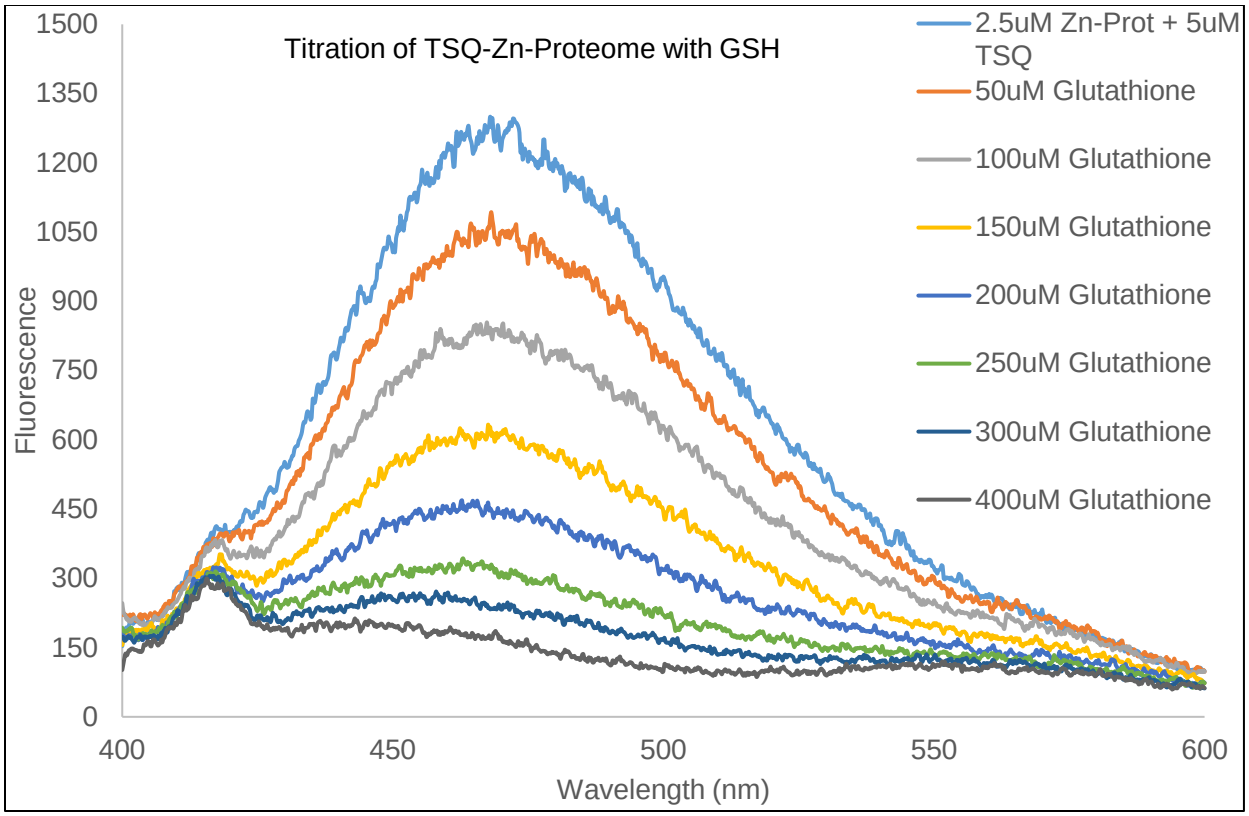

Figure 4.21

Titration of TSQ-Zn-Proteome with GSH. 2.5 µM Zn-Proteome in 20 mM Tris pH 7.4 was incubated with 5 µM TSQ for 60 mins prior to addition of Glt. 5 minutes in between additions of GSH. Excitation wavelength was 365 nm. Emission wavelength span was 400-600 nm.

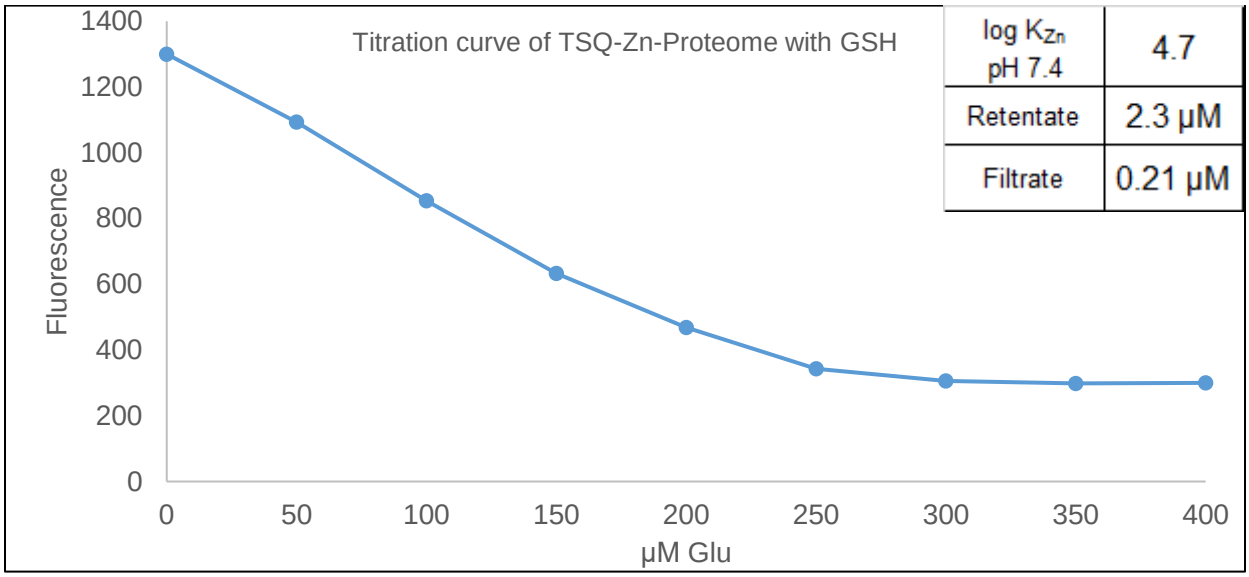

Figure 4.22

Titration curve of TSQ-Zn-Proteome with GSH. 2.5 µM Zn-Proteome in 20 mM Tris pH 7.4 was incubated with 5 µM TSQ for 60 mins prior to addition of GSH. 5 minutes in between additions of Glt. Excitation wavelength was 365 nm. Emission wavelength span was 400-600 nm.

In contrast to Cys, GSH is a more effective competitor of TSQ. As seen in **figure 4.22**, approximately 50% of the overall reaction was complete at 110 µM GSH. At 400 µM GSH, little Zn^{2+} bound to the Zn-Proteome was available for formation of Zn-$(GSH)_{1-2}$ (8%). Since the concentration of GSH in cells lies in the mM range, it seems likely that some Zn-proteins exist as GS-Zn-proteins in the intracellular steady state.

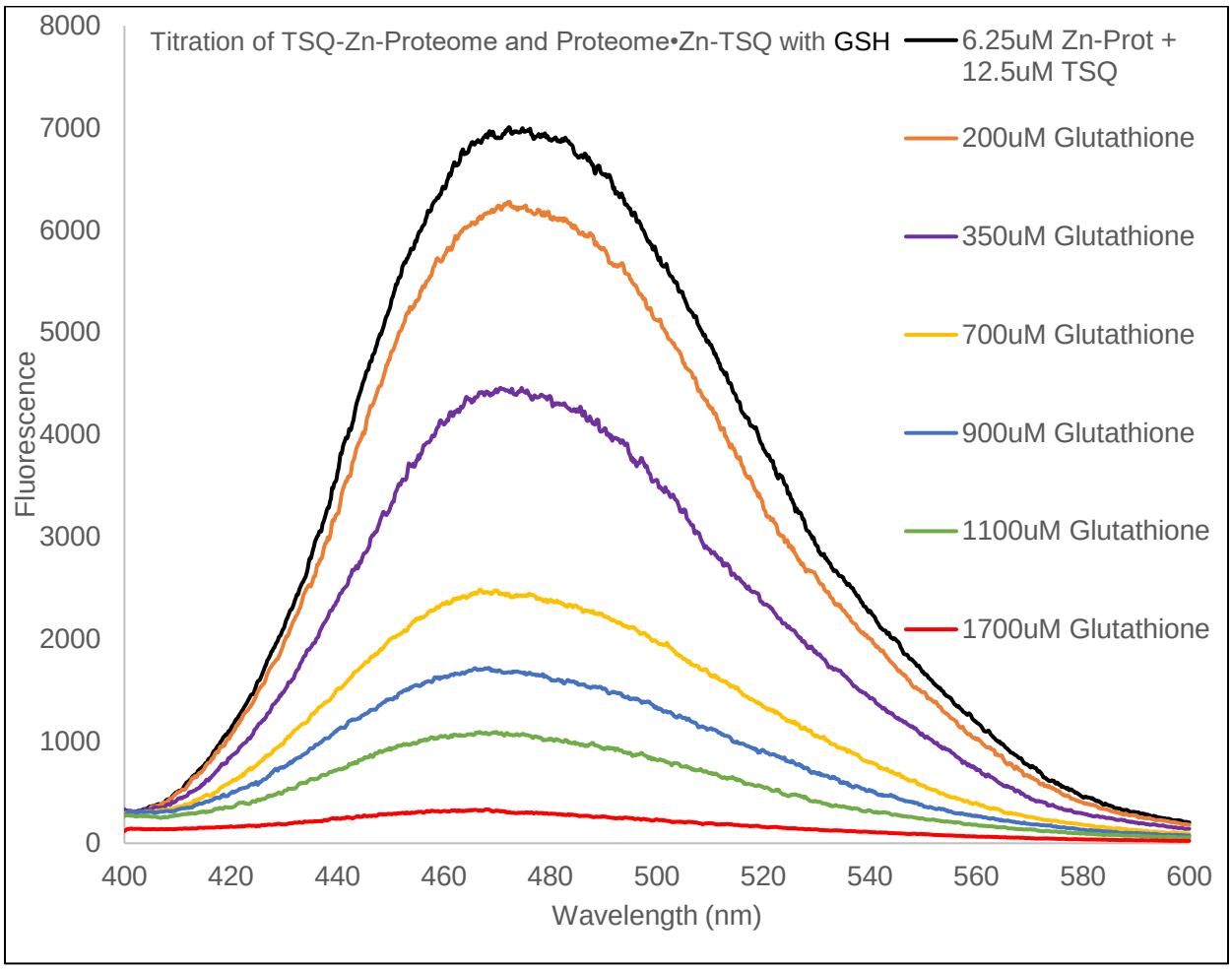

Figure 4.23

Titration of TSQ-Zn-Proteome and Proteome•Zn-TSQ with GSH. 2.5 µM Zn-Proteome in 20 mM Tris pH 7.4 was incubated with 5 µM TSQ for 60 mins prior to addition of 3.75 µM extra Zn^{2+}. Additional 7.5 µM TSQ was added, after 30 minutes of Zn^{2+} addition, prior to addition of GSH. 5 minutes in between additions of GSH. Excitation wavelength was 365 nm. Emission wavelength span 400-600 nm.

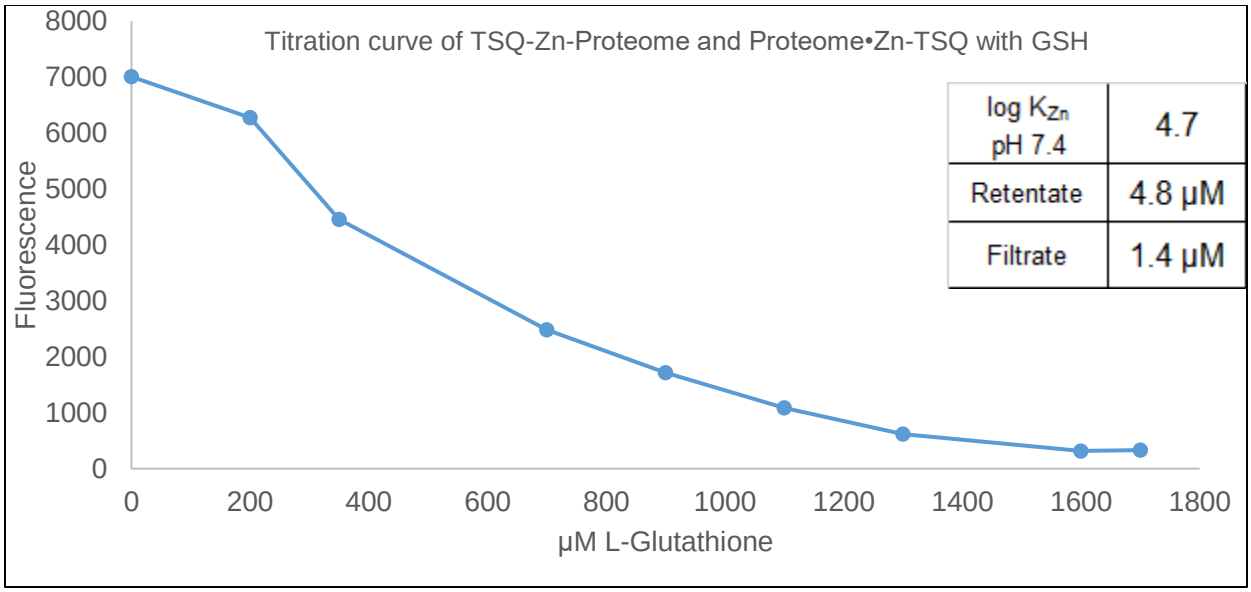

Figure 4.24

Titration curve of TSQ-Zn-Proteome and Proteome•Zn-TSQ with GSH. 2.5 µM Zn-Proteome in 20 mM Tris pH 7.4 was incubated with 5 µM TSQ for 60 mins prior to addition of 3.75 µM extra Zn^{2+}. Additional 7.5 µM TSQ was added, after 30 minutes of Zn^{2+} addition, prior to addition of GSH. 5 minutes in between additions of GSH. Excitation wavelength was 365 nm. Emission wavelength span 400-600 nm.

In the presence of extra Zn^{2+} the overall reaction of Glu with Proteomic zinc binding sites required more GSH (**figure 4.24**). About 500 µM GSH was needed to quench the fluorescence 50%; over 4 times the amount needed to quench TSQ-Zn-Proteome (**figure 4.22**). The relatively large concentration needed to drive this reaction in comparison with those involving Phen or PYR could be due in part to the lower stability constant of GSH with Zn^{2+} when compared to the calculated stability constants for Phen and PYR.

The reaction neared completion at 1.6 mM and chelated a modest 22% of Proteomic zinc at that point. Proteome•Zn is the presumed form of chelatable Zn^{2+}, considering that GSH did not remove a significant amount of zinc when reacting with Zn-Proteome (8%) (**figure 4.22;** inset). This explanation bolsters recently completed experiments in the Petering lab that show that GSH enhances the rate that Proteome•Zn donates Zn^{2+} to apo-Zn-proteins such as apo-carbonic anhydrase (Petering et al. 2019).

3.2.5 Pyridine-2,6-dicarboxylic acid (Dipicolinic Acid)

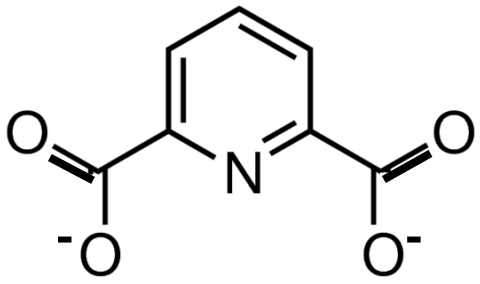

Figure 4.25

Structure of pyridine-2,6-dicarboxylic acid pH 7.4 (recreated from Sigma website)

Dipicolinic acid (DCP) (**structure figure 4.25**) was originally used to chelate cations within spores of bacteria in a 1:1 ratio (Setlow et. al. 2006). This ligand is also the standard ligand employed to extract Zn^{2+} from Carbonic Anhydrase. **Figures 4.26-4.29** describe its reactions with TSQ-Zn-Proteome and Proteome•Zn-TSQ.

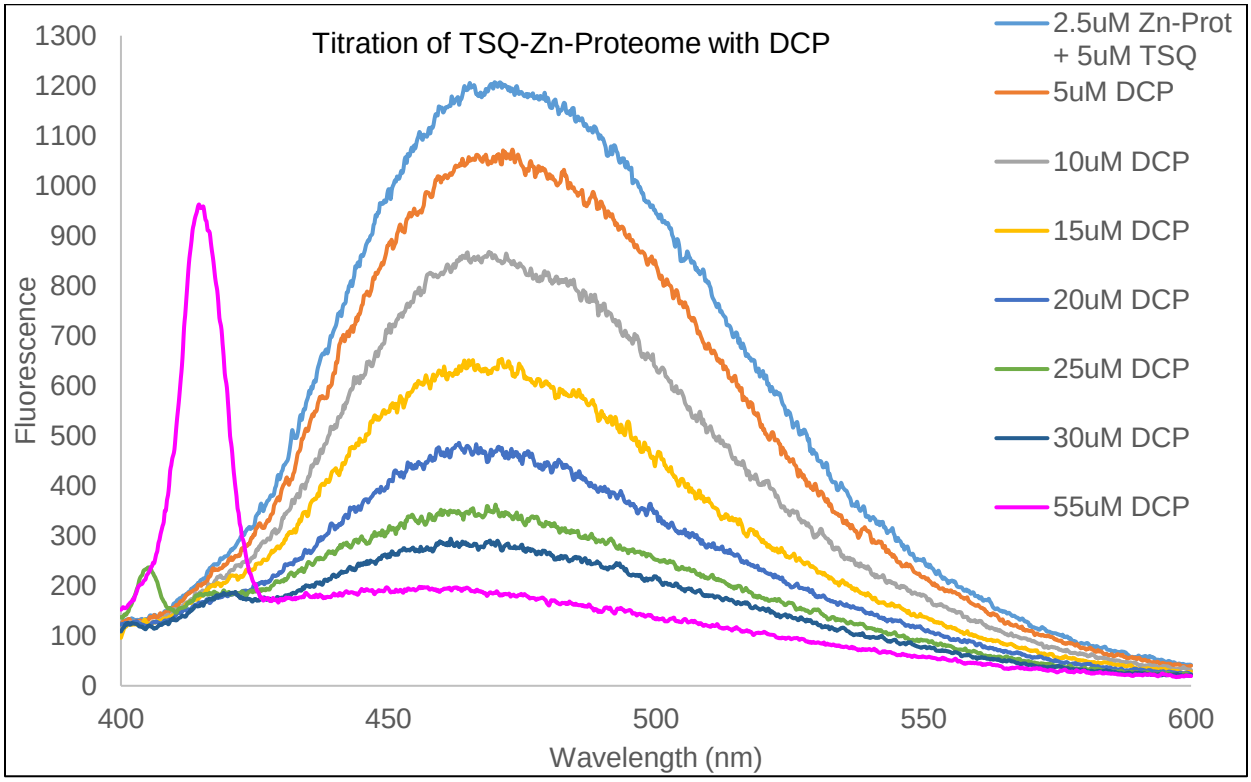

Figure 4.26

Titration of TSQ-Zn-Proteome with DCP. 2.5 µM Zn-Proteome in 20 mM Tris pH 7.4 was incubated with 5 µM TSQ for 60 minutes prior to addition of DCP. 5 minutes in between additions of DCP. Excitation wavelength was 365 nm. Emission wavelength span was 400-600 nm.

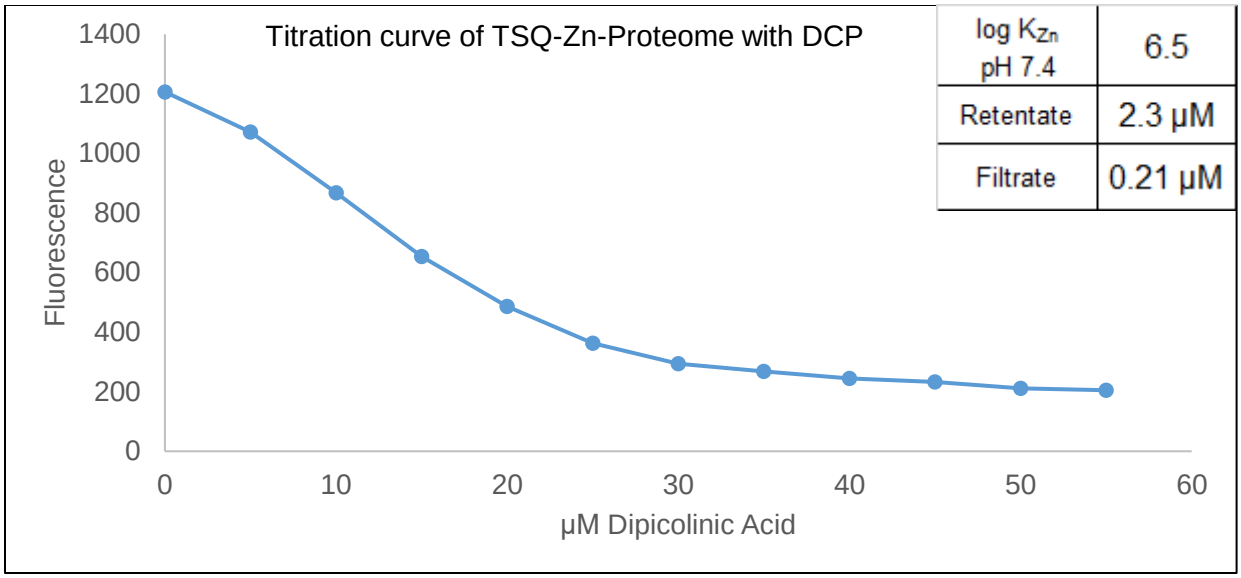

Figure 4.27

Titration curve of TSQ-Zn-Proteome with DCP. 2.5 µM Zn-Proteome in 20 mM Tris pH 7.4 was incubated with 5 µM TSQ for 60 minutes prior to addition of DCP. 5 minutes in between additions of DCP. Excitation wavelength was 365 nm. Emission wavelength span was 400-600 nm.

The competitive exchange reaction between DCP and TSQ, bound to Zn-Proteome, was the most effective among the reactions investigated (**figure 4.27**). The reaction was 50% complete at about 13 µM and complete around 30 µM DCP, somewhat better than Phen at 25 µM and 50 µM, respectively. According to the inset of **figure 4.27**, DCP only mobilized 8% of Proteomic zinc as filterable Zn-$(DCP)_{1\text{-}2}$; so, the observed reaction was largely an exchange process (**reaction 4.2**).

Figure 4.28 shows the competitive reaction titration of Zn-Proteome and Proteome•Zn with DCP and **figure 4.29** displays the summary of the titration.

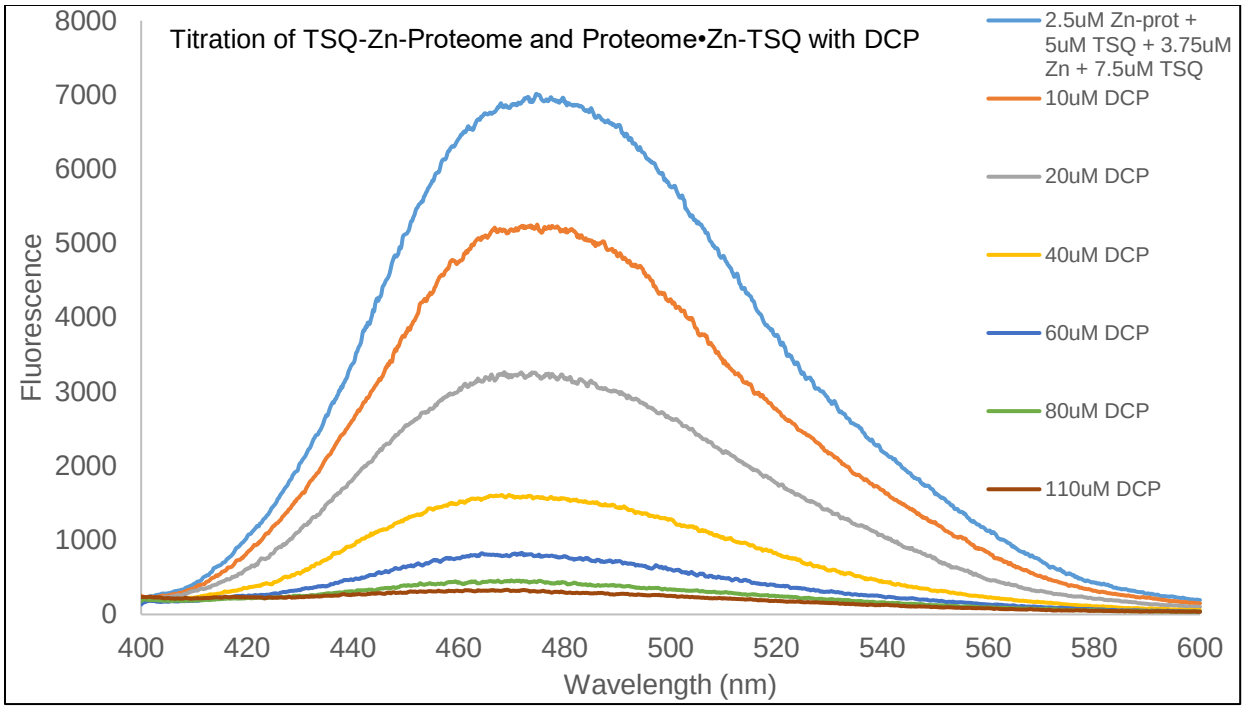

Figure 4.28

Titration of TSQ-Zn-Proteome and Proteome•Zn-TSQ with DCP. 2.5 µM Zn-Proteome in 20 mM Tris pH 7.4 was incubated with 5 µM TSQ for 60 mins prior to addition of 3.75 µM extra Zn^{2+}. Additional 7.5 µM TSQ was added, after 30 minutes of Zn^{2+} addition, prior to addition of DCP. 5 minutes in between additions of DCP. Excitation wavelength was 365 nm. Emission wavelength span 400-600 nm.

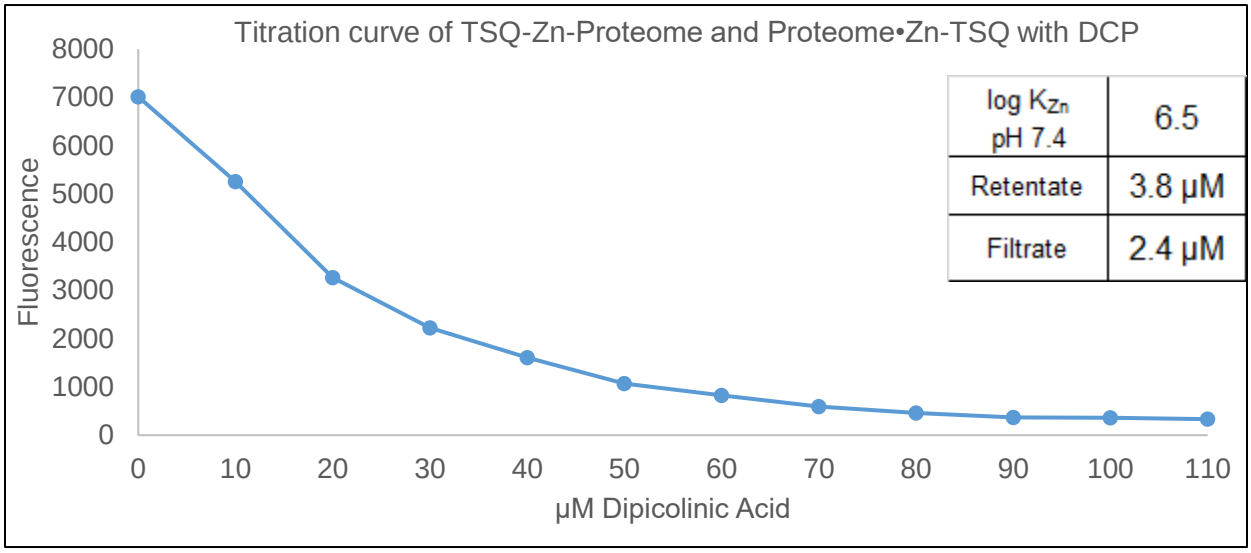

Figure 4.29

Titration of TSQ-Zn-Proteome and Proteome•Zn-TSQ with DCP. 2.5 µM Zn-Proteome in 20 mM Tris pH 7.4 was incubated with 5 µM TSQ for 60 mins prior to addition of 3.75 µM extra Zn^{2+}. Additional 7.5 µM TSQ was added, after 30 minutes of Zn^{2+} addition, prior to addition of DCP. 5 minutes in between additions of DCP. Excitation wavelength was 365 nm. Emission wavelength span 400-600 nm.

The titration of TSQ-Zn-Proteome plus Proteome•Zn-TSQ with DCP showed that DCP also competed with TSQ better than Phen for Proteome•Zn sites, lowering the fluorescence by 50% after the addition of about 13 µM DCP (25 µM for Phen) (**figure 4.29**). The inset table of **figure 4.29** indicates that a substantially larger chelation of Zn^{2+} by DCP than Phen. Specifically, 38% of the total zinc was found in the filtrate. This chelated Zn^{2+} is presumably in the form of Proteome•Zn, considering DCP chelated only 8 % of Zn^{2+} out of the Zn-Proteome.

4. Conclusion

Below is **Table 4.1** listing the concentration needed for the reaction of Proteomic zinc with ligands to be 50% complete from least to most.

	log K_{Zn} pH 7.4	50% Complete (µM)	Retentate (µM)	Filtrate (µM)	50% Complete (µM)	Retentate (µM)	Filtrate (µM)
8-OH	6.1	10	2.3	0.22	200	5.9	0.29
DCP	6.5	13	2.3	0.21	13	3.8	2.4
Phen	6.5	15	2.3	0.18	25	5.5	0.74
BP	5.0	50	2.3	0.18	100	5.0	1.2
PYR	5.9	70	2.3	0.15	125	4.0	2.2
GSH	4.7	110	2.3	0.21	500	4.8	1.4
Cys	5.9	16000	2.3	0.22	10000	5.3	0.96

Table 4.1

Zn^{2+} totals for ligands in the filtrate and retentate. BP – 2,2'-bipyridyl; 8-OH, 8-hydroxyquinoline

This study shows that a wide variety of bidentate and tridentate ligands can bind to native Zn-proteins in competition with TSQ to form ternary adducts. One of them, DCP, undergoes significant reaction with TSQ-Zn-Proteome and Proteome•Zn-TSQ at close to stoichiometric

concentrations. At the other end of the range of activity, very large excesses of Cys are required to replace TSQ in these adducts. Each of the competitive equilibria (**reactions 4.2**-**4.3**)

$$\text{TSQ-Zn-Proteome} + \text{L} \leftrightharpoons \text{L-Zn-Proteome} + \text{TSQ} \qquad K = K_{\text{L-Zn-Proteome}} / K_{\text{TSQ-Zn-Proteome}} \qquad (4.2)$$

$$\text{Proteome•Zn-TSQ} + \text{L} \leftrightharpoons \text{Proteome•Zn-L} + \text{TSQ} \qquad K = K_{\text{Proteome•Zn-L}} / K_{\text{Proteome•Zn-TSQ}} \qquad (4.3)$$

depends on the size of the ternary binding constants of L to Zn-Proteome and Proteome•Zn in comparison to those for TSQ. A relative scale of affinities of the ligands in **Table 4.1** for native Zn-Proteome and non-specifically bound zinc can be derived from the results. But they do not directly indicate whether such reactions may occur ***in vivo***. In the cell, TSQ is not normally present, so the reactions of interest may be

$$\text{Zn-Proteome} + \text{L} \leftrightharpoons \text{L-Zn-Proteome} \qquad (4.14)$$

$$\text{Proteome•Zn} + \text{L} \leftrightharpoons \text{Proteome•Zn-L} \qquad (4.1)$$

which will be more favorable in the absence of TSQ. However, in cells, instead of TSQ, GSH may bind to both classes of zinc-protein interactions. Potentially, such reactions of non-physiological metal binding ligands may be significant contributors to the cellular biochemistry of zinc, but more will need to be done to demonstrate their importance.

The one set of reactions that seems highly significant involves GSH as the ligand. GSH competes successfully with TSQ-Zn-Proteome and Proteome•Zn-TSQ at concentrations well below those commonly present in cells. Thus, it is reasonable to hypothesize that both members of the Zn-Proteome and Proteome•Zn exist *in vivo* as ternary adducts with glutathione.

Part V: Concluding Remarks

Does Cd^{2+} replace Zn^{2+} in Zn-proteins within the cell Proteome of LLC-PK_1 kidney epithelial cells? This initial hypothesis (**reaction 2.1**-**2.3**) was examined using $Cd(PYR)_2$ incubated with LLC-PK_1 cells for 30 minutes and the distribution of Zn^{2+} and Cd^{2+} monitored at six time points: 0 hour (30 minutes), 1 hour, 2 hours, 3 hours, 6 hours, 24 hours. The results indicate a majority of cadmium reacted and became bound to the Proteome within 30 minutes of incubation (**figure 2.4**). We assume that originally, Cd^{2+} becomes bound non-specifically to the Proteome:

$$Cd(PYR)_2 + \text{Proteome} \leftrightharpoons \text{Proteome•Cd} + 2\ PYR \qquad (2.2)$$

Once in the cells, PYR must redistribute itself back outside cells to bind more Cd^{2+} and then transport it into cells in order to move most of the extracellular Cd^{2+} into cells within 30 min.

$$PYR_{inside} \leftrightharpoons PYR_{outside} \qquad (5.1)$$

In **Part IV**, we demonstrated that PYR can form ternary adducts with Zn-proteins and Proteome•Zn (**figure 4.11-4.14**). Thus, it is possible that besides these reactions, it is also binding intracellularly to form PYR-Zn-proteins, PYR-Cd-proteins, Proteome•Zn-PYR and Proteome•Cd-PYR.

Figure 2.18 demonstrated that Proteome•Cd rapidly replaced Zn^{2+} in Zn-proteins and in the process made the Zn^{2+} available for reaction with EDTA. Overall, the exchange reaction is consistent with a 1:1 stoichiometry of Cd^{2+} and Zn^{2+}:

$$\text{Proteome•Cd} + \text{Zn-proteins} \leftrightharpoons \text{Cd-proteins} + \text{Proteome•Zn} \qquad (2.3)$$

MT was synthesized at the 2- and 4-hour time points (**figure 2.6-2.8**), consistent with **reactions 2.8**-**2.12**, and sequestered cadmium out of the Proteome while zinc was restored into the Proteome (**reactions 2.14**-**2.15**) (**figure 2.19**).

After two hours of incubation, the induction and synthesis of apo-MT began to take place (**reactions 2.7-2.10**). The induction process depends on the activation of the transcription factor, MTF-1 by Zn^{2+}. The source of available Zn^{2+} must be Proteome•Zn. Because MTF-1 has high affinity for Zn^{2+}, it competes for this pool of Zn^{2+}:

$$\text{MTF-1} + \text{Proteome•Zn}_n \leftrightharpoons \text{Zn}_n\text{-MTF-1} + \text{Proteome} \qquad (1.17)$$

Proteome•Zn must be produced within 30 minutes of incubation with $Cd(PYR)_2$ because it is the cause for the induction and synthesis of apo-MT that occurs through a cascade of reactions within the cell.

Over time, MT sequestered a nearly equal amount of cadmium out of the Proteome as native protein-bound zinc reappeared in the Proteome (**reactions 2.10-2.12**). After 24 hours post-incubation, the majority of the Proteome-bound cadmium was sequestered into MT along with an equal amount of zinc, presumably from the extracellular medium (**figure 2.9**).

The exchange reaction of cadmium and zinc within Zn-proteins can be seen through the *in vitro* reaction of isolated Zn-Proteome with increasing amounts of $Cd(PYR)_2$ (**figure 2.14-2.15**). The results showed that as the concentration of Cd^{2+} increased, the amount of Zn^{2+} mobilized and accessible to EDTA increased in parallel, stoichiometric (1:1) fashion. This mobilization of Zn^{2+} from Zn-proteins must result in the production of Proteome•Zn that reacts with EDTA and appears in the filtrate. The exchange reaction was also monitored with the zinc fluorescence probe, TSQ. TSQ binds to about 25% of the total zinc in the Proteome (Meeusen et al. 2011). Upon reaction of Zn-Proteome with Cd^{2+}, a large increase in fluorescence was observed that must represent Proteome•Zn because Cd^{2+} only poorly enhances the fluorescence emission of TSQ (**figures 3.17-3.18**)

$$\text{Zn-proteins} + \text{TSQ} \leftrightharpoons \text{TSQ-Zn-proteins} \qquad (3.2)$$

$$\text{TSQ-Zn-proteins} + \text{Proteome•Cd-TSQ} \leftrightharpoons \text{TSQ-Cd-proteins} + \text{Proteome•Zn-TSQ} \qquad (5.2)$$

In order to study the he cellular biochemistry of zinc and cadmium at the molecular instead of the proteomic level, new methods were developed. A native high-resolution separation method for proteins, NSDS-PAGE, was coupled with two highly sensitive method to measure elemental isotopes, LA-ICP-MS, and fluorescence imaging of zinc by TSQ. Bovine Serum Albumin and Carbonic Anhydrase were individual Zn-proteins used for method development. Albumin was shown to retain the native structural characteristics under conditions of electrophoresis and retain its complement of moderately bound Zn^{2+} (**figure 3.21**). Carbonic anhydrase was employed to investigate the limit of ^{66}Zn-protein detection by LA-ICP-MS (**figure 3.22-3.25**). Increasing concentrations of CA protein bands revealed by LA-ICP-MS, TSQ and Coomassie staining were found to be coincident with the location of zinc on the gel indicating that the LA-ICP-MS measurements detect ^{66}Zn bound to CA after NSDS-PAGE separation. The linear relationship and the good agreement between applied and detected amounts of zinc shows that this method provides quantitative results with a limit of detection of 14 pmol applied Zn^{2+} for Zn-CA (**figure 3.26**).

HPLC fraction 60 from the separation of proteome from LLC-PK_1 cells was the first mixture of Zn-proteins utilized for furthering this method development. Reproducibility of separation (NSDS-PAGE) and metal ion detection (LA-ICP-MS) was seen on the same lane, between lanes on the same gel and between gels (**figure 3.28-3.39**).

An investigation of the Cd-Zn exchange process was undertaken with fraction 60 (**figure 3.42-3.48**). The results complete the studies of the Cd-Zn exchange process that began with the exposure of LLC-PK_1 cells to Cd^{2+} plus Pyrithione (**figures 2.3-2.9**). They show the replacement of Zn^{2+} by Cd^{2+} from protein sites with approximate one to one stoichiometry. Addition of Zn-MT to the mixture shifts Cd^{2+} out of Cd-proteins and restores a native distribution of Zn^{2+} among Zn-proteins. The underlying reactions are thought to involve the direct reaction of Zn-MT with Cd-proteins (**reaction 3.4**).

$$\text{Cd-proteins} + \text{Zn-MT} \leftrightharpoons \text{Cd-MT} + \text{Zn-proteins} \quad (3.4)$$

The potential of PYR to interact with metal ions bound to the Proteome raised the question about whether other ligands might be able to do so. A survey showed that L-Glutathione formed adducts with members of both the Zn-Proteome and Proteome•Zn well below its cellular concentrations (**figure 4.21-4.24**). Therefore, these forms of Zn^{2+} and possibly Cd^{2+} may exist *in vivo* as ternary adducts with glutathione. In a related study glutathione was shown to chelate Zn^{2+} from Proteome•Zn, showing GSH enhances the rate that Proteome•Zn donates Zn^{2+} to apo-Zn-proteins such as apo-carbonic anhydrase (Petering et al. 2019).

$$\text{Proteome•Zn-GS} \leftrightharpoons \text{Zn-SG} + \text{Proteome} \quad (5.3)$$

$$\text{Zn-SG} + \text{apo-protein} \leftrightharpoons \text{Zn-protein} + GS^{-} \quad (5.4)$$

The results from the competitive ligand titration experiment show that such reactions of non-physiological metal binding ligands may also be significant contributors to the cellular biochemistry of zinc, but more will need to be done to demonstrate their importance.

REFERENCES

1. Anderegg G. (1964) Komplexone XXXVI. Reaktionsenthalpie rind -entropie bei der Bildung der Metallkomplexe der hoheren EDTA-Homologen. Helv Chim Acta 50:1801–1815
2. Andreini C., Banci L., Bertini I., Rosato A. (2006) Zinc through the three domains of life. J Proteome Res 5: 3173-3178
3. Andreini C., Banci L., Bertini I., Rosato A. (2006) Counting the zinc-proteins encoded in the human genome. J Proteome Res 5:196–201
4. Armitage I, Drakenberg T, Reilly B (2013) Use of ^{113}Cd NMR to probe the native metal binding sites in metalloproteins: an overview. In: Sigel A, Sigel H, Sigel RKO (ed) Cadmium: from toxicity to essentiality. Met ions life sci, vol 11. Springer, Heidelberg, pp 117-144
5. Becker JS, Lobinski R, Becker JS. (2009) Metal imaging in non-denaturating 2D electrophoresis gels by laser ablation inductively coupled plasma mass spectrometry (LA-ICP-MS) for the detection of metalloproteins. Metallomics;1(4):312-6.
6. Berg JM (1988) Proposed structure for the zinc-binding domains from transcription factor IIIA and related proteins. Proc Natl Acad Sci U S A 85:99–102
7. Berg JM, Godwin HA (1997) Lessons from zinc-binding peptides. Annu Rev Biophys Biomol Struct 26: 357-371
8. Bernhardt M. L., Kim A. M., O'Halloran T. V., & Woodruff T. K. (2011). Zinc requirement during meiosis I-meiosis II transition in mouse oocytes is independent of the MOS-MAPK pathway. *Biology of reproduction*, *84*(3), 526–536

9. Bittel D, Dalton T, Samson SL, Gedamu L, Andrews GK (1998) The DNA binding activity of metal response element-binding transcription factor-1 is activated In vivo and in vitro by zinc, but not by other transition metals. J Biol Chem 273:7127–7133

10. Blumenthal SS, Lewand DL, Buday MA, Kleinman JG, Krezoski SK, Petering DH (1990) Cadmium inhibits glucose uptake in primary cultures of mouse cortical tubule cells. Am J Physiol 258: F1625–F1633

11. Blumenthal S, Lewand D, Sochanik A, Krezoski S, Petering DH (1994) Inhibition of Na^{1+}-glucose cotransport in kidney cortical cells by cadmium and copper: protection by zinc. Toxicol Appl Pharmacol 29: 177-187

12. Blumenthal S, Lewand D, Krezoski SK, Petering DH (1996) Comparative effects of Cd^{2+} and Cd-metallothionein on cultured kidney tubule cells. Toxicol Appl Pharmacol 136:220–228

13. Bonta M, Limbeck A, Quarles Jr C.D., Oropeza D, Russo R.E., Gonzalez J.J. (2015) A metric for evaluation of the image quality of chemical maps derived from LA-ICP-MS experiments J. Anal. At. Spectrom. 30, 1809-1815

14. Bradshaw, N.; Hall, E. F.; Sanderson, N. E. (1989) J. Anal. At. Spectrom. 4, 801−803

15. Cousins RJ (1979) Metallothionein synthesis and degradation: relationship to cadmium metabolism. Environ. Health Persp 28:131–136

16. Coutant C.C., Chen C.H. (1993) Strontium Microstructure in Scales of Freshwater and Estuarine Striped Bass (Morone saxatilis) Detected by Laser Ablation Mass Spectrometry Canadian Journal of Fisheries and Aquatic Sciences, 50:1318-1323

17. Cox EH, McLendon GL (2000) Zinc-dependent protein folding. Curr Opin Chem Biol 4: 162-165

18. Cromwell, E. F., & Arrowsmith, P. (1995). Fractionation Effects in Laser Ablation Inductively Coupled Plasma Mass Spectrometry. Applied Spectroscopy, 49(11), 1652–1660.

19. Dalton TP, Bittel D, Andrews GK (1997) Reversible activation of mouse metal response element-binding transcription factor 1 DNA binding involves zinc interaction with the zinc finger domain. Mol Cell Biol 17: 2781-2789

20. Diwakar P. K., Harilal S. S., LaHaye N. L., Hassaneina A., Kulkarnib P. (2015) The influence of laser pulse duration and energy on ICP-MS signal intensity, elemental fractionation, and particle size distribution in NIR fs-LA-ICP-MS J. Anal. At. Spectrom., 28, 1420-1429

21. Durrant S.F. (1999) Laser ablation inductively coupled plasma mass spectrometry: achievements, problems, prospects J. Anal. At. Spectrom.,14, 1385-1403

22. Durrant S.F., Ward N. (2005) Recent biological and environmental applications of laser ablation inductively coupled plasma mass spectrometry (LA-ICP-MS) J. Anal. At. Spectrom., 20, 821-829

23. Dyke B., Hegenauer J., Saltman P., Laurs R.M. (1987) Isolation and characterization of a new zinc-binding protein from albacore tuna plasma Biochemistry. Jun 2;26(11):3228-34.

24. Eggins, S.M., Kinsley, L.P.J., Shelley J.M.G. (1998): Deposition and element fractionation processes during atmospheric pressure laser sampling for analysis by ICPMS. Appl. Surf. Sci. 129, 278-286

25. Ejnik J, Munoz A, Gan T, Shaw CF 3rd, Petering DH (1999) Interprotein metal ion exchange between cadmium-carbonic anhydrase and apo- or zinc-metallothionein. J Biol Inorg Chem 4: 784-790

26. Ejnik J, Shaw Cf 3rd, Petering DH (2010) Mechanism of cadmium ion substitution in mammalian zinc metallothionein and metallothionein alpha domain: kinetic and structural studies. Inorg Chem 49: 6525-6534

27. Fanali G, di Masi A, Trezza V, Marino M, Fasano M, Ascenzi P (2012) Human serum albumin: From bench to bedside. Molecular Aspects of Medicine, Volume 33, Issue 3 Pages 209-290

28. Fatema, Kaniz (2015) "Reaction of Zinc Proteome with Biologically Important Metal Binding Ligands" *Theses and Dissertations*. 1100

29. Friberg L (1984) Cadmium and the kidney. Environ Health Perspect 54:1–11

30. Garcia C.C., Lindnera H., Niemaxa K. (2008) Laser ablation inductively coupled plasma mass spectrometry—current shortcomings, practical suggestions for improving performance, and experiments to guide future development J. Anal. At. Spectrom., 24, 14-26

31. Geertsen C., Briand A., Chartier F., Lacour J., Mauchien P., Sjöström S., Mermet J. (1994) Comparison between infrared and ultraviolet laser ablation at atmospheric pressure—implications for solid sampling inductively coupled plasma spectrometry J. Anal. At. Spectrom. 9, 17-22

32. Grubbs F.E., Beck G. (1972) “Extension of Sample Sizes and Percentage Points for Significance Tests of Outlying Observations”, Technometrics, 14(4), 847-854

33. Guerrerio AL, Berg JM (2004) Metal ion affinities of the zinc finger domains of the metal responsive element-binding transcription factor-1 (MTF1). Biochemistry 45: 5437-5444

34. Guillong M., Horn I., Günther D. (2003) A comparison of 266 nm, 213 nm and 193 nm produced from a single solid state Nd:YAG laser for laser ablation ICP-MS J. Anal. At. Spectrom.,18, 1224-1230

35. Gunter V, Lindert U, Schaffner W (2012) The taste of heavy metals: gene regulation by MTF-1. Biochim Biophys Acta 1823: 1416-1425

36. Hieftje G.M., Ross B.S. (1992) Selection of solvent load and first-stage pressure to reduce interference effects in inductively coupled plasma-mass spectrometry. J Am Soc Mass Spectrom. (2): 128-38

37. Houk R.S., Fassel V.A., Flesch G. D., Svec H.J., Gray A.L., Taylor C. E. (1980) Inductively coupled argon plasma as an ion source for mass spectrometric determination of trace elements Anal. Chem., 52, 14, 2283-2289

38. Huang M, Krepkiy D, Hu W, Petering DH (2004) Zn-, Cd-, and Pb-transcription factor IIIA: properties, DNA binding, and comparison with TFIIIA-finger 3 metal complexes. J Inorg Biochem 98:775–785

39. Hunt JA, Fierke CA. (1997) Selection of carbonic anhydrase variants displayed on phage. Aromatic residues in zinc binding site enhance metal affinity and equilibration kinetics. J Biol Chem; 272(33): 20364-72.

40. Hurst, T. K., Wang, D., Thompson, R. B., & Fierke, C. A. (2010). Carbonic anhydrase II-based metal ion sensing: Advances and new perspectives. Biochimica et biophysica acta, 1804(2), 393–403.

41. Jakubowski N., Moens L., Vanhaecke F. (1998) Sector field mass spectrometers in ICP-MS, Spectrochimica Acta Part B: Atomic Spectroscopy, Volume 53, Issue 13, Pages 1739-1763

42. Jarup L, Akesson A (2009) Current status of cadmium as an environmental health problem. Toxicol Appl Pharmacol 238:201–208

43. Jarvis I., Jarvis K. E. (1992) Inductively coupled plasma-atomic emission spectrometry in exploration geochemistry, Journal of Geochemical Exploration, Volume 44, Issues 1–3, Pages 139-200

44. Jeong S.H., Borisov O.V., Yoo J.H., Mao X.L., Russo R.E. (1999) Effects of Particle Size Distribution on Inductively Coupled Plasma Mass Spectrometry Signal Intensity during Laser Ablation of Glass Samples Anal. Chem. 71, 22, 5123-5130

45. Jiang P, Guo Z (2004) Fluorescent detection of zinc in biological systems: recent development on the design of chemosensors and biosensors, Coordination Chemistry Reviews, Volume 248, Issues 1–2: Pages 205-229

46. Karim MR, Petering DH (2016) Newport Green, a fluorescent sensor of weakly bound cellular Zn^{2+}: competition with proteome for Zn^{2+}. Metallomics 8: 201-210

47. Klaassen CD, Maitani T, Cuppage FE (1988) Nephrotoxicity of intravenously injected cadmium-metallothionein: critical concentration and tolerance. Fundam Appl Toxicol 10:98–108

48. Klaassen CD, Dorian C, Gattone VH 2nd (1992) Accumulation and degradation of the protein moiety of cadmium-metallothionein (CdMT) in the mouse kidney. Toxicol Appl Pharmaco 117:242–248

49. Klaassen Cd, Liu J, Choudhuri S (1999) Metallothionein: an intracellular protein to protect against cadmium toxicity. Annu Rev Pharmacol Toxicol 39: 267-294

50. Klaassen CD, Habeebu SS, Liu J, Liu Y (2000) Metallothionein-null mice are more susceptible than wild-type mice to chronic CdCl(2)-induced bone injury. Toxicol Sci 56:211–219

51. Klaassen CD, Liu J, Diwan BA (2009) Metallothionein protection of cadmium toxicity. Toxicol Appl Pharmacol 238: 215-220

52. Kothinti RK, Blodgett AB, Petering DH, Tabatabai NM (2010) Cadmium down-regulation of kidney Sp1 binding to mouse SGLT1 and SGLT2 gene promoters: possible reaction of cadmium with the zinc finger domain of Sp1. Toxicol Appl Pharmaco 244:254–262

53. Kothinti R, Tabatabai NM, Petering DH (2011) Electrophoretic mobility shift assay of zinc finger proteins: competition for Zn(2+) bound to Sp1 in protocols including EDTA. J Inorg Biochem 105:569–576

54. Krepkiy D, Forsterling FH, Petering DH (2004) Interaction of Cd^{2+} with Zn finger 3 of transcription factor IIIA: structures and binding to cognate DNA. Chem Res Toxicol 17:863–870

55. Krezel A, Bal W (1999) Coordination chemistry of glutathione. Acta Biochim Pol 46: 567-580

56. Krezel A, Maret W (2006) Zinc-buffering capacity of a eukaryotic cell at physiological pZn. J Biol Inorg Chem 11: 1049-1062

57. Laity JH, Andrews GK (2007) Understanding the mechanisms of zinc-sensing by metal-response element binding transcription factor-1 (MTF-1). Arch Biochem Biophys 463: 201-210

58. Lee MS, Gippert GP, Soman KV, Case DA, Wright PE (1989) Three-dimensional solution structure of a single zinc finger DNA-binding domain. Science 245:635–637

59. Li TY, Kraker AJ, Shaw CF 3rd, Petering DH (1980) Ligand substitution reactions of metallothioneins with EDTA and apo-carbonic anhydrase. Proc Natl Acad Sci U S A 77: 6334-38

60. Liu J, Habeebu SS, Liu Y, Klaassen CD (1998) Acute CdMT injection is not a good model to study chronic Cd nephropathy: comparison of chronic $CdCl_2$ and CdMT exposure with acute CdMT injection in rats Toxicol. Appl. Pharmacol. 153:48–58

61. Lund E., Krezoski S., Petering D. (2018) The Chemical Biology of Cadmium. In: Thévenod F., Petering D., M. Templeton D., Lee WK., Hartwig A. (eds) Cadmium Interaction with Animal Cells. Springer, Cham

62. Maret, W, Moulis JM (2013) The bioinorganic chemistry of cadmium in the context of its toxicity. In: Sigel A, Sigel H, Sigel RKO (ed) Cadmium: from toxicity to essentiality. Met ions life sci, vol 11. Springer, Heidelberg, pp 1-29

63. Margoshes M, Vallee BL (1957) A cadmium protein from equine kidney cortex. J Am Chem Soc 79: 4813-4814

64. Masuoka J, Hegenauer J, Van Dyke BR, Saltman P. (1993) Intrinsic stoichiometric equilibrium constants for the binding of zinc(II) and copper(II) to the high affinity site of serum albumin. J Biol Chem. Oct 15; 268(29): 21533-7.

65. Meeusen, J. W., Tomasiewicz, H., Nowakowski, A., & Petering, D. H. (2011). TSQ (6-methoxy-8-p-toluenesulfonamido-quinoline), a common fluorescent sensor for cellular zinc, images zinc proteins. *Inorganic chemistry*, *50*(16), 7563–7573.

66. Meeusen, J. W., Nowakowski, A., & Petering, D. H. (2012). Reaction of metal-binding ligands with the zinc proteome: zinc sensors and N,N,N',N'-tetrakis(2-pyridylmethyl)ethylenediamine. *Inorganic chemistry*, *51*(6), 3625–3632.

67. Meldrum, N. U., & Roughton, F. J. (1933). Carbonic anhydrase. Its preparation and properties. *The Journal of physiology*, *80*(2), 113–142.

68. Namdarghanbari MA, Meeusen J, Bachowski G, Giebel N, Johnson J, Petering DH (2010) Reaction of the zinc sensor FluoZin-3 with Zn(&)-metallothionein: inquiry into the existence of a proposed weak binding site. J Inorg Biochem 104: 224-231

69. Namdarghanbari M, Wobig W, Krezoski S, Tabatabai NM, Petering DH (2011) Mammalian metallothionein in toxicology, cancer, and cancer chemotherapy. J Biol Inorg Chem 16: 1087-101

70. Namdarghanbari MA, Bertling J, Krezoski S, Petering DH (2014) Toxic metal proteomics: reaction of the mammalian zinc proteome with Cd^{2+}. J Inorg Biochem 136:115–121

71. Nettesheim DG, Engeseth HR, Otvos JD (1985) Products of metal exchange reactions of metallothionein. Biochemistry 24: 6744-6751

72. Nordberg GF (2009) Historical perspectives on cadmium toxicology. Toxicol Appl Pharmacol 238: 192-200

73. Nowakowski, A. B., & Petering, D. H. (2011). Reactions of the fluorescent sensor, Zinquin, with the zinc-proteome: adduct formation and ligand substitution. *Inorganic chemistry*, *50*(20), 10124–10133.

74. Nowakowski, A. B., Wobig, W. J., & Petering, D. H. (2014). Native SDS-PAGE: high resolution electrophoretic separation of proteins with retention of native properties including bound metal ions. Metallomics : integrated biometal science, 6(5), 1068–1078.

75. Nowakowski AB, Meeusen JW, Menden H, Tomasiewicz H, Petering DH. (2015) Chemical-Biological Properties of Zinc Sensors TSQ and Zinquin: Formation of Sensor-Zn-Protein Adducts versus Zn(Sensor)2 Complexes. Inorganic Chemistry. 54: 11637-47.

76. Nowakowski AB, A, Karim, MR, Petering DH (2015) Zinc proteomics. In: RA Scott (ed) Encyclopedia of inorganic and bioinorganic chemistry. Wiley, Chichester. Eibc2332.

77. Otvos JD, Armitage IM (1980) Structure of the metal clusters in rabbit liver metallothionein. Proc Natl Acad Sci U S A 77: 7094-98

78. Otvos JD, Petering DH, Shaw CF (1989) Structure-reactivity relationships of metallothionein, a unique metal binding protein. Comments Inorg Chem 9: 1-35

79. Petering DH, Loftsgaarden J, Scheider J, Fowler B (1984) Metabolism of cadmium, zinc, and copper in the rat kidney: the role of metallothionein and other binding sites. Environ Health Perspect 54: 73-81

80. Petering DH, Zhu J, Krezoski S, Meeusen J, Kiekenbush C, Krull S, Specher T, Dughish M (2006) Apo-metallothionein emrging as a major player in the cellular activities of metallothionein. Exp Biol Med (Maywood) 231: 1528-1534

81. Petering DH, Krezoski S, Tabatabai NM (2009) In: Sigel A, Sigel H, Sigel RKO (ed) Metallothioneins and related chelators. Met ions life sci, vol 5. Springer, Heidelberg, pp 353-397

82. Petering, DH (2017) Reactions of the Zn Proteome with Cd^{2+} and other xenobiotics: trafficking and toxicity. Chem Res Toxicol 30: 189-202

83. Petering, D.H., & Mahim, A. (2017). Proteomic High Affinity Zn2+ Trafficking: Where Does Metallothionein Fit in? International journal of molecular sciences, 18(6), 1289.

84. Petering DH, Mahim A (2019) **in preparation**

85. Petering H. G. (1978). Some observations on the interaction of zinc, copper, and iron metabolism in lead and cadmium toxicity. Environmental health perspectives, 25, 141–145

86. Pinter TB, Stillman MJ (2014) The zinc balance: competitive zinc metalation of carbonic anhydrase and metallothionein 1A. Biochemistry 53: 6276-6285

87. Pizzorno J. (2014). Glutathione!. Integrative medicine (Encinitas, Calif.), 13(1), 8–12.

88. Raab, A., Pioselli B., Munro C., Thomas-Oates J., Feldmann J. (2009) "Evaluation of Gel Electrophoresis Conditions for the Separation of Metal-tagged Proteins with Subsequent Laser Ablation ICP-MS Detection." Electrophoresis. 30.2: 303-14.

89. Radtke, F., Heuchel, R., Georgiev, O., Hergersberg, M., Gariglio, M., Dembic, Z., & Schaffner, W. (1993). Cloned transcription factor MTF-1 activates the mouse metallothionein I promoter. The EMBO journal, 12(4), 1355–1362.

90. Rana U, Kothinti R, Meeusen J, Tabatabai NM, Krezoski S, Petering DH (2008) Zinc binding ligands and cellular zinc trafficking: apo-metallothionein, glutathione, TPEN, proteomic zinc, and Zn-Sp1. J Inorg Biochem 102: 489-499

91. Roesijadi G, Bogumil R, Vasak M, Kagi JH (1998) Modulation of DNA binding of a tramtrack zinc finger peptide by the metallothionein-thionein conjugate pair. J Biol Chem 273: 17425-17432

92. Sabolic I, Breljak D, Skarica M, Herak-Kramberger CM (2010) Role of metallothionein in cadmium traffic and toxicity in kidneys and other mammalian organs. Biometals 23:897–926

93. Satarug S, Moore MR (2004) Adverse health effects of chronic exposure to low-level cadmium in foodstuffs and cigarette smoke. Environ Health Perspect 112:1099–1103

94. Schechter I, Xu L, Bulatov V, Gridin V.V. (1997) Absolute Analysis of Particulate Materials by Laser-Induced Breakdown Spectroscopy *Anal. Chem.* 69, 11, 2103-2108

95. Setlow, B., Atluri, S., Kitchel, R., Koziol-Dube, K., & Setlow, P. (2006). Role of dipicolinic acid in resistance and stability of spores of Bacillus subtilis with or without DNA-protective alpha/beta-type small acid-soluble proteins. Journal of bacteriology, 188(11), 3740–3747

96. Shin, J. H., Jung, H. J., An, Y. J., Cho, Y. B., Cha, S. S., & Roe, J. H. (2011). Graded expression of zinc-responsive genes through two regulatory zinc-binding sites in Zur. *Proceedings of the National Academy of Sciences of the United States of America*, *108*(12), 5045–5050

97. Sovago I, Varnagy K (2013) Cadmium (II) complexes of amino acids and peptides. In: Sigel A, Sigel H, Sigel RKO (ed) Cadmium: from toxicity to essentiality. Met ions life sci, vol 11. Springer, Heidelberg, pp 275-302

98. Stillman MJ, Cai W, Zelazowski AJ (1987) Cadmium Binding to Metallothioneins: DOMAIN SPECIFICITY IN REACTIONS OF a AND p FRAGMENTS, APOMETALLOTHIONEIN, AND ZINC METALLOTHIONEIN WITH Cd The Journal of Biological Chemistry 262: 4538-4548.

99. Sussulini A, Becker JS (2011) Combination of PAGE and LA-ICP-MS as an analytical workflow in metallomics: state of the art, new quantification strategies, advantages and limitations Metallomics,3, 1271-1279

100. Tabatabai NM, Blumenthal SS, Lewand DL, Petering DH (2001) Differential regulation of mouse kidney sodium-dependent transporters mRNA by cadmium. Toxicol Appl Pharmacol 177:163–173

101. Tabatabai NM, Blumenthal SS, Lewand DL, Petering DH. (2001) Mouse kidney expresses mRNA of four highly related sodium-glucose cotransporters: regulation by cadmium. *Kidney International*. 64: 1320-30

102. Tabatabai NM, Blumenthal SS, Petering DH (2005) Adverse effect of cadmium on binding of transcription factor Sp1 to the GC-rich regions of the mouse sodium-glucose cotransporter 1, SGLT1, promoter. Toxicology 207:369–382

103. Tan S, Horlick G (1987) Matrix-effect observations in inductively coupled plasma mass spectrometry J. Anal. At. Spectrom. 2, 745-763

104. Teledyne (2018) Performance and Gas-Flow Effects of an Active 2-Volume Sampling Chamber

105. Thermo Fisher Scientific (2008) https://www.niu.edu/geology/_pdf/Element2.pdf

106. Thevenod F (2003) Nephrotoxicity and the proximal tubule. Insights from cadmium. Nephron Physiol 93:87–93

107. Thevenod F, Lee WK (2013) Toxicology of cadmium and its damage to mammalian organs. In: Sigel A, Sigel H, Sigel RKO (ed) Cadmium: from toxicity to essentiality. Met ions life sci, vol 11. Springer, Heidelberg, pp 415-490

108. Vasak M, Meloni G (2011) Chemistry and biology of mammalian metallothioneins. J Biol Inorg Chem 16: 1067-1078

109. Walsh M.J., Ahner B.A. (2013) Determination of stability constants of Cu(I), Cd(II) & Zn(II) complexes with thiols using fluorescent probes, Journal of Inorganic Biochemistry, Volume 128, Pages 112-123

110. Wildner H. (1998) Application of inductively coupled plasma sector field mass spectrometry for the fast and sensitive determination and isotope ratio measurement of non-metals in high-purity process chemicals J. Anal. At. Spectrom.13, 573-578

111. Yin J, Ren W, Yang G, Duan J, Huang X, Fang R, Li C, Li T, Yin Y, Hou Y (2016) l-Cysteine metabolism and its nutritional implications. Mol Nutr Food Res 60:134-146.

112. Youn CK, Kim SH, Lee DY, Song SH, Chang IY, Hyun JW, Chung MH, You HJ (2005) Cadmium down-regulates human OGG1 through suppression of Sp1 activity. J Biol Chem 280:25185–25195

113. Zhang B, Georgiev O, Hagmann M, Günes C, Cramer M, Faller P, Vasak M, Schaffner W (2003) Activity of metal-responsive transcription factor 1 by toxic heavy metals and H_2O_2 in vitro is modulated by metallothionein. Mol Cell Biol 23:8471–8485

CURRICULUM VITAE

Eric D. Lund

Education

University of Milwaukee-Wisconsin
Ph.D. in Chemistry May 2020
Advisor: Distinguished Professor Dr. David H. Petering
Dissertation: Zinc Proteomics: Interactions of Zn^{2+}, Cd^{2+}, and Metal-Binding Ligands with Zn-Binding Sites in the Proteome
Graduate Teaching Assistant: General Chemistry and Qualitative Analysis

University of Milwaukee-Wisconsin
B.S. in Biochemistry December 2011
GPA 3.27/4.00
Undergraduate Research Advisor: Associate Professor Dr. Nicholas Silvaggi, Professor David Frick
Undergraduate Teaching Assistant: General Chemistry and Qualitative Analysis

Experience

University of Wisconsin – Milwaukee; Milwaukee, WI Sept. 2012 – Dec. 2019
Laboratory in Chemistry Building on University Campus

Research Assistant with Dr. David Petering, Distinguished Professor of Chemistry

- NMR and GC technique for analysis of unknown organic samples
- Purified protein through Sephadex column chromatography including HPLC, G-25 and G-75.
- Quantitation of Cd^{2+} and Zn^{2+} reactions with LLC-PK_1 Proteome furthering zinc biochemistry with toxic metals
- Separation of proteins using Native SDS - Polyacrylamide Gel Electrophoresis: After separation of proteins by molecular weight using electrophoresis, passive drying technique was used to dry gels for further analysis using laser ablation.
- Laser ablation – Inductively Coupled Plasma – Mass Spectrometry analysis of polyacrylamide gels: Passively dried gels were subjected to laser ablation. Proteins were identified. Zinc and Cadmium ions were observed.

University of Wisconsin – Milwaukee; Milwaukee, WI Jan. 2010 – Dec. 2011
Chemistry Laboratory, University Campus

Research Assistant with Dr. David Frick, Professor of Biochemistry

- Purified protein through BioRad column chromatography including Ion Exchange, Size Exclusion, and immobilized metal affinity.
- Ran Bradford and enzyme assays to measure activity.
- Protein Crystallography

Research Assistant with Dr. Nicholas Silvaggi, Associate Professor of Biochemistry

- Extensive general protein biochemistry and molecular biology techniques using equipment
- Expressed protein and purified it from *E. coli* using immobilized metal affinity chromatography and a GE Akta purifier FPLC
- Crystallized purified protein for X-ray crystallographic structure determination
- Tested for enzyme activity using an HPLC-based assay with pre-column DABSYL-Cl derivatization

Teaching Assistant - General Chemistry and Qualitative Analysis

- Provided detailed one hour lectures of coursework twice a week in a classroom setting of 18 students.
- Corrected papers weekly (36 labs and 36 quizzes) for 72 students.
- Created one quiz per week and distributed to students.
- Counseled students for four office hours per week.
- Instructed two labs (3 hours in length) per week.

Selected Presentations and Awards

1. **University of Wisconsin - Milwaukee:** 15th Annual Research Symposium
2. **University of Wisconsin - Milwaukee:** 14th Annual Research Symposium
3. **North American Workshop on Laser Ablation:** 2nd Biannual Poster Symposium
4. **University of Wisconsin - Milwaukee:** 12th Annual Research Symposium
5. **Canadian Bioinorganic Chemistry Conference:** 5th Biannual Research Symposium
6. **University of Wisconsin - Milwaukee:** ACS - American Chemistry Society Vice President
7. **University of Wisconsin – Milwaukee:** Undergraduate Research Symposium
8. **Boy Scouts of America Troop 507** – Earned Eagle Scout Ranking

Publications

1. Lund E., Krezoski S., Petering D. (2018) The Chemical Biology of Cadmium. In: Thévenod F., Petering D., M. Templeton D., Lee WK., Hartwig A. (eds) Cadmium Interaction with Animal Cells. Springer, Cham